Dissertations - ALL   **SURFACE**

August 2018

Post-Orogenic Thermal History and Exhumation of the Northern Appalachian Basin: Low-Temperature Thermochronologic Constraints

Chilisa Marie Shorten
Syracuse University

Follow this and additional works at: https://surface.syr.edu/etd

Part of the Physical Sciences and Mathematics Commons

General Abstract

Since the early development of the fission-track dating method by Price, Walker and Fleischer in the 1960's and 1970's, the method has evolved into a robust tool for constraining thermal histories and determining exhumation rates within the upper continental crust. Low-temperature thermochronology, notably apatite fission-track thermochronology because it has a kinetic parameter (i.e. track lengths), is commonly used to constrain the tectonic history of orogenic belts and the thermal history within sedimentary basins for hydrocarbon resource assessment. Collisional tectonics in the Paleozoic which formed of the Appalachian Orogen and the foreland basin has been a subject of considerable study. The objective of this dissertation is to apply low-temperature thermochronology to constrain the post-orogenic thermal history and exhumation of the Northern Appalachian Basin. Previous work has identified that the post-rifting evolution of eastern North America involves a number of periods of rapid cooling and/or exhumation, yet significant debate remains on the temporal and spatial resolution of the periods of rapid cooling within the Mesozoic and Cenozoic, and hence their significance. Chapters one and two of this dissertation are focused on constraining the post-orogenic thermal history and exhumation of the Northern Appalachian Basin, within New York and Pennsylvania. Chapter three is a comprehensive analysis of the thermal history trends and variations synthesized from published low-temperature thermochronology studies across the Appalachian orogen in eastern North America.

Chapter one constrains the post-orogenic thermal history and exhumation of the Northern Appalachian Basin utilizing apatite fission-track (AFT) thermochronology and (U-Th)/He dating integrated with paleothermometers and geologic constraints. Samples were collected from

Devonian-aged Catskill delta wedge formations across New York and Pennsylvania (USA). The AFT age of samples decreases from west to east across the Northern Appalachian Basin (~180-120 Ma) a result of synchronous onset of exhumation, with greater amounts of burial and exhumation in the east. Apatite fission-track thermochronology data, apatite (U-Th)/He ages, and vitrinite reflectance maximum paleotemperature information provide inputs for inverse thermal models, which constrain a multi-stage post-orogenic history. Overall cooling rates documented in the Northern Appalachian Basin are slow, however we constrain two periods of "rapid" cooling separated by a long period of slower cooling: (1) Late Triassic to Early Jurassic onset of rapid cooling (1-3 °C/Myr) from maximum temperatures, generally higher than the retentivity of fission-tracks in apatite (i.e. >~110-120 °C); (2) Slow cooling (0.1-0.3 °C/Myr), which is referred to as a period of stabilization within the Northern Appalachian Basin, from the Cretaceous to Late Cenozoic; (3) Rapid cooling (1-2 °C/Myr) from the Mid-Miocene to present. Low-temperature thermochronology, combined with paleothermometers, constrains the thermal and exhumation history of Devonian strata and relates episodes of cooling to contemporaneous tectonic events occurring along the northeastern North American margin.

Chapter two focuses on the thermal history and exhumation of the Catskill Mountains, New York. A ~1 km age-elevation profile of samples collected from Catskill delta wedge units of Slide Mountain were analyzed with apatite fission-track thermochronology and apatite (U-Th)/He dating. The Catskill Mountains formed via exhumation and erosion of the Appalachian Plateau. The slope of the AFT age-elevation profile constrains an apparent exhumation rate of ~50 m/Myr in the Early Cretaceous. Multi-kinetic inverse thermal models reveal "rapid" cooling episodes from the Early Jurassic to the late Early Cretaceous and from the Mid-Miocene to recent. As documented in the Northern Appalachian Basin, these episodes of rapid cooling in the

Catskills are separated by a period where samples experienced stabilization and much slower cooling for ~100 Myr. This chapter discusses the debate surrounding the resolution and existence of a Miocene cooling event along eastern North America, which because of its low magnitude makes it challenging to document with low-temperature thermochronology. Miocene cooling constrained in modeling of the Catskills age-elevation profile samples is compared to previous low-temperature thermochronology studies that either rejected or confirmed this cooling. Studies rejecting Miocene cooling used mono-kinetic annealing algorithms in early generation AFT modeling programs, which often produced a spurious late-stage rapid cooling event. However, other low-temperature thermochronology and geomorphological studies in the central and southern Appalachians and a rapid Miocene increase offshore sedimentation rates suggest exhumation and erosion of Appalachian strata was necessary in the Miocene.

Chapter three collates low-temperature thermochronology data and thermal histories from 26 studies utilizing apatite fission-track thermochronology and/or apatite (U-Th)/He dating within the Appalachian physiographic provinces (the Appalachian low-temperature thermochronology database). While there is an abundance of thermochronology data from many studies scattered over the eastern U.S., an orogen-scale synthesis of the low-temperature thermal and exhumation history has not been undertaken. The objective is to determine temporal and spatial trends in the post-orogenic thermal histories, through identifying events which occurred throughout the Appalachian provinces, as well as province-specific events. Challenges exist in interpreting the thermal history trends given that the studies range in publication from the 1980's to present day and hence vary in style of analysis and objectives, contain synthesis of results from different methods, and utilize different data interpretation and modeling approaches with several generations of modeling programs. Many of the low-temperature thermochronology

studies undertaken along the eastern U.S. lie within present day catchments that drain into Mid-Atlantic offshore basins. We examine the onshore record and conclude episodes of rapid cooling and exhumation documented within these catchments correlate well with periods of increased sediment flux into offshore Mid-Atlantic basins. Synthesizing the temporal correlation between onshore exhumation and offshore sediment flux and the provinces' thermal histories, the post-orogenic low-temperature thermal history across the eastern U.S. passive margin is divided into three extended periods of cooling and exhumation. These periods are related to regional effects of Early Mesozoic continental rifting and post-rift crustal extension, Late Mesozoic variable cooling due to the development of the passive margin and to exogenic mechanisms, and Late Cenozoic (i.e. Miocene) rapid cooling related to the establishment of dynamic topography and drainage reorganization.

POST-OROGENIC THERMAL HISTORY AND EXHUMATION OF THE NORTHERN APPALACHIAN BASIN: LOW-TEMPERATURE THERMOCHRONOLOGIC CONSTRAINTS

by

Chilisa M. Shorten

B.S., University of Pittsburgh, 2010

Dissertation
Submitted in partial fulfillment of the requirements for the degree of
Doctor of Philosophy in Earth Sciences.

Syracuse University
August 2018

Acknowledgments

Table of Contents

List of Illustrative Materials

Chapter One

Post-Orogenic Thermal History and Exhumation of the Northern Appalachian Basin: Low-Temperature Thermochronologic Constraints

Abstract

The Appalachian Foreland Basin extends from New York to Alabama in the eastern United States and contains sediment derived from the Appalachian Orogen. The post-orogenic thermal history and exhumation of the Northern Appalachian Basin in New York and Pennsylvania is constrained with apatite fission-track (AFT) thermochronology and (U-Th)/He dating, also incorporating other paleothermometers and geologic constraints. Thirty-eight samples were collected across twelve formations from the Devonian-aged Catskill delta wedge, which is positioned stratigraphically above the hydrocarbon-rich Marcellus Shale. AFT ages range from ca.185-120 Ma, with a younging trend from west to east. Mean track lengths range from 10.6 to 13 µm, with unimodal, slightly negatively skewed distributions. Except for samples from the westernmost region, all samples reached temperatures higher than the retentivity of fission-tracks in apatite (i.e. >~110-120 °C). Inverse thermal models constrain a multi-stage post-orogenic evolution: (1) Late Triassic to Early Jurassic onset of cooling from maximum temperatures. Cooling at rates of ~1-2°C/Myr is likely due to erosion of the orogenic overburden, contemporaneous with extension and rifting along the eastern United States. Paleothermometers and AFT age trends indicate that eastern samples reached higher maximum temperatures and experienced greater erosion than western and central samples. (2) From the Early Cretaceous to the Late Cenozoic, cooling rates slow significantly as the basin stabilizes after the removal of most of the orogenic overburden and the transition to a passive margin. Western and west-central samples cooled more slowly (<0.5 °C/Myr) with longer residence times within the partial annealing zone than eastern samples (cooling rates <~1 °C/Myr). (3) Inverse models of western and central samples, including a drill core sample, indicate the onset of more rapid cooling (~1-2 °C/Myr) in the Late Cenozoic, continuing to present. This Late Cenozoic event is highly debated

but thermochronology results from this study indicate it is real and significant and most likely associated with landscape rejuvenation in Miocene to recent times. Low-temperature thermochronology, combined with paleothermometers, constrains the thermal history of Devonian strata, exhumation rates, and contemporaneous tectonic events occurring along the Eastern U.S. margin.

Introduction

Low-temperature thermochronology, paleothermometers and geologic constraints provide a valuable integrative approach to constrain upper crustal thermal histories (e.g. Naeser et al., 1989). Paleothermometers such as vitrinite reflectance (e.g. Zhang & Davis, 1993; Weary et al., 2000), fluid inclusion microthermometry and overpressure history (e.g. Wojcik et al., 1994; Lash & Blood, 2007; Wilkins et al., 2014) or a combination of those methods (e.g. Tobin & Claxton, 2000; Reed et al., 2005) are traditionally used to constrain thermal maximums and burial histories of sedimentary basins. Apatite fission-track (AFT) thermochronology applied to sedimentary basin strata can constrain maximum temperatures (T_{max}) up to ~100-120 °C, as well as assess the timing and rates of cooling (e.g. Gleadow et al., 1983; Bray et al., 1992; Green et al., 1995; Green & Duddy, 2012). AFT is also well-suited for characterizing potential hydrocarbon generation zones due to the overlap between the partial annealing zone (PAZ) temperature range and temperatures of initial source rock maturity (Figure 1). For sedimentary basins, combining thermochronology and paleotemperature methods, is often used to establish T_{max}, thermal cooling rates, exhumation histories, and provide insight into hydrocarbon source rock maturation levels (e.g. Green et al., 1989; Gallagher et al., 1998; Green & Duddy, 2012; Ketcham, 2012).

This study utilizes low-temperature AFT thermochronology, combined with apatite (U-Th)/He (AHe) dating and maximum paleotemperature indicators (i.e. vitrinite reflectance and conodont alteration indices), to constrain the thermal and exhumation history of the Northern Appalachian Foreland Basin (NAB), in the states of Pennsylvania (PA) and New York (NY; Figure 2). Previous work, which used AFT analysis to constrain the thermal history of the NAB in NY (Miller and Duddy, 1989), and this study observe similar AFT age trends but different thermal histories. Without inverse thermal modeling, Miller and Duddy (1989) schematically determined a thermal history based on spatial trends of AFT ages and the relationships between AFT age, mean track length and standard deviations (i.e. "boomerang plots", Figure 3 & 6 of Miller & Duddy, 1989). They hypothesized that all samples across the basin were exhumed to the near present surface within the Early Cretaceous (ca.120-140 Ma). In this paper precise measurements of confined fission track lengths and composition proxies are input into inverse thermal modeling, utilizing a multi-kinetic annealing algorithm (e.g. Ketcham et al., 2007), an approach not typically undertaken until the 1990's. With these advances, this study builds on previous work while revealing a more complex, multi-stage cooling history.

Geologic Setting

The formation of the Appalachian Mountains of eastern North America and the adjacent foreland basin is a result of the Taconic, Acadian and Alleghanian orogenies in the Paleozoic (e.g. Hatcher, 2010). Tectonic deformation and loading close to the orogenic front controlled the extent and shape of the basin, generating an asymmetrical accommodation space (Figure 3; e.g. Beaumont et al., 1987; Ver Straeten, 2010). The Devonian sedimentary units preserved in the NAB, referred to as the Catskill delta wedge, were deposited during the Acadian Orogeny in a series of westward-migrating depositional episodes (Faill, 1985; Ver Straeten, 2010). The

provenance of the Catskill delta wedge includes mainly sedimentary and low-grade metamorphic rocks from predominantly Acadian sources with lesser contributions of sediment from Taconic- (~30%) and Grenville-age (~5%) sources (Ver Straeten, 2009).

The total preserved Paleozoic sedimentary section in the NAB is estimated at 6-8 km thick in the west and 10-16 km thick in the east (Lindberg, 1985; Ver Straeten, 2010) as shown in a diagrammatic cross section (Figure 3). Paleocurrent analyses indicate detritus was carried westward from the mountains formed during the Acadian orogeny, resulting in a general fining of the grain-size from east to west (Faill, 1985; Ver Straeten, 2010). Basin units dip gently ~1-2° to the southwest, due to post-depositional tectonics associated with basin inversion and/or regional uplift (e.g. Johnsson, 1986; Isachsen et al., 1991; Eaton & Frederiksen, 2007). Thus, outcropping units are stratigraphically younger to the south.

A significant amount of sediment was deposited on top of the Catskill delta wedge during the Acadian and Alleghanian Orogenies and is reflected in maximum burial depths from T_{max} indicators (e.g. Johnsson, 1986; Levine, 1986; Beaumont et al., 1987; Reed et al., 2005; Lash & Blood, 2007). Estimates of the amount of sediment (i.e. "overburden") which has been removed from above the Catskill wedge range from ~2-4 km (Johnsson, 1986; Faill, 1998), with some estimates as high as 7 km (Friedman, 1987). The duration of T_{max} due to burial and the timing of temperatures within the hydrocarbon generation window is more elusive, since common indicators such as vitrinite reflectance and conodont alteration indices only constrain T_{max} and are dependent on heating rate and residence time (e.g. Green & Duddy, 2012). In the Late Triassic (ca. 237 Ma), after syn- and post-Alleghenian deposition westward into the NAB, Pangea began to break apart and a passive margin developed along the eastern North American continent (Withjack et al., 1998; Withjack & Schlische, 2005). As the Atlantic Ocean expanded,

drainage patterns shifted, and sediment was transported eastward across much of the NAB (Judson, 1975).

Methods

Sampling Strategy

Devonian sandstones from the Catskill delta wedge were collected in a broad swath along the NY-PA border (Figure 2). Samples were collected from Devonian Catskill delta wedge units, including several depositional groups (i.e. Conewango, Conneaut, Canadaway, West Falls and Hamilton) and 12 different formations (see supplementary file A). Sample locations were influenced by the availability of suitable sedimentary outcrops (i.e. medium sandstone or coarser, as immature as possible). Suitable outcrops are less abundant in the west, as this region was distal from the source region lying to the east (Figure 3). Fifty-four outcrop samples were collected and eight core samples were obtained from the PA Department of Conservation and Natural Resources Topographic and Geologic Survey. Thirty-seven outcrop samples and one core sample yielded sufficient apatite fractions for AFT analysis using conventional heavy liquid and magnetic separation techniques (Table 1).

Analytical Techniques

Apatite Fission-track Thermochronology is commonly applied to constrain the thermal and exhumation history within the upper ~4-5 km of the Earth's crust (e.g. Gallagher et al., 1998). This technique is a powerful tool for basin analysis (e.g. Gleadow et al., 1983; Naeser et al., 1989; Bray et al., 1992; Green et al., 1995; Green & Duddy, 2012), notably due to the kinetic parameter provided by measuring confined track lengths. Fission-track thermochronology is based on measuring the density and length distribution of fission tracks formed in a crystal as a result of the spontaneous fission of ^{238}U. In the external detector method, the density of tracks in

the apatite grain is determined along with the density of induced [235]U tracks for the same area within a mica external detector (e.g. Hurford & Green, 1983). This, in conjunction with the density of induced tracks in a mica over a standard glass of known [U], allows an age determination for each grain (e.g. Green et al., 1989). The length of a fission track is proportional to the maximum temperature experienced and thus the confined track length distribution (CTLD) within a sample can be used to constrain the thermal history of the sample (e.g. Gleadow et al., 1986; Green et al., 1986; Ketcham et al., 1999). A narrow distribution of long tracks indicates rapid cooling of the sample while a broad distribution of shorter and longer tracks indicates partial annealing and/or a more complex thermal history (e.g. Gleadow et al., 1986). AFT low-temperature thermochronology was undertaken at Syracuse University following standard procedures summarized in Table 1 as summarized in Riccio et al. (2014).

For samples with similar compositions to the Durango apatite standard, the AFT system has a closure temperature of 120 °C for cooling rates of ~10 °C/Myr (Gleadow & Duddy, 1981) over long-term durations of 10^8 years (Naeser, 1981). At temperatures higher than 120 °C all fission tracks are typically completely annealed, between ~110-60 °C fission track length is reduced in the partial annealing zone (PAZ), and at temperatures lower than 60 °C most tracks are retained (e.g. Gleadow & Duddy, 1981; Gleadow et al., 1986; Gleadow & Fitzgerald, 1987; Laslett et al., 1987; Gallagher et al., 1998). Closure temperature varies with chemical composition (~120-100 °C; Green et al., 1986; Barbarand et al., 2003) and D_{par}, the diameter of etch pits parallel to the c-axis, is a simple and efficient measurement of an apatite's resistance to annealing (e.g. Burtner et al., 1994; Carlson et al., 1999, Donelick et al., 1999; Ketcham et al., 1999; Donelick et al., 2005). D_{par} was measured on each apatite grain used for AFT analysis.

grains which are more resistant to annealing than standard fluoroapatites (e.g. Donelick et al.,

2005) and the base of the PAZ is extended to ~120 °C for those samples.

(U-Th)/He Dating is a low-temperature thermochronometric method that is used to calculate

an age from the concentrations of the daughter product (^{4}He) and the parent isotopes (^{238}U, ^{235}U,

^{232}Th, and ^{147}Sm). Retention of the daughter product depends on the temperatures experienced

and He diffusivity of the mineral (e.g. Zeitler et al., 1987; Farley, 2002; Harrison & Zeitler,

2005). The closure temperature for the AHe dating method is ~65-70 °C and the partial retention

zone (PRZ), the temperature range over which radiogenic He is partially lost due to diffusion out

of the crystal, is typically ~30-90 °C (e.g. Flowers et al., 2009). Single-grain ages can vary

considerably as a result of a number of factors including the presence of [U]-rich inclusions,

effective uranium (i.e. [eU], a parameter that weights the decay of the parent isotopes, calculated

as [U] + 0.235 × [Th]), grain size and/or zonation, plus cooling rate and residence time in the

PRZ which tends to magnify any single-grain age variation (e.g. Wolf et al., 1996; 1998; Reiners

& Farley, 2001; Farley, 2002; Meesters & Dunai, 2002; Fitzgerald et al., 2006; Flowers et al.,

2009). The variation of single-grain ages, the cause of this dispersion, the significance, and how

to interpret the data has been a topic of continued discussion for >10 years (e.g. Fitzgerald et al.

2006; Flowers & Kelley, 2011; Brown et al., 2013; Wildman et al., 2016; Green & Duddy,

2018).

Two of the ten samples screened for apatite quality (i.e. crystal size, shape, and inclusion

presence) yielded suitable grains for AHe dating (Table 2). Five grains were analyzed per sample

to reveal possible single-grain age dispersion, common in AHe dating, especially in detrital

samples (e.g. House et al., 1999; Armstrong, 2005). In this study, as reference, mean AHe ages

are reported with 1 σ error and variation of the single-grain ages from the mean age. Similar to

other low-temperature techniques, ages do not necessarily correlate to specific geological events. AHe analyses were performed by the University of Colorado, Boulder, Thermochronology Research and Instrumentation Lab (CU TRaIL) and the methods, summarized in Table 2, are detailed in Weisberg et al. (2018).

Maximum Paleotemperature Indicators included in this study are published vitrinite reflectance ($\%R_o$) values and measured conodont alteration index (CAI) values (Table 1). The percentage of light reflected off vitrinite, an organic substance naturally occurring in rocks, is a proxy for thermal maturity primarily controlled by temperature and time (Burnham & Sweeny, 1990). Published maps of $\%R_o$ values from Devonian shale drill core and cuttings samples (East et al., 2012; Ryder et al., 2013) were used to estimate $\%R_o$ values for this study's samples. Values for individual samples were estimated based on their proximity to $\%R_o$ isograds or, if they were within <15 km of a drill core location, values were estimated directly from measured values (Table 1). $\%R_o$ values were used to estimate maximum paleotemperatures experienced by this study's samples using the Easy$\%R_o$ model (Burnham & Sweeny, 1990). Given that the Devonian shales measured by East et al. (2012) and Ryder et al. (2013) are stratigraphically below this study's samples (Figure 3), $\%R_o$ values were interpreted as an absolute maximum bound for potential T_{max} experienced by this study's samples.

Conodont alteration index (CAI) values were measured on the four samples which contained conodonts in their >200 µm apatite separates (Table 1). Conodonts are an index microfossil (0.1-1 mm in size) found in Cambrian to Triassic aged marine rocks (Epstein et al., 1977). During burial and resultant temperature increase, conodonts irreversibly change color from pale yellow (unaltered) to dark brown then black (Epstein et al., 1977). CAI is the systematic measurement of the color of the basal portion of the conodonts, which is a proxy for maximum temperature

experienced. Variation in color within a sample may be due to the dimensions or maturity of the individual pieces, as larger, thicker, and/or adult elements are darker in color (Epstein et al., 1977; Repetski et al., 2008). CAI determines a range of T_{max} possible for durations between 1-500 Myr (Figure 1), however the low end of the range is commonly used to estimate T_{max} of the sample since the higher end of the range indicates extreme conditions (Epstein et al., 1977). Conodonts were examined under binocular microscope using unfiltered reflected light and matched to Munsell soil color chips to determine CAI values, following the procedures of Epstein et al. (1977).

Inverse Thermal Modeling

Inverse thermal modeling was undertaken using the modeling program HeFTy (Ketcham, 2005). HeFTy uses a Monte Carlo approach to evaluate the time-temperature (T-t) space by modeling many mutually independent trials. Modeled thermal histories are compared to measured data and evaluated using "goodness of fit" tests, specifically equations 31-34 in Ketcham (2005) for age and the Kolmogorov-Smirnov (K-S) test for CTLD. Both tests determine the probability of a modeled T-t path to recreate the data (age or CTLD) and are weighted equally in a combined merit function, which evaluates if a T-t path is supported by the data (good fit at a significance level of 0.5) or is not ruled out by the data (acceptable fit at a significance level of 0.05; Ketcham, 2005).

AFT thermochronology data (i.e. AFT single-grain ages, confined track lengths, their angle to the c-axis, and D_{par} for each grain used in determining age or measuring track lengths; Table 1) were the primary inputs into inverse thermal models (Ketcham, 2005). Models were run using c-axis projection which has been demonstrated to fix user bias (Ketcham et al., 2007). The Ketcham et al. (2007) multi-kinetic annealing algorithm was used. As proposed by Sobel and

Seward (2010), I applied a user specific calibration factor (0.96) to this study's D_{par} measurements to convert measurements to an equivalent D_{par} value measured by Raymond A. Donelick (reported in Carlson et al., 1999). Calibration of D_{par} is recommended in the HeFTy manual (Donelick et al., 2005; Ketcham, 2005) and accounts for the influence of etching conditions and user error on measuring apatite fission-track etch pit diameter (Sobel & Seward, 2010). In modeling, the calibration affects the kinetic behavior estimate of the grains, but there is very little difference between calibrated and uncalibrated models.

AHe data included in modeling used the radiation damage accumulation and annealing model RDAAM (Flowers et al., 2009) and the alpha ejection correction for age (Farley et al., 1996). AHe data provides a lower temperature constraint to inverse models. Fixed constraints were specified for the stratigraphic (depositional) age range with paleo-mean annual temperature (MAT) ($25 \pm 10\ °C$; Woodrow et al., 1973) and present-day MAT ($5 \pm 5\ °C$; Hijmans et al., 2005). Post-depositional time-temperature constraint boxes are broad, which allows the model paths full latitude to explore T-t space (see supplementary file B1). $\%R_o$ values, estimated from published isograd maps (East et al., 2012; Ryder et al., 2013), were included in models using the Easy$\%R_o$ method of Sweeney and Burnham (1990). In models, $\%R_o$ values were calculated in passive mode, which allows AFT data full latitude to constrain thermal histories with $\%R_o$ values functioning as a confirmation point (Ketcham, 2005).

Results

AFT Data

AFT ages from 37 outcrop samples, and 1 core sample, range from 115 ± 6 Ma to 185 ± 11 Ma ($\pm 1\sigma$) (Table 1, Figure 2). Mean track lengths vary from 10.6 to 13.2 µm (Table 1). CTLDs have a weak negative skewness, which indicates that the NAB experienced a protracted cooling

history (e.g. Corrigan et al., 1998). Twenty-one samples pass the chi-square probability test (χ^2) while 17 samples fail. The χ^2 test determines the probability that the grains are from a single age population given the single-grain age variation (e.g., Galbraith and Laslett, 1993). Since these samples are sandstones, with grains likely sourced from multiple provenances that have experienced long-term residence within the PAZ, magnification of single-grain age dispersion between multiple kinetic populations is to be expected. Samples were examined for D_{par} variation and RadialPlotter (Vermeesch, 2008) was used to determine multiple kinetic populations, which were input as guides for inverse thermal modeling (see supplementary file C).

AHe Data

The central region contained two samples (3P and 43P) which yielded apatites of sufficient size (radius > 60 µm) for (U-Th)/He dating (e.g. Flowers et al., 2009). There was significant variation of AHe single-grain ages (~16-17%) with single-grain ages ranging from 188 to 116 Ma (Table 2). Including outliers, mean ages of 154 and 134 Ma were calculated for 3P and 43P respectively using the methods of Ault et al. (2013). Most of the AHe single-grain ages from samples 3P and 43P are younger than the sample's AFT central age but there are older ages, especially for sample 3P. Single-grain age variation is likely due to residence time within the PRZ which magnifies age differences due to varying [eU], zonation and/or grain size (e.g. Reiners & Farley, 2001; Meesters & Dunai, 2002; Fitzgerald et al., 2006). Age variation may also be affected by the poor quality of the detrital apatites (Ehlers & Farley, 2003). Grains analyzed were sub-rounded with surface pits and striations indicative of transportation, and as such were difficult to evaluate for the presence of inclusions.

AHe single-grain ages plotted against [eU] and grain size display weak or no trends (see supplementary file D). Thus it is not recommended to use AHe as the only data to constrain the thermal history (e.g. Green and Duddy, 2018). F_T measures of the amount of He ejected from the crystal with lower values (i.e. <0.65) indicating greater loss (e.g. Farley et al., 1996; Ketcham et al., 2011). Grain sizes are small (33-61 µm), which means the alpha ejection correction (F_T) values are low and hence the correction of a raw age for alpha-particle ejection is high (up to ~60-70%), with larger non-analytical uncertainties. These non-analytical uncertainties can affect the thermal history and its precision (e.g. Ketcham et al., 2011). AHe single-grain ages are shown overlain along inverse thermal model output as reference points in Figure 5. Where appropriate, AHe data was used as another constraint in HeFTy inverse thermal models, in all cases, providing verification of AFT constrained thermal histories.

Regional Trends

There is a younging trend of AFT ages from west to east across the NAB (Figure 4). Samples were divided into the same three regions as did Miller and Duddy (1989). The oldest AFT ages (>160 Ma) generally lie in the western region (west of 78 °W) and the youngest ages (<140 Ma) occur in the eastern region (east of 75.5 °W; Figure 2 & 3). The central region contains the greatest range of AFT ages (115-159 Ma), a core sample (28Pc), and two samples with AHe data (3P and 43P). Depositional age of samples ranges from Early Devonian to Early Mississippian which may cause some variation between samples' AFT ages (Table 1). Published %R$_o$ and measured CAI data also indicate a trend of increasing maximum paleotemperatures from west to east, ~100 °C to >200 °C (Repetski et al., 2008; East et al., 2012; Ryder et al., 2013).

Western Region: Sampled lithologies (sandstones) in the western region are finer-grained than those preserved closer to the orogenic front in the east. AFT ages from 8 samples yield ages

from 185 ± 11 to 146 ± 8 Ma (Table 1). Four samples fail the χ^2 test, while single-grain age variance ranges from 0-37%. Mean track lengths are 11.9 to 12.5 µm with standard deviations of 1.3 to 1.9 µm (Table 1). Several samples retain single AFT grain ages between ca. 385-250 Ma, which are older than the depositional age (383-359 Ma), indicating that the samples were not fully reset after deposition and burial temperatures did not exceed ~120 °C. Three samples in this region contained conodonts that yielded CAI values between 2-2.5, which agree with published values (Repetski et al., 2008; Weary et al., 2000). Vitrinite reflectance (VR) isograds range from 0.6-1.5 %R_o (East et al., 2012; Ryder et al., 2013).

Central Region: AFT ages range from 159 ± 10 to 118 ± 6 Ma for the 22 outcrop samples (Table 1). The core sample (28Pc at 1048-1051 m depth) is the youngest at 115 ± 7 Ma, which is expected since it is stratigraphically below the central region outcrop samples and passed through the PAZ more recently. The outcrop sample closest to the core (55P) has an AFT age of 150 ± 8 Ma. Ten samples fail the χ^2 test, while single-grain age variance ranges from 0-29%. This region contains the largest AFT age range and variability, possibly because it incorporates more samples and/or that samples are from a greater number of depositional groups/formations. Mean track lengths range from 10.9 to 13.2 µm with standard deviations of 1.5 to 2.5 µm (Table 1). Sample 35N contains conodonts that yielded a range of CAI values between 2.5-3 and VR isograds range from 0.77-3 %R_o (Table 1). As discussed above, sample 3P and 43P yielded mean AHe ages of 154 and 134 Ma respectively with ~16-17% variation of AHe single-grain ages (Table 2).

Eastern Region: Seven samples yielded AFT ages ranging from 141 ± 7 to 120 ± 9 Ma (Table 1). Three samples fail the χ^2 test, while single-grain age variation ranges from 9-27%. Mean track lengths vary from 12.7 to 13.1 µm with standard deviations of 1.3 to 1.6 µm. VR

isograds range from 2.45-3 %R_o (Table 1) and no samples contained conodonts. Given %R_o values estimate temperatures between ~215-230 °C (using Easy%R_o model; Sweeny & Burnham, 1990), AFT ages likely represent cooling from temperatures greater than the base of the PAZ.

Thermal History Interpretation

The initial part of the samples' thermal histories, representing Taconic and Acadian uplift/erosion, is unconstrained by AFT and AHe data. The complete thermal history is included in model output to provide geologic context and to prevent introduction of bias, such as operator-imposed T-t constraints. Due to the geologic history of the samples, all models were started between 500 to 375 Ma at temperatures >140 °C (e.g. Ver Straeten, 2009). In Figure 5, the parts of the model that are not directly constrained have been made semi-opaque (i.e. temperatures higher than the base of the PAZ and times before the oldest modeled track).

AFT ages are relatively "old" (Jurassic to Cretaceous) and have experienced a protracted history with significant time spent in the PAZ. Thus, only significant cooling events are distinguishable. Cooling rates constrained in the thermal models, and throughout the Appalachian Basin (e.g. Blackmer et al., 1994; Boettcher & Milliken, 1994; Reed et al., 2005), are slow (<2.75 °C/Myr) in comparison to other tectonic settings, such as young, active collisional orogens (~40-50 °C/Myr; e.g. Thiede et al., 2004). In this study, Early Jurassic cooling and Late Cenozoic cooling is referred to as "rapid" in comparison to the Cretaceous period of slower cooling.

Six representative inverse thermal models are presented which demonstrate the T-t history trends while also capturing variability within, and between the regions (Figure 5). From the central region the core sample (28Pc) and near-by surface sample (55P) are also included, as they

add a vertical element to the data. However, trends are based on the models from all included

samples (HeFTy output for all samples is included in supplementary file B2). Across the NAB,

inverse models exhibit multi-stage post-orogenic cooling patterns with similar timing of events:

(1) Onset of cooling from maximum temperatures began in the Late Triassic to Early Jurassic;

(2) Cooling rates slow significantly in the western and west-central NAB from the Early

Cretaceous to Late Cenozoic while the eastern and east-central NAB cooling rates only slow

slightly within the Cenozoic; (3) Western and west-central models suggest a rapid cooling event

initiated in Late Cenozoic times. In context with these events, the differences across the NAB

(i.e. T_{max}, rate of cooling, and resolution of a Late Cenozoic rapid cooling event) are discussed

below.

(1) Early Jurassic to Cretaceous Cooling: Thermal models from sample results across the

NAB indicate initial cooling rates of 1-2 °C/Myr, from the Late Triassic to Early Jurassic (Figure

5). Faster initial cooling is recorded in eastern samples. For example, the weighted mean path of

3P (east-central) indicates a cooling rate of ~1.7 °C/Myr while 51N (western) cooling rate is

~0.9 °C/Myr. That the oldest modeled track in the western most sample (51N) is 256 Ma and a

0.6 %R_o value (Table 1) suggests the sample did not exceed ~125 °C. Thus, this sample has

fission tracks that formed prior to T_{max} and the timing of T_{max} is constrained to ca. 187 Ma. Most

of the samples reached temperatures greater than the PAZ, annealing all pre-existing tracks.

In the central region, samples 3P and 43P AHe ages were incorporated as inputs for inverse

thermal modeling (Figure 5). These models constrain cooling to ~70 °C by the end of the Early

Cretaceous, placing samples within the upper part (lower temperatures) of the PAZ and the lower

part (higher temperatures) of the PRZ. Models that do not utilize AHe ages (because there were

none for those samples) also constrain that samples were at temperatures lower than 90 °C by the end of the Early Cretaceous.

(2) Cretaceous to Late Cenozoic Stabilization: Thermal histories from western and central samples constrain that initial rapid cooling was followed by extended residence time in the PAZ and slow cooling (~0.15-0.25 °C/Myr) during the Cretaceous to Late Cenozoic (i.e. "stabilization period"). In the east and east-central region, the best-fit T-t paths for samples 3P and P12 constrain periods of slower cooling during the Cretaceous, at rates of ~0.13 °C/Myr and ~0.20 °C/Myr respectively. However, overall the thermal histories of the eastern and east-central samples suggest only slightly reduced cooling, at average rates of ~0.8 °C/Myr beginning in Cretaceous times to present. AHe single-grain ages for sample 43P lie within the modeled T-t envelopes during this period of slow cooling while AHe ages from sample 3P do not (Figure 5). Based on these results, the interpretation is that eastern samples spent less time resident in the PAZ than western and central samples.

(3) Late Cenozoic Cooling: Models from western and central samples show an increase in cooling rates to ~1-2 °C/Myr from the Late Cenozoic to present (Figure 5). The core sample (28Pc) constrains the onset of Late Cenozoic cooling in the Miocene (ca. 23 Ma), with the model paths cooling from within the PAZ. Inverse thermal models from the east-central (3P) and eastern samples (P12) do not clearly reveal the Late Cenozoic "rapid" cooling event. This can be explained as follows: As eastern samples cooled more rapidly through the PAZ, the proportion of tracks that were shortened by residence within the PAZ is not significant, and this relative lack of shorter tracks from the stabilization period means that inverse modeling does not detect this Late Cenozoic accelerated cooling. Therefore, although multi-stage cooling may have occurred, the eastern models cannot resolve between initial stabilization and the later rapid cooling.

Given the importance of identifying Late Cenozoic cooling, CTLD of western and central samples were measured multiple times to verify data. Note that modeling using early apatite mono-kinetic annealing algorithms (e.g. Laslett et al., 1987; Crowley et al., 1991) often produced a spurious late stage cooling event (e.g. De Bruijne & Andriessen, 2002). Early algorithms were based on annealing experiments on Durango apatite and this these models ran on the assumption that all apatite's had the same annealing characteristics as Durango. However, annealing is variable, depending on the composition of the apatite. Thus, multi-kinetic models used since ca. 1999 measure kinetic parameters for each grain (e.g. Ketcham et al. 1999; Ketcham et al., 2007). This later generation models do not produce an apparent late-stage cooling artifact. In other words, the Late Cenozoic initiation of rapid cooling in these western and central samples is regarded as significant and real.

Discussion

AFT Age Trends

A younging trend in AFT ages from west to east is clearly documented in this study (Figure 4). Miller and Duddy's (1989) data also shows this trend in the NAB but contains more scatter due to greater N-S distribution of their sampling and the inclusion of more northerly samples from older stratigraphic units that yielded older AFT ages (Figure 4). Blackmer et al. (1994) noticed AFT ages are generally older in the NAB in western PA than eastern PA but determined that the intervening ages did not define an eastward decreasing trend. Roden & Miller (1989) identify tectonic provinces with different thermal regimes but state that their AFT ages do not exhibit a clear trend of eastward younging across the basin in Pennsylvania.

The pattern of younging AFT ages from west to east across the NAB may reflect either diachronous onset of exhumation across the NAB or differential amounts of burial. Most studies

that present maximum temperatures, burial curves and/or regional thermal history trends in the Appalachian region conclude that the primary control on trends in thermal proxies is the varying magnitude of burial across the foreland basin (e.g. Friedman & Sanders, 1982; Gerlach & Cercone, 1993; Lakatos & Miller, 1983; Blackmer et al., 1994; Johnsson, 1986; Gurney & Friedman, 1986; Miller & Duddy, 1989; Roden & Miller, 1989). Data from this study also supports this interpretation. AFT samples in the east are younger since they reached greater temperatures due to greater burial (documented with $\%R_o$ and CAI values; e.g. East et al., 2012; Ryder et al., 2013), and thus cooled through the base of the PAZ more recently than shallower western samples, some of which have not exceeded temperatures at the base of the PAZ.

Paleogeothermal Gradient in the NAB

To convert cooling rates to exhumation rates in the NAB, a paleogeothermal gradient must be assumed. This can be estimated based on reasonable geologic assumptions for similar situations (i.e. 20-30 °C/km is common for sedimentary basins), through independent means, or from modeling programs that provide thermal gradients as an output. Several low-temperature thermochronology studies in the Appalachian Basin and New England assumed a steady state paleogeothermal gradient between 25-30 °C/km throughout the thermal history considered (e.g. Roden & Miller, 1989; Roden, 1991; Roden-Tice & Tice, 2005; Lash & Blood, 2007; Roden-Tice et al., 2009). However, other studies utilizing heat flow models, T_{max}, and/or subsidence histories have estimated an elevated paleogeothermal gradient of ~30-45 °C/km during and directly after the Alleghanian Orogeny (Vitorello & Pollack, 1980; Chyi et al., 1987; Weary et al., 2000), with some estimates as high as 50 °C/km (Hulver, 1997).

Studies based on the presence of authigenic clay minerals (Daniels et al., 1990), coal rank patterns (Hower and Gayer, 2002), heat-flow calculations based on fluid-inclusions (Harrison et

al., 2004), and %R_o trends (Ruppert et al., 2010) determined that an elevated paleogeothermal gradient during the Alleghanian Orogeny was produced as overthrust terranes forced migration of hot fluids through the newly formed basin sedimentary package. An increased geothermal gradient (~35 °C/km) due to regional fluid flow would not continue long after the end of the Alleghanian Orogeny, as it requires thrusting to force fluid migration, and estimated rates of hot fluid flow are high and short-lived (Oliver, 1986; Dorobek, 1989). There is significant evidence to indicate that the geothermal gradient has varied over time in the Appalachian Basin (e.g. Weary et al., 2000; Ruppert et al., 2010) but has decreased to average estimates (~20-30 °C/km) since the Alleghanian Orogeny (e.g. Reed et al., 2005). AFT data and thermal models in this study do not constrain the part of the thermal history that may have experienced an elevated geothermal gradient (i.e. the Alleghenian Orogeny until the Late Permian) since samples were still being buried and had not reached T_{max}, which reset most samples.

It is evident, given the overall slow cooling rates documented in this study, that the samples experienced a relatively stable, post-orogenic thermal regime without much advection or significant changes in the paleogeothermal gradient, such as may be caused by rapid cooling due to fault movement (e.g. Ehlers & Farley, 2003). Small, local kimberlite intrusions (ca. 146-110 Ma; Heaman & Kjarsgaard, 2000; Bailey & Lupulescu, 2015) occur in the central region of the NAB in NY, but there is no evidence that they have regionally influenced the paleogeothermal gradient (e.g. Johnsson, 1986), such as would be caused by a large magmatic intrusion (e.g. Gleadow & Duddy, 1984; Gleadow & Fitzgerald, 1987). Core sample 28Pc was collected from an exploration drill hole with a present-day maximum downhole temperature of ~48 °C at ~2 km depth, indicating a present-day geothermal gradient of 24 °C/km. Also, the offset between the T-t paths for the core sample in the central region and the closest surface sample (55P) is on the

order of ~25 °C during the Cretaceous to Late Cenozoic stabilization (Figure 5). Therefore,

assuming a relatively stable, unperturbed geothermal gradient during the post-orogenic history of

the NAB, cooling rates are converted to exhumation rates using a geothermal gradient of

25 °C/km (Figure 6).

    Post-Orogenic Exhumation

This section discusses the exhumation history, constrained by inverse thermal modeling and

converted to exhumation rates using the assumptions discussed above. The exhumation history is

divided into the same three stages as the cooling history: (1) Early Jurassic to Cretaceous initial

onset of exhumation; (2) Cretaceous to Late Cenozoic stabilization in the west with continuous

and slower exhumation documented in the east; (3) a Late Cenozoic increase in exhumation rates

(Figure 6).

(1) Early Jurassic to Cretaceous Exhumation: All models suggest the onset of exhumation

in the Late Triassic to Early Jurassic with the western sample (51N) constraining onset of

exhumation to the Early Jurassic, ca. 187 Ma (Figure 6). This initial exhumation event continued

until the Early Cretaceous, at rates of 40-50 m/Myr in western samples and slightly higher rates

of 50-70 m/Myr in eastern samples (Figure 5 & 6). The differences in exhumation rates across

the NAB further support the conclusion regarding the west to east younging AFT age trend. That

is, the AFT age trend is due to differential burial, and thus the region experiences differential

amounts/rates of exhumation which was initiated at about the same time across the NAB.

Concurrent with the onset of exhumation, was the rift initiation and the formation of the

Northern Atlantic Ocean in the Late Triassic (ca. 237 Ma; Withjack et al., 1998; Withjack &

Schlische, 2005). This provided accommodation space for sediment eroded from the

Appalachian Highlands and NAB basin. As the eastern U.S. margin underwent rifting and the

lowering of regional base levels, river incision, backwearing and valley widening may have allowed the re-excavation and erosion of the NAB, similar in style to Late Neogene re-excavation of the Ebro Basin, Spain (e.g. Coney et al., 1996; Babault et al., 2006; Beamud et al., 2010). Initial exhumation of the NAB correlates well with rapid unroofing rates estimated by Blackmer et al. (1994) in the western Appalachian basin of Pennsylvania during the Late Permian through the Early Jurassic. They suggested that this event may be due to flexural rebound of the lithosphere related to the erosion of the Alleghenian overburden. The variation in exhumation rates from west to east constrained in this current study further supports this mechanism, as samples were buried more deeply in the east and thus the flexural response was greater, recorded as higher exhumation rates.

The timing of initial exhumation within the NAB (this study) generally agrees with low-temperature thermochronology studies across the Appalachian Basin and New England, which constrain exhumation beginning in the Triassic to Late Jurassic (Roden & Miller, 1989; Roden, 1991; Roden & Miller, 1991; Blackmer et al., 1994; Roden-Tice & Wintsch, 2002; Reed et al., 2005). Other low-temperature thermochronology studies constrain the onset of rapid exhumation in the Early Cretaceous, referring to it as the "Early Cretaceous rapid cooling event" (e.g. Miller & Duddy, 1989; Boettcher & Milliken, 1994; Roden-Tice et al., 2000; Spotila et al., 2004; Roden-Tice & Tice, 2005; Roden-Tice et al., 2009; Taylor & Fitzgerald, 2010; McKeon et al., 2014). However, most of the studies reporting rapid cooling and exhumation onset in the Early Cretaceous are based on samples that reached temperatures greater than the PAZ and, though they document timing of rapid cooling through the PAZ, they do not constrain when cooling was initiated from T_{max}.

(2) Cretaceous to Late Cenozoic Stabilization: From the Cretaceous until the Late Cenozoic, significantly slower rates of exhumation are documented in the NAB (Figure 6). Western and west-central thermal models indicate relatively slow cooling and exhumation at rates of 6-9 m/Myr. These rates are the slowest rates in their post-orogenic exhumation histories, which indicate a period of basin stability. The central model (55P) and corresponding core sample (28Pc) indicate slow exhumation rates of 8-11 m/Myr. However, models within the central region show the greatest variation in exhumation rates during this time (i.e. 3P; Figure 6). Eastern models suggest exhumation at rates of 25-30 m/Myr, which is approximately half the rate of initial exhumation but is still more rapid than western and central samples during this period. Also, the easternmost sample (P12) records a short period (ca. 35 Myr) of slower exhumation (~10 m/Myr) in the Cretaceous (Figure 5). Other studies throughout the Appalachian Basin also document variable exhumation rates similar to these during the Cretaceous to Late Cenozoic (i.e. Blackmer et al., 1994; Reed et al., 2005; McKeon et al., 2014).

During the early Middle Jurassic, the east coast of North America transitioned from an active continental rift zone into a passive continental margin (e.g. Klitgord et al., 1988; Ettensohn, 2008) and flexural rebound due to erosion no longer contributed to exhumation (Blackmer et al., 1994). Most models in the NAB constrain significantly reduced exhumation rates, implying relative stability, during the Cretaceous to Late Cenozoic (Figure 6). Stability during the Late Cretaceous to Late Cenozoic is also observed in models from the Appalachian Basin in PA (Blackmer et al., 1994) and Kentucky (KY; Boettcher & Milliken, 1994). Models for the eastern samples tend to indicate continuous exhumation during this period – albeit slightly slower than initial rates – as this region continued to erode, likely a result of additional flexural rebound. However, the eastern region may have also experienced relative stability but the AFT data (i.e.

relative components of confined tracks) are not sensitive enough to constrain variations in exhumation rate. Western and central region samples are more sensitive to changes in exhumation rates due to slower exhumation rates throughout their post-orogenic history and longer residence in the PAZ, and these changes are discussed below.

(3) Late Cenozoic Exhumation: Beginning in the Late Cenozoic, rapid exhumation is well constrained in models for western and central samples (Figure 5 & 6). As discussed above, this event is real and significant. Since the core sample cooled from within the PAZ, its thermal model best constrains the onset of Late Cenozoic exhumation as Miocene (ca. 23 Ma). Western and west-central samples (i.e. 51N and 43P) record exhumation rates of 40-50 m/Myr and central samples record rates of 50-65 m/Myr, beginning in the Oligocene to Miocene (ca. 30-20 Ma).

The Late Cenozoic history of the Appalachian basin is enigmatic. Several thermochronology studies suggest rapid exhumation in the Cenozoic (i.e. Roden, 1991; Blackmer et al., 1994; Boettcher & Milliken, 1994; Roden-tice & Wintsch, 2002; Reed et al., 2005), but some of these studies used mono-kinetic annealing algorithms which produce spurious late-stage cooling, as discussed above. Also, there are no direct AFT or AHe (i.e. Late Miocene ages) to document rapid cooling at that time (e.g. Spotila et al., 2004; McKeon et al., 2014). Thus, the identification of this Late Cenozoic cooling event in these previously published models should be regarded as suspect until confirmed. However, there are other lines of evidence which support the identification of a Late Cenozoic pulse of rapid exhumation, such as evidence of uplift from knickpoint migration in stream profiles (Miller et al., 2013) or the increase in sediment flux to mid-Atlantic basins during the Miocene (Pazzaglia & Brandon, 1996). Sediment flux is reportedly too rapid to be primarily driven by decreasing sea level or climate change (Poag &

Sevon, 1989) and it has been suggested that it was controlled by uplift and erosion of the Appalachian source terrane (Poag & Sevon, 1989; Pazzaglia & Brandon, 1996).

Studies constraining rapid exhumation within the Miocene (ca. 15 Ma) attribute exhumation as an isostatic flexural response (Pazzaglia & Gardner, 1994; Blackmer et al., 1994) or to landscape rejuvenation caused by dynamic topography (e.g. Pazzaglia & Brandon, 1996; Miller et al., 2013). Isostatic flexure is estimated to produce 35-130 m of rock uplift of the Appalachian terrane (Pazzaglia & Gardner, 1994) and dynamic topography induces long-wavelength, low amplitude uplift of ~100 m over the last 30 Ma (Moucha et al., 2008). This study constrains an increase in exhumation rates (~30-65 m/Myr) across the NAB beginning in the Late Cenozoic (30-20 Ma), which accounts for the removal of ~1 km of sediment since then (Figure 6). Isostatic flexure or dynamic topography alone does not induce enough exhumation to explain the Late Cenozoic exhumation constrained in models from this study. Instead, the documented exhumation is likely due to a complex combination of drivers causing landscape rejuvenation, including dynamic topography (e.g. Pazzaglia & Brandon, 1996; Gallen et al., 2013; Miller et al., 2013), climatic changes causing increased mechanical erosion within the Appalachian Basin (e.g. Poag & Sevon, 1989; Boettcher & Milliken, 1994), and flexural response of the continental crust to sediment deposition offshore (Pazzaglia & Gardner, 1994; Blackmer et al., 1994).

Conclusions

This study constrains the post-orogenic history of the Northern Appalachian Basin, adding insight into the timing and rates of cooling, thermal regimes, and exhumation events. AFT thermochronology, AHe dating, T_{max} indicators, and stratigraphic constraints are integrated to constrain the cooling and exhumation history of the NAB as occurring in 3 stages:

(1) A Late Triassic to Early Jurassic onset of cooling from T_{max} with the first event extending to the Early Cretaceous (1-2 °C/Myr cooling rate; ~40-70 m/Myr exhumation rate). The younging trend of AFT ages from west to east across the NAB is due to differential amounts of burial and subsequent unroofing, which causes the difference in exhumation rates as the lithosphere experiences flexural rebound related to overburden removal. This event is contemporaneous with rifting (Withjack & Schlische, 2005) and includes the "Early Cretaceous" rapid cooling documented by other studies, since most studies document the passage of samples through the base of the PAZ and not onset from T_{max} (e.g. Miller & Duddy, 1989; Roden, 1991; Boettcher & Milliken, 1994; Roden-Tice et al., 2000; Spotila et al., 2004; Roden-Tice & Tice, 2005; Roden-Tice et al., 2009; McKeon et al., 2014).

(2) The Cretaceous to Late Cenozoic event is a period of stabilization within the NAB. Slow cooling and exhumation are documented in the western and central regions of the NAB (0.15-0.25 °C/Myr; ~6-9 m/Myr) while inverse models in the eastern region constrain cooling and exhumation at rates of 0.5-1 °C/Myr and ~25-30 m/Myr, which are slightly slower than initial cooling rates. Although it is undocumented in thermal models, eastern region samples may have experienced relative stability at this time. The slow exhumation experienced in the NAB is related to the stabilization of the interior of the craton, which is contemporaneous with the transition of the east coast of North America to a passive continental margin (e.g. Klitgord et al., 1988; Ettensohn, 2008).

(3) Rapid exhumation is documented from the Late Cenozoic (30-25 Ma) to present (1-2 °C/Myr; ~30-65 m/Myr) and accounts for the removal of ~1 km of sediment. This event was not constrained in all samples across the NAB, likely due to the relative sensitivity of the AFT and AHe systems. The cause of increased exhumation during this time is highly debated and

often beyond the resolution of low-temperature thermochronology datasets, especially those techniques that lack a kinetic parameter (e.g. McKeon et al., 2014). However, there is other evidence, such as sediment flux to mid-Atlantic basins and knickpoint migration in stream profiles, which indicates that there were increased exhumation rates during the Late Cenozoic along the eastern U.S. (e.g. Blackmer et al., 1994; Boettcher & Milliken, 1994; Pazzaglia & Brandon, 1996; Miller et al., 2013). Neither dynamic topography or isostatic flexural response can be attributed as the primary cause of the increase in exhumation rates. This Late Cenozoic cooling is a real and significant event, likely due to combination of drivers causing landscape rejuvenation.

Acknowledgments

Figures and Tables

Figure 1. Comparison of hydrocarbon (HC) maturity, organic diagenetic stages, maximum paleotemperature (T_{max}) indicators (i.e. vitrinite reflectance (%R_o) and conodont alteration index (CAI)), and the apatite fission track (AFT) partial annealing zone (PAZ) (modified from: Tissot & Welte, 1978; Gleadow et al., 1983). Organic diagenetic stages (meta. for metagenesis) and illite percentage in the illite/smectite mixed layer included as reference for hydrocarbon generation zone identification (modified from Foscolos et al., 1976; Tissot & Welte, 1978; Jiang, 2012). Generation windows for oil and gas included within the organic stage column (Tissot & Welte, 1978). %R_o values based on a heating rate of 2.8 °C/Myr from 10 °C (Nielsen et al., 2017), with the easy %R_o model in italics (Sweeny & Burnham, 1990) and the basin %R_o model in bold (Nielsen et al., 2017). CAI values characterizes a maximum temperature range and the coloration of the conodont fossils (Epstein et al., 1977). The AFT PAZ (shaded green) the age profile is included (black line) is from ~60 to 110-120 °C, depending on composition, and closely overlaps with the hydrocarbon generation window (e.g., Gleadow et al., 1983; Green et al., 1989).
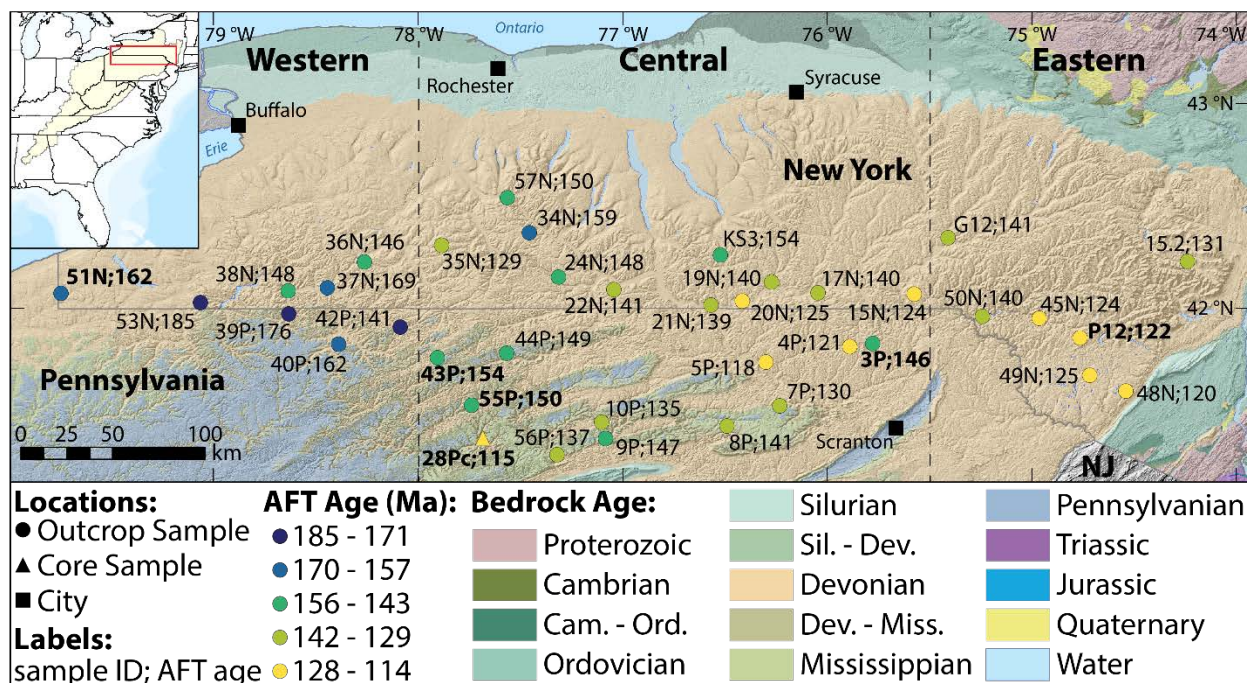
Figure 2. Map of the Northern Appalachian Basin showing 37 Devonian sedimentary outcrop samples (circles) and a core sample (triangle) with AFT ages (sample ID; AFT age (Ma)). Sample colors highlight the AFT age trend. Insert shows study location (red) and extent of the Appalachian Basin (yellow). Included are regional divides and the six representative samples used in the results and discussion section are bolded. Base map generated in ArcGIS using STRM 90m DEM relief shaping overlain by bedrock geologic ages for NY and PA (Dicken et al., 2005; Jarvis et al., 2008).
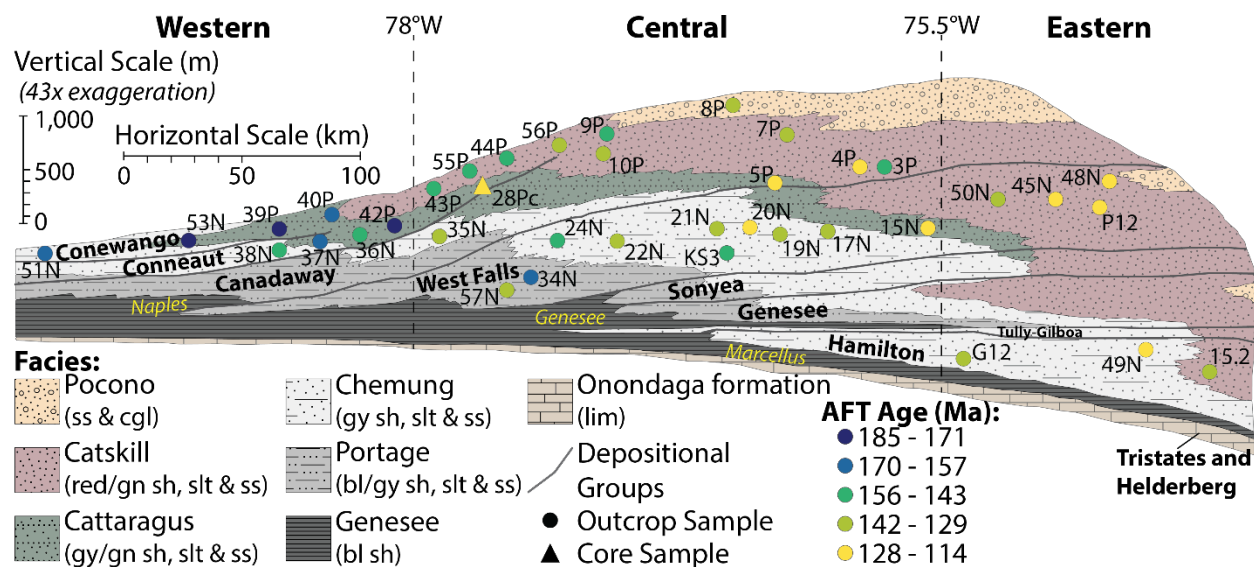
Figure 3. Diagrammatic cross section of the outcropping Catskill Delta strata in the NAB (modified from Isachsen et al., 1991) with stratigraphic locations of the samples, labeled and colorized by AFT age. The section is flattened on the Genesee Formation, with thickness of units exaggerated 43x width of the units to show details (Isachsen et al., 1991). Given that the sedimentary Paleozoic rocks of the Appalachian Basin gently dip (~1-2°) to the southwest (e.g. Johnsson, 1985; Isachsen et al., 1991; Eaton and Frederiksen, 2007), the facies at the base of the cross section (i.e. the Onondaga Formation) outcrop in the northern most parts of the basin (e.g. Buffalo, NY). The Catskill Delta strata are divided into groups based on episodes of deposition (in bold) and the facies indicate the depositional environment (detailed in Isachsen et al., 1991). Abbreviations: cgl – conglomerate; ss – sandstone; sh – shale; lim – limestone; bl – black; gy – grey; gn – green.
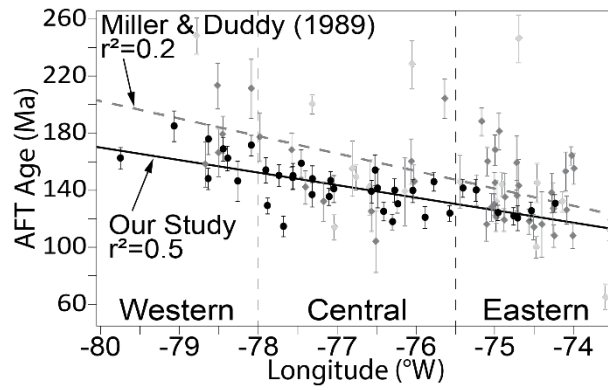
Figure 4. AFT ages (± 1σ) from this study (black points, solid best-fit trend line) and Miller and Duddy's (1989; grey diamonds, dashed best-fit trend line) plotted against longitude. Miller and Duddy's samples are further divided by distance from this study's samples (i.e. samples >15 km north of this study's samples are light grey).

Figure 5. Inverse thermal (time-temperature) models undertaken using HeFTy v1.9.1 (Ketcham, 2005) arranged from west to east, with regional divides. Dark grey envelope indicates the good paths, light grey envelope are the acceptable paths, thick blue path is the weighted mean, and the thin black line is the best-fit path. The timing and duration of the thermal/exhumation events (1, 2, 3) is included for reference. Constraints used include: stratigraphic age (Late Devonian, 383-359 Ma), paleo-surface temperature (25 ± 10 °C; Woodrow et al., 1973), present-day surface temperature (7 ± 5 °C; Hijmans et al., 2005), and present-day core sample temperature (25 ± 5 °C). PAZ (~60-120 °C, depending on composition) and PRZ (~30-90 °C) are marked with dashed lines. Semi-opaque white shading over the models masks parts unconstrained by AFT data (i.e. older than the oldest modeled track and/or at temperatures greater than the base of the PAZ). AFT central age (circles colorized same as Figure 2 and 3) is included on weighted mean path and AHe single-grain ages (orange diamonds) are included in the PRZ, when measured. Published %R_o values (East et al., 2012; Ryder et al., 2013) used passively in inverse thermal modeling are included when they are within bounds of figure (i.e. <200 °C). Goodness-of-fit
(GOF) statistics for model age and track length distributions in bottom left corner of models. Track length distributions with mean track length (μ), standard deviation (σ), and number of tracks measured (N) in bottom right.
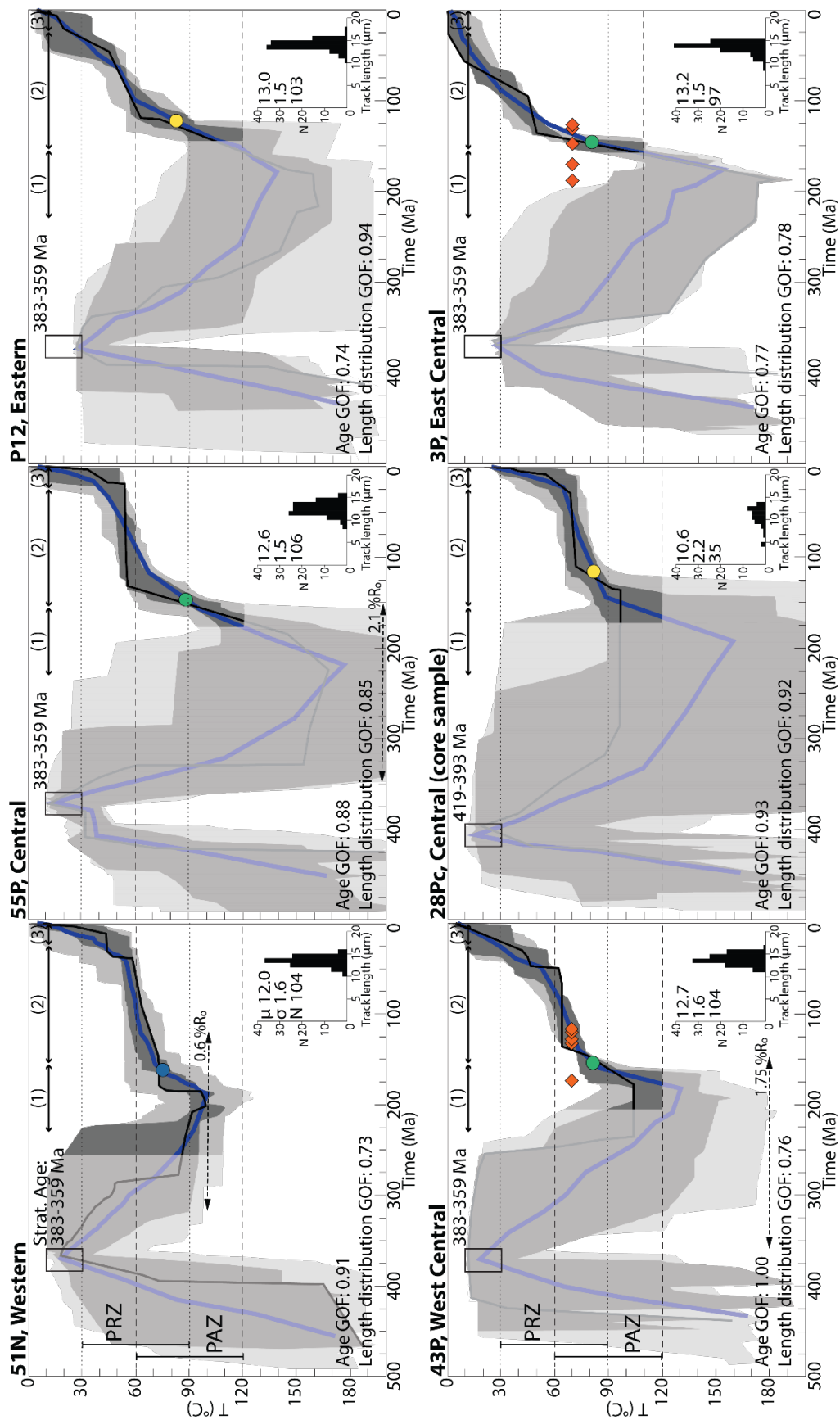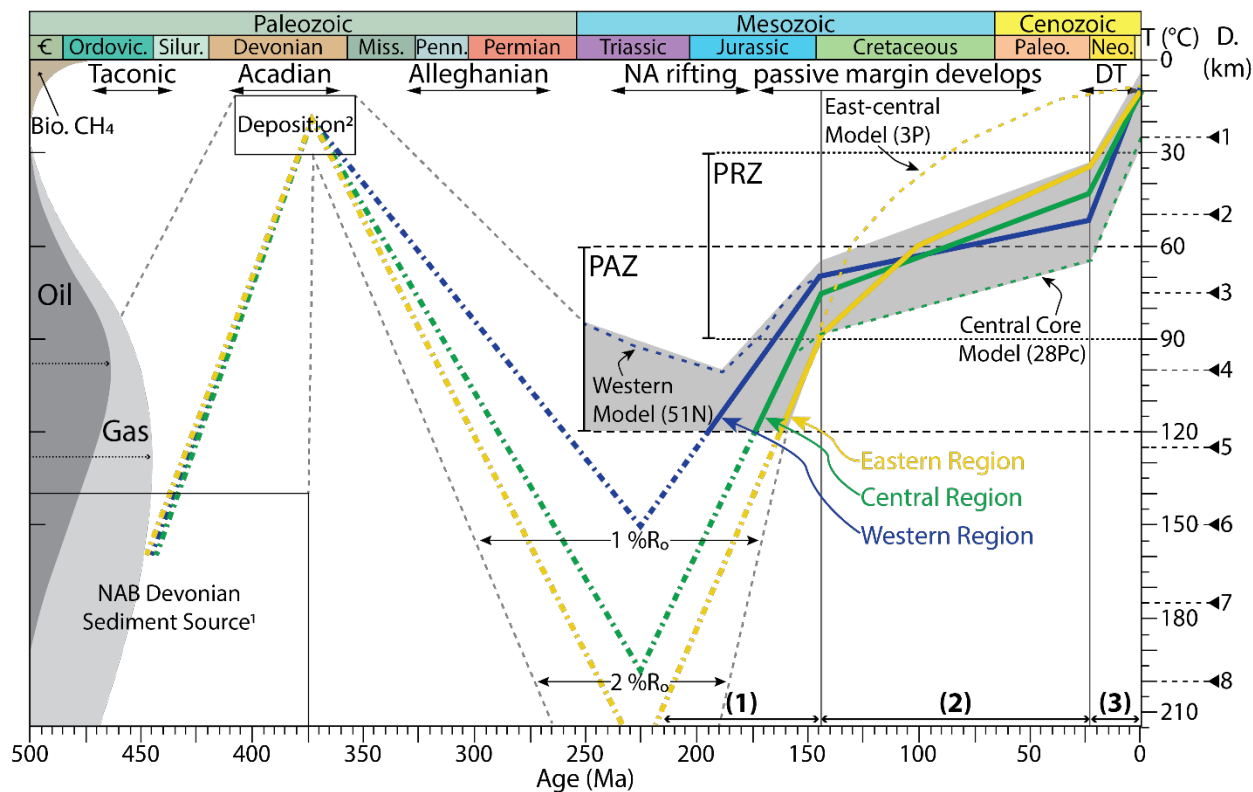
Figure 6. Schematic time-temperature histories of the eastern (yellow), central (green), and western (blue) region – based on AFT ages and CTLD, AHe ages, T_{max} indicators (CAI and %R_o), and geologic constraints ([1]Ver Straeten, 2009; [2]Woodrow et al., 1973) – with portions unconstrained by AFT data dashed. The grey envelope indicates the temporal trends across the NAB, solid grey where constrained by thermal modeling and dashed extent where unconstrained. Temperature converted to depth using a geothermal gradient of 25 °C/km, as discussed. Hydrocarbon maturity window and peak oil and gas generation temperatures included (modified from: Tissot and Welte, 1978; Gleadow et al., 1983). Appalachian orogenies and geologic events occurring along the eastern USA included along the top (summarized from: Klitgord et al., 1988; Poag and Sevon, 1989; Pazzaglia and Brandon, 1996; Withjack et al., 1998; Withjack and Schlische, 2005; Ettensohn, 2008; Hatcher, 2010; Miller et al., 2013). Along the bottom are the three cooling/exhumation events identified in this paper with vertical reference lines.
Table 1 page 1

Table 1. Summary of apatite fission-track thermochronology results.

Sample (Strat. Age)	Lat., Long. (°) Elev. (m)	No. of Grains	Standard Track Density (x 10^6cm^{-2})	Spontaneous Track Density (x 10^6cm^{-2})	Induced Track Density (x 10^6cm^{-2})	χ^2 prob. (%)	Var. (%)	Age (Ma) (±1σ)	Mean Track Length (μm)	Std. Dev. (μm)	D_{par} (μm)	%R$_o$ {CAI}
Western Region												
36N (LD)	42.226, -78.2598 504	23	1.124 (6976)	1.7081 (568)	2.574 (856)	0.0	37	146 ± 14	11.9 ± 0.2 (41)	1.5	2.13 (0.3)	0.8
37N (LD)	42.1001, -78.4433 441	25	1.027 (6589)	2.2654 (934)	2.433 (1003)	41.4	7	169 ± 8	12.4 ± 0.2 (93)	1.8	1.83 (0.3)	1.2
38N (LD)	42.0835, -78.6338 447	25	1.13 (6976)	1.8752 (667)	2.522 (897)	76.7	0	148 ± 8	12.5 ± 0.1 (101)	1.4	2.28 (0.4)	1.2 {2}
39P (LD)	41.9713, -78.6302 403	25	0.993 (6679)	2.116 (950)	2.156 (968)	5.0	18	176 ± 11	12.5 ± 0.2 (100)	1.8	2.43 (0.4)	1.3 {2-2.5}
40P (LD)	41.824, -78.3859 618	25	1.001 (6679)	2.0179 (1638)	2.269 (1842)	0.0	20	162 ± 9	12.4 ± 0.1 (101)	1.3	2.37 (0.3)	1.5
42P (LD)	41.9045, -78.087 495	25	1.029 (6589)	2.4414 (2412)	2.63 (2598)	0.1	15	171 ± 8	12.2 ± 0.2 (101)	1.9	1.56 (0.2)	1.4
51N (LD)	42.0731, -79.7453 443	25	1.04 (6679)	2.3798 (848)	2.68 (955)	58.8	0	162 ± 8	12.0 ± 0.2 (104)	1.6	2.08 (0.2)	0.6
53N (LD)	42.0265, -79.0644 618	25	1.049 (6679)	2.9793 (1236)	3.093 (1283)	0.1	20	185 ± 11	12.0 ± 0.2 (101)	1.5	2.15 (0.3)	1.2 {2}
Central Region												
3P (LD)	41.8265, -75.7744 326	25	1.083 (6881)	1.5306 (1335)	1.992 (1737)	13.5	11	146 ± 7	13.2 ± 0.2 (97)	1.5	1.64 (0.2)	2.75
4P (LD)	41.8116, -75.8852 491	19	1.086 (6881)	1.8536 (831)	2.969 (1331)	0.1	22	121 ± 8	12.4 ± 0.2 (97)	2.0	1.62 (0.2)	2.75
5P (ED)	41.7358, -76.2975 323	25	1.092 (6881)	1.8362 (1207)	3.123 (2053)	5.9	12	118 ± 6	13.1 ± 0.2 (101)	1.6	1.65 (0.3)	2.5
7P (LD)	41.5206, -76.2312 377	20	1.098 (6881)	1.7436 (683)	2.591 (1015)	92.2	0	130 ± 7	12.5 ± 0.2 (93)	1.9	1.62 (0.3)	3*
8P (EM)	41.4228, -76.4886 570	17	1.048 (6976)	0.8979 (514)	1.246 (713)	0.0	29	141 ± 14	10.9 ± 0.4 (53)	2.5	1.88 (0.5)	3
9P (LD)	41.363, -77.082 242	25	1.008 (6589)	1.2861 (1671)	1.572 (2043)	4.9	13	147 ± 7	13.2 ± 0.2 (102)	1.6	1.67 (0.2)	2.54*
10P (LD)	41.4414, -77.1006 389	25	1.010 (6589)	2.6588 (1705)	3.482 (2233)	0.8	14	135 ± 6	12.8 ± 0.2 (103)	2.0	1.85 (0.3)	2.54*
15N (LD)	42.0681, -75.5716 464	22	1.017 (6589)	1.228 (851)	1.772 (1233)	97.9	0	124 ± 6	13.1 ± 0.2 (98)	1.6	1.81 (0.3)	2.45
17N (LD)	42.0751, -76.0418 328	25	1.054 (6976)	1.7958 (514)	2.39 (684)	54.1	4	140 ± 8	12.2 ± 0.2 (47)	1.6	1.93 (0.3)	2.12*
19N (LD)	42.1258, -76.2702 233	25	1.066 (6976)	1.7639 (506)	2.37 (680)	65.1	0	140 ± 8	12.2 ± 0.3 (65)	2.1	1.98 (0.3)	1.9
20N (LD)	42.0333, -76.4116 242	25	1.022 (6589)	1.793 (602)	2.886 (969)	91.0	0	125 ± 7	12.6 ± 0.2 (99)	1.9	1.79 (0.3)	1.75
21N (LD)	42.014, -76.5657 396	25	1.072 (6976)	1.5341 (594)	2.102 (814)	35.3	9	139 ± 8	12.1 ± 0.2 (102)	1.7	2.03 (0.3)	1.75
22N (LD)	42.0904, -77.0414 359	25	1.083 (6976)	1.8573 (620)	2.549 (851)	2.6	20	141 ± 10	12.7 ± 0.2 (102)	1.9	2.00 (0.3)	1.4
24N (LD)	42.1515, -77.3132 315	25	1.095 (6976)	2.0116 (546)	2.649 (719)	15.3	14	148 ± 10	12.5 ± 0.2 (103)	1.5	2.20 (0.3)	1.2
28Pc (ED)	41.3649, -77.6804 1048-1051 depth	23	1.107 (6976)	2.495 (620)	1.4113 (1096)	17.0	7	115 ± 7	10.6 ± 0.4 (35)	2.2	2.08 (0.4)	2.22*
34N (LD)	42.3659, -77.4529 446	25	1.024 (6589)	2.5243 (729)	2.926 (845)	14.9	15	159 ± 10	12.2 ± 0.2 (96)	1.9	1.75 (0.3)	0.77*
35N (LD)	42.3053, -77.8841 592	25	1.113 (6976)	2.4506 (848)	3.725 (1289)	92.9	0	129 ± 6	12.6 ± 0.1 (101)	1.3	2.12 (0.2)	1.05* {2.5-3}
43P (LD)	41.7573, -77.9034 621	25	1.142 (6976)	1.7604 (1044)	2.342 (1389)	0.4	19	154 ± 9	12.7 ± 0.2 (104)	1.6	2.32 (0.2)	1.75
44P (EM)	41.7785, -77.5638 427	25	1.01 (6679)	1.454 (1892)	1.826 (2376)	0.0	21	149 ± 8	13.0 ± 0.1 (105)	1.5	2.54 (0.4)	1.75

Table 1. Summary of apatite fission-track thermochronology results.

Sample (Strat. Age)	Lat., Long. (°) Elev. (m)	No. of Grains	Standard Track Density (x 10^6cm^{-2})	Spontaneous Track Density (x 10^6cm^{-2})	Induced Track Density (x 10^6cm^{-2})	χ^2 prob. (%)	Var. (%)	Age (Ma) (±1σ)	Mean Track Length (μm)	Std. Dev. (μm)	D_{par} (μm)	%R$_o$ {CAI}
55P (LD)	41.5253, -77.7366 373	25	1.058 (6679)	1.7099 (2006)	2.214 (2597)	0.0	20	150 ± 8	12.6 ± 0.1 (106)	1.5	2.51 (0.4)	2.1
56P (LD)	41.2836, -77.3185 180	24	1.067 (6679)	1.7536 (829)	2.454 (1160)	0.9	20	137 ± 9	13.0 ± 0.1 (103)	1.5	2.21 (0.3)	2.29*
57N (LD)	42.5379, -77.5593 453	25	1.075 (6679)	1.663 (722)	2.124 (922)	10.2	15	150 ± 9	12.8 ± 0.1 (106)	1.4	2.24 (0.3)	0.77*
KS3 (LD)	42.2585, -76.5184 337	22	1.084 (6679)	1.4717 (1400)	1.917 (1824)	0.0	26	154 ± 11	12.9 ± 0.2 (94)	1.6	2.48 (0.5)	1.5*
Eastern Region												
45N (LD)	41.9492, -74.9608 390	25	1.019 (6679)	0.881 (1148)	1.279 (1667)	12.6	9	124 ± 6	13.0 ± 0.1 (105)	1.3	2.15 (0.3)	3
48N (LD)	41.6726, -74.7131 442	25	1.027 (6679)	0.7998 (749)	1.24 (1161)	0.0	27	120 ± 9	12.9 ± 0.1 (107)	1.4	2.34 (0.3)	3
49N (MD)	41.5954, -74.5389 457	25	1.031 (6589)	1.1589 (1212)	1.7 (1778)	0.7	16	125 ± 7	12.8 ± 0.1 (146)	1.6	1.61 (0.3)	3
50N (LD)	41.957, -75.2388 341	25	1.036 (6679)	1.1867 (932)	1.548 (1216)	3.2	16	140 ± 8	13.0 ± 0.1 (100)	1.3	2.31 (0.2)	2.75
G12 (MD)	42.3423, -75.4055 339	24	0.983 (6671)	1.6355 (1113)	2.006 (1365)	15.2	9	141 ± 7	13.1 ± 0.2 (100)	1.5	1.87 (0.2)	2.45
P12 (LD)	41.8541, -74.7617 552	25	0.993 (6671)	1.0465 (867)	1.51 (1251)	8.8	11	122 ± 6	13.0 ± 0.2 (103)	1.5	1.84 (0.2)	3
15.2 (MD)	42.2281, -74.2372 595	25	1.014 (6671)	1.659 (1001)	2.269 (1369)	19.1	11	131 ± 6	12.7 ± 0.1 (100)	1.4	1.94 (0.2)	3

Samples listed numerically within regions, with stratigraphic age: EM – Early Mississippian (359-345 Ma); LD – Late Devonian (383-359 Ma); MD – Middle Devonian (393-383 Ma); ED – Early Devonian (419-393 Ma). All samples were crushed and apatites were separated using conventional heavy liquid and magnetic separation techniques. Apatites were mounted and prepared for AFT thermochronology using standard methods (e.g. Kohn et al., 2018). As is preferred, 25 grains (no. of grains) were counted to determine AFT ages when possible. Standard and induced track densities were counted on mica external detectors and spontaneous track densities were counted on internal apatite mineral surfaces, with the track count in parentheses. Chi-square probability (χ^2 prob.) determines if grains are from a single age population; if the χ^2 value is >5%, it is likely that there is a single age population. Age variation (Var.) is the relative standard deviation of the central age and when variation is low (<~15%) the data are consistent with a single population. The external detector method (e.g. Gleadow, 1981) and zeta calibration approach (Hurford and Green, 1983) was used with a zeta of 353 ± 13 (± 1σ) for Shorten (Supplementary File E). Central ages are reported (Galbraith and Laslett, 1993). When possible and as is preferred, at least 100 horizontal confined fission track lengths per sample were measured using a projection tube and a digitizing tablet (number of tracks measured in parentheses) and standard deviation of fission-track lengths (Std. Dev.) is reported. Mean D_{par} calculated from D_{par} measurements on grains used for AFT age, with std. dev. in parentheses. Vitrinite reflectance (%R$_o$) is estimated from Devonian %R$_o$ isograds (Ryder et al., 2013 and East et al., 2012) or nearest (<15 km) measured reading (*; Ryder et al., 2013). Conodont alteration index values (in {}) were measured following the procedures of Epstein et al. (1977) and, when a range of CAI values were present, the range was reported as is common practice (e.g. Repetski et al., 2008).

Table 2. Summary of (U-Th)/He results.

Grain #	Dim. Mass (mg)	r (μm)	l (μm)	U (ppm)	Th (ppm)	Sm (ppm)	eU	^{4}He (nmol/g)	F_T	Raw Age (Ma)	Corr. Age (Ma)	Error (Ma)
3P, Catskills facies (Late Devonian), East-Central Region, 41.8265°, -75.7744°												
a1	5.1	61	204	38.1	62.9	41.4	52.8	29.1	0.76	101	131	1.0
a2	2.8	50	217	17.1	56.4	54.9	30.4	22.3	0.70	133	188	1.3
a3	1.1	37	153	27.7	101.0	81.4	51.4	25.6	*0.61*	90	148	1.2
a5	1.7	44	162	94.7	117.3	81.0	122.3	77.7	0.67	116	171	1.2
a6	4.5	60	168	36.9	63.6	36.9	51.8	28.3	0.76	100	130	1.0
										Mean age ± 1σ (% std. dev): 154 ± 25 (16 %)		
43P, Catskills facies (Late Devonian), West-Central Region, 41.7573°, -77.9034°												
a1	1.1	35	106	75.7	216.6	71.0	126.6	72.3	*0.59*	104	175	0.7
a2	1.3	34	149	37.7	272.5	50.0	101.7	36.9	*0.57*	66	116	0.8
a3	1.1	33	130	22.9	161.1	30.5	60.8	22.3	*0.55*	67	120	0.7
a4	1.1	34	123	16.6	311.2	34.7	89.7	36.4	*0.56*	74	133	1.3
a6	1.2	33	149	68.9	564.0	72.2	201.5	78.0	*0.55*	71	128	0.6
										Mean age ± 1σ (% std. dev): 134 ± 24 (17 %)		

Analyses were completed by CU TRaIL. Dim. Mass = dimensional mass of grain calculated from crystal volume and average apatite density; r = radius of a sphere with equivalent surface area to volume ratio as the grain; l = longest dimension of the grain. Concentrations of U, Th and Sm measured via isotope dilution on an ICP-MS. eU is the effective Uranium, calculated as [U] + 0.235[Th] (e.g. Flowers et al., 2009). Grains were degassed by heating with a laser to determine the amount of ^{4}He (nmol/g) in the grain. Alpha ejection correction (F_T) is a measure of the amount of He ejected from the crystal, values <0.65 (italicized, grey) indicate that a significant amount of He was ejected (Farley et al., 1996). Ages and F_T were calculated using methods described in Ketcham et al. (2011). Raw Age = age calculated from isotope concentrations, without F_T correction; Corr. Age = age calculated from isotope concentrations, with F_T correction; Error = 2σ analytical uncertainty (not incorporating F_T uncertainty). Summarized in bold italics, is the mean age of the single-grain corr. ages with 1σ error on the ages (1 standard deviation). In parenthesis is the coefficient of variation (% std. dev.), calculated from the ratio of the standard deviation to the mean. Coefficient of variation is used to show the variation of single-grain ages from the mean age.

Chapter Two

Episodic Exhumation of the Appalachian Orogen in the Catskill Mountains

Abstract

An increasing abundance of evidence documenting episodic post-rift exhumation indicates eastern North America is not a tectonically quiescent passive margin. The timing, resolution and significance of post-orogenic exhumation events are debated, notably an enigmatic Miocene event. We add insight to this post-orogenic exhumation history by constraining the thermal history of the Catskill Mountains of New York (USA) utilizing apatite fission-track (AFT) thermochronology and apatite (U-Th)/He (AHe) ages from a 1 km age-elevation profile collected from Slide Mountain. While the overall cooling rates are slow, multi-kinetic inverse thermal models reveal relatively rapid cooling at rates of ~1-3 °C/Myr from the Early Jurassic to Early Cretaceous and rates of ~1-2 °C/Myr from the Miocene to Recent. These "rapid" episodes are separated by much slower cooling at rates <~0.5 °C/Myr, during which samples resided for ca. 100 Myr in the partial annealing zone (for AFT) and partial retention zone (for AHe). Cooling was due to erosional exhumation and cooling episodes can be correlated with Early Jurassic rifting of the Atlantic margin, development of the passive margin, and a period of landscape rejuvenation likely associated with dynamic topography in the Miocene. The relatively low magnitude of the Miocene event means that documentation using low-temperature thermochronology constraints has been elusive. However, onshore thermochronology correlates with the sedimentation record in offshore Mid-Atlantic basins that indicate an increase in Miocene sedimentation rates, while geomorphologic studies in the southern Appalachians document accelerated erosion in the Miocene due to landscape rejuvenation. Our findings contrast with previous thermochronologic studies that were unable to verify the existence of Miocene exhumation and those that rejected the Miocene cooling as a spurious artifact of an early generation of thermal models.

Introduction

Post-orogenic development of topography along the Eastern North American passive margin and persistence of mountainous topography in the Appalachian Mountains has been a source of debate over the past 50 years (e.g. Hack, 1960, 1982; Miller and Duddy, 1989; Pazzaglia and Brandon, 1996; Roden-Tice et al., 2009; Miller et al., 2013 McKeon et al., 2014; Amidon et al., 2016). Conventionally, after initial rifting, passive margins were considered tectonically quiescent regions with decreasing topographic relief attributed to exponentially-decaying relict topography (Davis, 1899). Since the 1990's there has been a renewed interest in exploring the correlation between tectonics and topography and demonstrating a more dynamic post-rift history along passive margins (c.f. Bishop, 2007). Pulses of accelerated sediment flux into offshore Mid-Atlantic basins, such as in the Baltimore Canyon Trough, since the Late Jurassic – including a strong Miocene pulse – suggests renewed periods of tectonic uplift and/or erosion along the Appalachian orogen and eastern North America (e.g. Poag, 1985; 1992; Poag and Ward, 1993; Pazzaglia and Brandon, 1996). There is also onshore geomorphologic evidence of Miocene surface uplift of ~100-200 m, documented in the central and southern Appalachians (e.g. Miller et al., 2013; Gallen et al., 2013).

The interpretation of Miocene exhumation based on low-temperature thermochronology in the Appalachian highlands has not yielded definitive results where this approach has been applied, for example in the Blue Ridge Mountains, New England, and central Appalachians in New Jersey (e.g. Spotila et al., 2004; Roden-Tice et al., 2009; McKeon et al., 2014; Amidon et al., 2016). No Miocene ages have been documented, even with low-temperature techniques such as apatite (U-Th)/He (AHe) dating. There are 3 AFT Paleogene ages (48-33 Ma) recorded in the Appalachian Basin and Ridge and Valley provinces of southwestern Pennsylvania and West

Virginia, however these ages are considered anomalous and related to thermal resetting, possibly due to decreasing temperatures of thermal springs in the Cenozoic which were at temperatures >100 °C in Mesozoic (Roden, 1991). The absence of younger ages, associated with Miocene exhumation, suggests that erosion since the Miocene must be less than ~2 km (e.g. McKeon et al. 2014). Interpretation of thermochronologic data from studies utilizing inverse thermal modeling is mixed, for a variety of reasons. Two studies have constrained accelerated Miocene cooling in their thermal history interpretations of data from the central and southern Appalachian basin (Blackmer et al., 1994; Boettcher and Milliken, 1994). However, these studies employed modelling that used mono-kinetic annealing algorithms (e.g. Laslett et al., 1987; Crowley et al., 1991) that often produced a late-stage cooling artifact (i.e. Miocene cooling) which, without supporting geologic evidence makes the interpretation of modeling results unreliable and lacking confidence (e.g. De Bruijne and Andriessen, 2002; Ketcham et al., 1999). Miocene cooling was modeled in other thermochronologic studies within the Blue Ridge Mountains and New England, also using mono-kinetic annealing algorithms of Laslett et al. (1987) and Crowley et al., (1991), but in contrast these studies rejected Miocene cooling revealed in their thermal models as a spurious artifact because of these issues with modeling programs at that time (Spotila et al., 2004; West et al., 2008; Roden-Tice et al., 2009).

In this study low-temperature thermochronologic results are presented for a suite of samples collected over short-wavelength topography and significant relief (~1 km) from Slide Mountain, near West Shokan, New York (Figure 1). The AFT age-elevation profile and multi-kinetic inverse thermal modeling of AFT data, AHe ages, and maximum paleotemperature (T_{max}) indicators constrains the episodic cooling and exhumation history of the Catskill Mountains (Catskills) during the Mesozoic and Cenozoic. AFT thermochronology utilizes confined track

lengths as a kinetic parameter (e.g. Gleadow et al., 1986). Multi-kinetic models characterize individual apatite grains' variability to annealing within a sample and does not produce a spurious late-stage cooling artifact (Ketcham et al., 1999). From the Slide Mountain data it is possible to document two episodes of accelerated cooling: Late Jurassic to Early Cretaceous; and Miocene to present, separated by a period from the Cretaceous to Miocene of much slower cooling ("stabilization"). Results are discussed in context of previous studies and correlate events with regional tectonics and proposed Cenozoic mantle upwelling along eastern North America (NA).

Geologic Setting

The Catskill Mountains are comprised of Devonian, near-horizontal, undeformed sedimentary strata of the Catskill delta wedge (Figure 1; Faill, 1985; Ver Straeten, 2013). The Catskill wedge consists of a series of delta-alluvial wedges and submarine facies that coarsen up-section as the delta front prograded cratonward (Ettensohn, 1985; Ver Straeten, 2013). Sediments reflect a dominant Acadian provenance with lesser contributions from Taconic and Grenville sources (Ver Straeten, 2009). The preserved sediments (~2.7 km in thickness) were deposited during the Acadian orogeny (ca. 419-365 Ma; Ver Straeten, 2013). Younger sedimentary packages were deposited on top of the currently preserved sediments in the Catskill region during the Acadian and the Alleghenian orogeny (ca. 330-265 Ma, Ettensohn, 2008) are missing as they have since been eroded. The thickness of eroded sediments in the Catskills is estimated as ~5 km (e.g. Friedman and Sanders, 1982; Lakatos and Miller, 1983; Miller and Duddy, 1989).

Thrusting during the Alleghenian orogeny led to over-pressurization of sediments, and formation of joints in the Catskill wedge strata (Lash and Engelder, 2009; Ver Straeten, 2013). However, there is no other deformation of the Middle to Late Devonian strata in the Catskills

(Ver Straeten, 2013). Alleghenian thrusting also resulted in regional hot fluid-flow within the Catskill wedge, which elevated the geothermal gradient, but not after the Alleghenian Orogeny (Dorobek, 1989). At the end of the Alleghenian Orogeny the Catskill Delta wedge and overlying Early Pennsylvanian to Permian units comprised the expansive, flat-lying Alleghenian Plateau (Ver Straeten, 2013). The Catskill Mountains' peaks all have similar elevations (summit-height concordance), indicating that they were formed from the erosional incision and exhumation of the Alleghenian plateau (e.g. Ettensohn, 2008; Ver Straeten, 2013). The timing of this post-orogenic exhumation, documented throughout the Appalachian Basin in various thermochronology studies, is episodic but variable (e.g. Blackmer et al., 1994; Reed et al., 2005; Amidon et al., 2016) and does not occur as one rapid pulse (e.g. Miller and Duddy, 1989) or as a result of slowly decaying topography due to erosion (Davis, 1889).

Methods, Results, and Geothermal Gradient

Five samples of Middle to Late Devonian sandstones were collected at elevations ranging from 281 to 1,272 m to generate an age-elevation profile (Figure 1, Supplementary Table 1). Samples were collected along the shortest, most direct trail to the peak of Slide Mountain and in the surrounding valleys, within ~8 km of the peak. The vertical profile was collected over short wavelength topography to minimize modification of the slope due to topographic effects on sub-surface isotherms (e.g. Reiners et al., 2003; Fitzgerald and Malusà, 2018). AFT low-temperature thermochronology (Supplementary Table 1) was undertaken at Syracuse University following standard procedures (e.g. Riccio et al., 2014) and AHe dating (Supplementary Table 2) at CU TRaIL (Colorado Thermochronology Research and Instrumentation Laboratory, University of Colorado, Boulder, e.g. Weisberg et al., 2018). T_{max} information is from published Vitrinite reflectance (%R_o) isograd maps of Devonian shales (Ryder et al., 2013). Apatite grains from

these samples are well-rounded, often pitted and semi-opaque (stained) likely due to transportation prior to burial and diagenesis since, making the selection of appropriate grains for AHe difficult (Supplementary Table 3).

AFT central ages range from 133 ± 7 to 114 ± 8 Ma ($\pm 1\sigma$). For all samples, the variation of single-grain AFT ages is low (0-16%) and all pass the χ^2 test, indicating that grains for each sample define a single age population (Supplementary Table 1). AFT ages increase with increasing elevation, with the slope representing an apparent exhumation rate of ~50 m/Myr during the Early Cretaceous (Figure 2). Mean track lengths vary from 13.1 to 12.8 µm with standard deviations of 1.6 to 1.1 µm. Confined track length distributions (CTLDs) exhibit a weak negative skewness (Figure 2). Track length data thus indicates a complex thermal history involving partial annealing and/or an episodic cooling (e.g. Gleadow et al., 1986, Green et al., 1986). D_{par} values range from 2.15 to 2.39 µm, which indicate that the apatite grains are more resistant to annealing than standard fluorapatites (i.e. $D_{par} > 1.75$ µm; e.g. Donelick et al., 2005). This means that the partial annealing zone (PAZ), the temperature range in which fission-tracks are annealed, is ~120-60 °C.

AHe single-grain ages on samples C1, C3, and C5 range from $1,850 \pm 69$ to 83 ± 1 Ma with significant variation about the mean (e.g. 52-125%; Supplementary Table 2). There are obvious outliers, potentially due to the influence of one or more well documented factors such as poor grain quality or inclusions with high uranium content (Supplementary File A; e.g. Ehlers and Farley, 2003; Fitzgerald et al., 2006; Wildman et al., 2016). Green and Duddy (2018) summarize problems of "excessive dispersion" of single-grain ages, use of mean AHe ages for interpretation, and He retentivity due to radiation damage. They also discuss that models (i.e. RDAAM; Flowers et al., 2009) cannot yet accurately replicate single-grain age dispersion. There

is no clear age-elevation trend in the AHe ages from Slide Mountain. Overall challenges remain for the interpretation of AHe data (e.g. Green and Duddy, 2018), however the interpretation of such data, including that from Slide Mountain are fortified by the use of inverse thermal models that rely dominantly on AFT data (see below). Mean AHe ages calculated from AHe single-grain ages without obvious outliers (e.g. Ault et al., 2013) decreases variation to 27-31 %. Mean AHe ages for samples C1 (highest elevation), C3, and C5 are 159 ± 49 Ma ($\pm 1\sigma$), 111 ± 3 Ma, and 128 ± 34 Ma respectively.

Samples are estimated to have reached maximum temperatures of ~215-235 °C, estimated from %R_o values (Ryder et al., 2013; Supplementary Table 1) using the Basin %R_o model (Nielsen et al., 2017). Fission tracks in apatite grains have therefore been reset and thermochronology data does not constrain the timing of T_{max} but does constrain the post-orogenic thermal history. Inverse thermal modeling of AFT and AHe data, using the modeling program HeFTy v1.9.1 (Ketcham, 2005), constrains cooling since the Late Jurassic (Figure 3; Supplementary File B). Overall, cooling rates are low enough that effects of advection due to rapid exhumation or distortion of the geothermal gradient are likely to be insignificant (e.g. Braun, 2002). Fluid-flow influenced the geothermal gradient during the Alleghenian orogeny, but it did not continue after thrusting ceased (Dorobek, 1989). The cooling history is therefore converted to exhumation rates using a relatively stable, modern geothermal gradient of 25 °C/km, similar to other studies in eastern North America using this approach (e.g. Reed et al., 2005; Amidon et al., 2016; Shorten and Fitzgerald, in review).

Episodic Cooling and Exhumation History

The age-elevation profile combined with track length information and inverse modeling (Figure 3) indicates episodic cooling (Figure 4). Initial, relatively rapid cooling from T_{max} is

model constrained to begin in the Early Jurassic and samples pass into the PAZ by the Late Jurassic (event 1-1a). Between the Early Cretaceous and Miocene, thermal models constrain a time of slower cooling ("stabilization") when samples are resident in the upper crust (event 2). Beginning in the Miocene models constrain an acceleration in cooling to present day (event 3).

Event 1-1a: Initial cooling from T_{max} and exhumation of Appalachian basin strata began in the Early Jurassic. This timing is not revealed clearly in Slide Mountain inverse models (Figure 3) but is revealed in AFT data from the northern Appalachian Basin lying to the west of Slide Mountain (Shorten and Fitzgerald, in review). The Catskill samples cooled into the PAZ in the Late Jurassic. Thus, we break this initial exhumation event into (1 – northern Appalachian Basin samples) and (1a – Catskills samples). Estimated cooling rates between the start of rapid cooling and ca. 120 Ma (end of event 1a) are 0.6-2.4 °C/Myr (weighted mean paths), with rates up to 2.1-9.6 °C/Myr constrained in individual best-fit model paths. Assuming a geothermal gradient of 25 °C/Myr for the weighted mean paths, suggests the removal of ~3-6 km of overburden at rates of 24-95 m/Myr during this event (Figure 4). These rates correlate well with the apparent exhumation rate derived from the slope of the age-elevation profile (~50 m/Myr).

We relate initial rapid cooling (events 1 and 1a) to rift flank uplift, extension and subsequent rifting that led to the formation of the North Atlantic Ocean (Figure 4). This period of rapid cooling and exhumation in the Catskills correlates well with an increase in sediment flux into the Baltimore Canyon Trough, starting in the Late Jurassic (Pazzaglia and Brandon, 1996). Lowering of regional base levels due to the extension and rifting, and formation of the Atlantic passive margin likely increased river incision and backwearing resulting in re-excavation and increased erosion rates of the onshore Appalachian orogen and sedimentary strata in the Catskills (c.f. Wildman et al., 2018). In the Appalachian Basin in Pennsylvania, Blackmer et al. (1994)

state that initial exhumation at this time is likely due to erosion of the sedimentary overburden in response to flexural rebound of the lithosphere after the cessation of deposition. Our timing of initial cooling also overlaps with Miller and Duddy's (1989) estimate of 140-120 Ma for the Catskills. However, our estimates of the amount of exhumation differ from Miller and Duddy (1989), who suggested this event accounted for the removal of almost all the orogenic overburden.

Event 2: Inverse thermal models clearly indicate residence of samples in the PAZ and AHe partial retention zone (PRZ, ~30-90 °C; Flowers et al., 2009) from the Early Cretaceous to Miocene. Cooling is very slow, with rates of 0.2-0.5 °C/Myr. Event 2 accounts for <1 km of exhumation over ca. 100 Ma at rates of ~9-21 m/Myr. AHe Single-grain age variations often result from variations in grain size, zonation patterns, and/or effective uranium (eU) concentrations (e.g. Fitzgerald et al., 2006; Flowers et al., 2009). Long-term residence within the PRZ is also well-known for magnifying the effect of these factors, causing significant single-grain age dispersion (e.g. Reiners et al., 2003; Fitzgerald et al., 2006). Offshore sedimentation rates decrease significantly during this time (Pazzaglia and Brandon, 1996). Thus, we propose that event 2 is associated with stabilization with decreasing relief within the Catskills as eastern North America transitioned into a passive continental margin (Figure 4; e.g. Withjack and Schlische, 2005; Ettensohn, 2008).

Event 3: Following long-term residence within the PAZ and PRZ, thermal models constrain an increase in cooling rates, to 0.9-1.9 °C/Myr (based on weighted mean paths), with best-fit model rates ranging from 1.2-3.2 °C/km (Figure 3). The timing of this increase in cooling rate occurs at ca. 23 Ma (Miocene), but the timing is variable between models for samples from different elevations (ca. 30 to 20 Ma). Since higher elevation samples pass into the PAZ earlier

than those at lower elevations, models from higher elevation samples suggest onset of rapid cooling earlier, as to be expected. Exhumation rates are between 34-75 m/Myr on average, with peak best-fit estimates up to 128 m/Myr. This period of relatively rapid exhumation accounts for the removal of the final 1-2 km of overburden and the exposure of the Devonian strata to the surface (Figure 4).

The increase in exhumation in the Miocene documented for samples in this study and the offshore sedimentation record have a positive correlation (Pazzaglia and Brandon, 1996). The mechanisms responsible for this increase in Miocene exhumation and sedimentation are highly debated. Initially, studies hypothesized that the Miocene increase in offshore sedimentation rates resulted from a change to a cool/dry climate in the Miocene, causing increased mechanical weathering and exhumation of the onshore Appalachian region (e.g. Poag and Sevon, 1989; Boettcher and Milliken, 1994). However, given the timing and amount of exhumation documented in the Appalachian Basin, most studies now agree that tectonic processes must be the driving factor in the Appalachian Basin thermal history trends and pulses of offshore sedimentation (e.g. Pazzaglia and Gardner, 1994; Blackmer et al., 1994; Pazzaglia and Brandon, 1996; Miller et al., 2013; Gallen et al., 2013). Both geomorphologic and low-temperature thermochronology studies that constrain Miocene cooling conclude the mechanism was either due to interaction of isostatic forces on the ancient foreland and flexural response due to sedimentation along the margin (Pazzaglia and Gardner, 1994; Blackmer et al., 1994) or a result of dynamic topography (e.g. Pazzaglia and Brandon, 1996; Miller et al., 2013; Gallen et al., 2013). Given that our models constrain 1-2 km of exhumation, we conclude that there must have been a complex combination of factors causing broad, regional landscape rejuvenation.

Eastern US Context for Miocene Exhumation

Offshore Mid-Atlantic basins (e.g. Salisbury Embayment, Baltimore Canyon Trough, and the Hatteras Basin) record pluses of increased sediment flux rates during the Jurassic, Late Cretaceous, and Miocene, suggested as due to tectonic uplift and erosion of Appalachian terranes (e.g. Poag and Sevon, 1989; Pazzaglia and Brandon, 1996; Amidon et al., 2016). Sediment flux into the basins and erosion rate in the Appalachian hinterland is greatest in the Miocene, requiring >1.1 km of rock to be removed from catchments across the central Appalachians to New England (Braun, 1989). Zircon fission track analysis conducted on Atlantic Coastal Plain sediments and in Blue Ridge Mountains of Virginia and North Carolina suggest that headwaters of catchment basins incised westward and began to transport western Appalachian detritus eastward beginning in the late early Oligocene to middle early Miocene (Naeser et al., 2016). Naeser et al. (2016) suggested that the increase in offshore sedimentation is partially due to rivers gaining access to easily eroded Paleozoic sedimentary rocks of the western Appalachians. Geomorphological evidence also constrains an onshore increase in erosion rates in the Miocene. Stream profile analysis and ^{10}Be erosion rates of the Susquehanna River catchment basin in PA indicates ~100-150 m of river incision propagating upstream in the Miocene due to rock uplift (Miller et al., 2013). Also, generation of knickpoints and preservation of relict landscape in North Carolina (NC) is interpreted as surface response to broad, regional uplift of the Appalachians by dynamic mantle forcing during the mid-Miocene (Gallen et al., 2013).

Thermochronology studies have struggled to confidentially verify this Miocene exhumation signal. There are no recorded Miocene AFT or AHe ages (e.g. Spotila et al., 2004; McKeon et al., 2014), and there is contradictory information from thermal models. As discussed above, early studies utilizing mono-kinetic annealing algorithms either concluded that there was

real Miocene cooling (e.g. Blackmer et al., 1994; Boettcher and Milliken, 1994) or that it has not occurred and is a model artifact (e.g. Spotila et al., 2004; West et al., 2008; Roden-Tice et al., 2009). The reason why mono-kinetic models often indicated spurious late-stage cooling was because these models used annealing algorithms based on annealing experiments undertaken on Durango apatite (e.g. Laslett et al., 1987). Fission-tracks in Durango tend to be more resistant to annealing than the average fluorapatite, thus using Durango kinetics during modeling of a fluorapatite would cause tracks to not be annealed early in the model, which would then produce a late-stage rapid cooling as the model sought to end at present day temperatures. Late-stage cooling (often Miocene) documented with mono-kinetic algorithms are therefore questionable given the input assumption of uniform apatite composition and annealing characteristics (e.g. De Bruijne and Andriessen, 2002; Roden-Tice et al., 2009).

Documentation of Early Cretaceous AHe ages in several studies from New England, was also cited as a reason against Miocene cooling, since samples would have to be within the PRZ during the Mesozoic (e.g. West et al., 2008; Roden-Tice et al., 2009). Our AHe ages in the Catskills are also, generally Cretaceous in age but, as discussed above, samples also contain outliers of Paleozoic and Precambrian AHe single-grain ages (Supplementary Table 2). West et al. (2008) comment on the discordance of several of their AHe ages and corresponding AFT ages, such as AHe ages significantly older or within standard error of AFT ages. They state that it is possible that single-grain age dispersion is caused by retention of He in apatite due to radiation damage and/or high eU concentrations. Further south in the Blue Ridge Mountains, McKeon et al. (2014) used the lack of Miocene ages as evidence that any Miocene exhumation was <2 km in magnitude. Otherwise, reset AHe ages would have been present at the surface, assuming a typical continental geotherm (e.g. 20-30 °C/km). Mesozoic (and older) AHe ages do

not preclude Miocene cooling, as documented in the multi-kinetic thermal models, they simply constrain the amount of Miocene cooling and hence estimates on exhumation.

It is important to note that offshore sedimentation flux is calculated for the ten major catchments, spanning from New Hampshire to northern Virginia, which feed sediment to the Mid-Atlantic margin (Pazzaglia and Brandon, 1996). Thus, onshore exhumation and erosion required to account for a Miocene plus in offshore Mid-Atlantic basin sedimentation should be focused on that region, which includes the Catskills. Also, there is an inherent assumption in this study and Pazzaglia and Brandon's (1996) work that the catchment basins have not greatly changed extent through geologic time. Some of the studies which do not constrain Miocene cooling (e.g. Spotila et al., 2004; West et al., 2008; Roden-Tice et al., 2009; McKeon et al., 2014) either completely or partially lie within catchments (i.e. Mississippian or St. Lawrence catchments) which drain into the North Atlantic or Gulf of Mexico, something that was also commented on by McKeon et al. (2014). Given that our study area is in the Hudson river catchment, which directly drains into the Baltimore Canyon Trough, it is plausible that Miocene exhumation of the relatively high-standing Catskills region is more closely correlated with documented offshore sedimentation.

Conclusions

Our results show that the Catskills experienced an episodic cooling history since the end of the Alleghenian orogeny. Initial cooling and exhumation from the Late Triassic to Early Cretaceous is contemporaneous with rifting (events 1-1a), followed by a long period of stabilization as eastern North America drifted and developed into a passive margin (event 2), then a final period of rapid cooling and exhumation in the Miocene (event 3), due to landscape rejuvenation. Triassic to Cretaceous and Miocene exhumation correlates with increases in

offshore sedimentation rates (e.g. Pazzaglia and Brandon, 1996). Significant Miocene to present rapid cooling due to erosional exhumation is revealed in multi-kinetic inverse thermal models. Miocene cooling has previously been regarded as controversial and highly debated due to the late-stage rapid cooling artifact of first-generation inverse thermal models that used mono-kinetic annealing algorithms, as well as the lack of Miocene AFT and AHe ages (e.g. Spotila et al., 2004; Roden-Tice et al., 2009). Miocene-Recent exhumation in the Catskills is constrained as 1-2 km, most likely resulting from a combination of mechanisms, each of which produce relatively small magnitude effects. These include isostatic flexural response to offshore sedimentation and dynamic topography causing landscape rejuvenation. We note that the detection of this Miocene event is often near the resolution of the methods employed, and that the causes of this Miocene-recent exhumation remain enigmatic and offer future avenues for research and greater understanding.

Acknowledgments
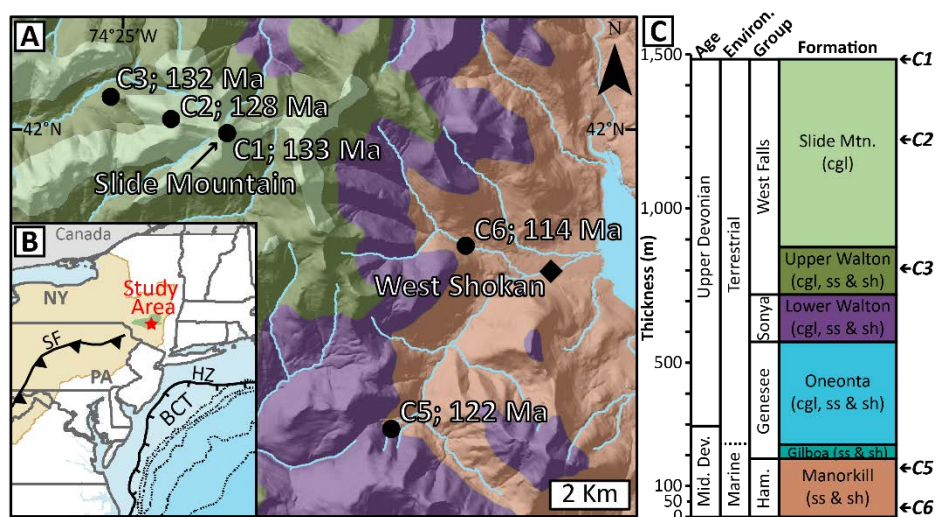
Figures

Figure 1. (A) Geologic map with samples and AFT ages. (B) Insert of study area (red star), Catskill state park (green), Appalachian Basin (tan), Appalachian structural front (SF), North American passive margin hinge zone (HZ), Baltimore Canyon Trough (BCT), and bathymetry (dashed lines represent 200, 1000, 2000, 3000 and 4000 m depth, from west to east). (C) Stratigraphic column of Catskill Delta Wedge units from Slide Mountain to West Shokan, NY (modified from Ver Straeten, 2013) with estimated stratigraphic sample locations. Mid. Dev. – Middle Devonian; Environ. – environment; Ham. – Hamilton; cgl – conglomerate; ss – sandstone; sh – shale.
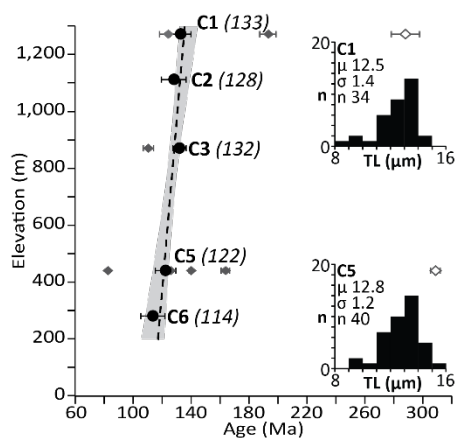
Figure 2. Age vs. elevation profile. AFT central ages (±1σ, black), with sample ID and AFT age. AHe single-grain ages (±2σ, dark grey), with outliers made hollow. Trendline of AFT ages (dashed) and 1σ error envelope (light grey). CTLD of C1 and C5 include: track lengths (TL), mean track length (μ), standard deviation (σ) and number of tracks measured (n).
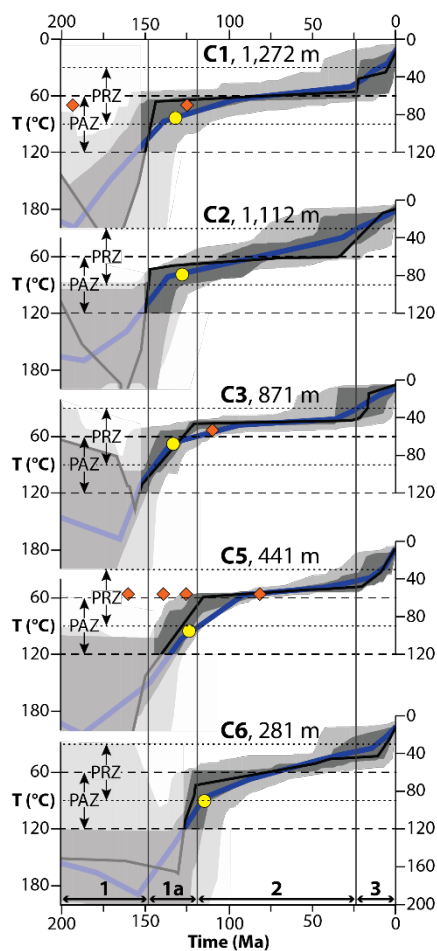
Figure 3. Inverse thermal models from HeFTy (Ketcham, 2005) arranged according to elevation. AFT central ages (yellow circles) and single-grain AHe ages (orange diamonds). Black line is the "best fit", thick blue line is the weighted mean, dark gray envelopes are "good fit" paths (i.e. T-t paths supported by the data) and light gray envelopes are "acceptable fit" paths (i.e. T-t paths not ruled out by the data). Areas unconstrained by AFT data are semi-transparent. Vertical lines (numbered 1, 1a, 2, 3) highlight thermal history trends. PAZ – partial annealing zone; PRZ – partial retention zone; T – temperature.

56
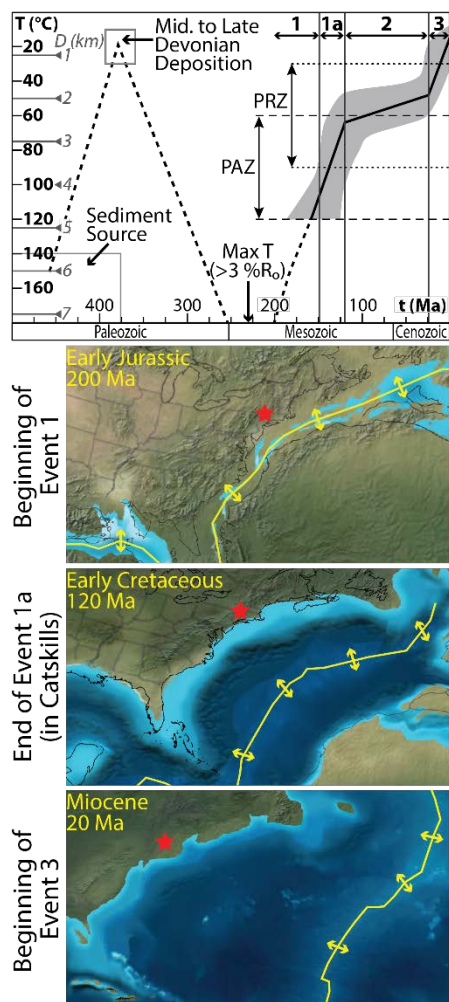
Figure 4. Schematic T-t history of the Catskills. Dashed line is the history constrained by geologic information, sediment source (Ver Straeten, 2009), deposition time/paleo-surface temperature (25 ± 10 °C; Woodrow et al., 1973), and T_{max} %Ro data (Ryder et al., 2013). Solid line and grey envelope is the average history and range constrained with low-temperature thermochronology data. Present-day surface temperature is 7 ± 5 °C (Hijmans et al., 2005). Temperature (T) and estimated depth (D), using geothermal gradient of 25 °C/km, are along the left side and cooling/exhumation events (1, 1a, 2, 3) with vertical reference lines are listed along the top. Paleogeographic maps (Blakey, 2013) include the study location (red star) and divergent boundary (yellow), illustrating the rifting of Pangea and transition to drift and passive margin development (e.g. Withjack and Schlische, 2005).

Chapter Three

Synthesis of Post-Orogenic Low-Temperature Thermal Histories along the eastern United States

Abstract

Following the Appalachian orogeny, the eastern United States (U.S.) has experienced a complex, episodic cooling and exhumation history. To constrain major orogen-wide thermal and tectonic events as well as distinguish those events that are localized or only occur within a small region, we undertake a comprehensive synthesis of data from 26 low-temperature thermochronology studies along the eastern U.S. Challenges exist in comparing thermal histories from studies which are spread across the entire Appalachian orogen, have different sampling strategies and objectives, apply different methods and span in publication from the early 80's to today. There are also variations in timing, duration, rates and resolution of the different events across the various physiographic provinces of the eastern U.S. (i.e. the Taconic and Acadian province in New England, the Adirondacks, the Appalachian Basin, and the Ridge and Valley province).

Many of the low-temperature thermochronology studies undertaken along the eastern U.S. lie within present day catchments that drain into Mid-Atlantic offshore basins. We examine the onshore record and conclude episodes of rapid cooling and exhumation documented within these catchments correlate well with periods of increased sediment flux into offshore Mid-Atlantic basins. Synthesizing the temporal correlation between onshore exhumation and offshore sediment flux and the provinces' thermal histories, the post-orogenic low-temperature thermal history across the eastern U.S. passive margin is divided into three extended periods of cooling and exhumation. These periods are related to regional effects of Early Mesozoic continental rifting and post-rift crustal extension, Late Mesozoic variable cooling due to the development of the passive margin and to exogenic mechanisms, and Late Cenozoic (i.e. Miocene) rapid cooling related to the establishment of dynamic topography and drainage reorganization.

Introduction

The Paleozoic collisional and other tectonic events that formed the Appalachian Mountains, followed by the Mesozoic to Cenozoic evolution of the passive margin of the eastern United States (U.S.) are the subject of considerable study (e.g. Hatcher et al., 1989; Miller and Duddy, 1989; Poag and Sevon, 1989; Faill, 1997a; Roden-Tice and Tice, 2005; Ettensohn, 2008; Moodie et al., 2018). The geologic processes controlling post-orogenic passive margin development are complex (e.g. Green et al., 2018) and often involve episodic syn- and post-rift magmatic and thermal events (e.g. de Boer et al., 1988). Low-temperature thermochronology is a method often applied to constraining the post-orogenic thermal history and exhumation rates of passive margins such as the eastern U.S. (Table 1). While there is an abundance of thermochronology data from many studies scattered over the eastern U.S., an orogen-scale synthesis of the low-temperature thermal and exhumation history has not been undertaken. This comprehensive, thermal and exhumation history synthesis of available data provides insight into the exogenic forces (i.e. tectonics, dynamic topography or climate change) which are responsible for the larger, orogen-scale cooling and exhumation events as well as the more localized events.

To undertake this synthesis, apatite fission-track (AFT) thermochronology and (U-Th)/He (AHe) data was collated from 26 low-temperature thermochronology studies located throughout eastern U.S. (24 published studies and Chapters 1 and 2; Figure 1 and 2). In regions where the rate of cooling is overall very slow, such as the post-orogenic history of the eastern U.S., AFT and AHe ages can be meaningless when taken out of context with the thermal history that the sample has experienced (e.g. Gleadow and Brown, 2000). In other words, AFT and AHe ages cannot be simply interpreted as closure temperature ages. AFT ages are a function of time and temperature, that when combined with the measurement of fission-track lengths (as a kinetic

parameter) and D_{par} (as a compositional proxy) allows for inverse thermal modeling of the time-temperature paths at temperatures <120-100 °C (e.g. Gleadow et al., 1986; Gallagher et al., 1998). The distribution of fission-track lengths constrains the thermal history that a rock has experienced, with broad distributions and mean fission-track lengths (MTL) < 14 µm indicative of complex or slow cooling while narrow distributions with MTL ≥14 µm are indicative of rapid cooling (e.g. Gleadow et al., 1986; Green et al., 1989). AHe ages reflect the interaction of in-situ radiogenic He production and diffusive loss at temperatures <~70 °C that can help constrain the lower-temperature thermal history (e.g. Reiners and Farley, 2001). Trends identified and discussed in the paper are thus mainly based on model-constrained cooling histories with the aid of data-drive interpretations (i.e. AFT ages of samples with MTL ≥14 µm).

Thermal histories from different studies, both within and across physiographic provinces of the Appalachian orogen (i.e. Taconic and Acadian province, Adirondacks, Appalachian Basin, Ridge and Valley province, Blue Ridge Mountains, Piedmont, Mesozoic rift basins), often constrain differential rates of cooling with variation in resolution, duration and significance of cooling events. The episodicity of cooling events and variation of such across the provinces reveal which events occur throughout the entire orogen as compared to those events which are more localized (i.e. province-specific and more likely to originate from a localized geologic event) during the post-orogenic history. There are challenges in comparing thermal histories from studies published over the last 40 years. Different studies focused on constraining different specific geologic events, may incorporate a range of thermal and geologic constraints, and utilize several generations of thermal models (i.e. mono-kinetic (e.g. Laslett et al., 1987; Crowley et al., 1991) verses multi-kinetic annealing algorithms (e.g. Ketcham et al., 1999; 2007)). However, commonality and differences between thermal histories at different scales can be determined.

After providing an overview of the geologic history of the eastern U.S. for context, this chapter discusses the database created from the 26 low-temperature thermochronology studies and the challenges of interpreting thermal histories. The synthesis is undertaken in 2 stages. (1) Comparing thermal histories from samples that lie within catchment basins which drain into Mid-Atlantic offshore basins (i.e. Salisbury Embayment, Baltimore Canyon Trough and Hatteras Basin; Poag and Sevon, 1989). The onshore thermal record from these samples record cooling and exhumation related to North American rifting and 4 periods of increased sediment flux to offshore Mid-Atlantic basins, calculated by Pazzaglia and Brandon (1996). (2) Determining major thermal trends documented within individual provinces and across the eastern U.S. These are analyzed to determine which events are orogen-wide in scale and which are more localized and hence what exogenic events are responsible. Despite the challenges in comparing the different generations of studies, we provide new insight into the temporal and spatial patterns of the post-orogenic exhumation history and landscape evolution of the passive margin of the eastern U.S.

Geologic overview

Eastern U.S. is geologically complex, containing several provinces that formed from collision and terrane accretion along the eastern Laurentian margin during different orogenic and exhumation events since the beginning of a Wilson cycle in the Neoproterozoic (Rast, 1989; Hatcher, 2010). Figure 1A shows the main physiographic provinces, including the Adirondack mountains (Grenville), accreted island arcs and terranes (i.e. Taconic and Acadian provinces), preserved structural features (i.e. Blue Ridge Mountains, Alleghenian structural front and Paleozoic contractional structures), and thick sedimentary packages of both deformed (i.e. Ridge and Valley province) and flat lying strata (i.e. Appalachian Basin). The present drainage divide

between the Atlantic Ocean and Gulf of Mexico is thought to have been relatively steady since the early-Mid Mesozoic (Hack, 1982), with local westward migration in the southern Blue Ridge province since Oligocene (e.g. Spotila et al., 2004; Naeser et al., 2016). Modern catchment basins are used in this study to approximate areas which drain into the Northern, Middle and Southern North Atlantic Ocean and the Gulf of Mexico (Figure 1B).

Paleozoic Era: The Appalachian Mountains stretch from Alabama, U.S. to Newfoundland, Canada (Hatcher et al., 1989; Hatcher, 2010). The development of the Appalachian Mountains and resulting foreland basin are well-documented (e.g. Hatcher et al., 1989; Rast, 1989; Faill, 1997a; Faill, 1997b; Faill, 1998; Ettensohn, 2008; Hatcher, 2010). To briefly summarize, the Appalachian orogen was formed from 3 diachronous orogenic events: (i) the Taconic orogeny, in the Middle Ordovician to Early Silurian (ca. 472 – 436 Ma; Ettensohn, 2008), during which the eastern margin of Laurentia collided with volcanic island arc terranes (Hatcher, 2010); (ii) the Acadian orogeny, in the Early Devonian–earliest Mississippian (ca. 410 – 360 Ma; Rast and Skehan, 1993), marking the transpressional accretion of terranes to the Laurentian proto-North American craton (Ettensohn, 2008); and (iii) the Alleghanian orogeny, Early Pennsylvanian–Permian (ca. 330-265 Ma; Hatcher, 2002), which closed the Iapetus ocean from north-to-south as Gondawana rotated and collided against the southeastern margin of Laurentia to form supercontinent Pangea.

Mesozoic Era: A massive rift zone developed within Pangea during the early Mesozoic time (ca. 237 Ma), separating North America from Gondwana, beginning with the north-central Atlantic basin and progressing southward (Withjack et al., 1998; Withjack and Schlische, 2005). Rifting occurred along the entire boundary of North America and Gondwana by the Late Triassic (Withjack et al., 2012). Crustal extension produced asymmetric rift basins, bounded to the west

by extensional faults (Figure 1; Faill, 1997). During continental rifting and before development of oceanic crust, the Central Atlantic Magmatic Province (CAMP), one of the largest igneous provinces on Earth, was emplaced ca. 200 ± 4 Ma (Marzoli et al., 1999; Hames et al., 2003; Nomade et al., 2007). Igneous intrusions (e.g. basaltic lava flows and diabase sheets) in the Mesozoic rift basins are associated with the CAMP (e.g. Hames et al., 2003; Withjack et al., 2012).

As the Atlantic basin continued to open in the Early Jurassic, the margin experienced vertical crustal rebound (e.g. Faill, 1997a). This resulted in tilting of the Mesozoic rift basins and of crustal blocks in New England (Faill, 1973; Withjack et al., 2012) as well as the formation of a prominent topographic ridge along the eastern edge of the Piedmont (e.g. Hack, 1982; Faill, 1997a). Onset of seafloor spreading and the cessation of rifting along the North American margin occurred first in southeastern North America (latest Triassic) and progressed to northeastern North America by Early Jurassic and into Newfoundland by the Early Cretaceous (Schettino and Turco, 2009; Withjack et al., 2012).

Post-rift exhumation eroded the Appalachian highlands and greatly modified the Appalachian landscape (e.g. Ettensohn, 2008). Sediment was transported eastward to the newly formed Atlantic basin, extending the coastal plain, covering Mesozoic rift basins and filling offshore basins (e.g. Poag, 1992; Steckler et al., 1993). There are several generations of syn- and post-rift magmatic/thermal events recorded along the Appalachian orogen (de Boer et al., 1988). In the Early Cretaceous (ca. 120-100 Ma), the regions of northern New York (Adirondacks) and New England translated to the northwest over the Great Meteor hotspot (GMHS; Figure 1). Timing of this event and the trace of the hotspot trail NW to SE across northern North America is constrained through U-Pb dating on progressively younger kimberlitic intrusions (Heaman and

Kjarsgaard, 2000). In the Late Cretaceous, ca. 85 to 65 Ma, there was a change in the Atlantic stress regime from due to a temporary 45° shift in seafloor spreading direction from NW-SE to W-E (Klitgord and Schouten, 1986; Fairhead and Binks, 1991).

Cenozoic Era: The Early Cenozoic history is tectonically quiescent, exhibiting background erosion rates of 20-30 m/Myr (e.g. Boettcher and Milliken, 1994; Blackmer et al., 1994; Roden-Tice et al., 2009; McKeon et al., 2014; Amidon et al., 2016 Shorten and Fitzgerald, in review). The Late Cenozoic history, Oligocene to present, contains evidence to support the development of long-wavelength, low-amplitude dynamic topography due to mantle flow (e.g. Moucha et al., 2008; Miller et al., 2013; Gallen et al., 2013). Geomorphology studies in the central and southern Appalachian regions have documented Miocene (ca. 15 Ma) rock uplift and erosion of ~100-200 m (e.g. Miller et al., 2013; Gallen et al., 2013). There is also zircon fission-tracks (ZFT) and lithic detritus data to indicate that the drainage divide in the southern Appalachian migrated westward in the Oligocene and Miocene (Naeser et al., 2016). Offshore sediment flux records a 5x increase in sedimentation rates in the mid-Miocene, decreasing slightly at ca. 8 Ma (Pazzaglia and Brandon, 1996).

Database and Thermal History Interpretation Challenges

Thermal history trends were determined based on 24 published studies, Chapter 1 and Chapter 2 (Table 1 and Figure 2). Studies range across 23 catchments, drain to 4 different offshore oceanic basins, and are in 7 different physiographic provinces of the Appalachian orogen (Figure 1). The collection of data and the challenges of the thermal history trend analysis will be discussed in this section.

Database: There are 26 low-temperature thermochronology studies along the Appalachian orogen in eastern U.S. from which we collated AFT and AHe data, creating the

"Appalachian low-temperature thermochronology database" (AppLTDB; Appendix C). The

AppLTDB consists of the following information for each datapoint: location, elevation, AFT age

data and chi-squared values (when reported), AHe ages and single-grain age variation (when

reported), tectonic provinces (Hack, 1989; Soeder et al., 2014), Mesozoic rift basins (Withjack et

al., 2012), lithology (Horton, 2017), catchment area (Lehner et al., 2008) and drainage outlets.

Location and thermochronology data were collated directly from published tables and/or

georeferenced figures in ArcGIS. GoogleEarth was used to determine approximate elevation

when it was not reported. Drainage outlets (i.e. which offshore basin/ocean does the catchment

ultimately lead to) were determined from the following sources: Pazzaglia and Brandon (1996);

the HydroSHEDS database (i.e. hydrological data and maps based on shuttle elevation

derivatives at multiple scales; Lehner et al., 2008); and Hack (1989). Additional information on

source material and the AppLTDB can be found in Appendix C.

Study focus and scale: Studies from different provinces, as well as when they were

published which is important with respect to how evolved thermal modeling was at the time,

focus their analysis on constraining different regional thermal or tectonic processes. For

example, the determination of the development of relief in the Appalachian Mountains of New

Hampshire during the Cretaceous (Roden-Tice et al., 2012) or the origin and evolution of the

Blue Ridge escarpment in Virginia and North Carolina since the Mesozoic era (Spotila et al.,

2004). There are also differences in the scale of the studies. The analysis includes smaller and/or

more focused studies which constrained thermal histories and trends based on <10 samples (e.g.

Doherty and Lyons, 1980) and/or age-elevation or age-depth profiles (e.g. Reed et al., 2005;

Taylor and Fitzgerald, 2010; Amidon et al., 2016; Shorten and Fitzgerald, in prep. Chapter 2) as

well as large regional studies which include up to ~100 samples (e.g. Miller and Duddy, 1989;

Roden-Tice and Tice, 2005; Shorten and Fitzgerald, in review). Smaller and/or more focused studies can provide precise, well constrained thermal histories and exhumation through time but are limited in geographical coverage (e.g. Taylor and Fitzgerald, 2010) while regional studies provide information on the generalized thermal history over a larger area but can result in imprecise thermal histories, which may combine smaller events so that only an average cooling histories are revealed (e.g. Roden-Tice et al., 2000; Roden-Tice and Tice, 2005).

"Rapid" Cooling: Within all the studies, differential cooling rates constrained by thermal modeling are all relatively slow (i.e. <12 °C/Myr) in comparison to other tectonic settings such as young, active collisional orogens (on the order of ~40-50 °C/Myr; e.g. Thiede et al., 2004). For this paper, slow cooling is defined as cooling at rates <1 °C/Myr (e.g. Amidon et al., 2016). Slow cooling and long residence in the partial annealing zone (PAZ; ~110-60 °C), referred to as "stabilization", is due to low rates of erosion, isostatic flexure, and/or post-rift decay of the passive margin interior (e.g. Boettcher and Milliken, 1994). "Rapid" cooling is defined as cooling at rates >1 °C, usually relative to preceding or subsequent slow cooling rates constrained in thermal modeling (i.e. changing from 0.2 to 1 °C/Myr; Shorten and Fitzgerald, in review). Relatively rapid cooling may be due to several different mechanisms, such as: rock uplift caused by a combination of surface uplift and exhumation of strata; erosion due to lowering of base level bringing strata closer to surface; or geothermal gradient decreases causing strata to cool in place, also referred to as relaxation of isotherms (e.g. Malusà and Fitzgerald, 2018).

Most studies identify periods of rapid cooling through forward or inverse thermal modeling, however there are 30 AFT samples from 7 studies which record mean fission-track lengths (MTL) and distributions indicative of rapid cooling through the PAZ (Supplementary Table 2). Samples with MTL >14 µm and narrow standard distributions (<~1.5 µm) did not

reside for a significant amount of time in the PAZ and thus retain longer fission-tracks with less variation (e.g. Gleadow and Brown, 2000; Hurford, 2018). These samples are used as reference points for rapid cooling events while constraining and analyzing thermal history trends (e.g. Gleadow et al., 1986; Green et al., 1989).

Data Interpretation: Studies range in publication date, from the early 1980's to today, and contain various methods of data interpretation (i.e. schematic data-driven thermal histories, forward and inverse modeling, age-elevation profiles to estimate exhumation timing and rates). Also, AHe dating which is now a commonly applied method was not applied until the 2000's. The 26 studies all include at least AFT and/or AHe data, while some also included other geochronometers or maximum paleotemperature indicators such as ZFT or vitrinite reflectance (Table 1). Given that AFT and AHe ages are a function of their thermal history and may or may not represent a real cooling event, thermal histories cannot necessarily be interpreted simply using the closure temperature principle (c.f. Gleadow and Brown, 2000; Malusà and Fitzgerald, 2018). There are 3 included studies which interpret thermal events via closure temperatures of AFT and ZFT ages (Lakatos and Miller, 1983; Roden and Miller, 1989; Steckler et al., 1993).

Collecting samples over significant relief (i.e. vertical profiles from steep terrane) or down boreholes and plotting age vs. elevation is a useful method for determining timing and rates of apparent exhumation, in which a break in slope may reveal the timing of transition from slow, tectonically stable cooling to rapid cooling and exhumation (e.g. Fitzgerald and Malusà, 2018). There are 2 studies which rely on age-elevation profiles and 7 more which combine age-elevation profile interpretations with inverse thermal modeling (Table 1).

Modeling Programs and their Influence on Interpretation: 17 studies constrained thermal histories with forward and/or inverse thermal modeling. The challenge with interpreting

model results is that due to the range in publication date, there are several different generations of annealing algorithms utilized in forward and inverse models (Table 1). First-generation models utilize mono-kinetic annealing algorithms (Laslett et al., 1987; Crowley et al., 1991) while second-generation models utilize multi-kinetic annealing algorithms (e.g. Ketcham et al., 1999; 2007). Mono-kinetic annealing models assume modeled apatite grains contain uniform apatite composition and identical annealing characteristics as the annealing algorithm experimental samples (i.e. Durango apatites used in Laslett et al. (1987) and Crowley et al. (1991)). Given this input assumption, first-generation models often produced spurious late-stage cooling (e.g. Ketcham et al., 1999). Thus, interpretations of Late Cenozoic cooling documented using first-generation models requires geologic constraints to confirm the cooling is real and not a model artifact (e.g. Ketcham et al., 1999; de Bruijne and Andriessen, 2002). More recently, second-generation multi-kinetic annealing models characterize individual apatite grains' variability to annealing within a sample and do not produce a spurious late-stage cooling artifact (e.g. Ketcham et al., 1999). In studies that utilize second-generation multi-kinetic modeling, Late Cenozoic rapid cooling, if present, is not a model artifact and thus can be determined to be a real event with more confidence than first-generation models.

The studies utilized the following modeling techniques (summarized in Table 1): 1 early study conducted forward modeling with time-temperature paths constrained based on geologic scenarios with model results then compared to measured data; 10 studies were conducted with first-generation mono-kinetic annealing modeling programs (i.e. AFTINV; Issler, 1996); 4 studies were conducted with second-generation multi-kinetic modeling programs (i.e. HeFTy; Ketcham, 2005); and 2 studies relied mostly on inverse modeling of AHe ages with the radiation damage accumulation and annealing model (RDAAM; Flowers et al., 2009). Amidon et al.

(2016) also employed HeFTy forward models (Ketcham, 2005), to test if AHe data best fit a

linear, long-term cooling or an episodic cooling model.

Cooling History Interpretation: Most of the 26 studies indicate that samples cooled from

temperatures greater than the retentivity of fission-tracks in apatite (i.e. >~110-120 °C). There

are a few examples of western Appalachian Basin samples cooling from <120 °C because of a

shallower their burial depth prior to post-orogenic cooling (e.g. Blackmer et al., 1994; Shorten

and Fitzgerald, in review). Five studies utilize ZFT, with a closure temperature ~250 °C for

cooling rates of 1-15 °C/Myr (Doherty and Lyons, 1980; Lakatos and Miller, 1983; Roden and

Miller, 1991; Steckler et al., 1993; Roden-Tice and Wintsch, 2002). ZFT ages from those

5 studies suggest temperatures prior to the Middle Triassic were >250 °C in the Taconic and

Acadian province of New England and temperatures were ~175 °C from deposition (ca. 360 Ma)

to 125 Ma in the Catskills of New York. We acknowledge that "onset" of cooling constrained in

some studies, without the use of a higher temperature constraint, is not the onset of cooling and

exhumation from maximum temperatures but rather documents when that sample cooled into the

PAZ and began retaining fission-tracks (~110°C for AFT) (e.g. Steckler et al., 1993; West and

Roden-Tice, 2003; Kunk et al., 2005; Shorten and Fitzgerald, in review).

Cooling rates documented in the various studies may also be an averaging of short-term,

intermittent rapid and slow cooling events (e.g. McKeon et al., 2014). Averaging of differential

rates, notably in modeled time-temperature paths, may be due to the resolution of the models or

the brevity/magnitude of the rapid cooling episode(s). There are a few studies that model

samples which constrain the onset of cooling in the Early Jurassic, followed by monotonic

cooling (e.g. Roden-Tice and Wintsch, 2002; Roden-Tice and Tice, 2005). However, monotonic

cooling does not rule out episodic cooling as it may be due to averaging of more subtle peaks due to the sensitivity of the methods/models.

Onshore thermal histories related to Offshore Mid-Atlantic deposition

Pazzaglia and Brandon (1996) calculated sediment flux rates into Mid-Atlantic offshore basins (i.e. Salisbury Embayment, Baltimore Canyon Trough and Hatteras Basin; Figure 1), using estimates of siliciclastic sediment volumes from 23 stratigraphic time intervals (Poag, 1985; 1992; Poag and Sevon, 1989). Pazzaglia and Brandon (1996) determined 4 peaks in sediment flux, the volume delivered into the basins per million years (Figure 3). They suggested that the peaks are best explained by tectonic forcing causing episodic increase in onshore erosion. Thus, while they caution against the dogmatic use of their end-member tectonic model to explain increased sediment flux, they state that the model adds a quantitative prediction to the distribution, timing and magnitude of onshore erosional events in the Mesozoic and Cenozoic. Low-temperature thermochronology studies often correlate cooling and exhumation events recorded onshore to periods of increased offshore sediment flux (e.g. Reed et al., 2005; Miller et al., 2013; McKeon et al., 2014).

In similar fashion, while we acknowledge that there are variations in timing and duration seen within the studies, we use the timing of North American rifting and the four peaks in sedimentation flux to contextualize thermal history trends (Figure 3 and 4). Since Pazzaglia and Brandon's (1996) study constrained offshore sediment flux in Mid-Atlantic basins, this section only includes low-temperature thermochronology studies which currently drain into the Mid-Atlantic Ocean (Figure 3 and 4). Although there is evidence of westward shifting of drainage divides and catchment boundaries (e.g. Spotila et al., 2004; Naeser et al., 2016; Moodie et al., 2018), modern catchment basins were used as an (Figure 1B). 7 studies are located completely

outside of Mid-Atlantic drainage basin and drain into the North Atlantic (Miller and Lakatos, 1983; West and Roden-Tice, 2003; West et al., 2008; Roden-Tice et al., 2012; Amidon et al., 2016) or the South Atlantic and Gulf of Mexico (Boettcher and Milliken, 1994; Spotila et al., 2004).

Event 1. Middle Triassic to Early Jurassic (ca. 237-175 Ma)

The first event spans from the Middle Triassic to the Early Jurassic (ca. 237-175 Ma), representing cooling which is concurrent with rifting of North America from Gondwana (e.g. Withjack et al., 2012). Eleven studies located in catchments which drain to Mid-Atlantic basins identify rapid cooling beginning during event 1 (Figure 3B). These studies span across all the physiographic provinces except for the Adirondacks. Within the Adirondacks and parts of the Taconic and Acadian province, there are samples that were at temperatures greater than the PAZ during this time and thus do not record event 1 in their thermal histories (Figure 4.1).

The Taconic and Acadian province contains one study (Roden and Tice, 2005) which constrains the onset of cooling ca. 200-180 Ma, however most of the area is at temperatures greater than the PAZ. In the northern Appalachian Basin in New York and Pennsylvania, western samples from Devonian sedimentary strata were not completely reset and constrain onset of rapid cooling to ca. 187 Ma at rates of 1-3 °C/Myr (Shorten and Fitzgerald, in review). There are several northern Appalachian Basin samples with mean track lengths (MTL) >14 µm which also indicate rapid cooling between ca. 245-200 Ma (Figure 3B; Miller and Duddy, 1989). Further south in the Appalachian Basin and the Ridge and Valley province rapid cooling is constrained to begin ca. 250-245 Ma (according to one rapidly cooled sample) and continues until 180 Ma (e.g. Roden and Miller, 1989; Roden, 1991; Blackmer et al., 1994). Reed et al. (2005) also present a schematic thermal history based on VR and AFT data interpreted as closure

temperature ages in the southern Appalachian Basin which estimates slow cooling of ~0.2-0.3 °C/Myr between the late Permian to Early Cretaceous from ~145 °C to ~110 °C.

To the east, within Early Mesozoic rift basins, samples record onset of cooling from temperatures >175 °C between 225-200 Ma to temperatures near the base of the PAZ (~100 °C) by ca. 180 Ma (e.g. Roden and Miller, 1991; Steckler et al., 1999; Tseng et al., 1999). In North Carolina's Blue Ridge Mountains there is a suggestion of rapid cooling from the base of the zircon (U-Th)/He window (~160-200 °C) at ca. 250-220 Ma (Triassic) to the upper part of the AHe partial retention zone (PRZ, ~40-80 °C) by ca. 170 Ma (McKeon et al., 2014). However, this event is only constrained in one (of two) presented thermal histories and their other model does not constrain the high-temperature cooling history prior to 120 Ma (McKeon et al., 2014).

In Summary, cooling begins in the region as early as the mid-Triassic, with most studies indicating temperatures within the PAZ by the Early Jurassic. In the rift basins along the U.S. east coast and in the Acadian and Taconic province, rapid cooling at this time is mainly attributed to crustal extension and an elevated geothermal gradient associated with rifting of North America (e.g. Roden and Miller, 1991; Steckler et al., 1999; Tseng et al., 1999). The thermal effect of lithospheric extension and hydrothermal fluid flow during the continental phase of rifting caused a higher geothermal gradient which reset AFT and ZFT ages (e.g. Roden and Miller, 1991; Tseng et al., 1999). Also during continental rifting, diabase sheets and dykes were intruded ca. 200 Ma (i.e. CAMP), which may have also contributed to resetting or partially-resetting ages (Marzoli et al., 1999; Olsen et al., 2003). To the west in the Appalachian Basin and Valley and Ridge provinces cooling during event 1 is attributed to far-field affects of rifting causing a regional lowering of base level and thus increasing erosion and exhumation (e.g. Blackmer et al., 1994; Shorten and Fitzgerald, in review). Overall, the timing of event 1 and the

proposed mechanisms relate to the geologic consequences of continental rifting of North America and formation of the North Atlantic Ocean.

Event 2. Middle Jurassic to Early Cretaceous (ca. 170-140 Ma)

The second event, during the Middle Jurassic to Early Cretaceous (170-130 Ma), correlates with the first peak of offshore sediment flux increase by ~2x followed by a ~3x decrease (Figure 3C). Rapid cooling at this time is identified in 13 studies during event 2, across all provinces except for the Blue Ridge Mountains (Figure 4.2). In the Taconic and Acadian province located in New England, cooling rates of ~0.5-1 °C/Myr are constrained in regional studies located along Paleozoic contractional faults in southern Maine, Massachusetts and Connecticut (e.g. Roden-Tice and Wintsh, 2002; West et al., 2008). Models of AFT data from south-central Maine indicate cooling to temperatures <120 °C did not occur until 140 Ma (West et al., 2008), which is also suggested by one sample from western CT with an AFT age of 143 Ma with MTL >14 µm (Roden-Tice and Wintsch, 2002).

Samples from the western side of the northern Appalachian Basin constrain rapid cooling beginning in event 1 and extending until ca. 145 Ma while eastern samples continue to cool until ca. 120 Ma. To the south, within the Ridge and Valley province of Pennsylvania, AFT and ZFT samples from the Alleghenian structural front indicate rapid cooling from ca. 150-105 Ma (Roden and Miller, 1989). Along the coastal piedmont and within the Newark and Taylorsville rift basins (New Jersey and Virginia), rapid cooling at rates between ~1-4 °C/Myr are documented to begin during event 1, and extend into event 2 (Steckler et al., 1993) or continue through event 3 (Tseng et al., 1999). There is evidence of rapid cooling during this time preserved in AFT ages from samples with MTL >14 µm as well (Figure 3, Supplementary Table

2). Along the coast of the eastern U.S., the Potomac terrane of the Piedmont province constrains rapid cooling at rates of 1-2 °C/Myr (Kunk et al., 2005).

In summary, no periods of modeled cooling are entirely contained in event 2 (Figure 3B). There are studies which show a continuation of rapid cooling which began in event 1 and other studies which document the onset of cooling during event 2 and extend into event 3. Pazzaglia and Brandon (1996) suggest the offshore sedimentation increase during event 2 was due to increased onshore erosion rates caused by surface uplift due to upwelling of hot mantle during rifting. Then, the subsequent decrease in sediment flux to lower rates is attributed to thermal relaxation and loss of thermal buoyancy (Pazzaglia and Brandon, 1996). In the Taconic and Acadian province, cooling is explained by either a change in the local stress field from extension to horizontal compression causing tilting of crustal blocks (Roden-Tice and Wintsch, 2002; Roden-Tice and Tice, 2005) or a discontinuous reactivation of major orogen-parallel faults (e.g. West et al., 2008). While variable cooling recorded in Appalachian Basin at this time is likely due to differential erosional exhumation caused by differential burial (e.g. Miller and Duddy, 1989; Roden and Miller, 1989). Rift basin and Piedmont cooling is suggested to be due to differential uplift in the Jurassic (Tseng et al., 1999) and thermal relaxation in the Late Jurassic to Early Cretaceous (Steckler et al., 1993; Tseng et al., 1999) or kilometer scale Early Cretaceous tilting of crustal blocks (Kunk et al., 2005). Cooling during event 2 cannot be attributed to a unique tectonic event occurring along eastern NA and instead is a continuation of cooling due to rifting, post-rift thermal relaxation and onset of seafloor spreading.

Event 3. Early Cretaceous (ca. 133-119 Ma)

Offshore, the third event is related to a small 1x increase in sediment flux during the Early Cretaceous (ca. 133-119 Ma; Figure 3C). This event is the smallest offshore sediment

pulse and onshore there is variation in the cooling rates (Figure 4.3). Rapid cooling is seen during event 3 in 4 studies in the Taconic and Acadian province, 1 study along the southeastern edge of the Adirondacks, 1 in the Ridge and Valley, and 2 in the Mesozoic Rifts and Piedmont. However, most studies document slow cooling (< 1°C/Myr) and several studies contain both rapid and slowing cooling samples within their study area during event 3.

Within the Taconic and Acadian province, all studies constrain continuous rapid cooling since at least the Late Jurassic (Figure 3B). In the southeastern margin of the Adirondacks, at the boundary between the Adirondacks and the Taconic and Acadian province, Roden-Tice et al. (2000) suggest slightly faster cooling (0.9-1.3 °C/Myr) beginning in event 2 and continuing through event 3. However, overall rates in the Adirondacks during the Early Cretaceous are slow, ≤0.6 °C/Myr (e.g. Roden-Tice et al., 2000; Taylor and Fitzgerald, 2010).

In the northern Appalachian Basin, Miller and Duddy (1989) schematically determined that samples rapidly cooled to near surface temperatures between 140-120 Ma (red dots in Figure 4.3). They used closure temperature principles and AFT ages from samples with MTL ≥14 µm, measured using binned track lengths, and my previous chapters further discuss this interpretation. Through using precise fission-track length measurements and second-generation inverse thermal modeling, Chapter 1 and 2 of this dissertation constrains cooling at rates of ~1-2 °C/Myr began in the Early Jurassic (event 1) and continued into event 3. Samples from the eastern region of the Appalachian Basin and the Catskills record rapid cooling (1-1.5 °C/Myr) continuing from initial onset during event 1 until the end of event 3, ca. 120 Ma (Shorten and Fitzgerald, in review; Shorten and Fitzgerald, in prep. Chapter 2) while western samples constrain rapid cooling ending in event 3 and slow cooling (<0.5 °C) during event 3.

In the Appalachian Basin and the Ridge and Valley there are 2 other studies which identify differential cooling during event 3 (e.g. Roden, 1991; Reed et al., 2005). In the Appalachian Basin and Ridge and Valley of West Virginia, Roden (1991) constrains onset of rapid cooling (~1-1.5 °C/Myr) with northeastern samples while northwestern samples cooled earlier during events 1 and 2 (Figure 3B). In the same area, Reed et al. (2005) constrains rapid cooling (~1.5 °C/Myr) in Upper Pennsylvanian strata while Lower Pennsylvanian strata concurrently cool slowly (~0.8 °C/Myr). During event 3 in the Blue Ridge Mountains of Virginia and North Carolina, McKeon et al. (2014) constrains that valley bottoms cool at average rates of ~1 °C/Myr while summit ridges cool at ~0.5 °C/Myr (McKeon et al., 2014).

In summary, Event 3, in the Early Cretaceous, contains considerable variation in the documentation of rapid and slow cooling across the physiographic provinces. Event 3 is roughly coeval with when the GMHS was located to the northwest of Montreal, Canada (ca. 120 Ma) and with magmatic activity associated with GMHS in western New England and Quebec (e.g. Pazzaglia and Brandon, 1996; Heaman and Kjarsgaard, 2000). Pazzaglia and Brandon (1996) interpreted the short-term increase in sediment flux, followed by a decrease to lower rates, to support the idea that parts of northeastern U.S. were experiencing dynamically supported topography in the Early Cretaceous. This explanation accounts for the slow cooling and elevated geothermal gradient documented in the Adirondacks during event 3 (e.g. Taylor and Fitzgerald, 2010). While the Taconic and Acadian province document continuous cooling beginning in event 1 or 2 and continuing into event 3, which is most often attributed to continual cooling related to initial rifting and fault reactivation (e.g. Roden et al., 2009; 2012). To the south, in the Appalachian Basin, Ridge and Valley, and Blue Ridge Mountains, differential cooling is recorded and in previous chapters I have suggested that this difference is due to eastern samples,

buried to greater depths, experiencing greater post-orogenic exhumation (Shorten and Fitzgerald, in review; Shorten and Fitzgerald, in prep. Chapter 2). Other studies agree and relate differential cooling to landscape evolution and a more pronounced trend of stabilization in the Appalachian basin, concurrent with the development of the passive margin and possible drainage reorganization (e.g. Roden, 1991; Blackmer et al., 1994; Reed et al., 2005; McKeon et al., 2014).

Event 4. Late Cretaceous (ca. 100-65 Ma)

The fourth event occurs in the Late Cretaceous, constrained by a ~2x increase in offshore sediment flux (Figure 3C). Six studies in northeastern U.S. identify a rapid cooling event at this time (Figure 4.4). This event is the most province-specific event and is recorded onshore as two rapid cooling events, the first occurring between ca. 105-95 Ma in the Adirondacks and the second between ca. 85-65 Ma in the Taconic and Acadian province. The offshore sedimentary record records one pulse of sediment flux, which is the average of these two onshore events.

Large, regional studies in New England and the Adirondacks constrain Late Cretaceous (ca. 100-72 Ma) cooling at rates of ~0.7 -1.1 °C/Myr (Roden-Tice et al., 2009) and emphasize AFT age discontinuities and differential unroofing (e.g. Roden-Tice and Wintsch, 2002; Roden-Tice and Tice, 2005; Roden-Tice et al., 2009). An Adirondack regional study by Roden-Tice et al. (2000), identifies fault reactivation ca. 100 Ma and a period of rapid cooling ca. 110-80 Ma. Linked age-elevation profiles from Mt. Marcy in the High Peaks and Prospect Mountain provide the clearest constraints and resolve rapid cooling (~6 °C/Myr) ca. 105-95 Ma (Tayler and Fitzgerald, 2010).

Later during event 4, between 85-65 Ma there is documentation of rapid cooling at rates of 9-12 °C/Myr constrained in inverse thermal models and an age-elevation profile from the White Mountains of NH and coastal Maine (Amidon et al., 2016). AFT age discontinuities

across the Norumbega fault zone in Maine also constrain Late Cretaceous (ca. 80 Ma) rapid cooling (West and Roden-Tice, 2003). Throughout the Taconic and Acadian province, studies identify rapid cooling and fault reactivation during the Late Cretaceous (e.g. Roden et al., 2000; West and Roden-Tice, 2003; Roden et al., 2009).

In summary, studies in the Adirondacks constrain fault reactivation and movement ca. 105-95 Ma (Roden-Tice et al., 2000), which is contemporaneous with the transit of the GMHS from onshore to offshore (Figure 1 and 3B). It is suggested that this rapid cooling is due to the interplay of thermal doming causing surface uplift followed by thermal relaxation as the North American craton translated to the northwest over the hotspot until, the GMHS was located offshore ca. 100 Ma (Figure 1; Taylor and Fitzgerald, 2010). There is also regional evidence of the effects of the GMHS passage causing fault reactivation ca. 100 Ma along the eastern and southern edge of the Adirondacks (Roden-Tice et al., 2000).

Studies in the Taconic and Acadian province constrain rapid cooling and fault reactivation at the end of event 4, ca. 85-65 Ma (West and Roden-Tice, 2003; Roden-Tice et al., 2009; Amidon et al., 2016). Between ca. 85-65 Ma there was a 45° shift in Atlantic mid-oceanic ridge spreading direction from southeast-northwest to east-west (Klitgord and Schouten, 1986; Fairhead and Binks, 1991), which has been suggested as a far-field trigger for reactivation of faults and associated cooling at this time. This shift is suggested to have caused a change in the stress regime which reactivated the faults, which is a common mechanism to explain cooling documented during this event (e.g. Roden-Tice et al., 2000; Roden-Tice and Wintsch, 2002; Roden-Tice and Tice, 2005; Amidon et al., 2016). Age discontinuities across and rapid cooling documented in the Acadian and Taconic province may also be related to the effects of the

GMHS, as the thermal anomaly in the mantle may have caused NW-SE extension reactivating pre-exiting orogen parallel faults (Roden-Tice et al., 2009).

As highlighted in Figure 4.4, there are a few studies in the Southern Appalachian Basin, Blue Ridge Mountains and Rift Basins which constrain differential or continuous cooling rates during event 4 (Tseng et al., 1999; Reed et al., 2005; McKeon et al., 2014). However, the cause of these events related to a continuation of mechanisms that began in events 2-3. It is likely that cooling constrained in these studies is due to localized differential erosion and valley incision (e.g. McKeon et al., 2014; Moodie et al., 2018).

Event 5. Miocene to present (ca. 25-0 Ma)

The fifth event, spanning 25 Ma to present, marks the largest increase in offshore sediment flux (~5x; Figure 3C and 4.5), but is also the most poorly understood and most debated. There are four studies, including our work in the Northern Appalachian Basin, which have modeled Miocene cooling and concluded it is a real, significant cooling event (Blackmer et al., 1994; Boettcher and Milliken, 1994; Shorten and Fitzgerald, in review; Shorten and Fitzgerald, in prep. Chapter 2). Four studies in the Adirondacks and Taconic and Acadian provinces model rapid cooling in the Cenozoic, but state that more work is required to validate this event (e.g. Roden-Tice and Wintsch, 2002; West et al., 2008; Taylor and Fitzgerald, 2010; Roden-Tice et al., 2012). However, three of the listed studies which contain a Miocene cooling event lie outside of Mid. Atlantic drainage and thus are unlikely to contribute to the large increase in offshore sediment flux (Boettcher and Milliken, 1994; West et al., 2008; Roden-Tice et al., 2012). The challenge in revealing this event is that identification of Late Cenozoic cooling relies on thermal modeling, since the exhumation was not great enough to bring Miocene aged samples to surface (e.g. McKeon et al., 2014).

Using second-generation multi-kinetic annealing algorithms (Ketcham et al., 2007) and inverse thermal modeling (Ketcham, 2005), we have constrained Miocene rapid cooling at rates of 1-3 °C/Myr in the western/central Northern Appalachian Basin and in the Catskills (Shorten and Fitzgerald, in review; Shorten and Fitzgerald, in prep. Chapter 2). The two other studies which have modeled and accepted Miocene cooling as a real event are also within the Appalachian Basin and Ridge and Valley (e.g. Boettcher and Milliken, 1994; Blackmer et al., 1994). They constrain cooling rates of 1-2.75 °C/Myr beginning in the Late Oligocene to Early Miocene (ca. 25-20 Ma), using forward models (Blackmer et al., 1994) and first-generation inverse modeling (Boettcher and Milliken, 1994).

In Summary, there must have been no more than 2 km of Miocene exhumation within any one location, or else there would be Miocene AHe ages and possibly AFT ages (e.g. McKeon et al., 2014). A recent paper (Moodie et al., 2018) proposed that exogenic forces, such as flexural isostatic crustal response (Blackmer et al., 1994) and the development of dynamic topography (e.g. Pazzaglia and Brandon, 1996; Moucha et al., 2008), caused the westward migration of the eastern U.S. drainage divide. Thus, it is possible that cooling/exhumation is localized to the Appalachian Basin and Ridge and Valley provinces due to the westward shift of the continental divide in the Oligocene-Miocene which caused eastward flowing rivers to access the easily erodible strata of these areas (e.g. Naeser et al., 2016; Moodie et al., 2018). The mechanism controlling this cooling/exhumation remains enigmatic and, given the magnitude of cooling, there are most likely a combination of mechanisms driving cooling and causing landscape rejuvenation (c.f. Shorten and Fitzgerald, in prep. Chapter 2).

Province Thermal History Trends

To further analyze thermal history trends and expand the study to incorporate all available low-temperature thermochronology data in the eastern U.S., this section synthesizes major thermal history trends documented within individual physiographic provinces. There are challenges in comparing thermal models from different studies, as even models created from the same area may vary on details due to including different data, methods of data entry, model constraints, modeling program, and generation of annealing algorithm (Ketcham et al., 2018). However, despite the variation of details, models from the same area agree on major features and reveal key thermal history trends within provinces related to geologically relevant events. Synthesized thermal histories discussed in this section (Figure 5) include the full range of potential time-temperature paths presented in published modeled thermal histories for each province as well as a best-fit thermal history constrained by the major trends.

Taconic and Acadian

In the Taconic and Acadian province, regional studies constrain cooling at rates of ~0.6-2 °C/Myr, on average ~1 °C/Myr, beginning ca. 200 Ma and continuing until ca. 100 Ma (Figure 5A). There is documentation of differential cooling related to structural depth/elevation, resulting in the range of cooling contained in figure 5A (e.g. Roden-Tice and Tice, 2005; Roden-Tice et al., 2009; Roden-Tice et al., 2012; West et al., 2008). For example, along an age-elevation profile of Mt. Washington in New Hampshire, high elevation samples document cooling at ~1 °C/Myr during the Late Jurassic (160-140 Ma) while low elevation samples document cooling at ~2 °C/Myr during the Early Cretaceous (ca. 110-90 Ma; Roden-Tice et al., 2012).

While some regional studies constrain slow cooling in the Late Cretaceous, there is evidence in the White Mountains in New Hampshire of rapid cooling (9-12 °C/Myr) occurring

between ca. 85-65 Ma (e.g. Amidon et al., 2016). Several other studies in the Taconic and Acadian province also document Late Cretaceous cooling related to compressive fault reactivation causing as much as ~2 km of west-side-up vertical movement (e.g. Roden et al., 2000; West and Roden-Tice, 2003; Roden et al., 2009). As discussed in event 4, this cooling event may be related to a change in the stress regime due to a 20 Myr shift in seafloor spreading direction to more east-west direction (Klitgord and Schouten, 1986; Fairhead and Binks, 1991).

Since ca. 65 Ma, cooling histories across the Taconic and Acadian province converge with slow cooling to present day conditions (Figure 5). There is Miocene cooling event recorded in first-generation models, but most studies indicated that this event is an artifact of the annealing algorithm and/or that more research is needed to determine if it is a real event (e.g. Roden-Tice and Wintsch, 2002; West et al., 2008; Roden-Tice et al., 2012) The prevailing explanation for the Cenozoic cooling history of the region is that by the end of the Cretaceous the relief was established across New England and steady-state topography has persisted through the Cenozoic to the present (e.g. Roden-Tice et al., 2012).

Adirondacks

In the Adirondacks, the thermal history is the most different from the surrounding provinces and begins with slow cooling (≤0.5 °C/Myr) from the Middle Jurassic to Early Cretaceous (Figure 5B; Miller and Lakatos, 1983; Roden-Tice et al., 2000; Taylor and Fitzgerald, 2010). The slow cooling documented throughout the High Peaks suggests the Adirondacks were experiencing a relatively stable thermal and tectonic regime with samples resident at temperatures at or above the PAZ for long periods during the Middle Jurassic through Early Cretaceous (ca. 175-110 Ma; Roden-Tice et al., 2000; Taylor and Fitzgerald, 2010). Within the end of the Early Cretaceous (ca. 120-100 Ma), northeastern U.S. passed over the GMHS

(Figure 1) and, due to the proximity to the Adirondacks, there was an elevated geothermal gradient estimated at ~60-38 °C/Km (e.g. Taylor and Fitzgerald, 2010).

In the Late Cretaceous, ca. 105-95 Ma, the Adirondacks clearly resolves rapid cooling (~6 °C/Myr; Figure 5B). As previously discussed in event 4, it is suggested that rapid cooling is due to the interplay of thermal doming causing surface uplift followed by thermal relaxation as the North American craton translated to the northwest over the hotspot until, the GMHS was located offshore ca. 100 Ma (Figure 1; Taylor and Fitzgerald, 2010). There is also regional evidence of the effects of the GMHS passage causing fault reactivation ca. 100 Ma along the eastern and southern edge of the Adirondacks (Roden-Tice et al., 2000; Figure 5). Since the late Cretaceous rapid cooling event, the Adirondacks have slowly cooled to present day conditions (e.g. Roden-Tice et al., 2000; Taylor and Fitzgerald, 2010). There is some indication for an increase in cooling rates during the Miocene to present however resolution of this event is questioned and needs closer examination (e.g. Taylor and Fitzgerald, 2010).

Appalachian Basin/ Ridge and Valley

In the Appalachian Basin and Valley and Ridge province, rapid cooling (~1-2 °C/Myr) from temperatures above the PAZ began in the Early Jurassic and continued until the mid-Early Cretaceous (Figure 5C; e.g. Boettcher and Milliken, 1994; Shorten and Fitzgerald, in review). There is a general trend of AFT ages decreasing from west to east (e.g. Roden, 1991; Blackmer et al., 1994; Shorten and Fitzgerald, in review) and a range of AFT ages with MTL >14 µm, ranging from 246-114 Ma (Supplementary Table 2), measured using binned track lengths by Miller and Duddy (1989). Younger ages in the east are due to greater burial, resulting in samples passing through the PAZ at later times and cooling faster (~2 °C/Myr) than western samples (~1 °C/Myr). Cooling and exhumation in the Appalachian Basin and Ridge and Valley

are suggested to be due to lowering of regional base levels as the Atlantic Ocean opened causing higher rates of incision and erosion of the landscape, as well as a flexural feedback response as material is removed (e.g. Roden, 1991; Blackmer et al., 1994; Shorten and Fitzgerald, in review).

Beginning in the Early Cretaceous and extending until the Oligocene to Miocene, there is no record of rapidly cooled AFT ages and most thermal histories constrain slow cooling (~0.2-0.6 °C/Myr; e.g. Roden, 1991; Reed et al., 2005; Shorten and Fitzgerald, in review). This period marks a stabilization of terrain in the Appalachian Basin and Ridge and Valley province (e.g. Blackmer et al., 1994; Shorten and Fitzgerald, in review). Most of the orogenic overburden was removed during rifting and post-rift erosional exhumation, and the stabilization is likely a result of no additional overburden to be removed and the transition of the eastern U.S. to a passive margin.

Inverse thermal modeling of the Appalachian Basin and Ridge and Valley strata reveals rapid cooling from ca. 25 Ma to recent (e.g. Blackmer et al., 1994; Boettcher and Milliken, 1994; Shorten and Fitzgerald, in review). Miocene offshore sediment flux estimates require an average of >1.1 km of rock to be removed across the region that drains into the Middle Atlantic Basin (Figure 1 and 3C), but it does not indicate that erosion was uniform across the catchments (e.g. Braun, 1989; McKeon et al., 2014). Two recent studies in the central and southern Ridge and Valley and Blue Ridge Mountain provinces suggested a westward migration of the drainage divide in the Oligocene and Miocene, which gave catchments access to more easily erodible Valley and Ridge and Appalachian Basin detritus (Naeser et al., 2016; Moodie et al., 2018). Offshore sedimentation flux, geomorphologic studies and mantle flow simulations indicate that rapid cooling documented in event 5 may be due to the development of dynamic topography causing landscape rejuvenation (e.g. Pazzaglia and Brandon, 1996; Moucha et al., 2008; Miller et

al., 2013; Gallen et al., 2013). Although this event results in the largest increase in offshore sediment flux, the resolution of an onshore signature and determining the mechanisms are the most enigmatic of all the events.

Blue Ridge Mountains

The Triassic to Jurassic thermal history of the Blue Ridge Mountains is not well constrained, since the low-temperature thermochronology studies conducted in the region primarily utilized AHe dating (e.g. Spotila et al., 2004; McKeon et al., 2014). ZFT ages (Naeser et al., 2016) and available inverse models based on AHe data (McKeon et al., 2014) indicates that the area cooled between ca. 250-170 Ma at rates of ~1-1.5 °C/Myr from temperatures >150 °C to within temperatures of the AHe PRZ (~30-90 °C; Figure 5D). In the Cretaceous, from ca. 120-80 Ma, McKeon et al. (2014) constrain differential cooling in the Blue Ridge Mountains, with samples from the valley bottoms cooling approximately twice as rapidly as nearby ridge tops. This differential cooling is suggested to be due to short, episodic periods of valley incision and drainage reorganization (McKeon et al., 2014). Since ca. 80 Ma, the Blue Ridge Mountains may have slowly cooled to present day (Figure 5). However, there is ZFT data (e.g Naeser et al., 2016) and drainage divide discrepancies with topography (e.g. Moodie et al., 2018) which indicate that that drainage divide moved westward past the Blue Ridge Mountains into the Appalachian Basin in the Oligocene-Miocene. This migration may have caused an Oligocene-Miocene cooling event in the Blue Ridge Mountains, but if there was a cooling event it must account for ≤2 km of sediment removal via exhumation since there are no Miocene AHe ages (e.g. Spotila et al., 2004; McKeon et al., 2014).

Mesozoic Rift Basins

Mesozoic rift basins (i.e. Hartford, Deerfield, Newark and Taylorsville basins) along the east cost of the U.S. record cooling at rates of ~1-2 °C/Myr from the Late Triassic through the Late Jurassic (e.g. Roden and Miller, 1991; Steckler et al., 1999; Tseng et al., 1999). There is a range of AFT ages which indicate rapid cooling (196-136 Ma; Figure 5E and Supplementary Table 2), which may extend initial cooling into the earliest Early Cretaceous. There are also differences in the onset of cooling recorded across basins (e.g. Roden and Miller, 1991; Tseng et al., 1999). For example, samples in the eastern part of the Taylorsville basin (Virginia) began to cool ca. 30 Myr earlier than western samples (Tseng et al., 1999). This difference in timing may be related to the westward tilt of the rift basins (e.g. Withjack et al., 2012) and/or hydrothermal fluid flow along the western boarder fault during rifting (e.g. Steckler et al., 1999). Overall, rates indicate rapid cooling from the Late Triassic to Late Jurassic, which is likely due to rifting, compression of isotherms, and the subsequent post-rift the relaxation of the isotherms (e.g. Roden and Miller, 1991; Steckler et al., 1999; Tseng et al., 1999). Coastal-plain sediments were deposited over top of the rift basins in the Early Cretaceous, marking the end of rapid cooling related to exhumation (Steckler et al., 1999; Figure 5E). Since the Early Cretaceous, the Mesozoic rift basins cooled slowly to present day conditions and the coastal-plain sediments were removed by slow but steady erosion associated with Late Cretaceous sea-level fall and glaciation (e.g. Steckler et al., 1999).

Piedmont

The low-temperature thermal history of the piedmont, outside of the Mesozoic rift basins, is discussed only in Kunk et al. (2005) and contains similar temporal trends as the Mesozoic rift basins with differences in cooling rate. The coastal piedmont rapid cools at rates of 3-4 °C/Myr,

cooling to temperatures within the PAZ beginning in the Early Jurassic with rapid cooling continuing into the earliest Early Cretaceous (Figure 5F). There are two rapidly cooled AFT ages, 131 Ma in the western region of their study and 179 Ma in the east (Kunk et al., 2005; Supplementary Table 2). Kunk et al. (2005) note that AFT ages become older from west to east, spanning ca. 70 Myr, and attribute this pattern to differential amounts of cooling in the Cretaceous due to westward tilting of the Potomac terrane in the piedmont. Basin tilting and older ages in the east compared to the west was also noted in Mesozoic rift basins (Tseng et al., 1999). Tilting is related to the rifting and onset of seafloor spreading and rapid cooling ceases at ca. 150 Ma in the Piedmont. Since initial rapid cooling, the area has likely slowly cooled to present day at rates ~0.1-0.5 °C/Myr (Figure 5E).

Conclusions

This study presents a comprehensive synthesis of low-temperature data from 26 studies scattered across the Appalachian orogen of the eastern U.S. to constrain the cooling and exhumation history at a variety of scales (i.e. across catchments which drain into the Mid-Atlantic, within physiographic provinces, and across the orogen as a whole). The cooling and exhumation history of onshore regions that drain into Mid-Atlantic basins correlates well with rifting of the eastern U.S. and periods of increased sediment flux into offshore Mid-Atlantic basins. Province thermal histories, composed through synthesizing the available low-temperature thermochronology data and thermal models, identify major orogen-scale trends and localized, province-specific trends (figure 5).

1. Across the orogen, except for the Adirondacks, relatively rapid cooling is constrained from temperatures above the PAZ beginning in the Late Triassic to Early Jurassic (ca. 237-175 Ma). This orogen-wide, rapid cooling and exhumation event is contemporaneous with

rifting of the eastern U.S. and the formation of the Atlantic Ocean (i.e. event 1, rifting).

Within the Appalachian Basin and Ridge and Valley province, western samples cool to

temperatures within the PAZ earlier than eastern samples. This is due to differential burial

and hence differential exhumation during the initial unroofing phase (e.g. Roden, 1991;

Blackmer et al., 1994; Shorten and Fitzgerald, in review). Often, due to differential burial,

AFT-constrained cooling will not be recorded until the Middle Jurassic to Early Cretaceous

(ca. 170-140 Ma). The Middle Jurassic to Early Cretaceous also includes the first pulse in

offshore sediment flux calculated by Pazzaglia and Brandon (1996), referred to in the chapter

as event 2 (Figure 3). There is also variation in the timing of cooling closer to the coast as

recorded in Mesozoic rift basins and Piedmont, likely a result of westward block rotation

during rifting and extension (e.g. Steckler et al., 1993; Kunk et al., 2005). While the variable

rapid cooling and exhumation history suggests different mechanisms are operating at a

smaller scale or within a localized region, these mechanisms are likely all related to rifting

and erosional exhumation occurring at the orogen-scale through the eastern U.S. during the

Late Triassic to Cretaceous.

2. Within the Cretaceous, there is greater variation between province cooling histories. In the

Early Cretaceous (ca. 133-119 Ma; i.e. event 3), it appears that the eastern U.S. experienced a

period of tectonic quiescence and slow cooling with the continued evolution of the passive

margin. In comparison, in the Late Cretaceous (ca. 100-65 Ma; i.e. event 4), there are two

province-specific onshore events which resulted in an increase of sediment in the offshore

Mid-Atlantic basins. In the Adirondacks there is rapid cooling ca. 105-95 Ma. This has been

related to the passage of the GMHS (e.g. Taylor and Fitzgerald, 2010). In the Taconic and

Acadian province there is rapid cooling along normal faults ca. 85-65 Ma, which has been

related to compressional reactivation of faults during a ~20 Myr shift in the direction of seafloor spreading along the Mid-Atlantic ridge (e.g. Amidon et al., 2016). During the Cretaceous, the Appalachian Basin, Ridge and Valley and Blue Ridge Mountains also record differential cooling, albeit at slower than initial rates, likely due to continuing erosional exhumation (e.g. Roden, 1991; Blackmer et al., 1994; Reed et al., 2005) and/or episodic periods of valley incision and drainage reorganization (e.g. McKeon et al., 2014). In general, the eastern U.S. continues to cool through the Cretaceous with variations related to differential mechanisms influencing different regions.

3. The Cenozoic history for the eastern U.S. on the orogen-scale consists mainly of slow cooling to present day. However, from the Miocene to present (ca. 25-0 Ma), studies in the Appalachian Basin and Valley and Ridge province constrain relatively rapid cooling (e.g. Blackmer et al., 1994; Boettcher and Milliken, 1994; Shorten and Fitzgerald, in review; Shorten and Fitzgerald, in press). The ability to distinguish this period of cooling in low-temperature thermochronology data is often beyond the sensitivity of the method (e.g. Spotila et al., 2004; McKeon et al., 2014; Shorten and Fitzgerald, in review). However, with the use of AFT's kinetic parameter, several studies have concluded that Miocene cooling is real and significant (e.g. Blackmer et al., 1994; Boettcher and Milliken, 1994; Shorten and Fitzgerald, in review; Shorten and Fitzgerald, in press). So far, Miocene cooling and exhumation appears to be localized within catchments that drain into the Mid-Atlantic basins and relates to the largest offshore sediment pulse (event 5). It is likely that Miocene cooling is due to drainage reorganization and the westward migration of the continental drainage divide during the Oligocene-Miocene, allowing for increase erosional exhumation of Appalachian and Ridge and Valley provinces (e.g. Naeser et al., 2016; Moodie et al., 2018).

Figures and Tables
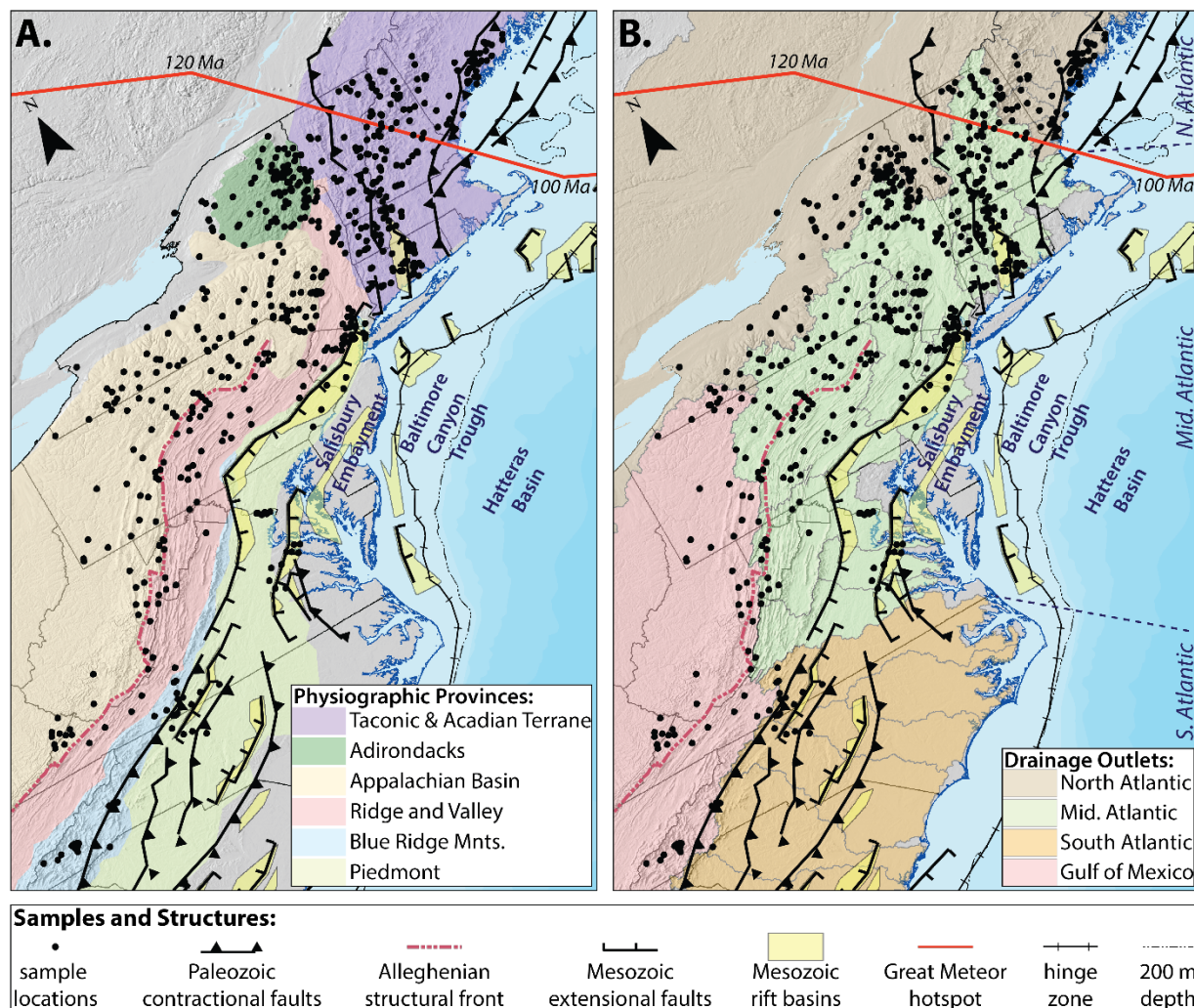
Figure 1. Map of eastern U.S. illustrating the sample locations from the 26 low-temperature thermochronology studies, structural features and rift basins (Withjack et al., 2012), path of the Great Meteor Hotspot (Heaman and Kjarsgaard, 2000), continental hinge zone, bathymetry (200 m depth and 1000 m shading), and the Middle (Mid.) Atlantic offshore basins (i.e. Salisbury embayment, Baltimore Canyon trough, Hatteras basin; Pazzaglia and Brandon, 1996) as well as the northern (N.) and southern (S.) Atlantic offshore basins. (A) General physiographic provinces (Hack, 1989; Soeder et al., 2014) and (B) catchments (Lehner et al., 2008) and drainage outlets (Hack, 1989; Pazzaglia and Brandon, 1996). Maps rotated 30° counterclockwise.
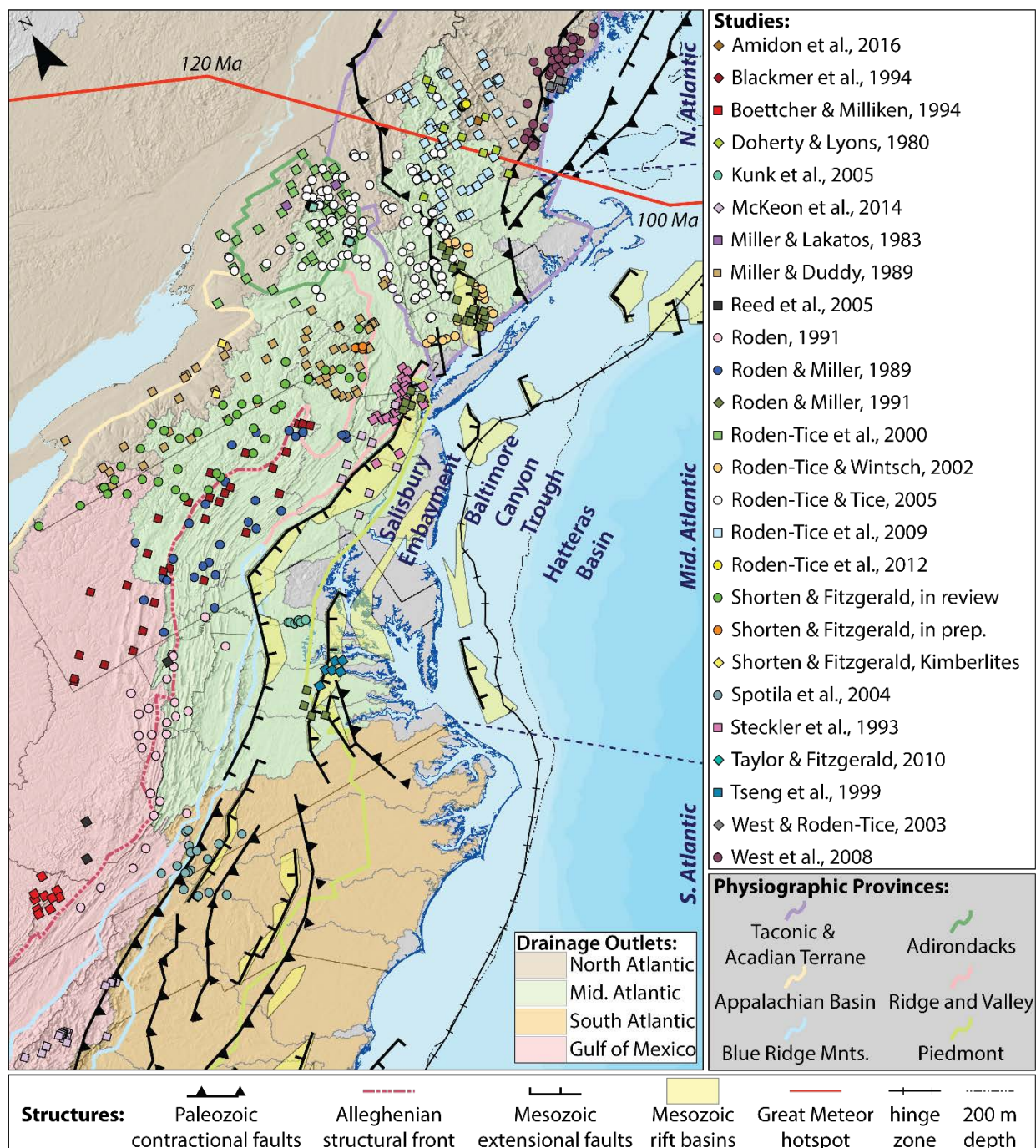
Figure 2. Map of eastern U.S. with sample locations from the 26 low-temperature thermochronology studies by color and symbol. Also included are the outline of the physiographic provinces (same colors as Figure 1), structural features and rift basins (Withjack et al., 2012), path of the Great Meteor Hotspot (Heaman and Kjarsgaard, 2000), continental hinge zone, bathymetry (200 m depth and 1000 m shading), and the Middle (Mid.) Atlantic offshore basins (i.e. Salisbury embayment, Baltimore Canyon trough, Hatteras basin; Pazzaglia and Brandon, 1996). Map rotated 30° counterclockwise.
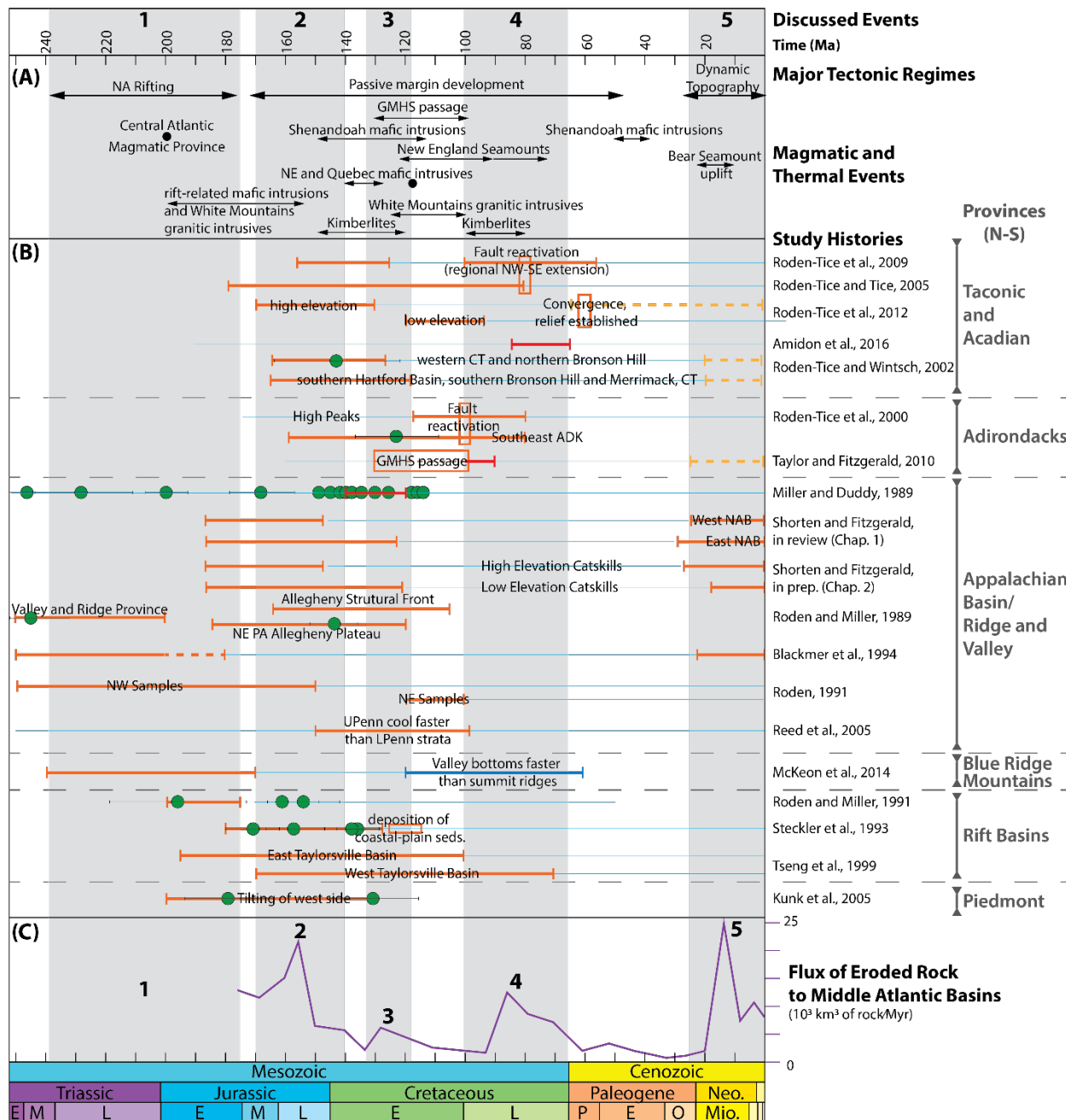
Figure 3. Comparison of modeled thermal histories (within catchments which drain into Mid. Atlantic) to geological events and offshore Mid. Atlantic sedimentation flux, highlighting the 5 periods of cooling discussed in text (grey shading). (A) Major tectonic regimes (Withjack et al., 1998; Moucha et al., 2008) and the syn- and post-rift magmatic intrusions of the eastern U.S. (de Boer et al., 1988; Pazzaglia and Brandon, 1996; Marzoli et al., 1999; Olsen et al., 2003). (B) Timing and duration of thermal events identified within low-temperature thermochronology studies which drain into the Mid. Atlantic, arranged from north to south and grouped by physiographic province. Colors and thickness differentiate periods and timing of very rapid cooling (>5 °C/Myr, red), rapid cooling (≥1 °C/Myr, orange), and slow cooling (<1 °C/Myr, blue). Green circles (± 1σ) are AFT ages with MTL >14 μm which indicate rapid cooling.

Figure 3. (continued) (C) Volume of solid-rock delivered into the Mid. Atlantic Basins (i.e. Salisbury Embayment, Baltimore Canyon Trough, and Hatteras Basin) per million years by mechanical erosion (i.e. sediment flux; Pazzaglia and Brandon, 1996).
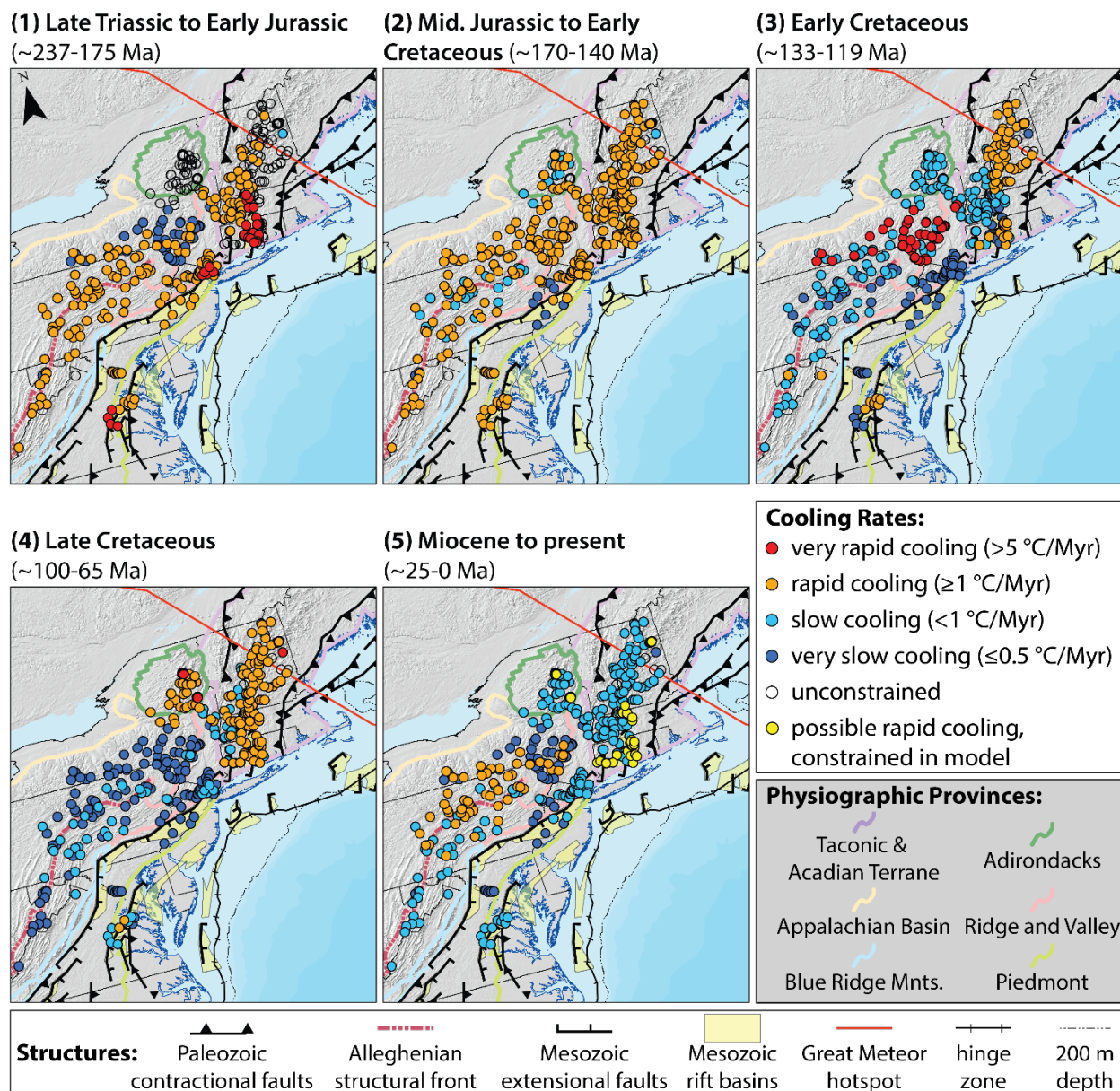
Figure 4. Maps of low-temperature thermochronology samples that lie within catchments which drain into Mid. Atlantic, colorized by rate of cooling during the 5 events discussed. Open circles indicate when a sample's thermal history does not include and/or constrain time-temperature paths within a time range. Yellow circles indicate model constrained Miocene cooling, which requires additional research to determine if it is real or which is an artifact of a first-generation annealing algorithm. Map rotated 15° counterclockwise.
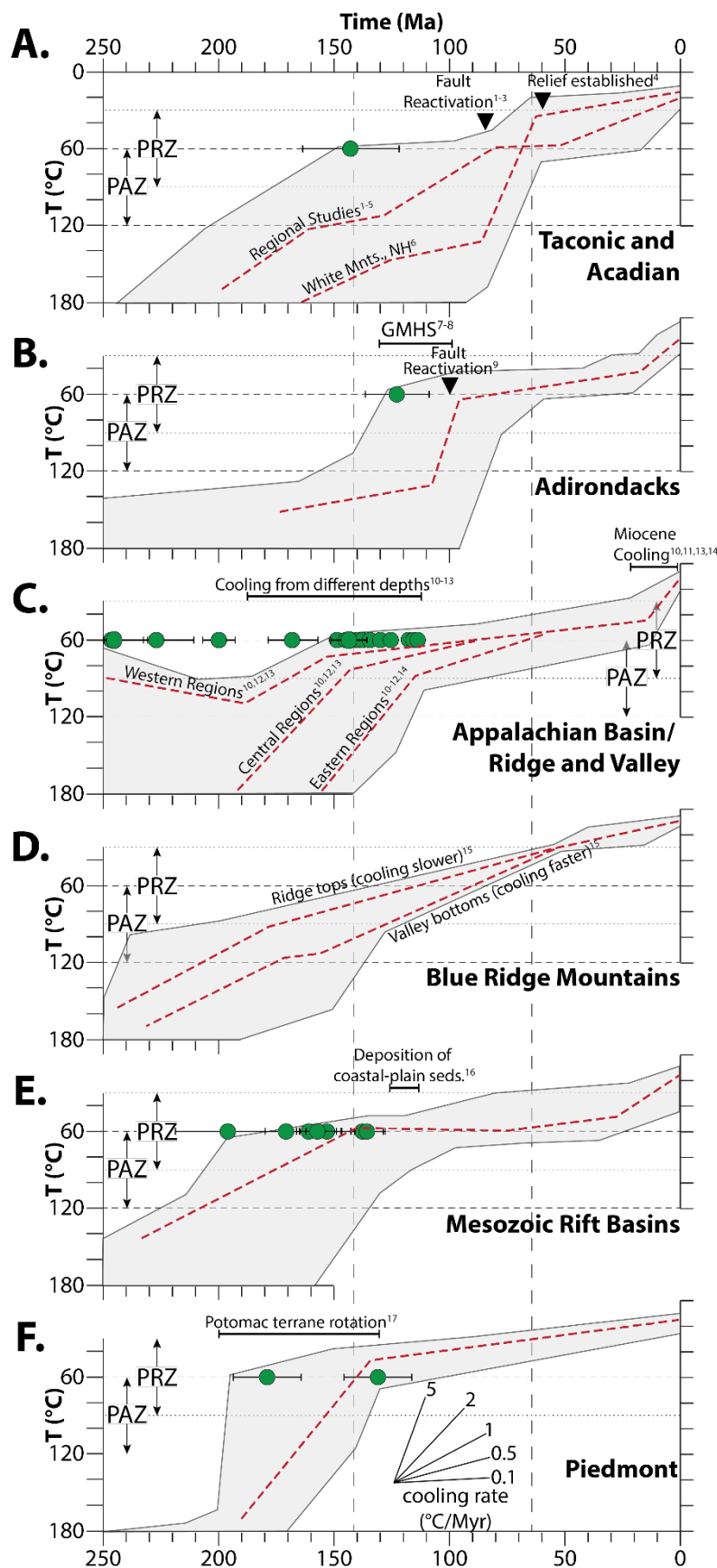
Figure 5. Schematic thermal history diagrams by province. Grey envelope represents the range of potential time-temperature (T-t) paths and the red dashed line is the best-fit thermal history constrained by published studies. AFT age of samples with mean track lengths >14 µm indicate rapid cooling (green circles ± 1σ). Timing and duration of relevant geologic events included. Dashed T-t paths illustrate differential cooling histories constrained within the province. Figure references: West and Roden-Tice, 2003[1]; Roden-Tice and Tice, 2005[2]; Roden-Tice et al., 2009[3]; Roden-Tice et al., 2012[4]; West et al., 2008[5]; Amidon et al., 2016[6]; Heaman and Kjarsgaard, 2000[7]; Taylor and Fitzgerald, 2010[8]; Roden-Tice et al., 2000[9]; Shorten and Fitzgerald, in review[10]; Shorten and Fitzgerald, in prep.[11]; Roden, 1991[12]; Blackmer et al., 1994[13]; Boettcher and Milliken, 1994[14]; McKeon et al., 2014[15]; Steckler et al., 1993[16]; Kunk et al., 2005[17].

Table 1. Summary of information in Eastern North America Low-temperature Thermochronology Studies

Study	Location (States)	Methods Measured	Where catchments drain to (% of Samples)	Provinces samples lie within (% of Samples)	Rock Type	Age-Elevation Profile	Low-T Therm. Modeling	Details
Amidon et al., 2017	NH	AFT, AHe, Zr U-Pb, U/Th zonation profiles	100% North Atlantic	100% Taconic/Acadian Terrane	Igneous	AFT and AHe	Forward and Inverse	modeling of AFT and AHe age data: two forward models in HeFTy and inverse in QTQt
Blackmer et al., 1994	PA	AFT and VR	69% Mid. Atlantic, 31% Gulf of Mexico	62% Appalachian Basin, 38% Valley and Ridge	Sedimentary	-	Forward	AFT annealing algorithm: Laslett et al., 1987; approach: Green et al., 1989
Boettcher & Milliken, 1994	KY & VA	AFT	100% Gulf of Mexico	100% Blue Ridge Mnts.	Sedimentary	-	Inverse	AFT annealing algorithm: Carlson, 1990; program: Corrigan, 1991
Doherty & Lyons, 1980	VT & NH	AFT and ZFT	78% Mid. Atlantic, 22% North Atlantic	100% Taconic/Acadian Terrane	Igneous	-	-	thermal conduction models, no AFT models
Kunk et al., 2005	VA & MD	AFT and Ar-Ar	100% Mid. Atlantic	100% Piedmont	Metamorphic	-	-	Schematic thermal history diagrams and Ar-Ar spectra
Lakatos and Miller, 1983	NY	AFT and ZFT	100% Mid. Atlantic	100% Appalachian Basin	Sedimentary	-	-	thermal trends based on AFT and ZFT ages and closure temperatures
McKeon et al., 2014	NJ, PA, NC & SC	AHe and Zhe	57% Gulf of Mexico, 27% Mid. Atlantic, 17% South Atlantic	73% Blue Ridge Mnts., 17% Valley and Ridge, 10% Piedmont	Metamorphic	AHe	Inverse	HeFTy models of AHe data (RDAAM; Flowers et al., 2009).
Miller & Lakatos, 1983	NY	AFT	100% North Atlantic	100% Adirondacks	Metamorphic	AFT	-	age-elevation profile used to estimate exhumation
Miller & Duddy, 1989	NY	AFT	74% Mid. Atlantic, 19% North Atlantic, 7% Gulf of Mexico	86% Appalachian Basin, 14% Valley and Ridge	Sedimentary	-	-	Schematic thermal history diagrams based on AFT data
Reed et al., 2005	WV	AHe, VR, fluid inclusion	50% Gulf of Mexico, 50% Mid. Atlantic	100% Appalachian Basin	Sedimentary	-	-	Schematic, exhumation rates calculated from T_{max}, AFT and AHe ages
Roden, 1991	MD, VA & WV	AFT	50% Gulf of Mexico, 46% Mid. Atlantic, 4% South Atlantic	69% Valley and Ridge, 31% Appalachian Basin	Sedimentary	-	Inverse	AFT annealing algorithm: Laslett et al., 1987; approach: Green et al., 1989
Roden & Miller, 1989	PA	AFT	96% Mid. Atlantic, 4% Gulf of Mexico	70% Valley and Ridge, 30% Appalachian Basin	Sedimentary	-	-	thermal history based on AFT data (ages and CTLDs) and their closure temperatures
Roden & Miller, 1991	MA, CT, NY, NJ & VA	AFT and ZFT	100% Mid. Atlantic	66% Taconic/Acadian Terrane, 31% Piedmont, 3% Valley and Ridge	Metamorphic & Sedimentary	-	Inverse	AFT annealing algorithm: Laslett et al., 1987
Roden-Tice et al., 2000	NY & VT	AFT and AHe	65% North Atlantic, 35% Mid. Atlantic	91% Adirondacks, 5% Appalachian Basin, 2% Taconic/Acadian Terrane, 2% Valley and Ridge	Metamorphic	-	Inverse	AFT annealing algorithm: Crowley et al., 1991; program: AFTINV (Issler, 1996)
Roden-Tice & Wintsch, 2002	CT, MA & NH	AFT, AHe, ZFT	100% Mid. Atlantic	100% Taconic/Acadian Terrane	Metamorphic & Sedimentary	-	Inverse	AFT annealing algorithm: Crowley et al., 1991; program: AFTINV (Issler, 1996)
Roden-Tice & Tice, 2005	NY, VT, NH, MA & CT	AFT and AHe	57% Mid. Atlantic, 43% North Atlantic	46% Taconic/Acadian Terrane, 44% Adirondacks, 7% Valley and Ridge, 2% Appalachian Basin, 1% Canada	Metamorphic & Sedimentary	AFT	Inverse	AFT annealing algorithm: Crowley et al., 1991; program: AFTINV (Issler, 1996)
Roden-tice et al., 2009	NH, ME & VT	AFT	70% Mid. Atlantic, 30% North Atlantic	100% Taconic/Acadian Terrane	Igneous & Metamorphic	-	Inverse	AFT annealing algorithm: Crowley et al., 1991; program: AFTINV (Issler, 1996)
Roden-tice et al., 2012	NH	AFT	100% North Atlantic	100% Taconic/Acadian Terrane	Metamorphic	AFT	Inverse	AFT annealing algorithm: Ketcham et al., 2007; program: HeFTy v1.6.7 (Ketcham, 2005)
Shorten & Fitzgerald, in review	NY & PA	AFT, AHe, CAI	71% Mid. Atlantic, 24% Gulf of Mexico, 5% North Atlantic	100% Appalachian Basin	Sedimentary	-	Inverse	AFT annealing algorithm: Ketcham et al., 2007; program: HeFTy v1.9.1 (Ketcham, 2005)
Shorten & Fitzgerald, in press Chap. 2	NY	AFT and AHe	100% Mid. Atlantic	100% Appalachian Basin	Sedimentary	AFT and AHe	Inverse	AFT annealing algorithm: Ketcham et al., 2007; program: HeFTy v1.9.1 (Ketcham, 2005)
Spotila et al., 2004	VA & NC	AFT and AHe	88% South Atlantic, 12% Gulf of Mexico	65% Piedmont, 35% Blue Ridge Mnts.	Metamorphic	AFT and AHe	-	used age-elevation profiles but no thermal modeling
Steckler et al., 1993	NY, PA & NJ	AFT and ZFT	100% Mid. Atlantic	62% Valley and Ridge, 38% Piedmont	Sedimentary, Igneous &	-	-	thermal history based on AFT data (ages and CTLDs) and ZFT ages and their closure temperatures
Taylor & Fitzgerald, 2010	NY	AFT and AHe	100% North Atlantic	100% Adirondacks	Metamorphic	AFT and AHe	Inverse	AFT annealing algorithm: Ketcham et al., 1999; program HeFTy (Ketcham, 2005)
Tseng et al., 1999	VA	AFT, Microthermometry, Gas Chromatography	100% Mid. Atlantic	100% Coastal Plain	Sedimentary	AFT depth profile	Inverse	AFT annealing algorithm: Laslett et al., 1987
West & Roden-Tice, 2003	ME	AFT	100% North Atlantic	100% Taconic/Acadian Terrane	Metamorphic & Sedimentary	-	Inverse	AFT annealing algorithm: Crowley et al., 1991; program: AFTINV (Issler, 1996)
West et al., 2008	ME & NH	AFT and AHe	97% North Atlantic, 3% Mid. Atlantic	100% Taconic/Acadian Terrane	Sedimentary, Igneous & Metamorphic	-	Inverse	AFT annealing algorithm: Crowley et al., 1991; program: AFTINV (Issler, 1996)

Methods measured only includes the methods that were calculated/measured in the study. Percent of samples located within drainage outlets (where catchments drain to) and provinces were determined using ArcGIS and published figures (e.g. Poag, 1992; Pazzaglia and Brandon, 1996). Modern United States postal code abbreviations used for states. HeFTy (Ketcham, 2005), QTQt (Gallagher, 2012), and AFTINV (Issler, 1996) are thermochronometric and maximum paleotemperature modeling software packages. AFT - apatite fission track; AHe - apatite (U-Th)/He dating; Zr - zircon; ZFT - zircon fission track; ZHe - zircon (U-Th)/He dating; VR - vitrinite reflectance; CAI - conodont alteration index; Mid. - Middle; Mnts. – Mountains; RDAAM - radiation damage accumulation and annealing model.

Appendices

Appendix A: Supplementary material for Chapter One

Supplementary File A. AFT Sample Matrix

Sample ID	State	Lat.	Long.	Elev. (m)	Dep. Age	Depositional Group	Formation	Ref. Map
Western Region								
36N	NY	42.226	-78.260	504	LD	Conneaut	Cattaragus facies	2,3
37N	NY	42.100	-78.443	455	LD	Conneaut	Cattaragus facies	2,3
38N	NY	42.083	-78.634	447	LD	Conneaut	Chemug facies	2,3
39P	PA	41.971	-78.630	403	LD	Conneaut	Chadakoin	4,5
40P	PA	41.824	-78.386	618	LD	Catskill facies	Catskill	1
42P	PA	41.904	-78.087	498	LD	Conneaut	Chadakoin	4,5
51N	NY	42.073	-79.745	443	LD	Conewango	Oswayo and Venango	2,3
53N	NY	42.026	-79.064	618	LD	Conewango	Oswayo and Venango	2,3
Central Region								
3P	PA	41.827	-75.774	336	LD	Catskill facies	Catskill	1
4P	PA	41.812	-75.885	499	LD	Catskill facies	Catskill	1
5P	PA	41.736	-76.297	394	ED	underlies Catskills (Canadaway	Lockhaven	1
7P	PA	41.521	-76.231	365	LD	Catskill facies	Catskill	1
8P	PA	41.423	-76.489	570	EM	above Catskill	Burgoon Sandstone	1
9P	PA	41.363	-77.082	233	LD	Catskill facies	Catskill	1
10P	PA	41.441	-77.101	384	LD	Catskill facies	Catskill	1
15N	NY	42.068	-75.572	464	LD	West Falls	Upper Walton	2,3
17N	NY	42.075	-76.042	328	LD	West Falls	Upper Walton	2,3
19N	NY	42.126	-76.270	233	LD	West Falls	Upper Walton	2,3
20N	NY	42.033	-76.412	304	LD	West Falls	Upper Walton	2,3
21N	NY	42.014	-76.566	396	LD	West Falls	Gardeau	2,3
22N	NY	42.090	-77.041	359	LD	West Falls	Nunda	2,3
24N	NY	42.152	-77.313	315	LD	West Falls	Nunda	2,3
28Pc	PA	41.365	-77.680	~ 1 km depth	ED	underlies Catskills (Canadaway	Lockhaven	1
34N	NY	42.366	-77.453	384	LD	West Falls	Nunda	2,3
35N	NY	42.305	-77.884	592	LD	Canadaway	Machias	2,3
43P	PA	41.757	-77.903	621	LD	Catskill facies	Catskill	1
55P	PA	41.525	-77.737	373	LD	Catskill facies	Catskill	1
56P	PA	41.284	-77.319	180	LD	Catskill facies	Catskill	1
57N	NY	42.538	-77.559	453	LD	West Falls	Nunda	2,3
KS3	NY	42.259	-76.518	337	LD	West Falls	Upper Walton	2,3
Eastern Region								
45N	NY	41.949	-74.961	390	LD	West Falls	Upper Walton	2,3
48N	NY	41.673	-74.713	442	LD	West Falls	Upper Walton	2,3
49N	NY	41.595	-74.539	428	MD	Hamilton	Moscow	2,3
50N	NY	41.957	-75.239	341	LD	West Falls	Upper Walton	2,3
G12	NY	42.342	-75.406	339	MD	Hamilton	Moscow	2,3
P12	NY	41.854	-74.762	552	LD	West Falls	Upper Walton	2,3
15.2	NY	42.228	-74.237	595	MD	Hamilton	Moscow	2,3

Samples listed numerically within regions.

Lat.: Latitude; Long.: Longitude; Elev.: Elevation; Dep. Age: Depositional age; Ref. Maps: Reference maps

EM: Early Mississippian (359-345 Ma); LD: Late Devonian (383-359 Ma); MD: Middle Devonian (393-383 Ma); ED: Early Devonian (419-393 Ma)

See next page for reference (ref.) maps.

Supplementary File B. Inverse Thermal Models

In this supplementary file, the development of post-depositional constraints and inverse
thermal models which did not work are discussed. Then, the models for all 38 of the samples are
presented. All samples were modeled using inverse thermal modeling in HeFTy (Ketcham, 2005)
and in this supplementary file the following information is presented for each sample: the time-
temperature history path envelopes (good paths in purple and acceptable paths in green), the
best-fit (black path) and weighted mean path (thick blue path), and the constraint boxes which
includes stratigraphic age and paleo-temperature (olive box; Woodrow et al., 1973); AFT track
length distribution, calculated track length distribution based on best-fit path; model goodness-
of-fit (GOF) statistics and the age of the oldest fission track that has not been completely
annealed ("Old"; Ketcham, 2005); AHe diffusion profile and GOF statistics when present; and
vitrinite reflectance (%R_o) output, which includes modeled and measured values (">" sign means
the %R_o calculation does not include a depositional event).

B1.   Development of post-depositional constraints used in inverse thermal modeling

Several iterations of models were run to determine the most likely thermal histories. First,
only the provenance (Acadian/Taconic sources; Ver Straeten, 2009), stratigraphic/depositional
age (Table 1) and paleo-temperature (25 ± 10 °C; Woodrow et al., 1973), and present-day
conditions (5 ± 5 °C; Hijmans et al., 2005) were used to constrain inverse thermal models
(Attempt 1). However, using only these constraints produced no good or acceptable paths. The
addition of a large post-depositional constraint box, ranging from ca. 360-0 Ma and ~0-190 °C,
allowed the models to explore the T-t space and begin to constrain T-t paths (Attempt 2).
Another constraint box was then added to resolve the Cenozoic thermal history (60-0 Ma), but
the box was left wide (0-100 °C) so as not to force paths to resolve a rapid cooling event

(Attempt 3). Finally, based on the thermal history trends constrained by the broad constraint

boxes (attempts 1-3) and the geologic events affecting the eastern North America, the constraint

boxes were further divided to better resolve the post-depositional thermal history (Attempt 4).

Constraint boxes are not tightly constrained by temperature but are divided into the following

time ranges: (1) ca. 360-200 Ma (deposition and rifting of eastern North America); (2) ca. 200-

60 Ma (post-rift passive margin development); (3) ca. 60-0 Ma (Cenozoic history and

development of dynamic topography). Note that with every attempt and addition of relevant

constraint boxes the goodness-of-fit statistics for the best-fit T-t path increased.

Attempt 1. Provenance, stratigraphic and present-day condition constraints only. For all models
10,000 paths were tried, with no constrained good or acceptable paths.

51N, Western
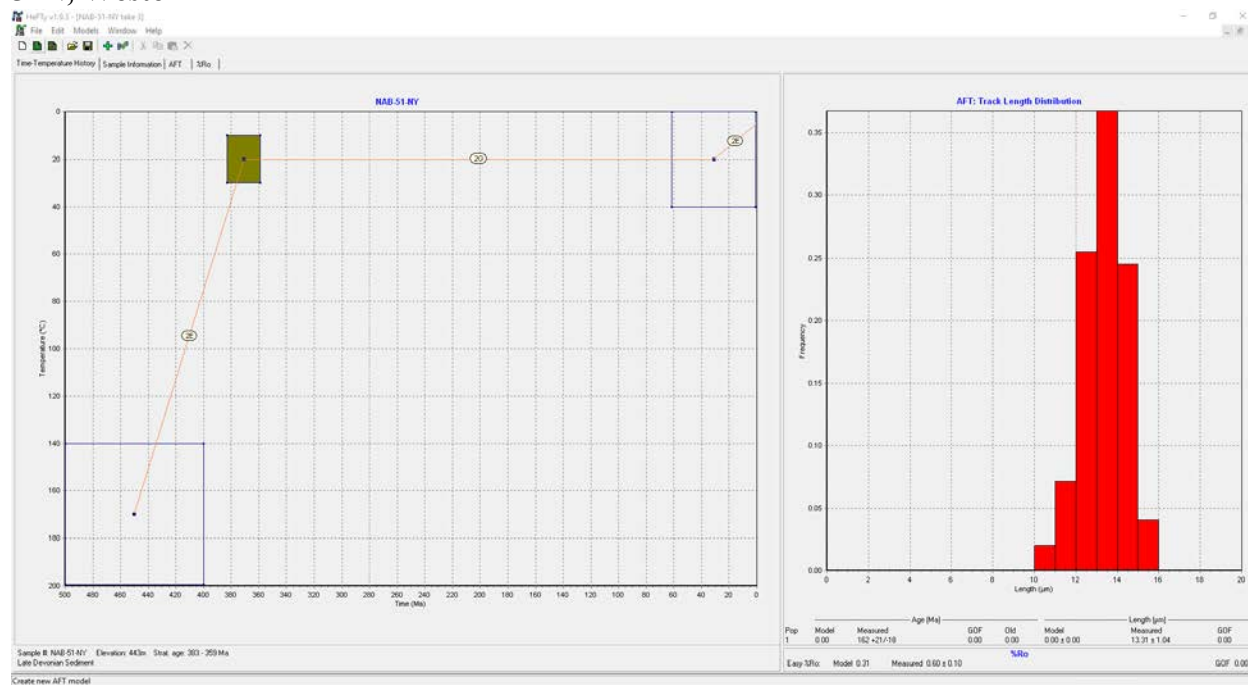
55P, Central
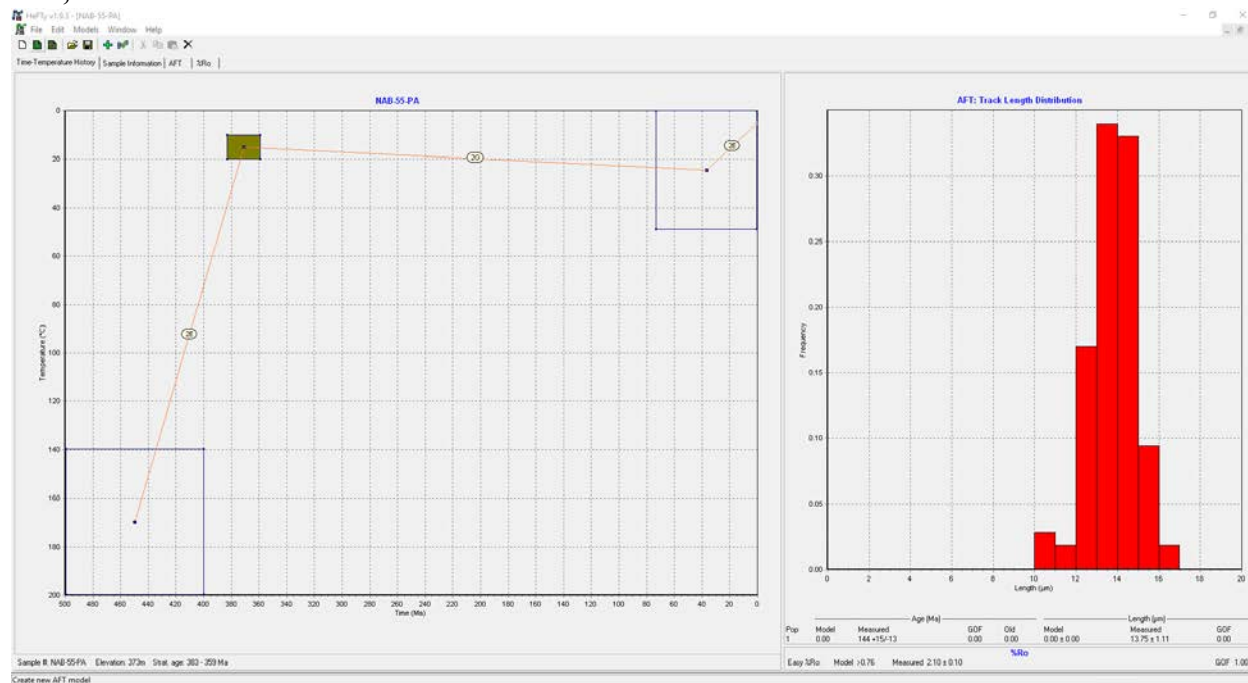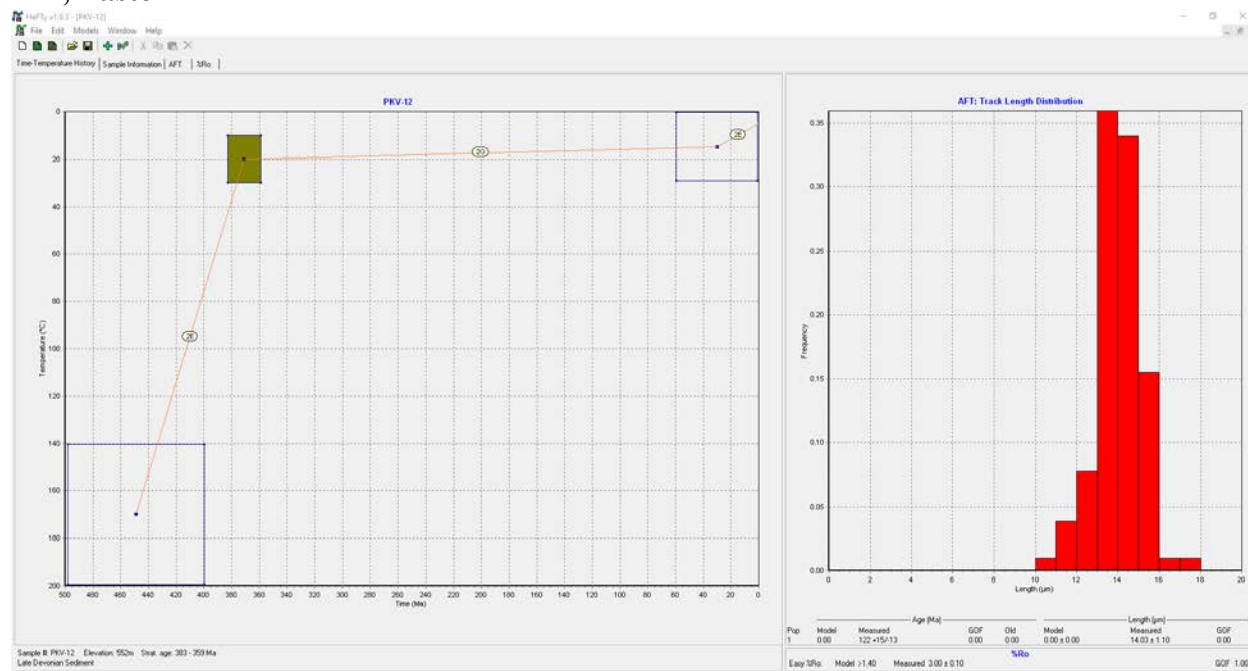
P12, Eastern

Attempt 2. Provenance, stratigraphic and large constraint box post-deposition. For all models 10,000 paths were tried with various resolution of thermal histories.

51N, Western
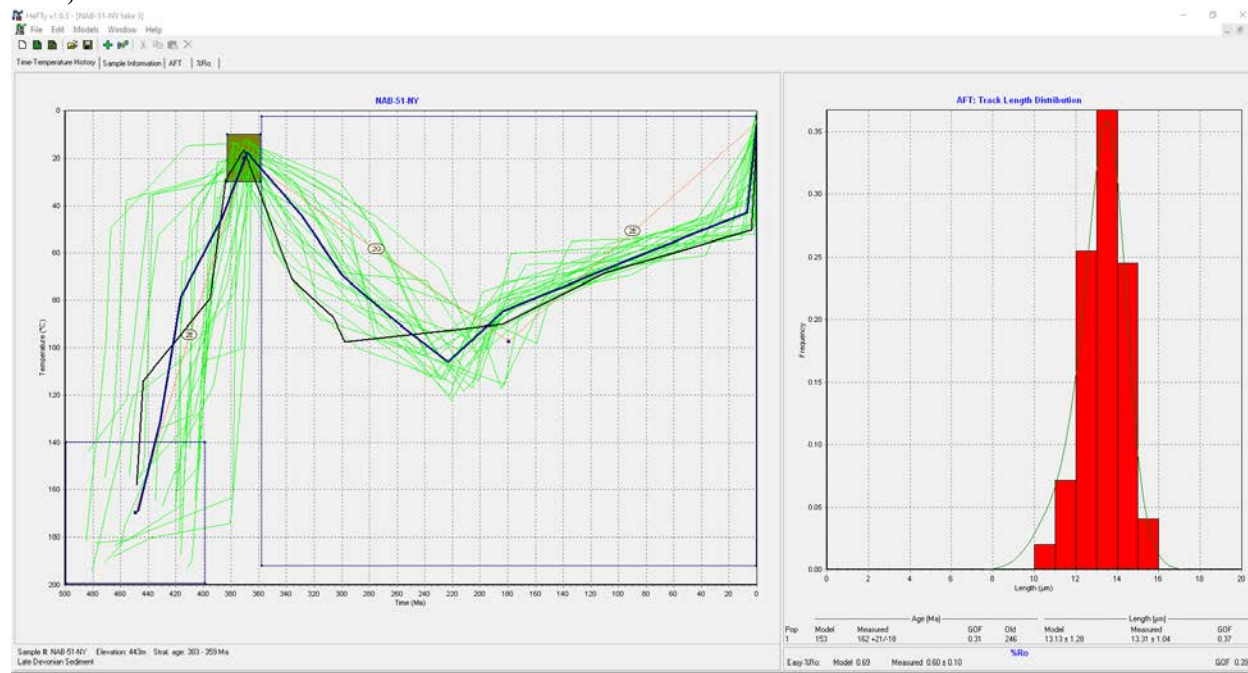
55P, Central
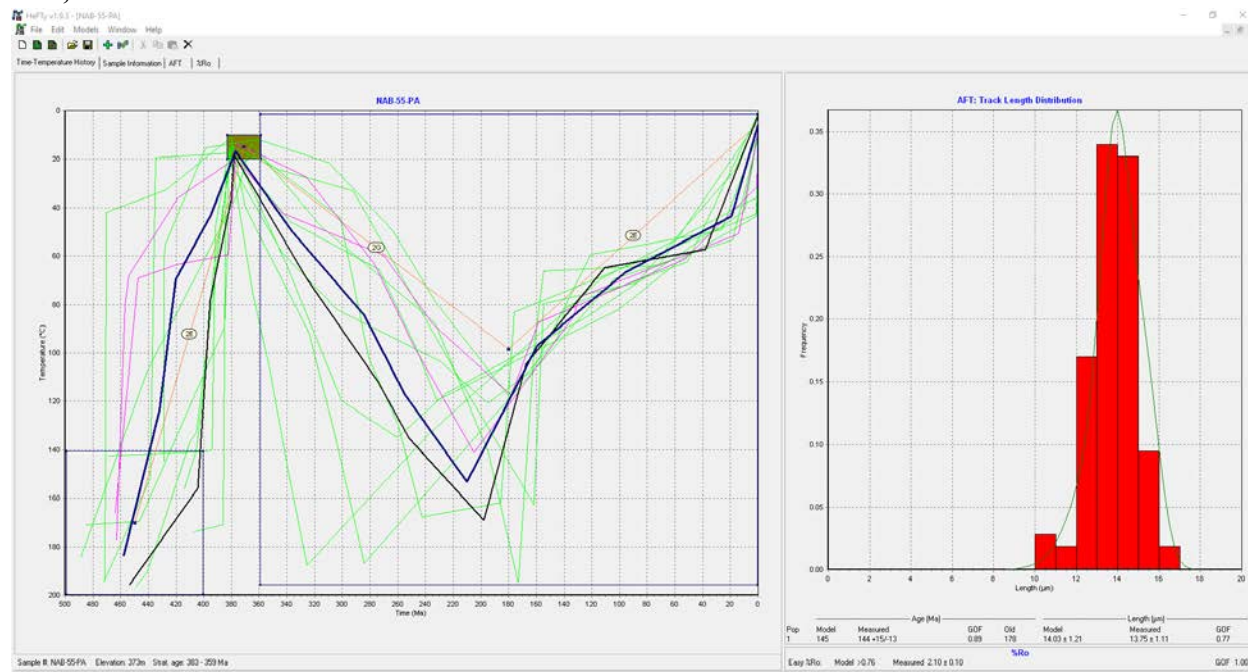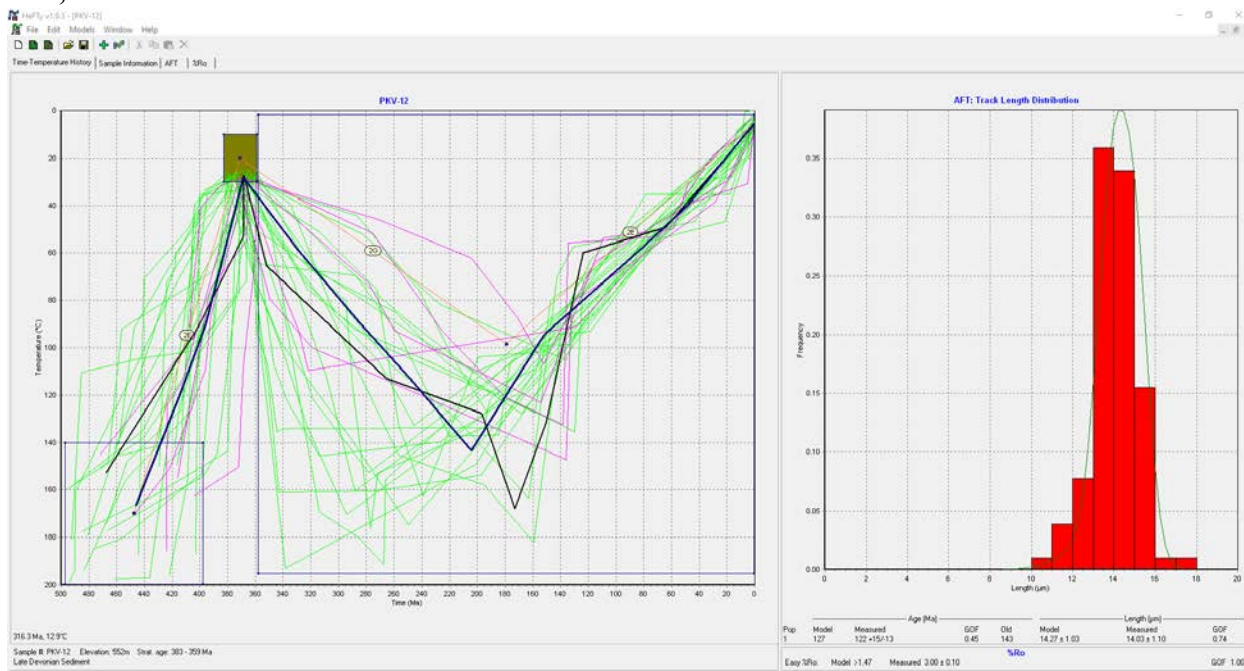
P12, Eastern

Attempt 3. Provenance, stratigraphic and two post-deposition constraint boxes with one focused on the Cenozoic thermal history. For all models 10,000 paths were tried.
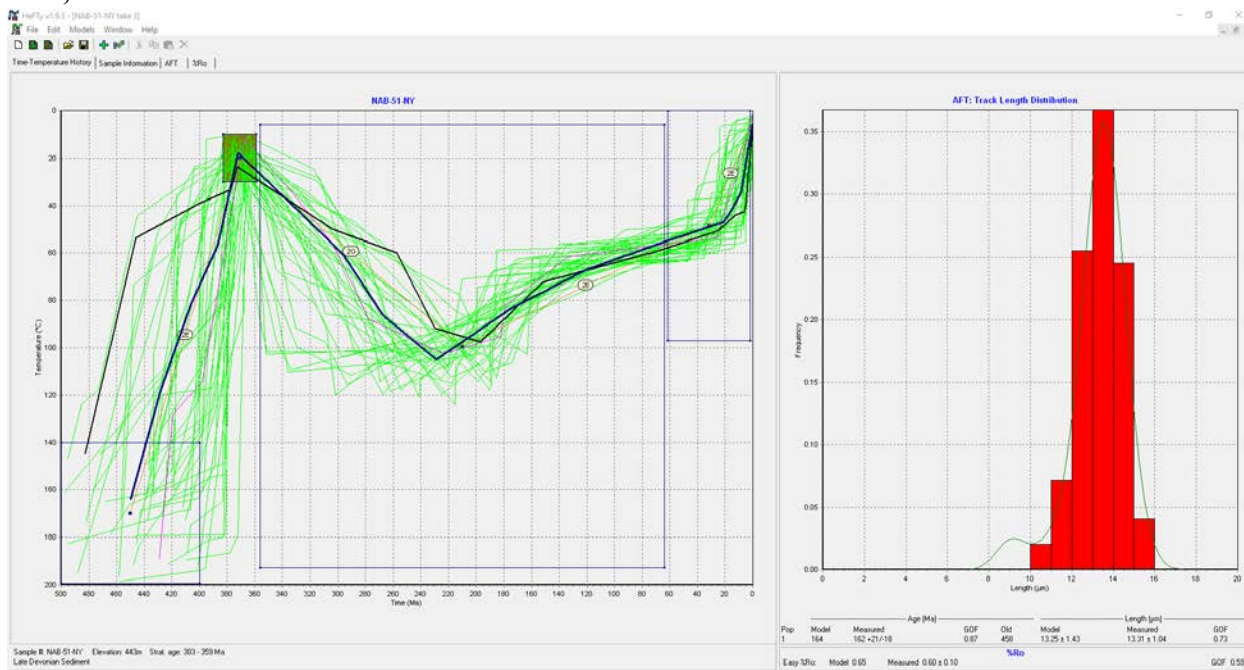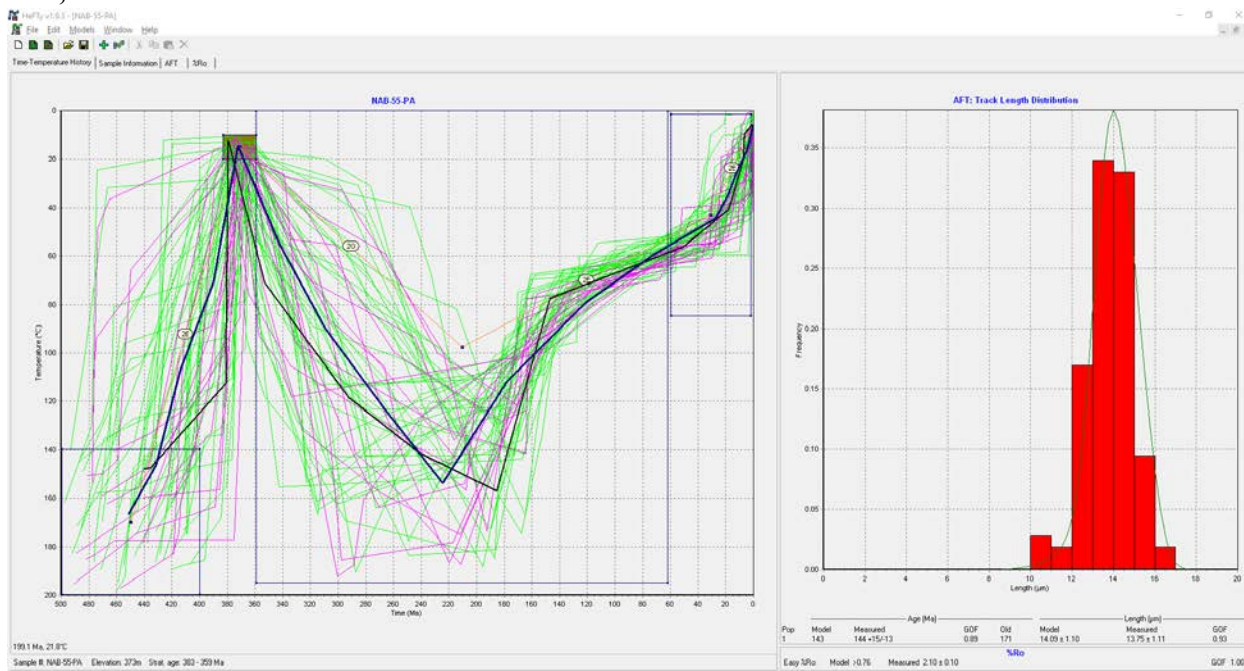
51N, Western
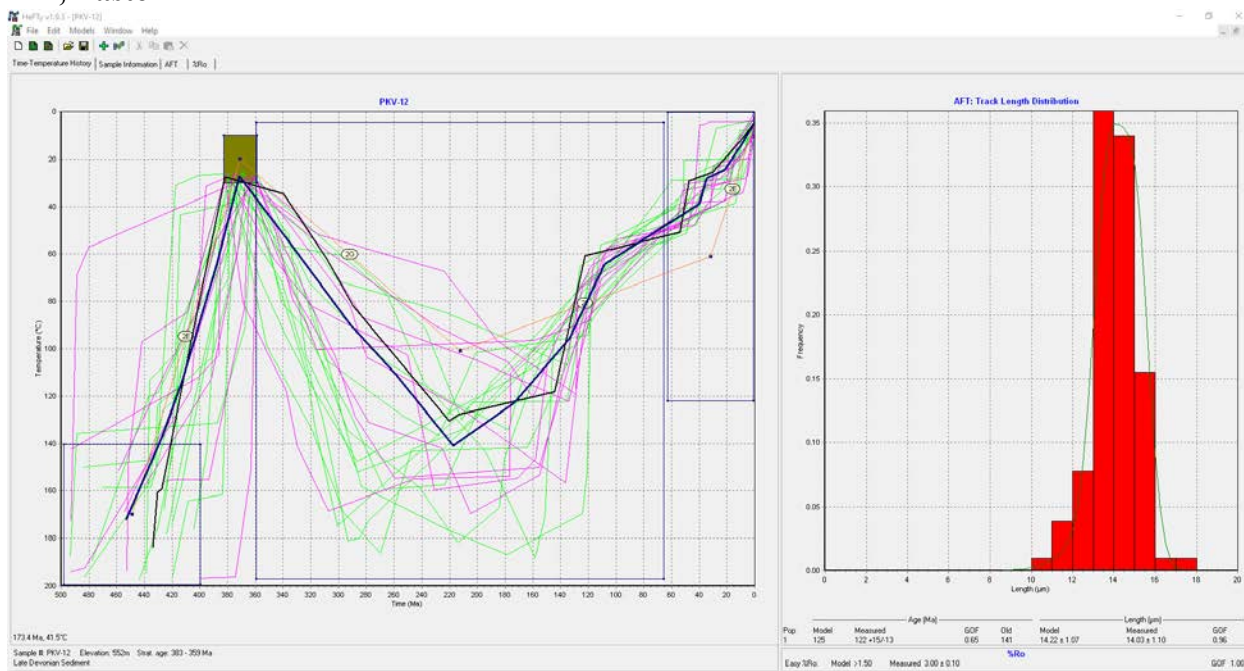
Attempt 4. Provenance, stratigraphic and three post-deposition constraint boxes. Both time-temperature paths and constraint points are shown. Points may represent local temperature minimums or maximums and can be useful in examining times/temperatures of peak heating and onset of changes in cooling rate constrained by inverse thermal models (Ketcham, 2005).

51N, Western

Paths
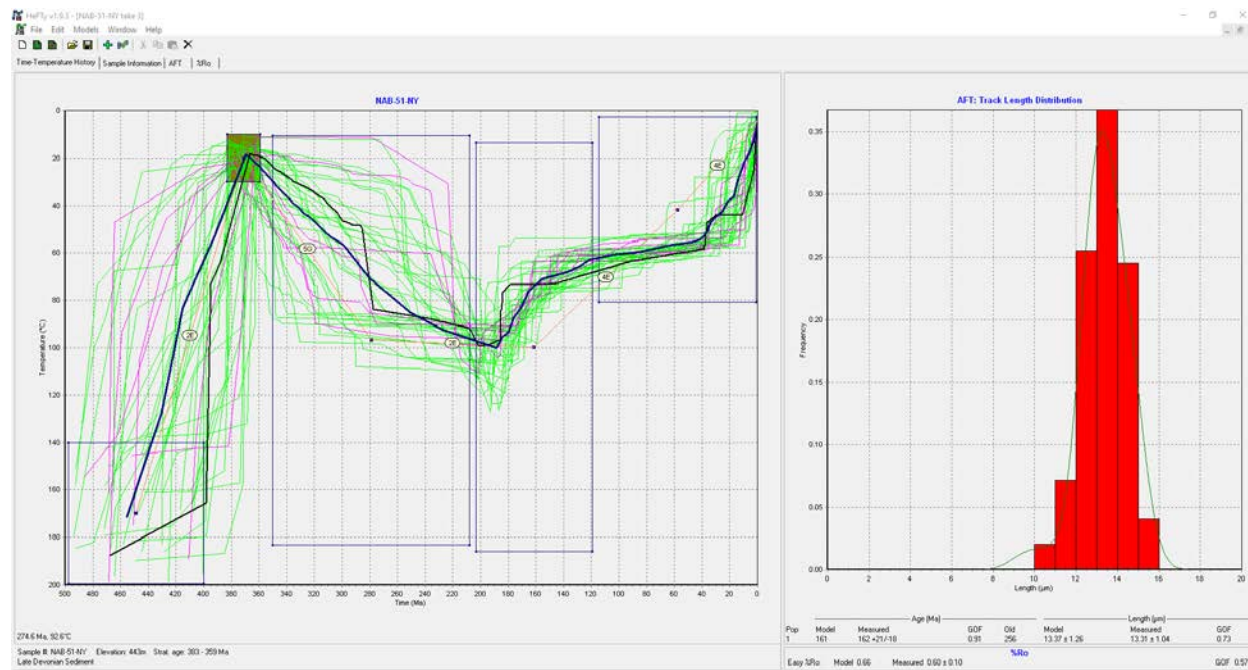
Constraint points
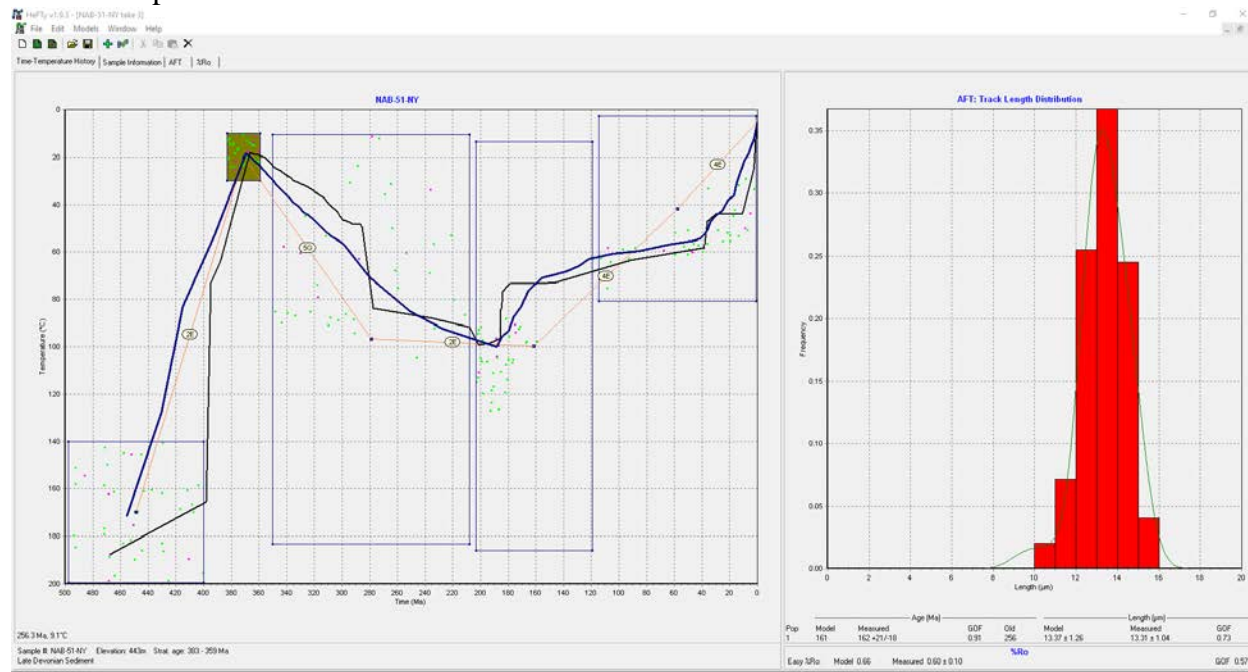
55P, Central

Paths
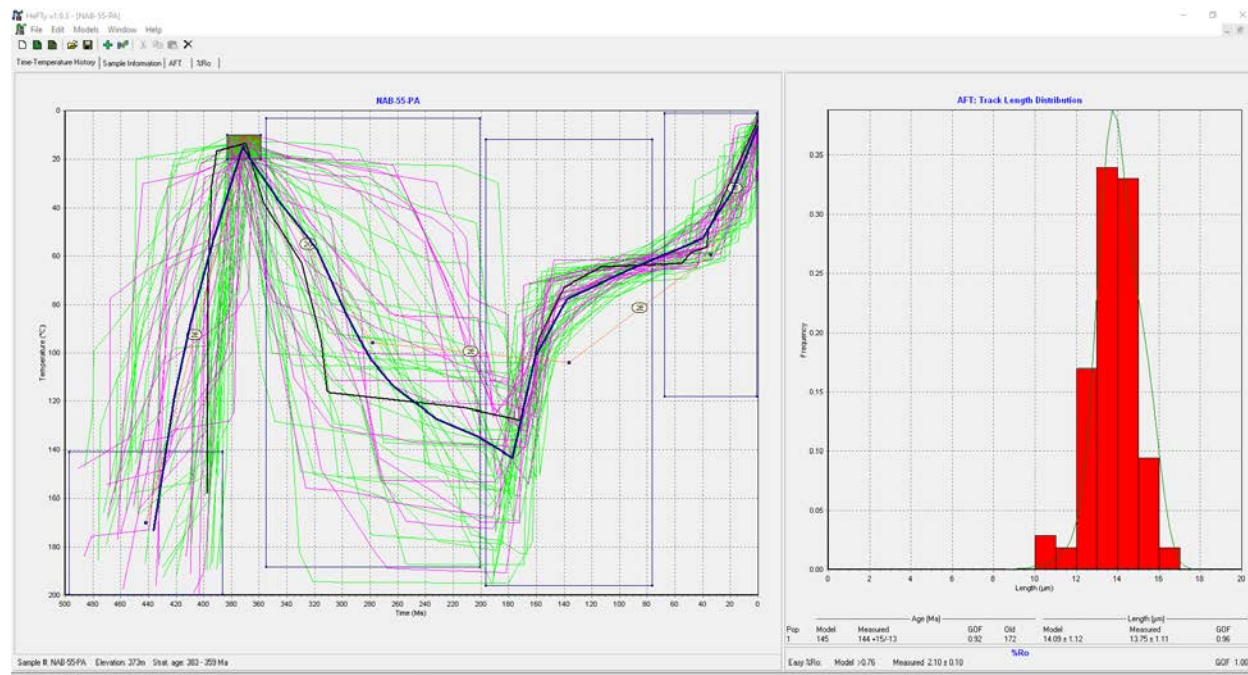
Constraint points
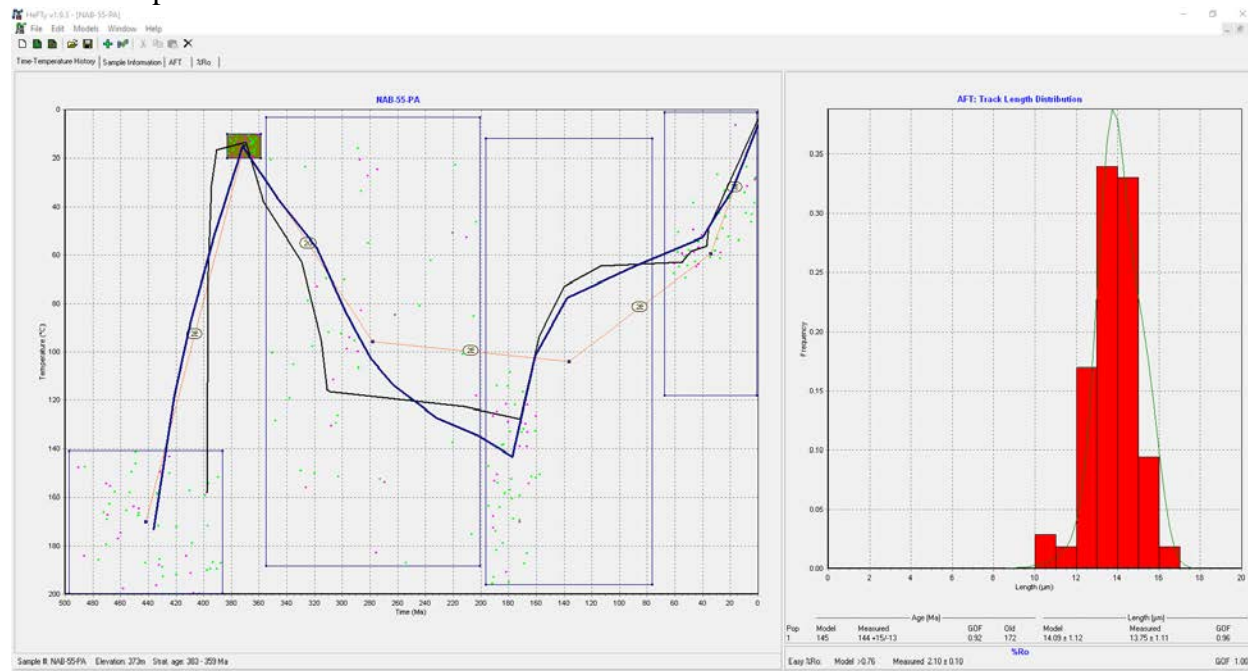
P12, Eastern

Paths
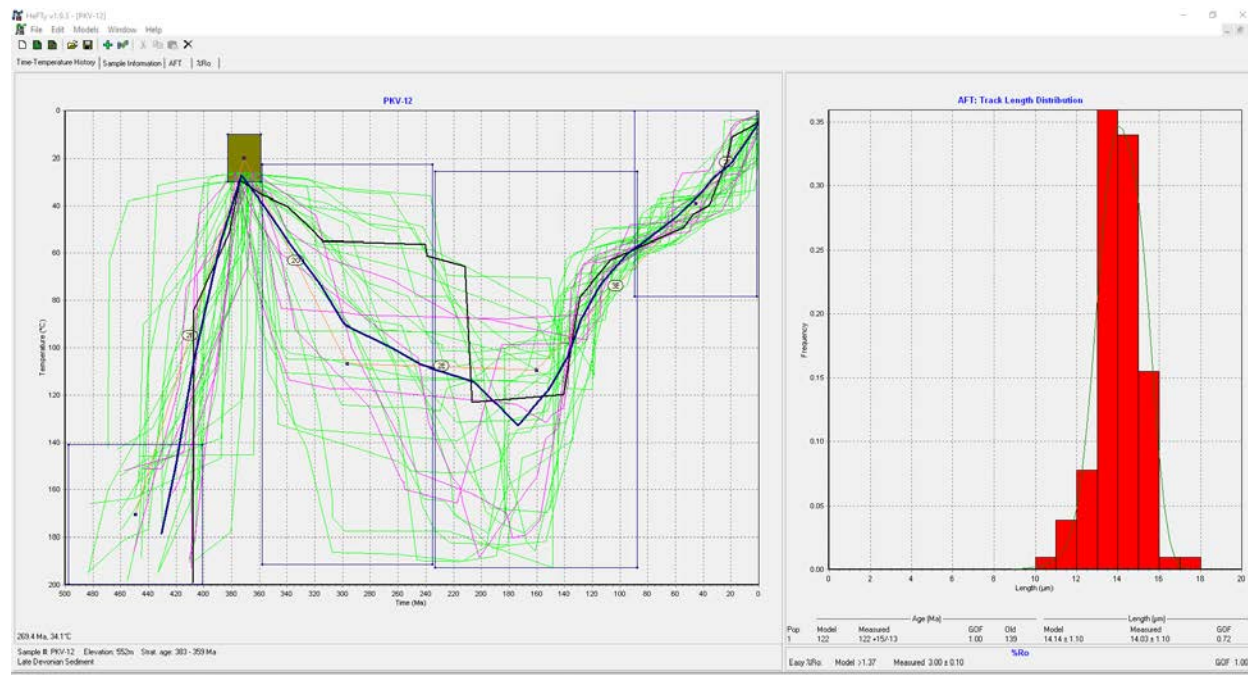
Constraint points
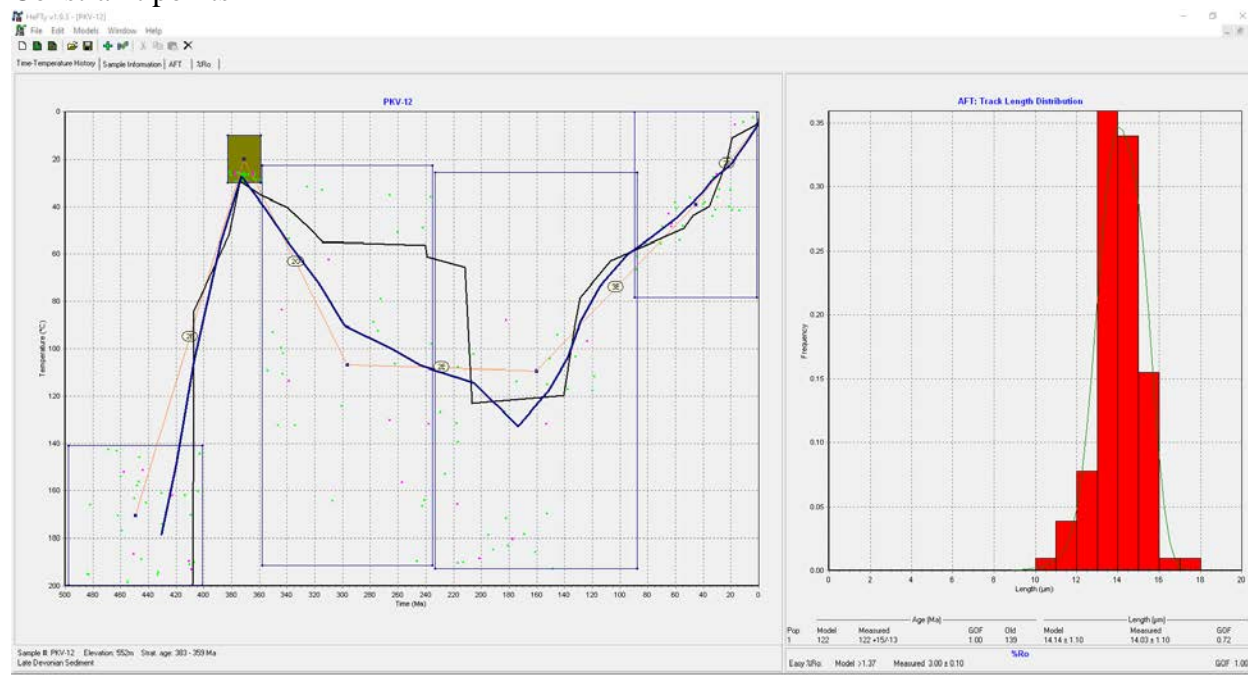
B2.   Inverse Thermal Models

As stated in the thermal history interpretation discussion within Chapter 1, six representative inverse thermal models were used to demonstrate the time-temperature history trends. However, the trends were based on the thermal trends revealed in models from all 38 of the samples. Inverse thermal models are presented in numerical sample order.

3P
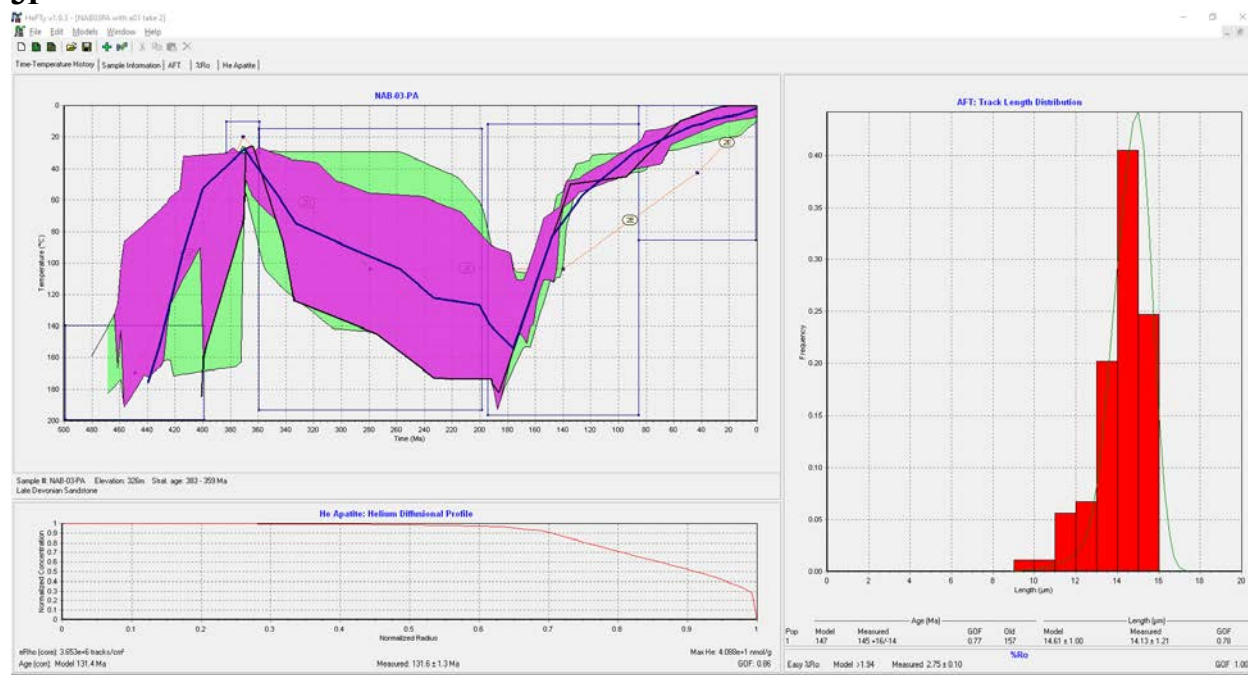
4P

5P
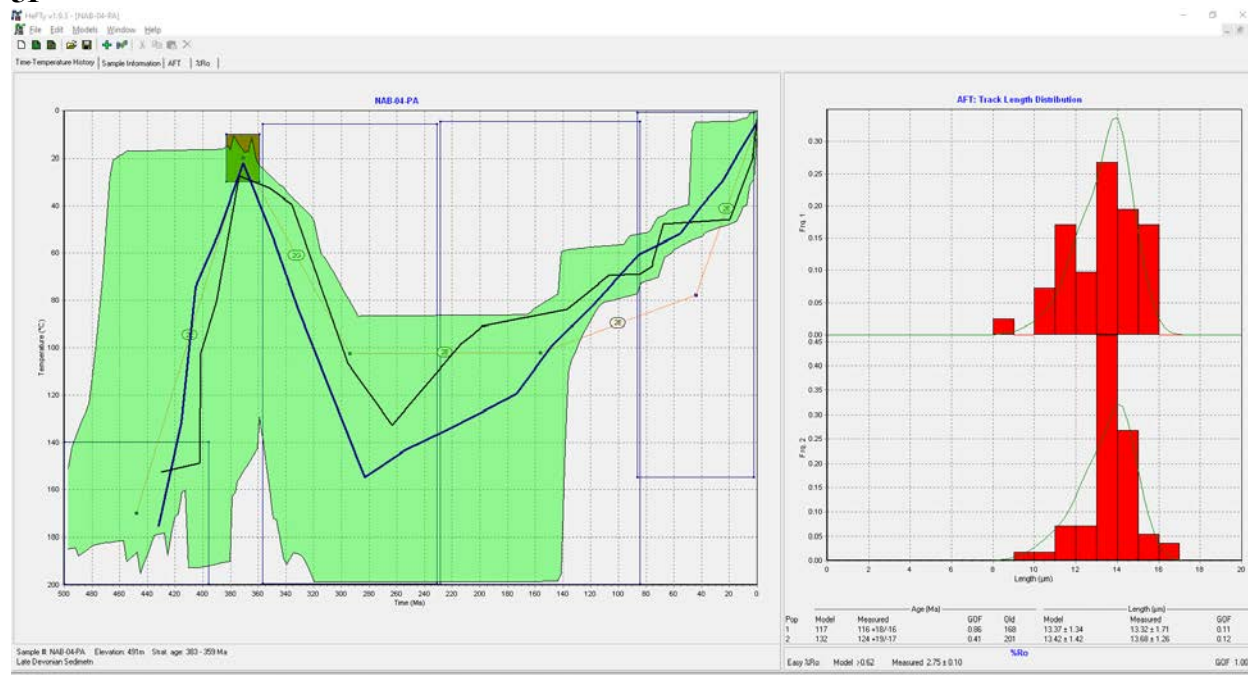
7P
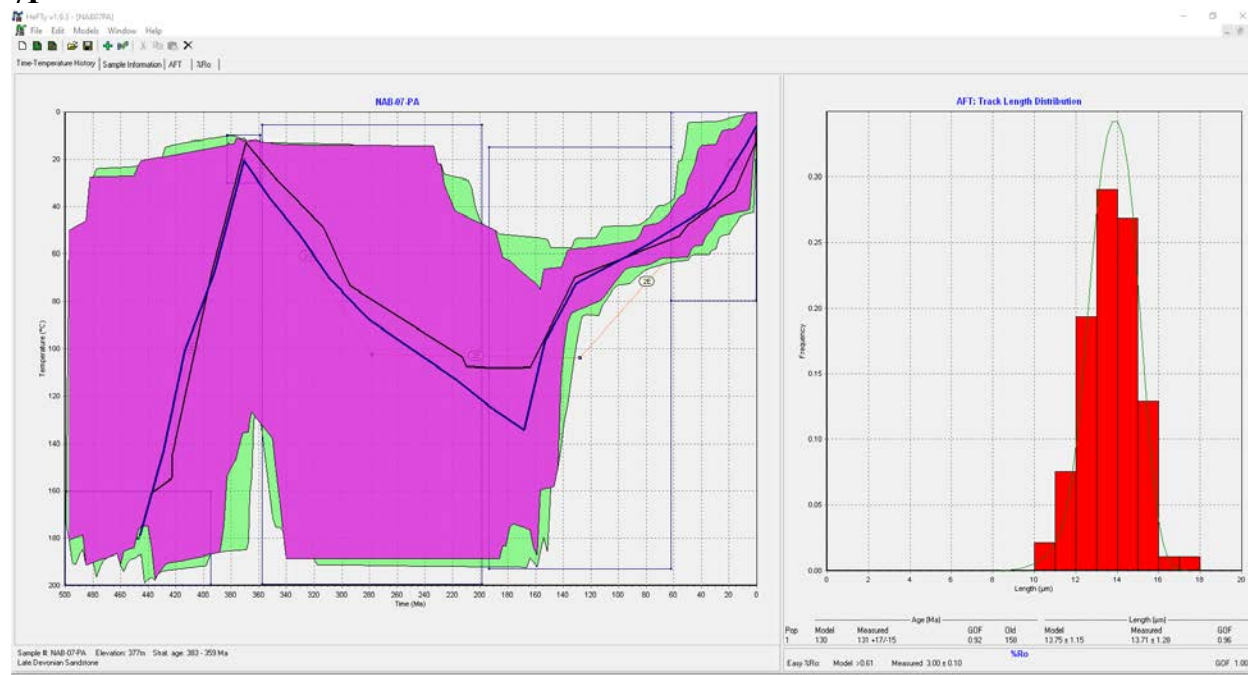
8P
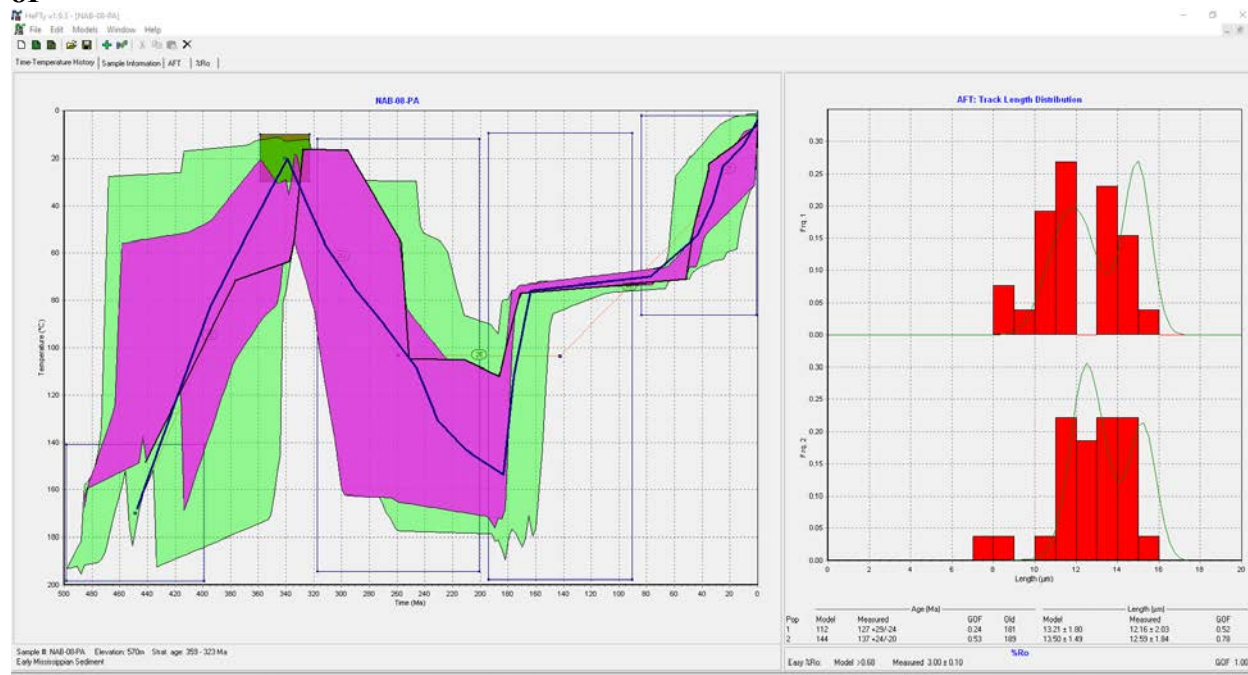
9P
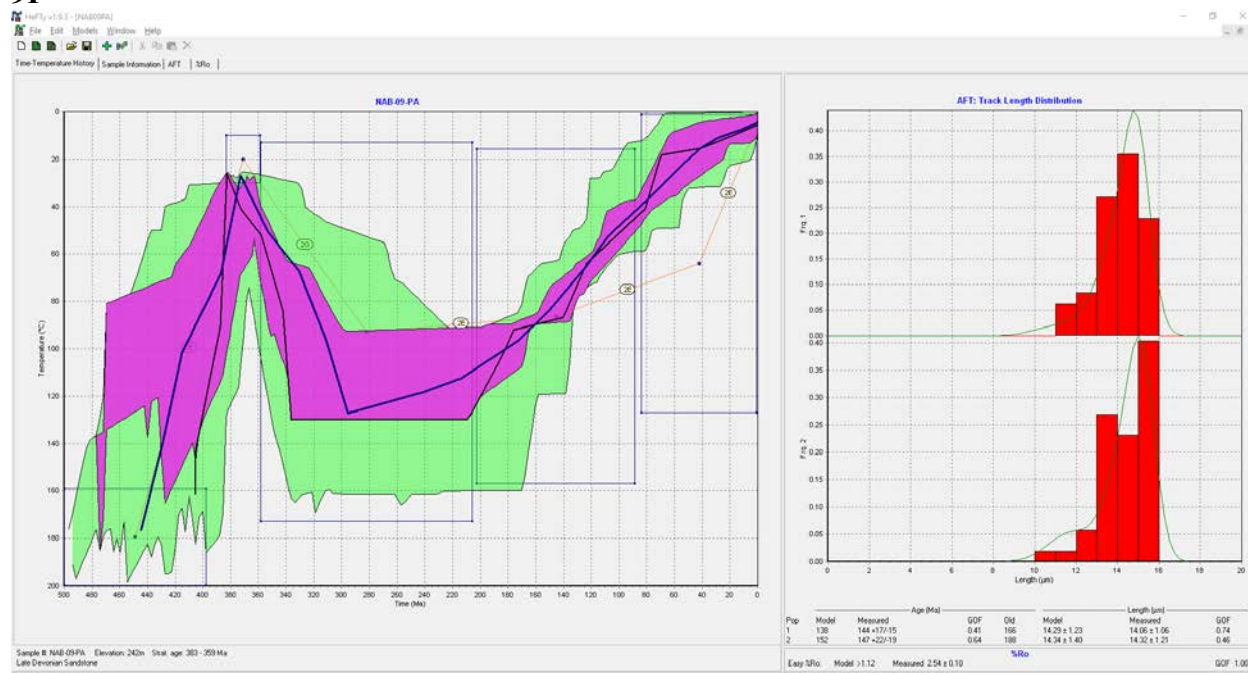
10P
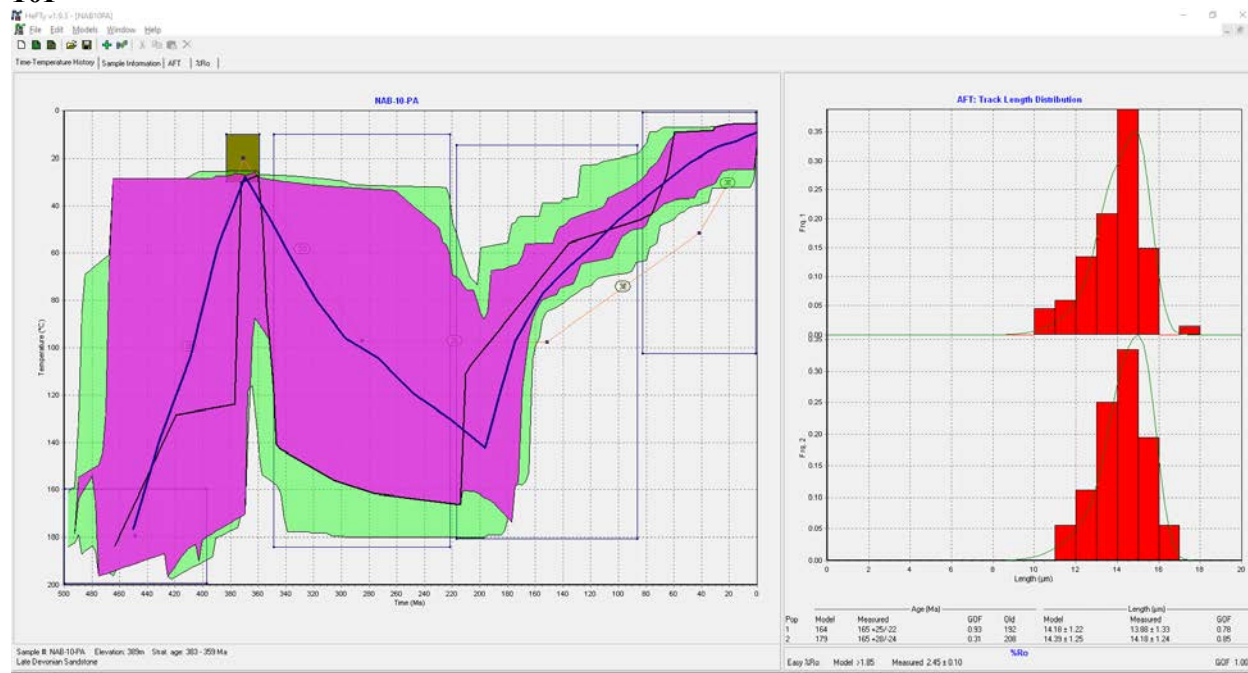
15N
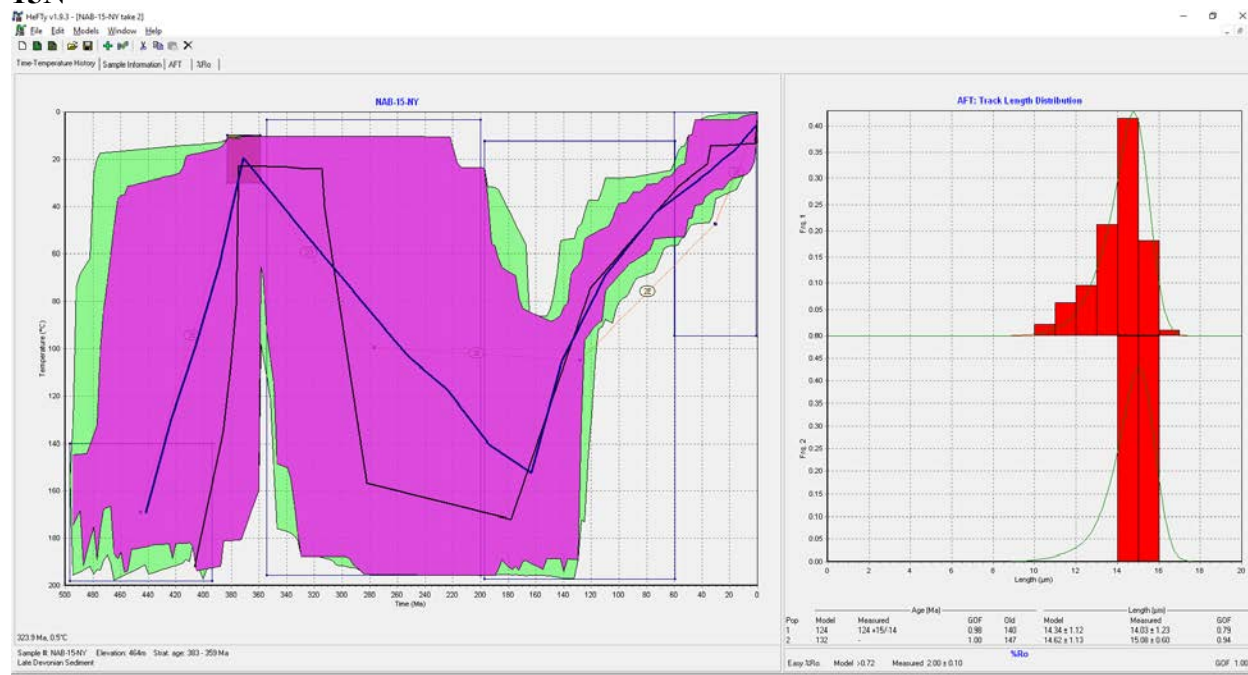
17N
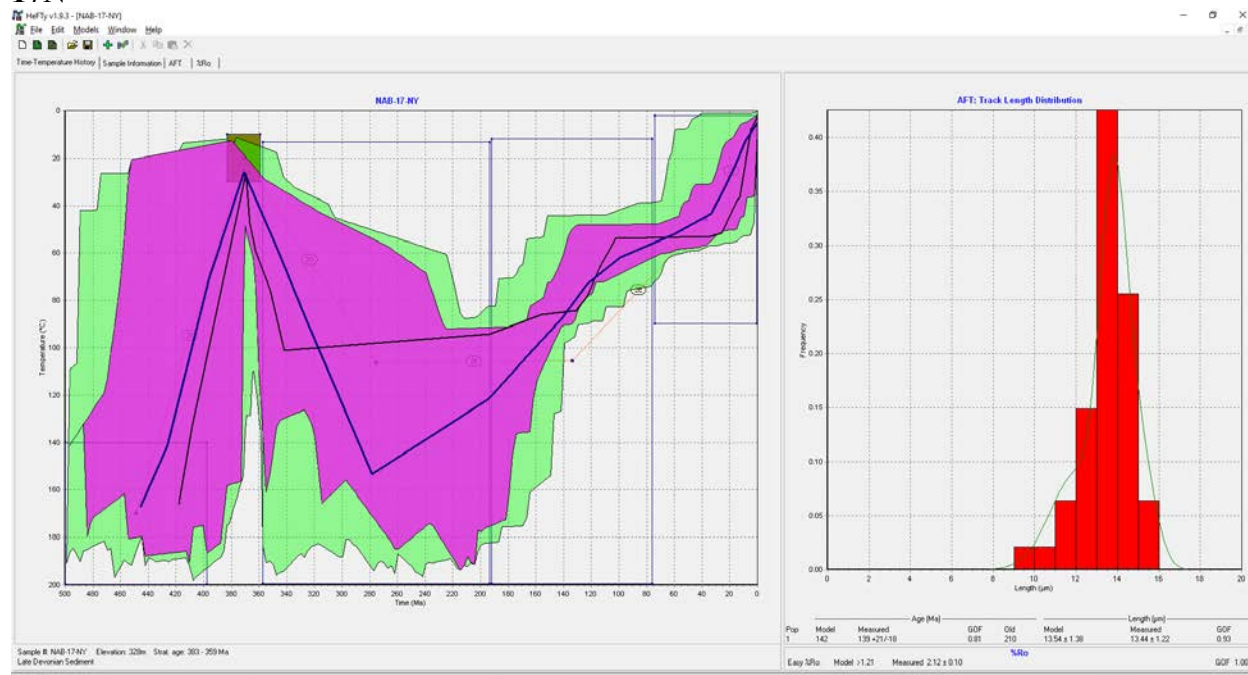
19N
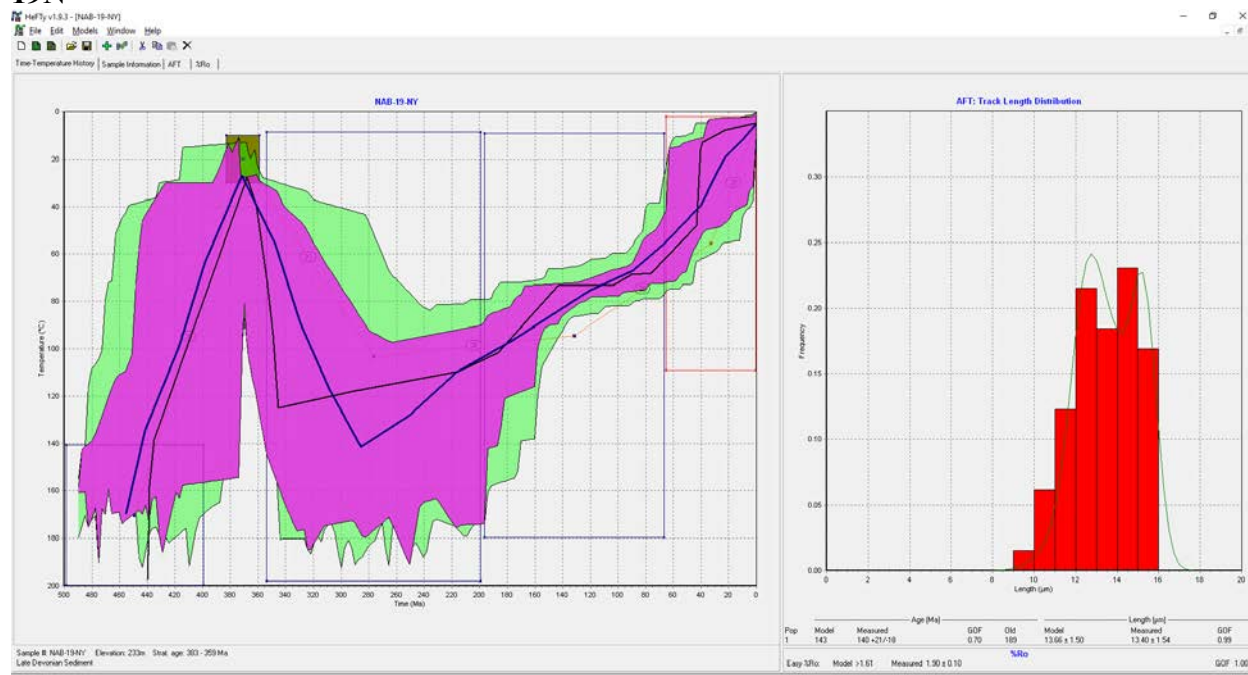
20N

21N

22N

24N

28Pc

117
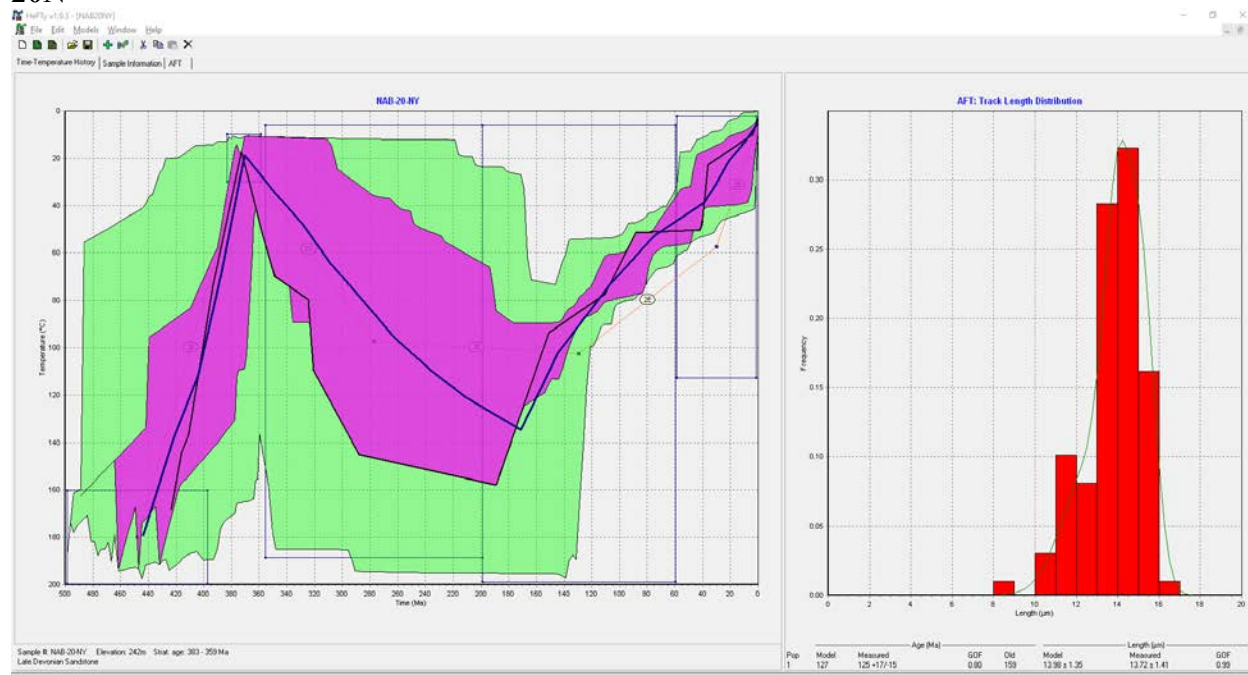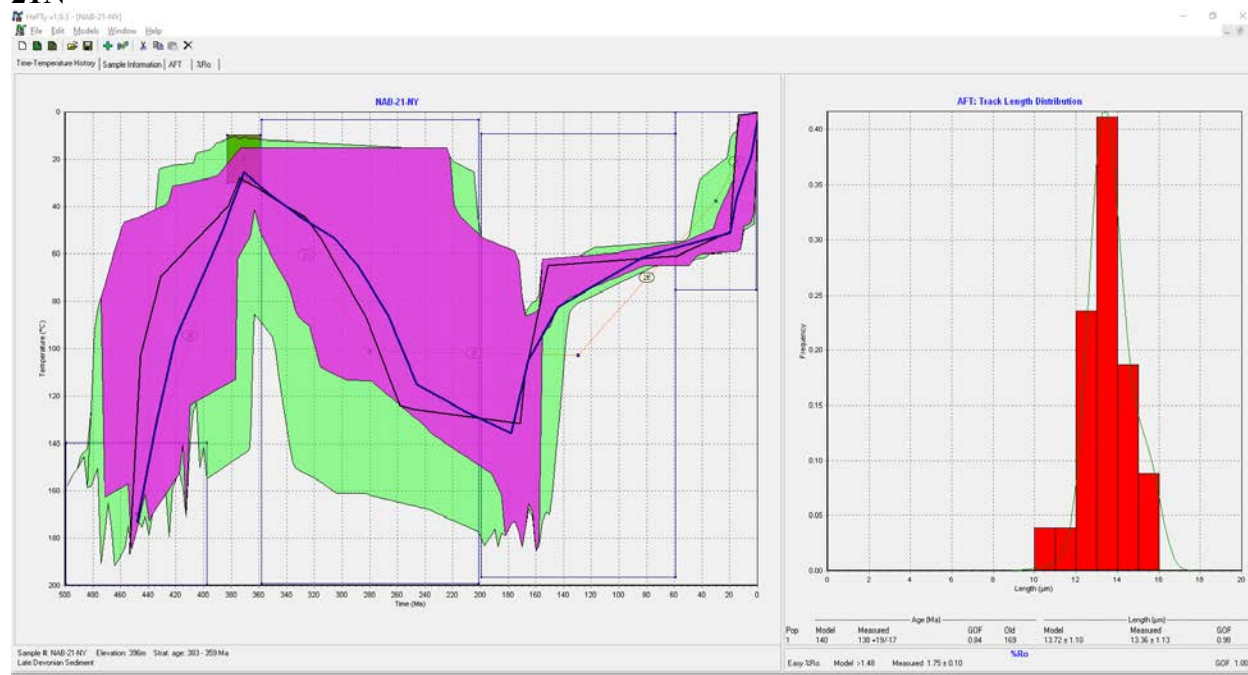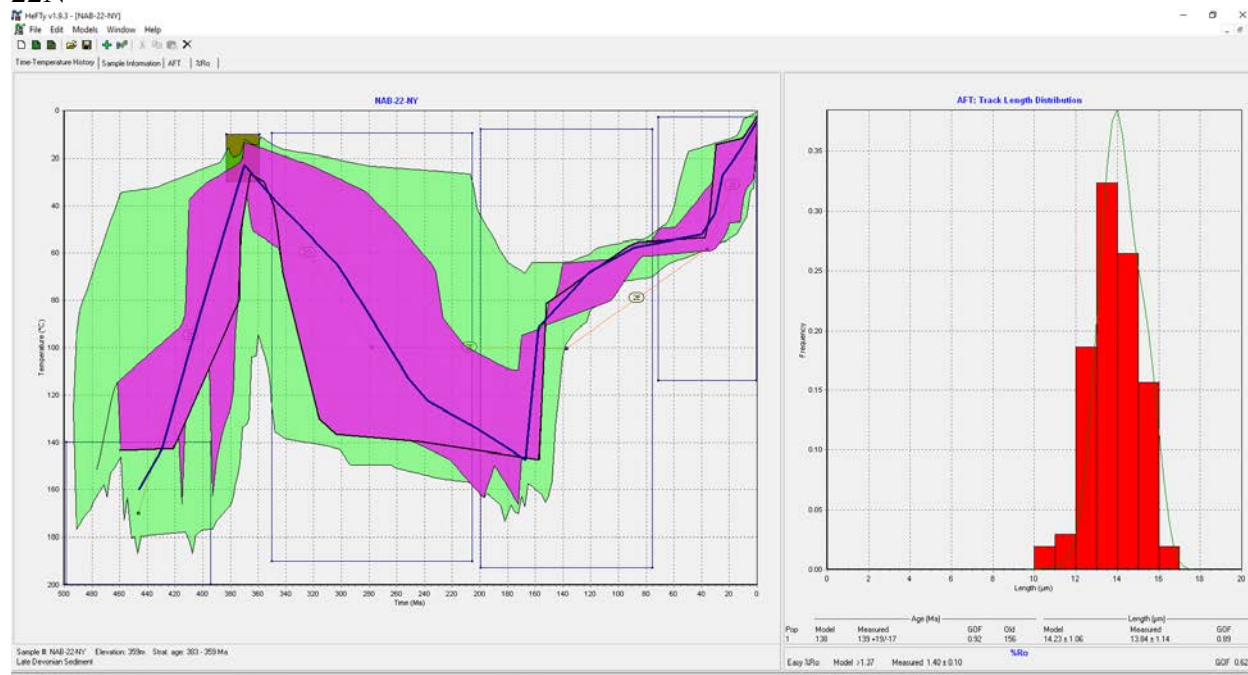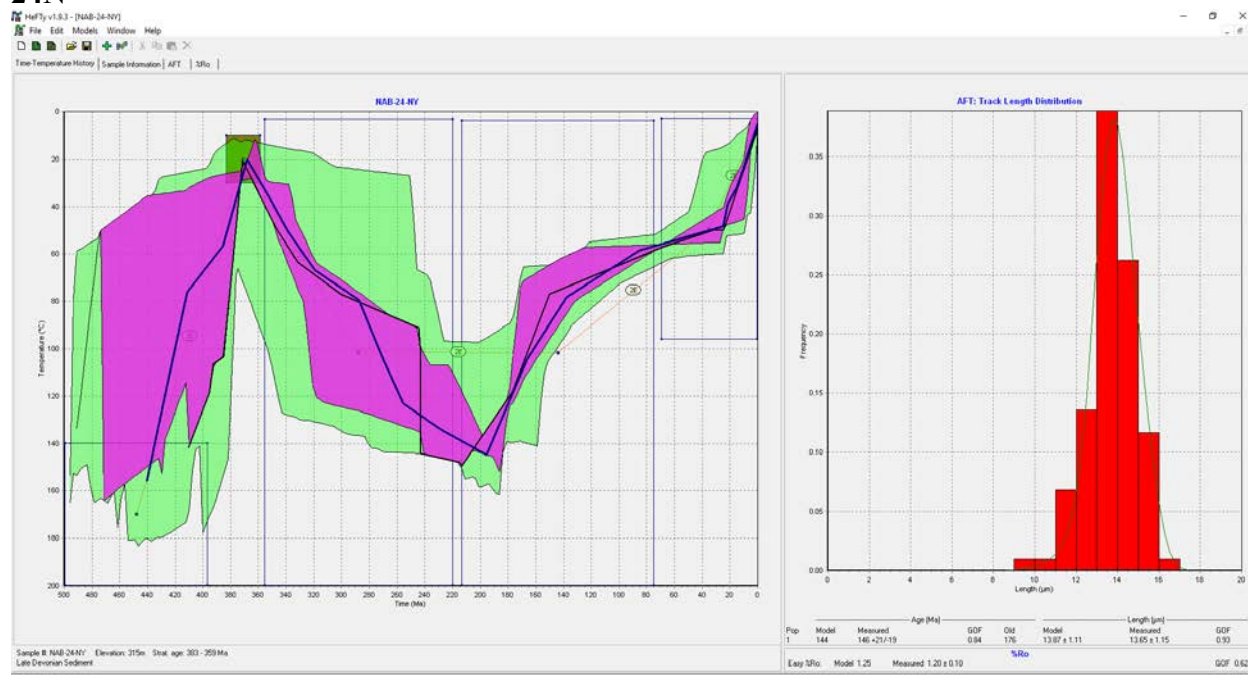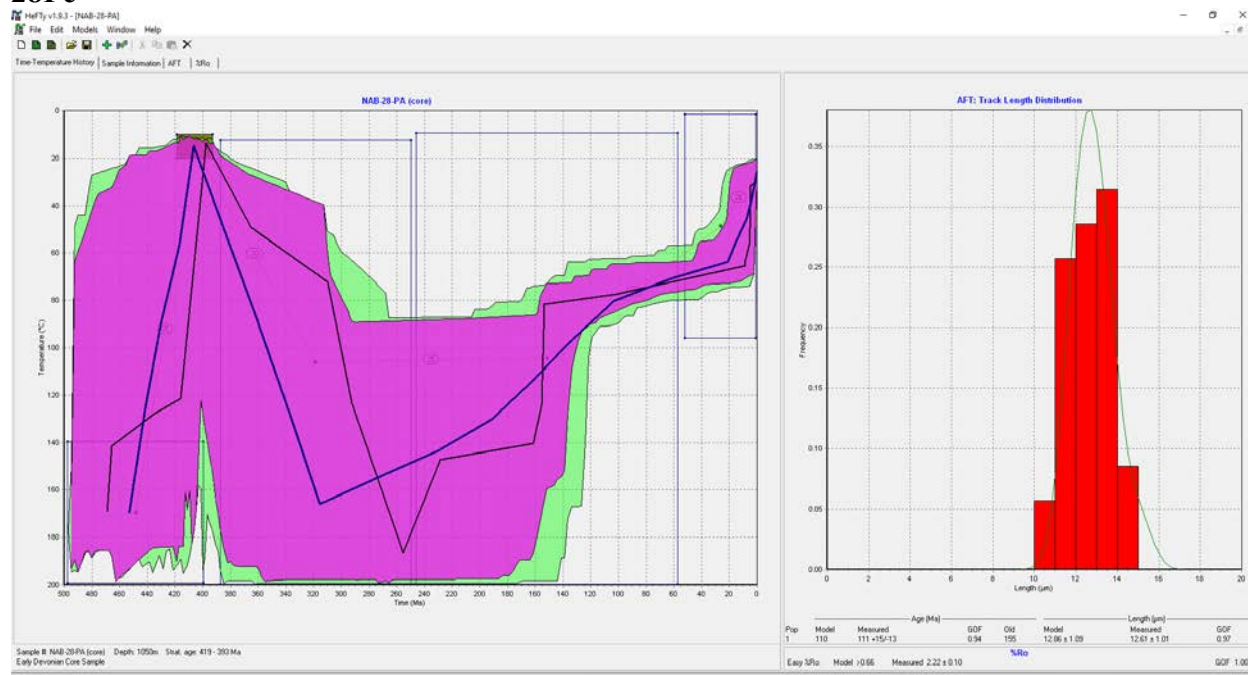
34N
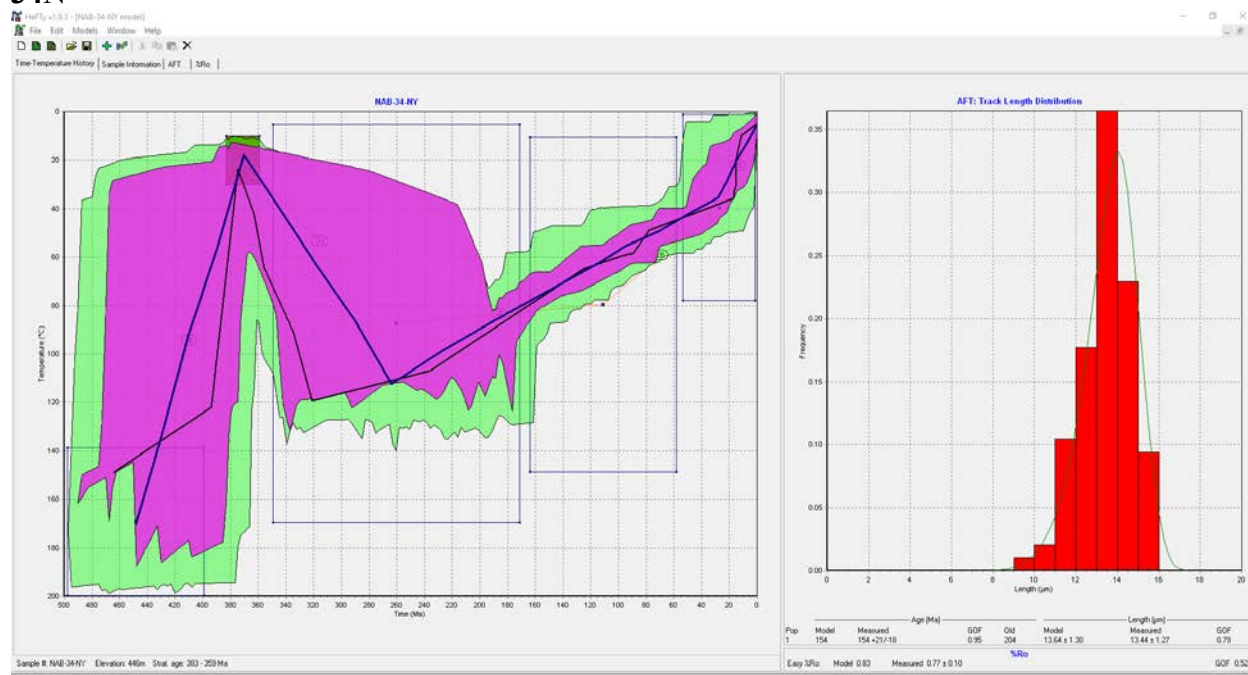
35N
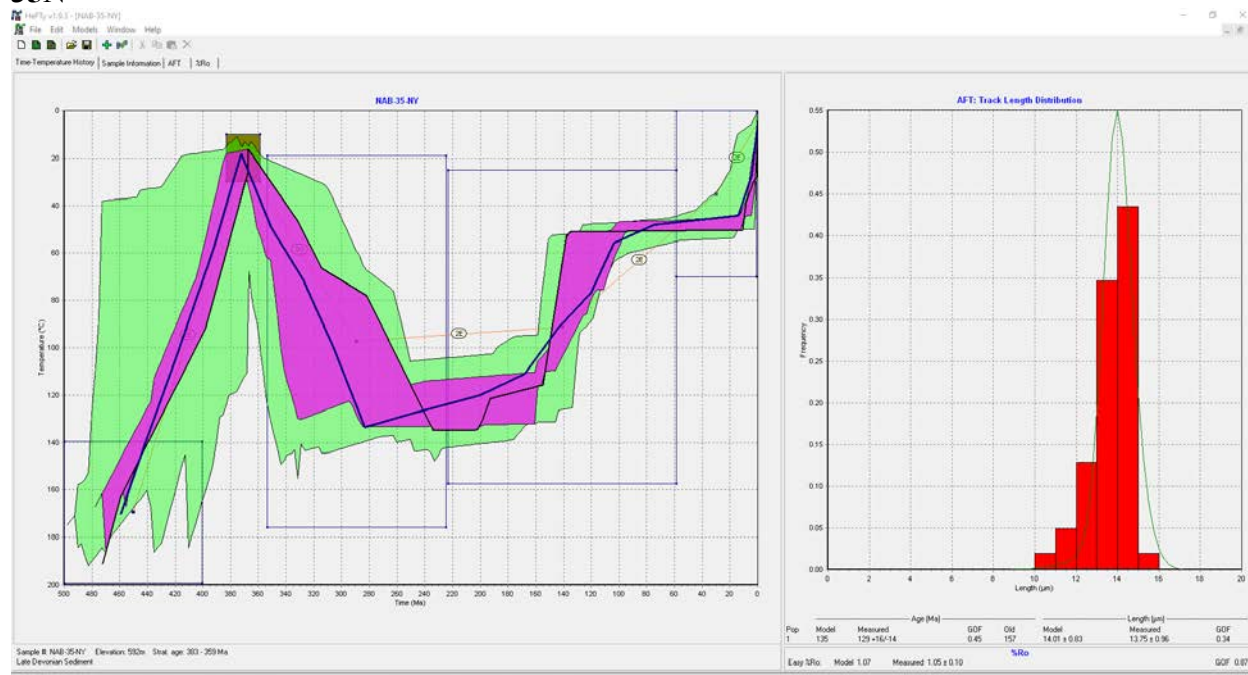
36N

37N
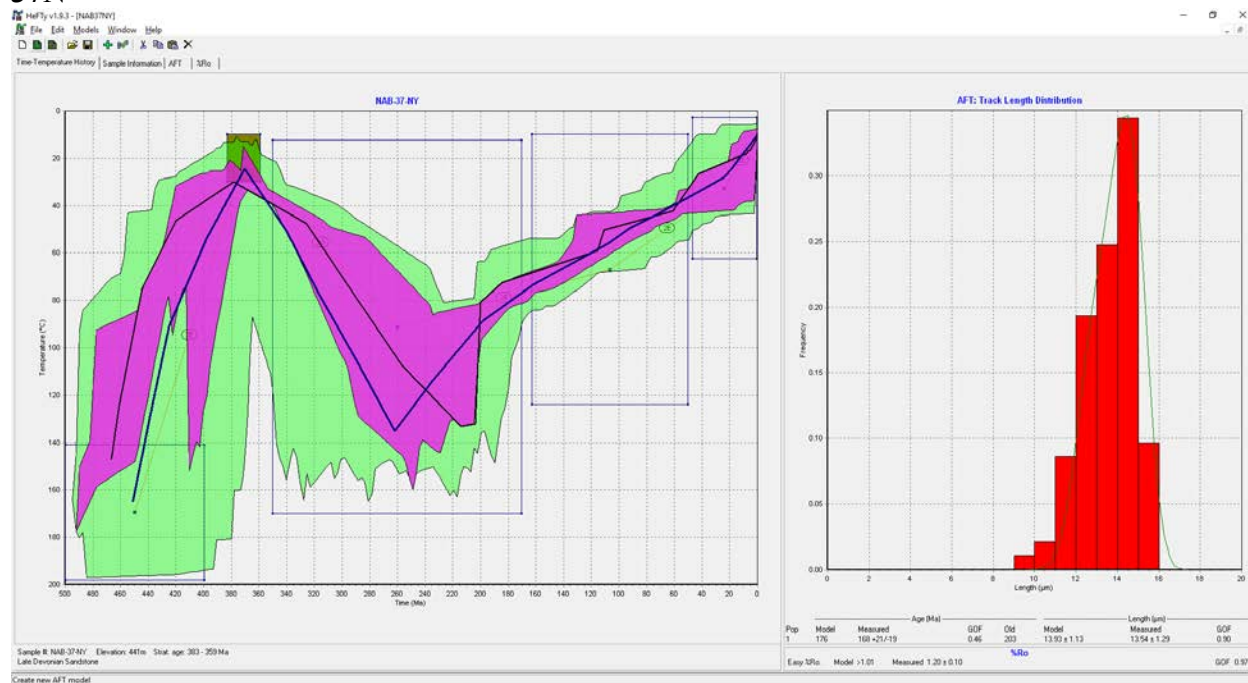
38N
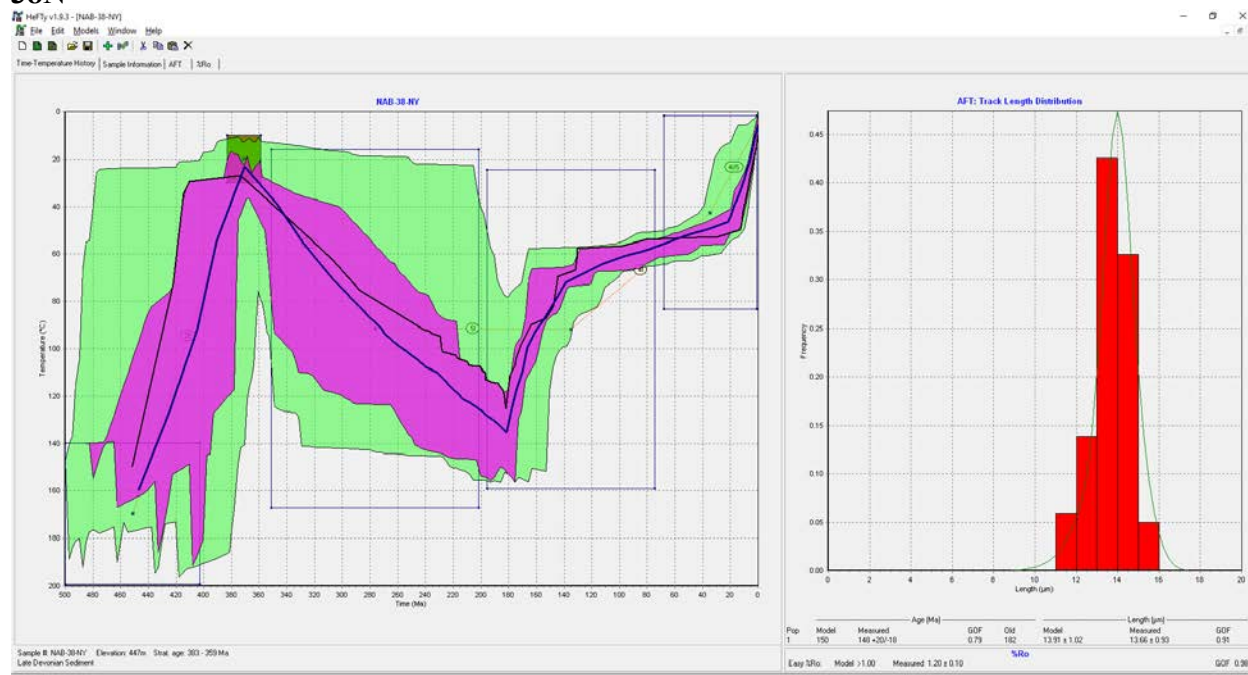
39P
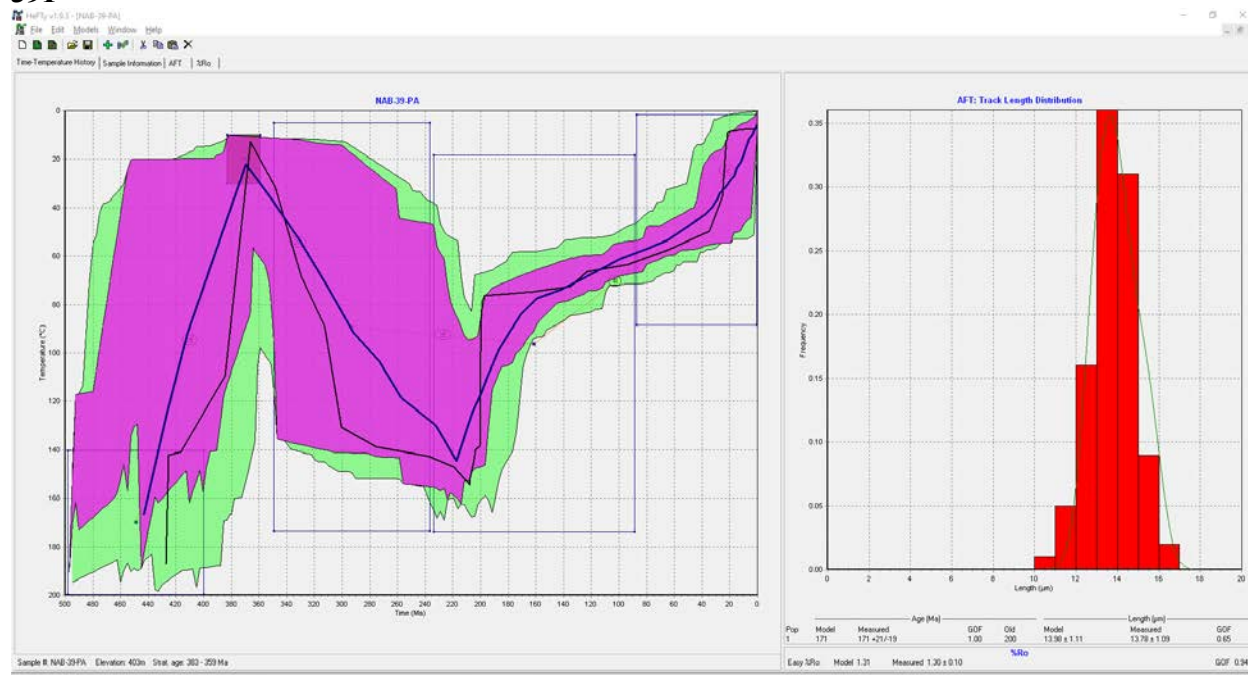
40P
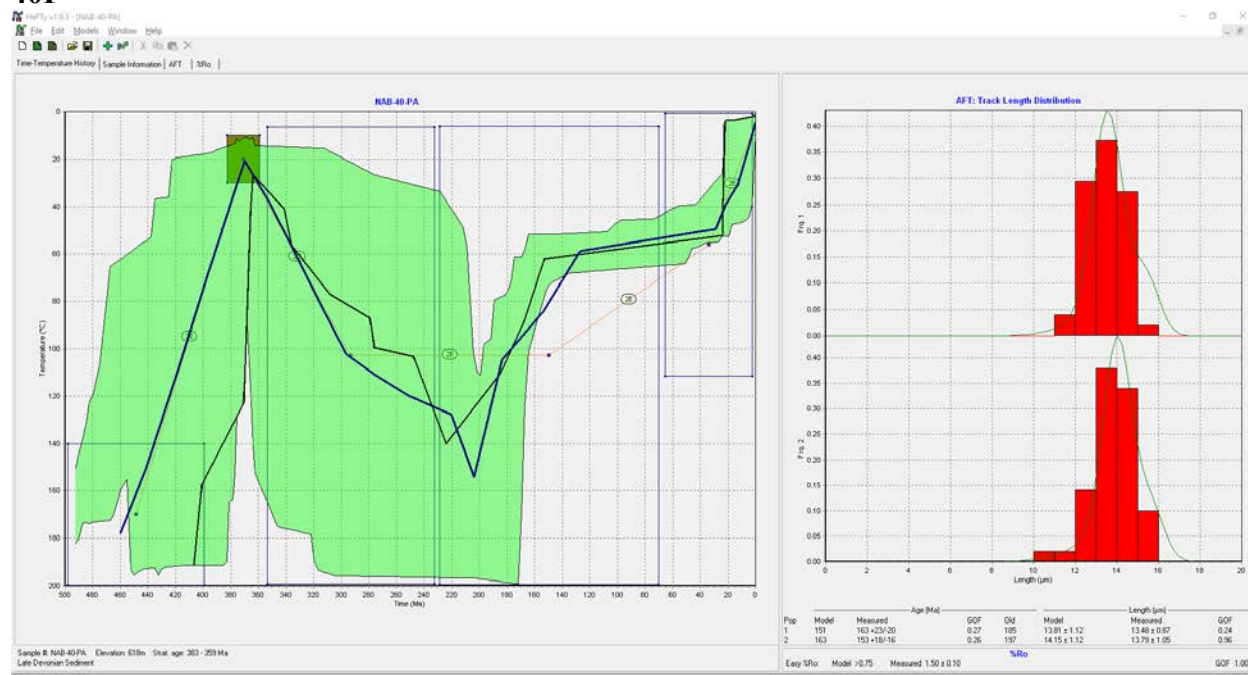
42P
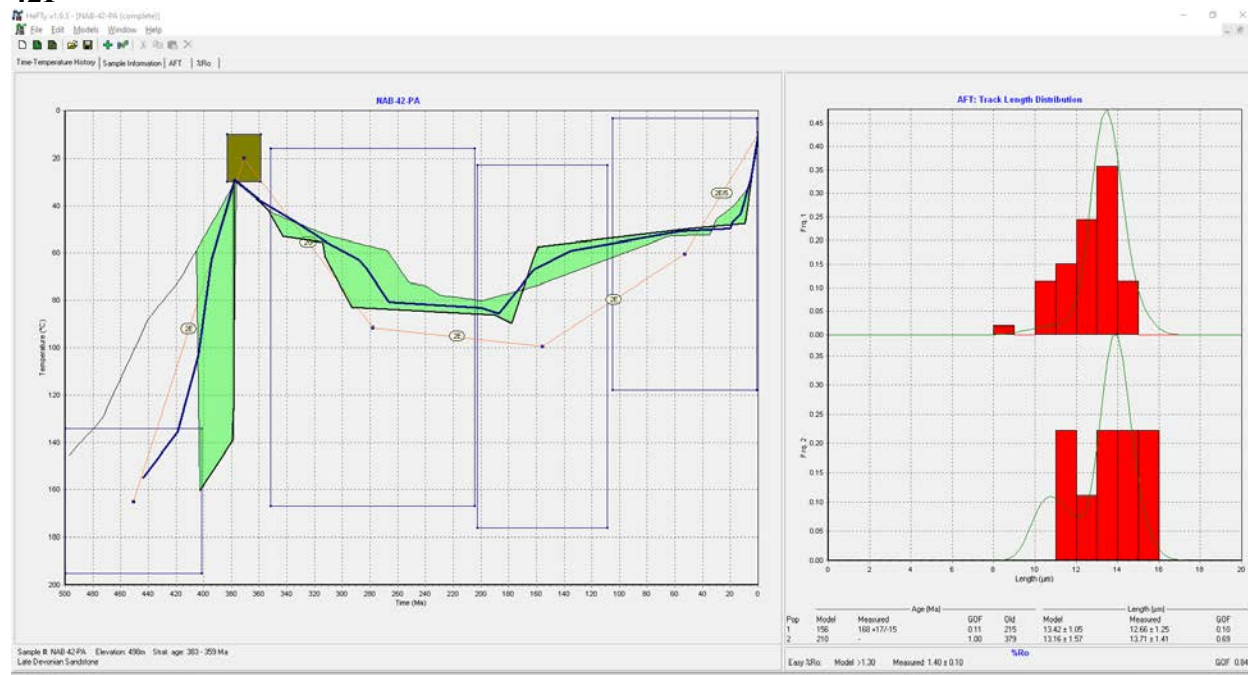
43P
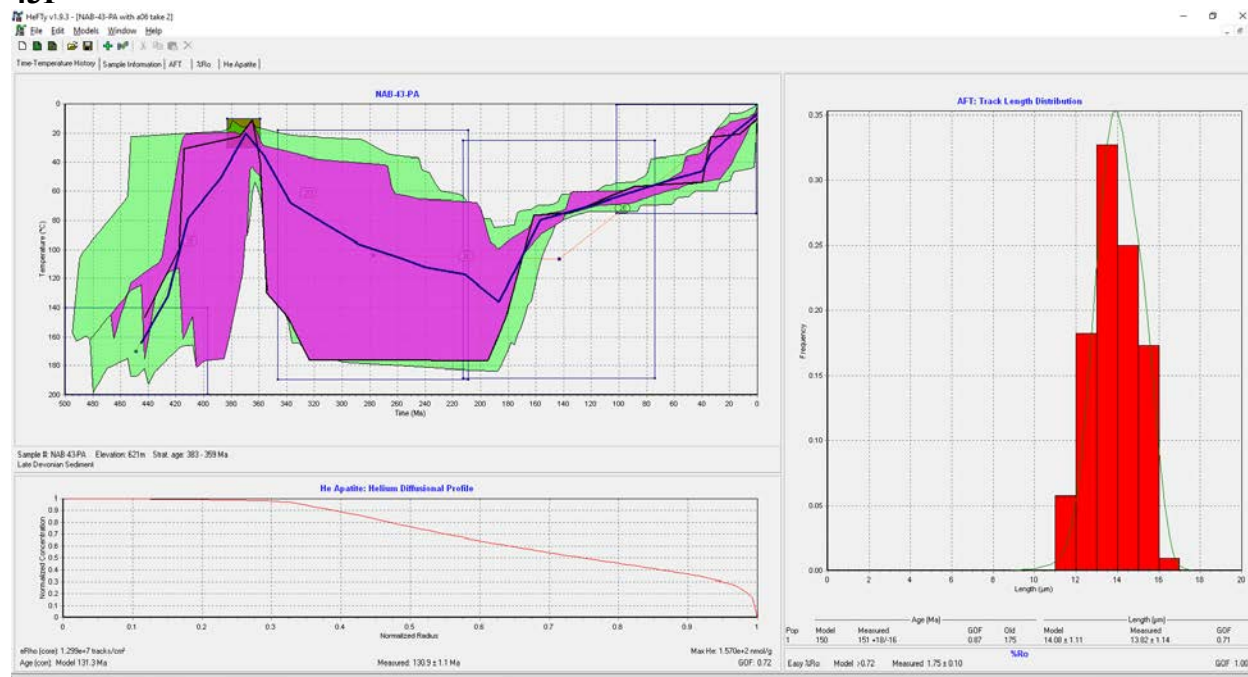
44P
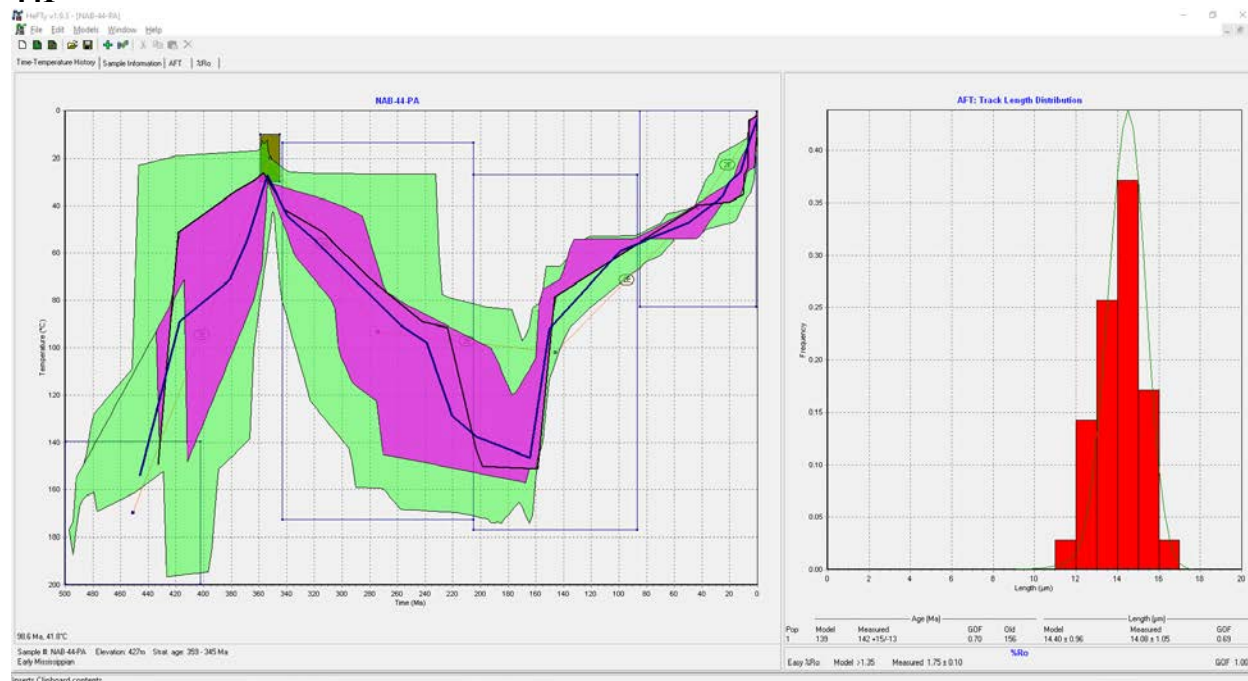
45N
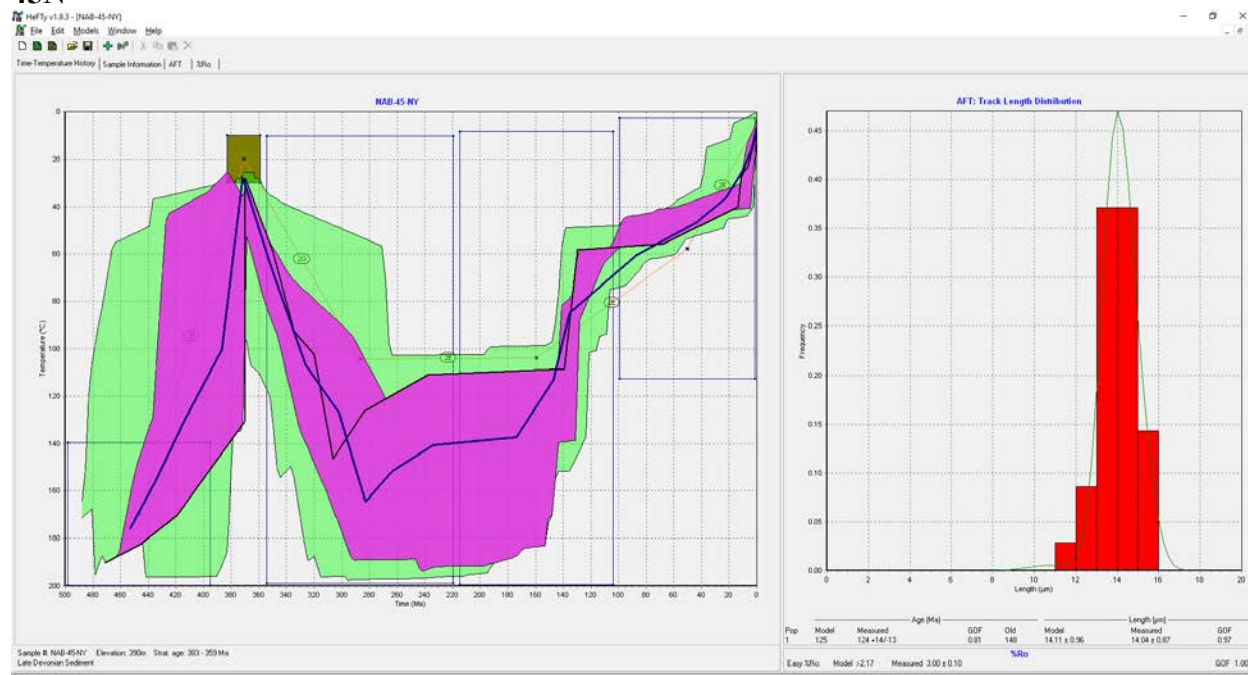
48N
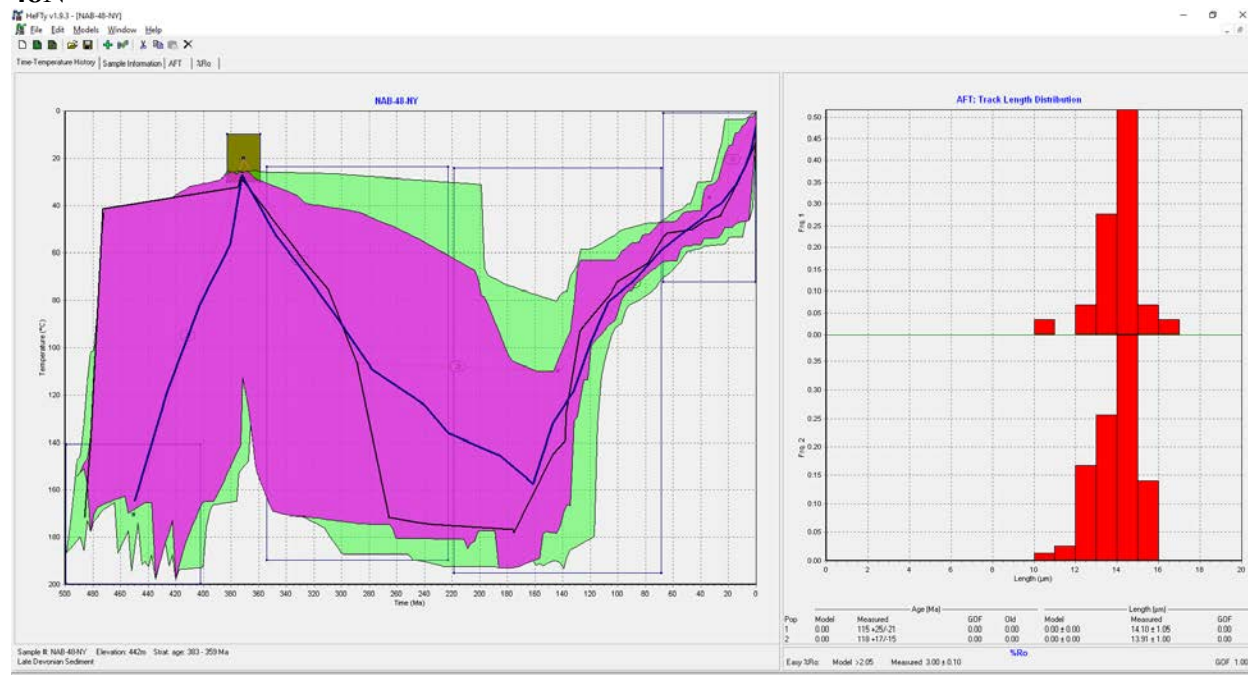
49N
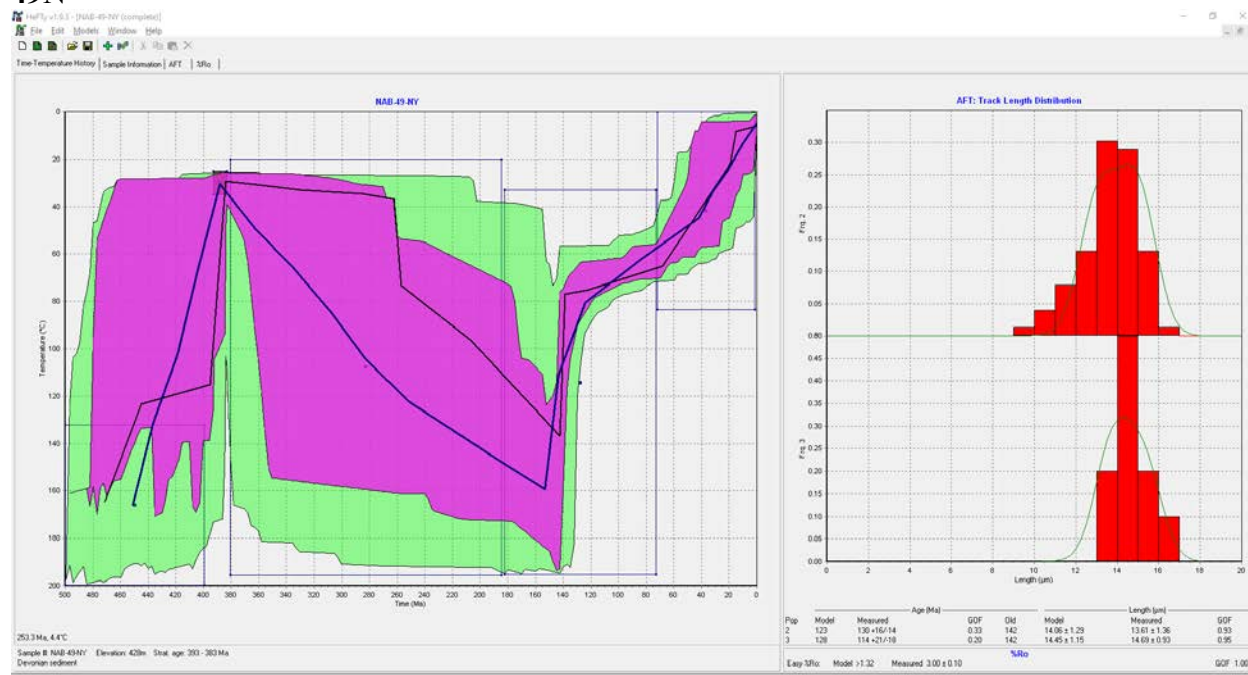
50N

51N
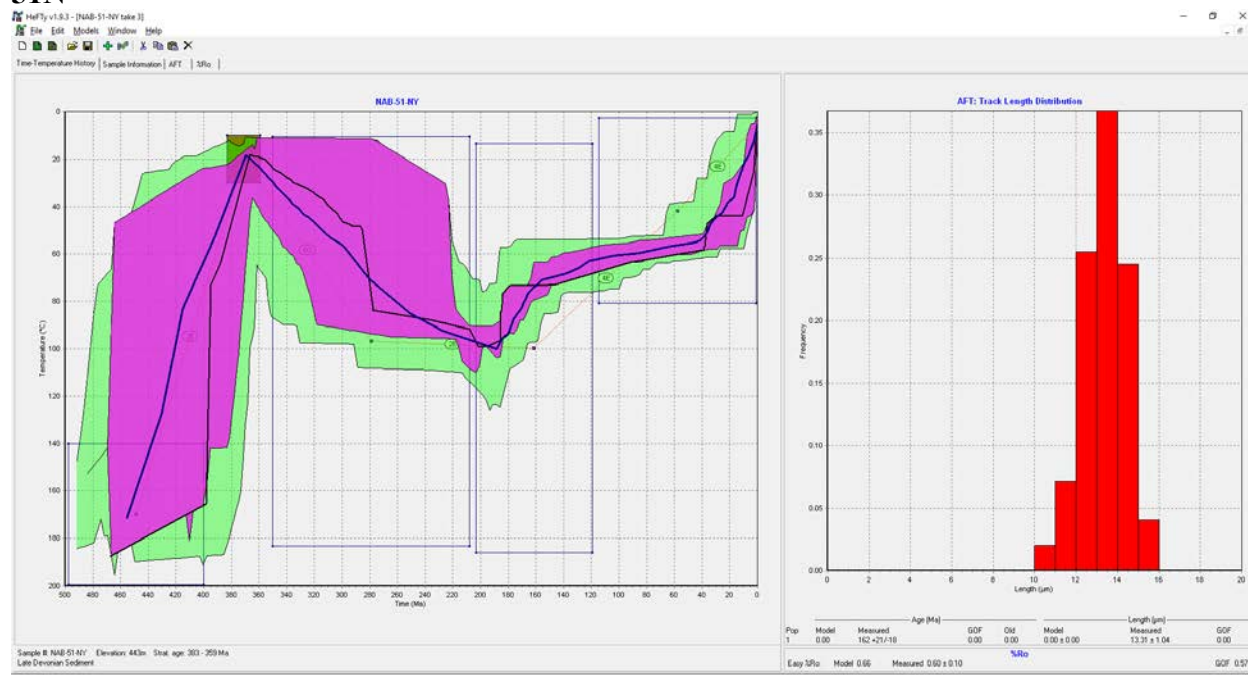
53N
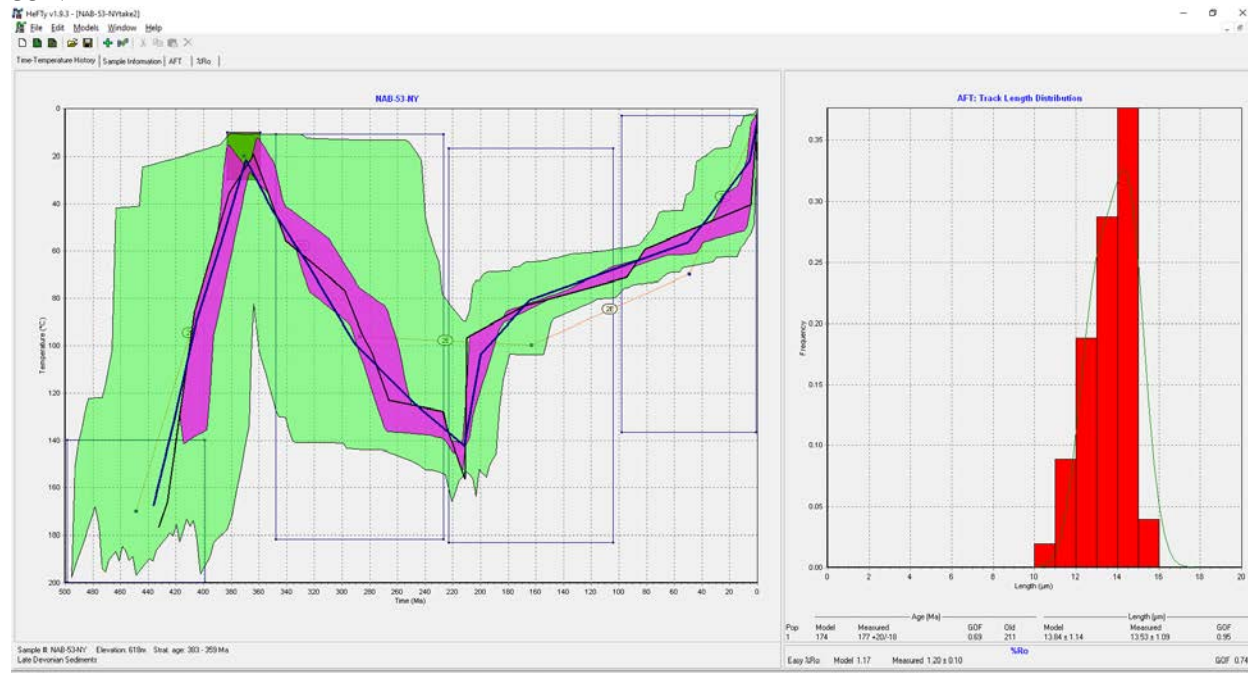
55P
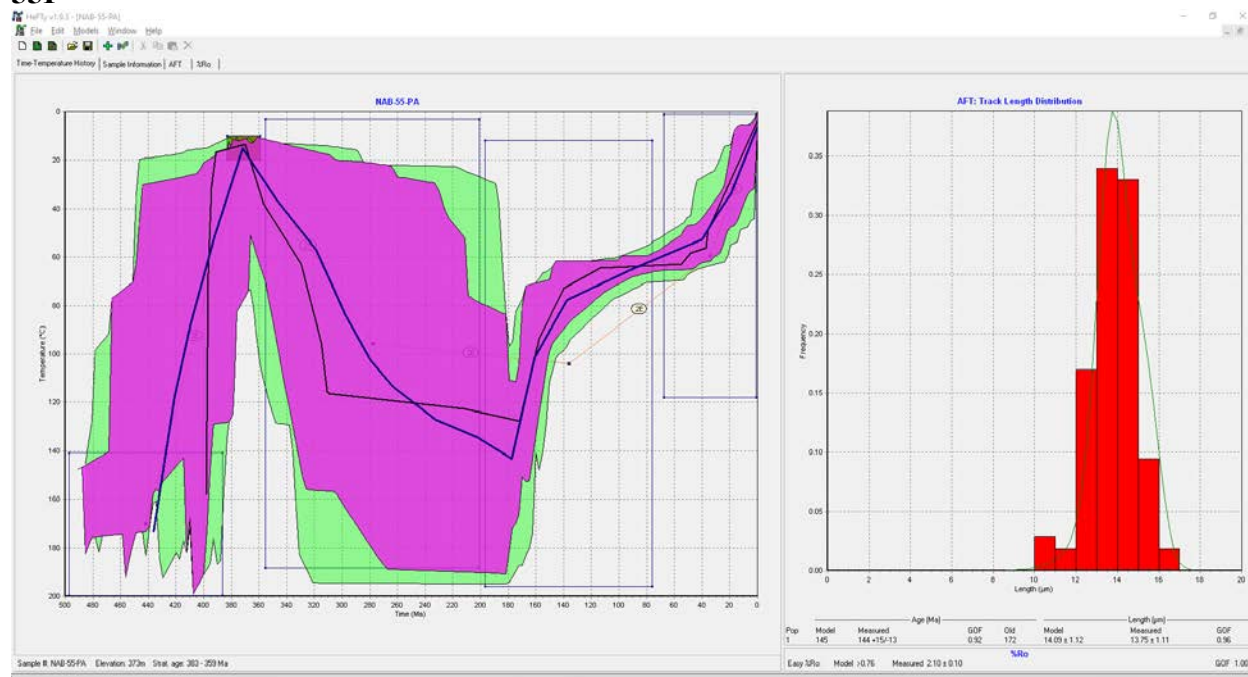
56P
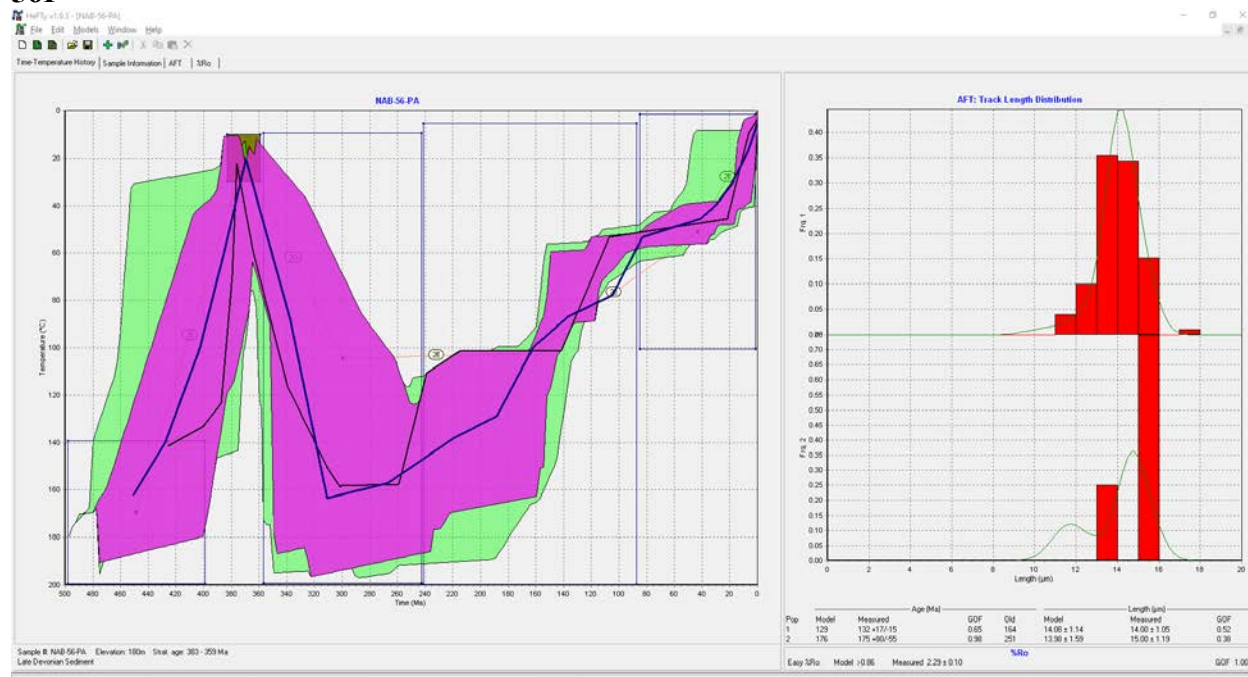
57N
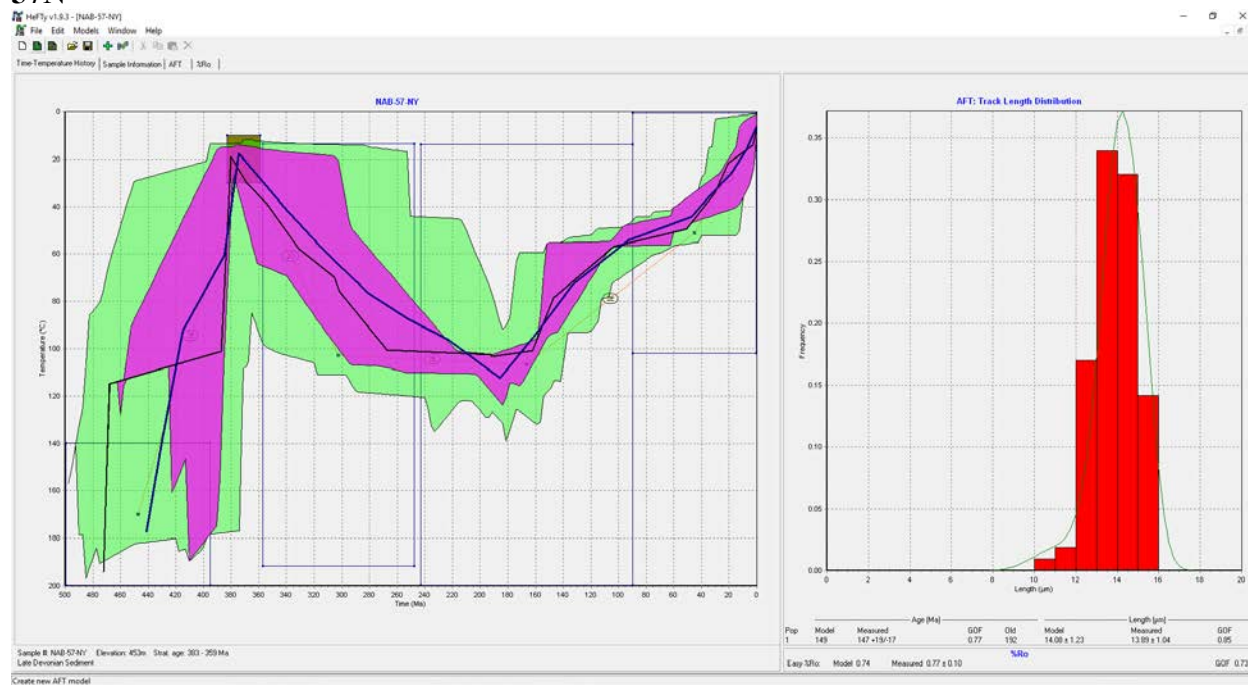
G12
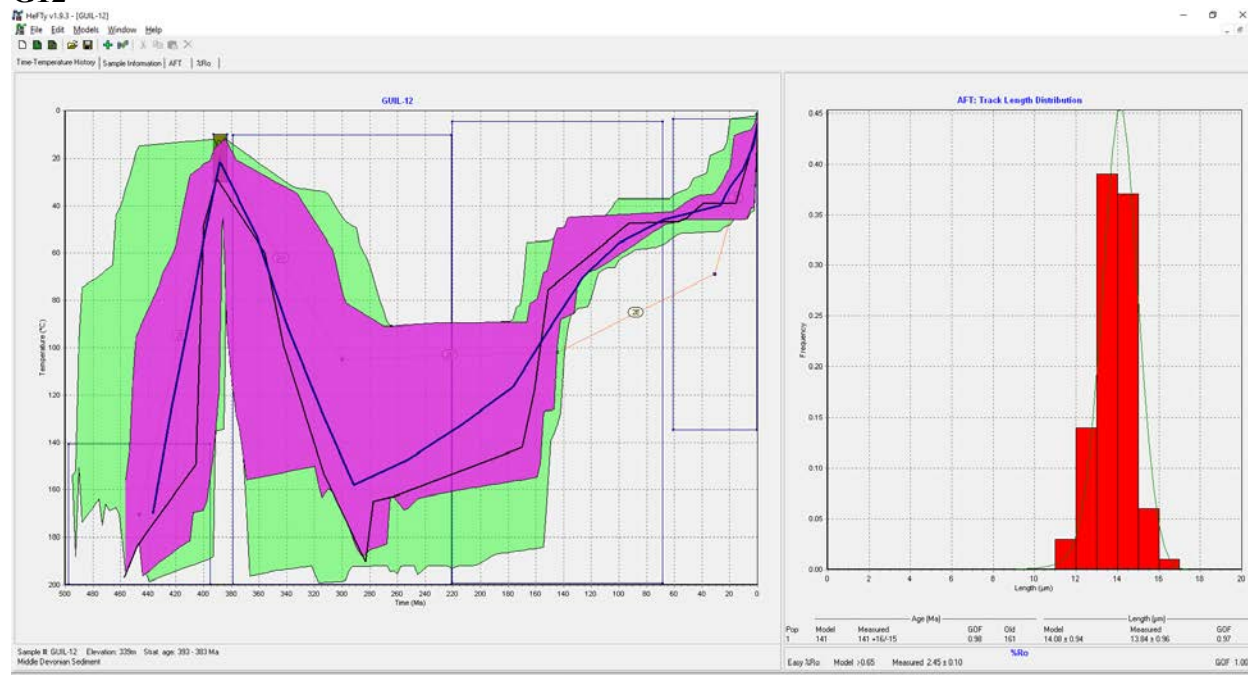
KS3
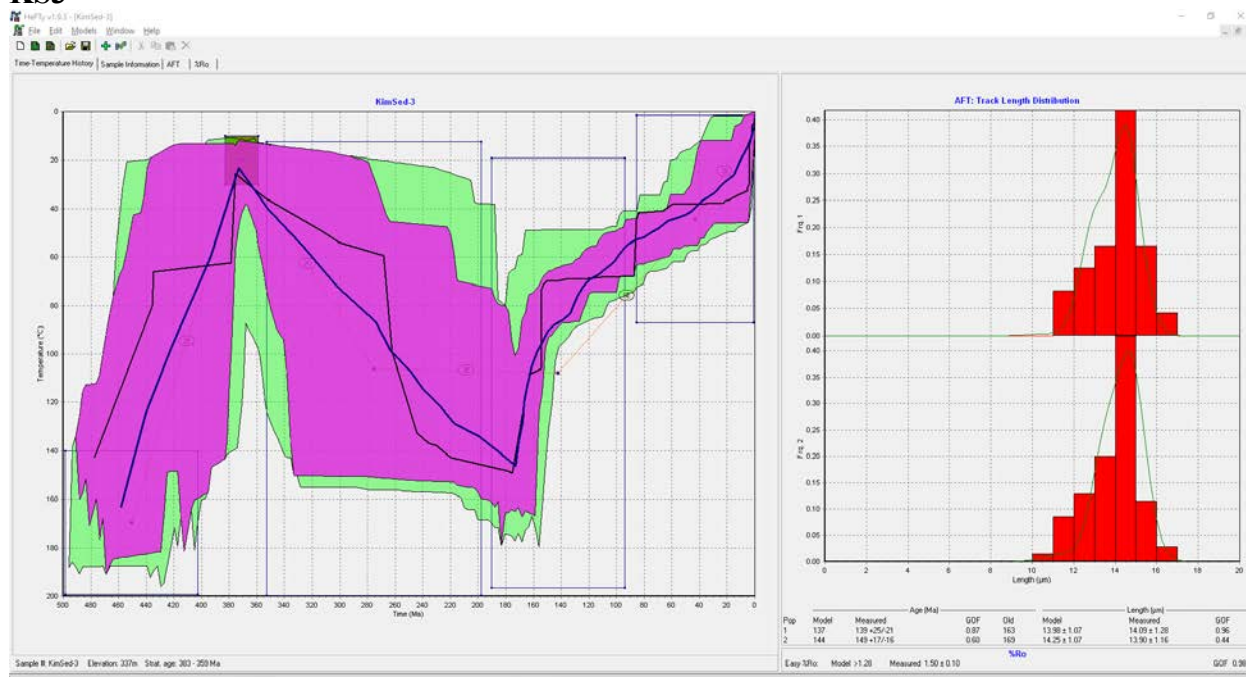
P12
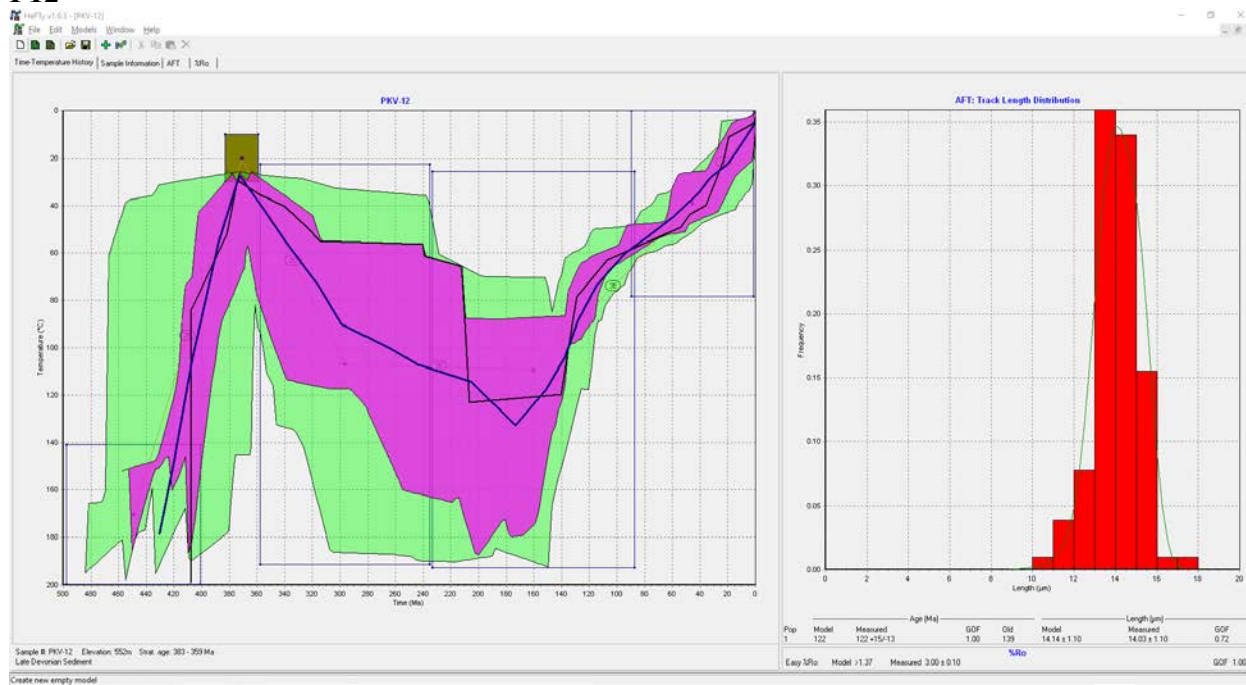
15.2
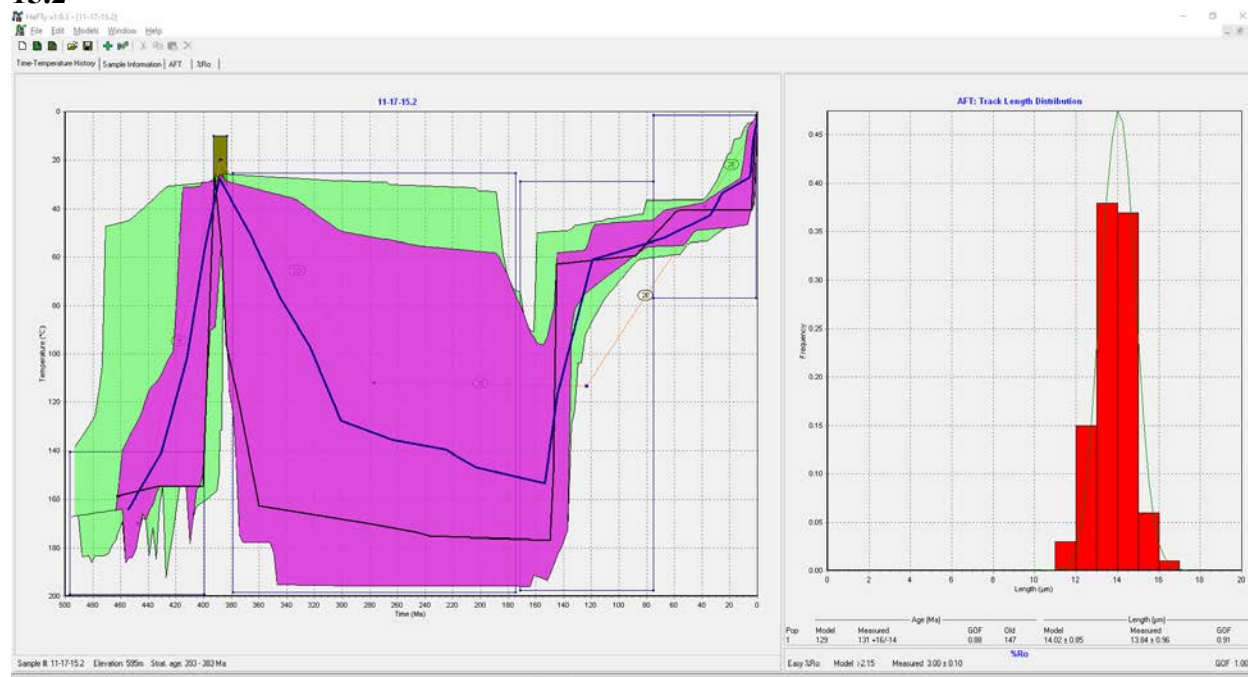
Supplementary File C. Radial Plots

It is common for detrital samples, such as this study's Devonian sandstone samples, to exhibit single-grain AFT age dispersion and contain multiple kinetic populations. Radial plots are a useful tool for displaying single-grain ages, analytical uncertainties and measurement precision (i.e. standard error; Galbraith, 1990). As stated in chapter 1, RadialPlotter (Vermeesch, 2008) was used to visualize the age spread and determine multiple kinetic populations on samples which failed the χ^2 test. Samples which passed the χ^2 test were not input into RadialPlotter as their radial plots would only constrain a single population or, if forced to constrain multiple populations, would result in populations of similar age (example below).
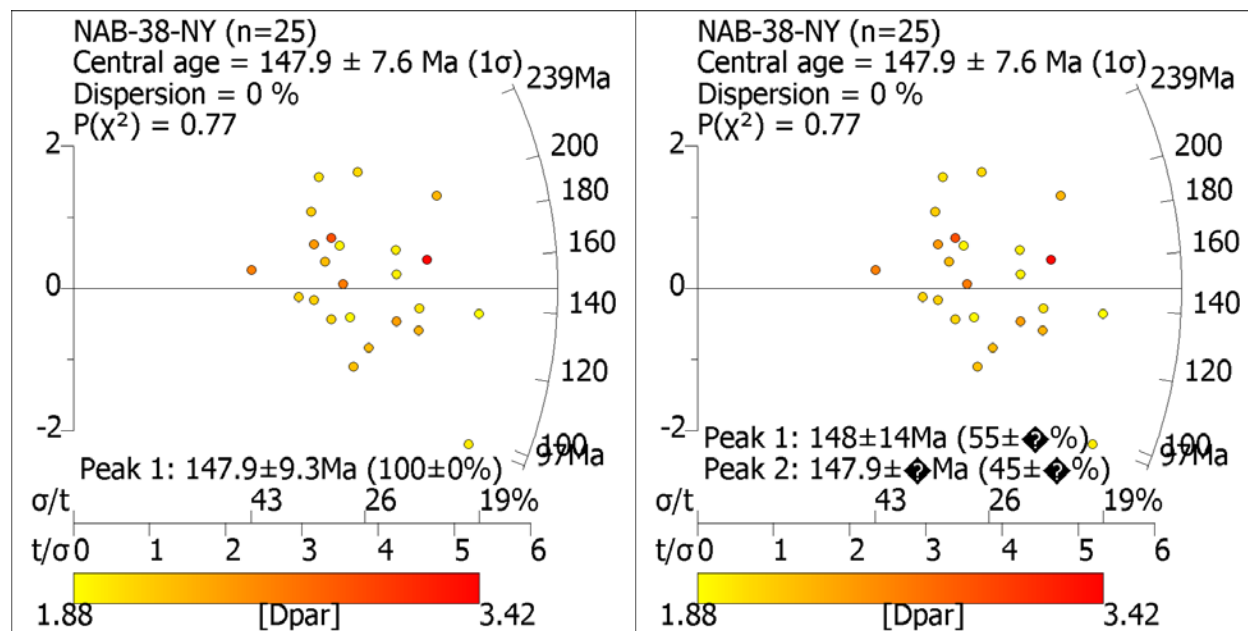
Example of radial plotting a sample (38N) which passed the χ^2 test (76.7 %). The plot on the right was allowed to automatically generate populations while the plot on the left was forced to produce two populations.

RadialPlotter automatically determined mixture models and generally produced two kinetic populations in samples which did not pass the χ^2 test (see Table 1 for χ^2 percentages). This information was utilized in inverse thermal modeling program HeFTy (Ketcham, 2005) to

define kinetic populations. Below are the radial plots of the 17 samples which did not pass the χ^2 test, displayed in numerical order.

NAB-22-NY (n=25)
Central age = 140.8 ± 9.6 Ma (1σ)
Dispersion = 20 %
P(χ²) = 0.03
Peak 1: 76±16Ma (9.7±8.1%)
Peak 2: 150±11Ma (90.3±8.1%)

NAB-36-NY (n=23)
Central age = 146 ± 14 Ma (1σ)
Dispersion = 37 %
P(χ²) = 0.00
Peak 1: 88±12Ma (31±15%)
Peak 2: 181±20Ma (69±15%)

NAB-40-PA (n=25)
Central age = 162.2 ± 8.7 Ma (1σ)
Dispersion = 20 %
P(χ²) = 0.00
Peak 1: 96±11Ma (8.2±6%)
Peak 2: 167.8±8.8Ma (91.8±6%)

NAB-42-PA (n=25)
Central age = 171.5 ± 7.2 Ma (1σ)
Dispersion = 15 %
P(χ²) = 0.00
Peak 1: 143±13Ma (38±28%)
Peak 2: 191±18Ma (62±28%)

NAB-43-PA (n=25)
Central age = 154.2 ± 8.8 Ma (1σ)
Dispersion = 19 %
P(χ²) = 0.00
Peak 1: 107±14Ma (18±14%)
Peak 2: 169±11Ma (82±14%)

NAB-44-PA (n=25)
Central age = 148.6 ± 8 Ma (1σ)
Dispersion = 21 %
P(χ²) = 0.00
Peak 1: 110.1±7Ma (35±11%)
Peak 2: 177±11Ma (65±11%)

NAB-48-NY (n=25)
Central age = 120.4 ± 8.8 Ma (1σ)
Dispersion = 27 %
P(χ²) = 0.00
Peak 1: 92±10Ma (51±21%)
Peak 2: 155±19Ma (49±21%)

NAB-49-NY (n=25)
Central age = 125.6 ± 6.4 Ma (1σ)
Dispersion = 16 %
P(χ²) = 0.01
Peak 1: 110±8Ma (65±17%)
Peak 2: 162±18Ma (35±17%)

NAB-50-NY (n=25)
Central age = 139.9 ± 7.8 Ma (1σ)
Dispersion = 16 %
P(χ²) = 0.03
Peak 1: 98±19Ma (19±20%)
Peak 2: 152±12Ma (81±20%)

NAB-53-NY (n=25)
Central age = 185 ± 11 Ma (1σ)
Dispersion = 20 %
P(χ²) = 0.00
Peak 1: 159±11Ma (67±15%)
Peak 2: 259±40Ma (33±15%)

NAB-55-PA (n=25)
Central age = 150.1 ± 7.8 Ma (1σ)
Dispersion = 20 %
P(χ²) = 0.00
Peak 1: 106±11Ma (20±11%)
Peak 2: 159.3±9.2Ma (80±11%)

NAB-56-PA (n=24)
Central age = 136.7 ± 8.6 Ma (1σ)
Dispersion = 20 %
P(χ²) = 0.01
Peak 1: 108±10Ma (48±18%)
Peak 2: 169±16Ma (52±18%)

KimSed-3 (n=22)
Central age = 154 ± 11 Ma (1σ)
Dispersion = 26 %
$P(\chi^2) = 0.00$

Peak 1: 133.7±7.4Ma (81±10%)
Peak 2: 252±30Ma (19±10%)

Supplementary File D. Apatite (U-Th)/He Dating

As discussed in AHe Data section of Chapter 1, AHe single-grain ages vs. [eU] display weakly

negative to no trend.
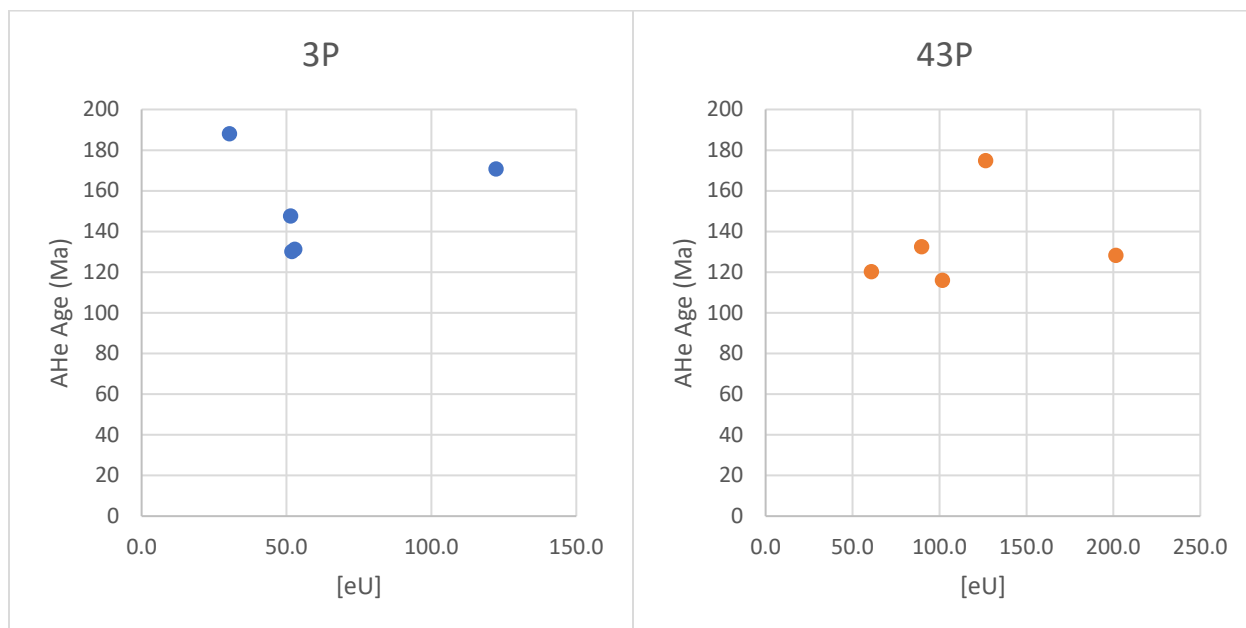
AHe single-grain ages vs. grain size (approximated by "r": radius of a sphere with an equivalent

surface area to volume ratio as the apatite grain) display a weakly positive trend.
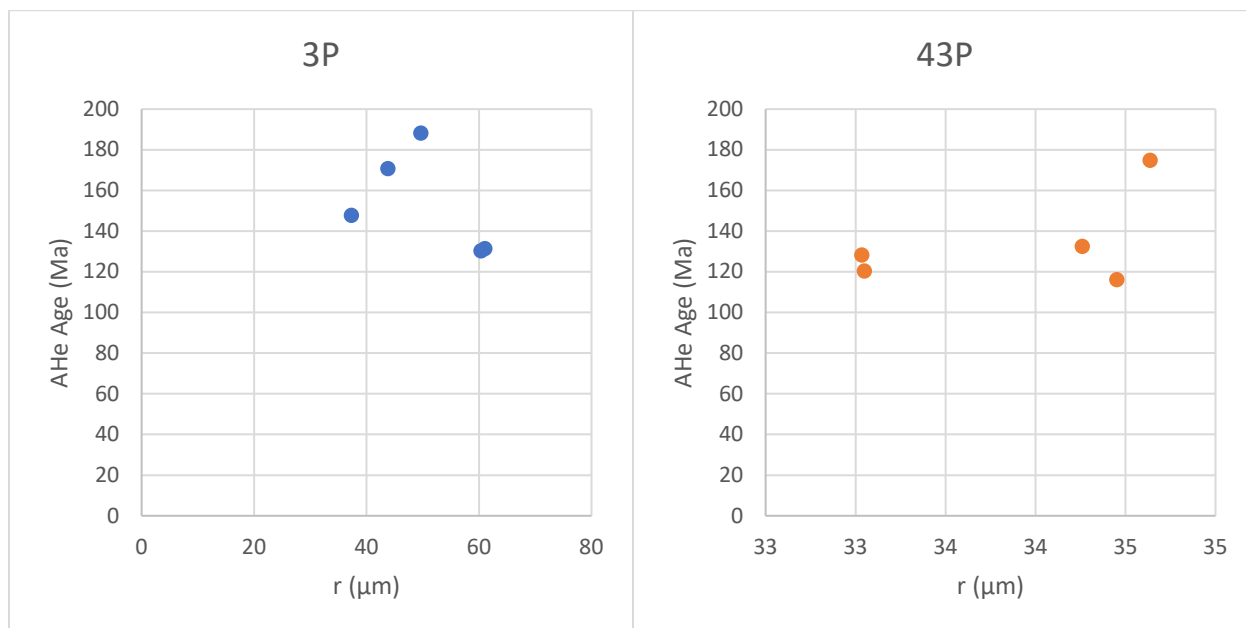
Supplementary File E. Shorten's Zeta Calibration

Apatite age standards (Fish Canyon Tuff, Durango, and Mt. Dromedary apatite) were counted to determine a personal zeta age calibration factor for fission-track dating (e.g. Hurford and Green, 1983). Before counting fission-tracks in apatite to familiarize Shorten with fission-track recognition and counting techniques, track densities in 6 external mica detectors of standard glasses (CN1, CN2 and CN5) were counted. Track densities counted from standard glasses were compared to those obtained by experienced fission-track workers at Syracuse University (e.g. Paul Fitzgerald and Paul O'Sullivan).

The zeta calibration results are listed in Table E1 and graphed in Fig. E2. A sample weighed mean zeta (the weighted mean of all determinations for each age standard) of 366 ± 35 was determined for the Fish Canyon Tuff apatite, 356 ± 10 for Durango apatite and 345 ± 26 for the Mt. Dromedary apatite. An overall weighted mean zeta of 356 ± 13 ($\pm 1\sigma$) was used when determining unknown apatite ages.

Table E1. Individual zeta determinations and SWMZ values for age standard apatites

Age standard (Age ±2σ) and apatite mount ID	No. of Grains	Standard Track Density (x 10⁶cm⁻²)	Spontaneous Track Density (x 10⁶cm⁻²)	Induced Track Density (x 10⁶cm⁻²)	χ^2 prob. (%)	Var. (%)	Zeta (±1σ)
Fish Canyon Tuff (27.8 ± 0.5 Ma)							
UA009-02 (FCT-11)	25	1.702 (5675)	0.1805 (256)	2.034 (2885)	99.7	0	369 ± 25
UA011-01 (FCT-14)	25	1.72 (5554)	0.1958 (276)	2.317 (3267)	93.6	0	383 ± 25
UA013-01 (FCT-3a)	25	1.967 (6475)	0.2132 (306)	2.537 (3640)	75.6	0	337 ± 21
							SWMZ = 366 ± 35
Durango (31.4 ± 0.5 Ma)							
UA009-01 (DUR-4)	29	1.69 (5675)	0.2205 (297)	2.21 (2976)	22.1	1	373 ± 24
UA009-11 (DUR-6a)	28	1.805 (5675)	0.2053 (362)	2.08 (3669)	80.8	0	353 ± 21
UA009-12 (DUR-6b)	25	1.816 (5675)	0.2386 (378)	2.369 (3753)	66.4	0	344 ± 20
UA009-13 (DUR-7b)	25	1.827 (5675)	0.2319 (361)	2.407 (3746)	65.9	0	358 ± 21
							SWMZ = 356 ± 10
Mt Dromedary (98.7 ± 0.5 Ma)							
UA009-03 (DROM-2b)	25	1.713 (5675)	0.9046 (576)	2.959 (1884)	6.9	15	380 ± 19
UA009-04 (DROM-2c)	25	1.725 (5675)	1.1154 (518)	3.583 (1664)	27.6	14	370 ± 19
UA011-04 (DROM-13a)	25	1.723 (5554)	1.1413 (577)	3.248 (1642)	60.2	0	329 ± 17
UA011-05 (DROM-13b)	25	1.725 (5554)	0.917 (499)	2.758 (1501)	8.1	14	347 ± 19
							SWMZ = 346 ± 26
							OWMZ = 356 ± 13

Brackets show number (no.) of tracks counted. Standard and induced track densities measured on mica external detectors (g=0.5) and spontaneous tracks densities on internal mineral surfaces (g=1). All samples pass the chi-squared test, with probabilities >5% (χ^2 prob.) and low single-grain age variation (Var.) indicating a single age population. SWMZ = sample weighted mean zeta (± 1σ); OWMZ = overall weighted mean zeta (± 1σ).
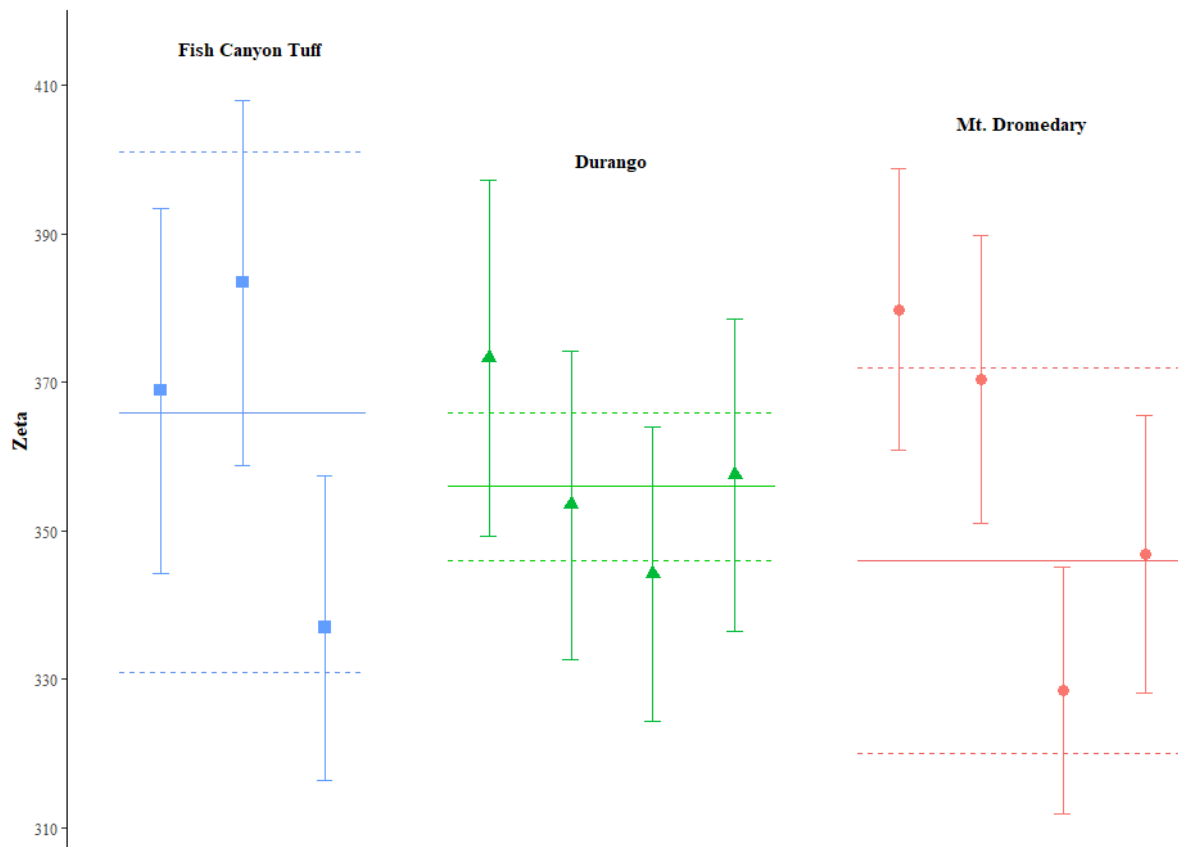
Figure E2. Repeated determinations of zeta for the apatite age standards Fish Canyon Tuff, Durango and Mt. Dromedary. Error bars are 1σ. The sample weighted mean zeta for each age standard is shown as a horizontal line ± 1σ (dashed lines).

Appendix B: Supplementary material for Chapter Two

Supplementary Table 1. Summary of apatite fission-track thermochronology results.

Sample (Strat. Age)	Lat. (°N), Long. (°W), Elev. (m)	No. of Grains	Standard Track Density (x 10^6 cm^{-2})	Spontaneous Track Density (x 10^6 cm^{-2})	Induced Track Density (x 10^6 cm^{-2})	χ^2 prob. (%)	Var. (%)	Age (Ma) (±1σ)	Mean Track Length (μm)	Std. Dev. (μm)	D_{par} (μm)
CAT-1 (LD)	41.9989, -74.3852 1272	18	1.05 (6671)	1.3152 (862)	1.831 (1200)	20.1	12	133 ± 7	12.5 ± 0.2 (34)	1.4	2.34 (0.3)
CAT-2 (LD)	42.0023, -74.4022 1112	14	1.06 (6671)	0.8939 (399)	1.304 (582)	71.0	0	128 ± 9	12.9 ± 0.3 (22)	1.6	2.15 (0.3)
CAT-3 (LD)	42.0074, -74.4204 871	25	1.071 (6671)	1.556 (1705)	2.224 (2437)	66.1	0	132 ± 5	12.9 ± 0.2 (100)	1.6	2.22 (0.3)
CAT-5 (MD)	41.9318, -74.3359 441	21	1.081 (6671)	1.0485 (698)	1.648 (1097)	16.0	11	122 ± 7	12.8 ± 0.2 (40)	1.2	2.39 (0.4)
CAT-6 (MD)	41.9731, -74.3128 281	20	1.091 (6671)	1.0609 (449)	1.843 (780)	17.6	16	114 ± 8	13.1 ± 0.2 (32)	1.1	2.38 (0.4)

Samples listed numerically from highest to lowest elevation, with stratigraphic age: LD – Late Devonian (383-359 Ma); MD – Middle Devonian (393-383 Ma). Location, elevation, and number of grains counted for AFT age included. Standard and induced track densities were counted on mica external detectors and spontaneous track densities were counted on internal apatite mineral surfaces, with the track count in parentheses. All samples were crushed and apatites were separated using conventional heavy liquid and magnetic separation techniques. Apatites were mounted and prepared for AFT thermochronology using standard methods (e.g. Kohn et al., 2018). Chi-square probability (χ^2 prob.) determines if grains are from a single age population; if the χ^2 value is >5%, it is likely that there is a single age population. Age variation (Var.) is the relative standard deviation of the central age and when variation is low (<~15%) the data are consistent with a single population. The external detector method (e.g. Gleadow, 1981) and zeta calibration approach (Hurford and Green, 1983) was used with a zeta of 353 ± 13 (± 1σ) for Shorten. Central ages are reported (Galbraith and Laslett, 1993). When possible, 100 horizontal confined fission-track lengths per sample were measured using a projection tube and a digitizing tablet (number of tracks measured in parentheses) and standard deviation of fission-track lengths (Std. Dev.) is reported. Mean D_{par} calculated from D_{par} measurements on grains used for AFT age, with std. dev. in parentheses.

Supplementary Table 2. Summary of (U-Th)/He results.

Grain #	Dim. Mass (mg)	r (μm)	length (μm)	U (ppm)	Th (ppm)	Sm (ppm)	eU	4He (nmol/g)	F_T	Raw Age (Ma)	Corr. Age (Ma)	Full Unc. (Ma)	Analytic Unc. (Ma)
CAT1, Honesdale Formation of the West Falls Group (Late Devonian), 41.9989 °N, -74.3852 °W, 1272 m elevation													
a1	2.9	50.27	124.80	6.78	23.57	17.68	12.3	6.025	0.711	89	124		5.9
a2	2.8	48.97	133.04	10.82	23.91	21.07	16.4	18.757	0.708	206	*288*		*9.8*
a4	5.4	63.79	186.75	0.18	2.25	1.36	0.7	1.281	0.758	323.66	*424*		*30.3*
a5	7.5	69.15	243.03	23.42	44.63	33.82	33.9	28.603	0.789	153	193		5.7
a6	8.7	75.88	194.29	0.11	3.05	32.58	0.8	9.593	0.792	1545.24	*1850*		*69.2*

Mean age ± 1 σ (% std. dev.) of all: 576 ± 721 (125%)
Mean age ± 1σ (% std. dev.) of grain 1 & 5: 159 ± 49 (31%)

Grain #	Dim. Mass (mg)	r (μm)	length (μm)	U (ppm)	Th (ppm)	Sm (ppm)	eU	4He (nmol/g)	F_T	Raw Age (Ma)	Corr. Age (Ma)	Full Unc. (Ma)	Analytic Unc. (Ma)
CAT3, Upper Walton Formation of the West Falls Group (Late Devonian), 42.0074 °N, -74.4204 °W, 871 m elevation													
a1	6.0	64.34	133.12	14.30	74.99	31.06	31.9	14.933	0.769	85	111		3.5

Mean age ± 1σ (% std. dev.): 111 ± 3 (0%)

Grain #	Dim. Mass (mg)	r (μm)	length (μm)	U (ppm)	Th (ppm)	Sm (ppm)	eU	4He (nmol/g)	F_T	Raw Age (Ma)	Corr. Age (Ma)	Full Unc. (Ma)	Analytic Unc. (Ma)
CAT5, Moscow Formation of the Hamilton Group (Middle Devonian), 41.9318 °N, -74.3359 °W, 441 m elevation													
a1	1.3	39.02	168.79	26.92	25.60	75.61	32.9	14.750	0.637	81	126	20.39	1.1
a2	1.4	40.16	141.41	14.47	0.00	21.92	14.5	8.720	0.652	109	164	22.23	2.8
a3	9.2	81.00	273.30	1.54	12.39	12.86	4.5	6.271	0.806	251	*309*	*22.61*	*3.4*
a4	6.0	75.59	137.58	5.43	108.06	21.46	30.8	10.986	0.786	65	83	5.99	0.6
a5	2.5	53.56	169.22	22.55	107.94	22.66	47.9	26.276	0.714	100	140	10.23	1.2

Mean age ± 1σ (% std. dev.) of all: 164 ± 86 (52%)
Mean age ± 1σ (% std. dev.) of grain 1, 2, 4 & 5: 128 ± 34 (27%)

Analyses were completed by CU TRaIL. Dim. Mass = dimensional mass of grain calculated from crystal volume and average apatite density; r = radius of a sphere with equivalent surface area to volume ratio as the grain; l = longest dimension of the grain. Concentrations of U, Th and Sm measured via isotope dilution on an ICP-MS. eU is the effective Uranium, calculated as [U] + 0.235[Th] (e.g. Flowers et al., 2009). Grains were degassed by heating with a laser to determine the amount of ^{4}He (nmol/g) in the grain. Alpha ejection correction (F_T) is a measure of the amount of He ejected from the crystal, values <0.65 (grey) indicate that a significant amount of He was ejected (Farley et al., 1996; Farley, 2002). Each grain degassed was followed by a re-extract to ensure there was no ^{4}He gas remaining in the crystal. If residual ^{4}He was measured the sample was rejected, as this typically indicates the presence of [U]-rich inclusions. Ages and F_T were calculated using methods described in Ketcham et al. (2011). Raw Age = age calculated from isotope concentrations, without F_T correction; Corr. Age = age calculated from isotope concentrations, with F_T correction (outliers in red, italics); Error = 2σ analytical uncertainty (not incorporating F_T uncertainty). Summarized in italics is the mean age of the single-grain corr. ages with 1σ error on the ages and in bold italics the mean age and 1σ error without outliers, with coefficient of variation (% std. dev.) in parenthesis. Exclusion of outliers is discussed in text. Averaging grain ages and determining variation of single-grain ages is after Ault et al. (2013). Coefficient of variation (% std. dev.) is calculated from the ratio of the standard deviation to the mean and indicates the variation of single-grain ages from the mean age.

Supplementary Table 3. CU TRaIL notes on apatite grains used for AHe analyses.

Grain #	Corr. Age (Ma)	Analytic Unc. (Ma)	Notes
CAT1, Honesdale Formation of the West Falls Group (Late Devonian), 41.9989 °N, -74.3852 °W, 1272 m elevation			
a1	124	5.9	broken segment, surface heavily pitted, tough to see inclusions, goes completely dark in XPL, fractures and brownish coloration
a2	*288*	*9.8*	broken segment, surface heavily pitted, tough to see inclusions, goes completely dark in XPL, fractures and brownish coloration
a4	*424*	*30.3*	broken end, many surface pits though interior appears clear. Crack visible inside. Goes completely dark in xpl, but may have small inclusions
a5	193	5.7	many surface pits, but interior appears clear. Fracture shines in XPL. Broken segment. May have inclusions
a6	*1850*	*69.2*	many surface pits, but interior appears clear. dark in XPL. Broken segment. Brownish coloration in the interior. May have small inclusions
			Mean age ± 1σ (% std. dev.) of all: 576 ± 721 (125%)
			Mean age ± 1σ (% std. dev.) of grain 1, 2 & 5: 202 ± 82 (41%)
			Mean age ± 1σ (% std. dev.) of grain 1 & 5: 159 ± 49 (31%)
CAT3, Upper Walton Formation of the West Falls Group (Late Devonian), 42.0074 °N, -74.4204 °W, 871 m elevation			
a1	111	3.5	large, 2 fractured ends, no visible inclusions, surface a bit marked but most is clear enough to see through
			Mean age ± 1σ (% std. dev.): 111 ± 3 (0%)
CAT5, Moscow Formation of the Hamilton Group (Middle Devonian), 41.9318 °N, -74.3359 °W, 441 m elevation			
a1	126	1.1	clear, no inclusions, looks like 2 pyr
a2	164	2.8	clear, no inclusions, looks like 1 pyr
a3	*309*	*3.4*	very rounded, heavily pitted, no obvious inclusions, some marks and fractures could obscure small incl., blue and reddish brown intf colors, seems to be apatite (lower relief than zircons in same sample)
a4	83	0.6	very rounded, heavily pitted, could be broken tip, no obvious inclusions, some marks and fractures could obscure small incl., blue and reddish brown intf colors, seems to be apatite (lower relief than zircons in same sample)
a5	140	1.2	very rounded, heavily pitted, no obvious inclusions, some marks and fractures could obscure small incl., blue and reddish brown intf colors, seems to be apatite (lower relief than zircons in same sample)
			Mean age ± 1σ (% std. dev.) of all: 164 ± 86 (52%)
			Mean age ± 1σ (% std. dev.) of grain 1, 2, 4 & 5: 128 ± 34 (27%)

Supplementary File A. Apatite (U-Th)/He Dating

AHe single-grain ages vs. effective urainium [eU] display a weakly negative to no trend.
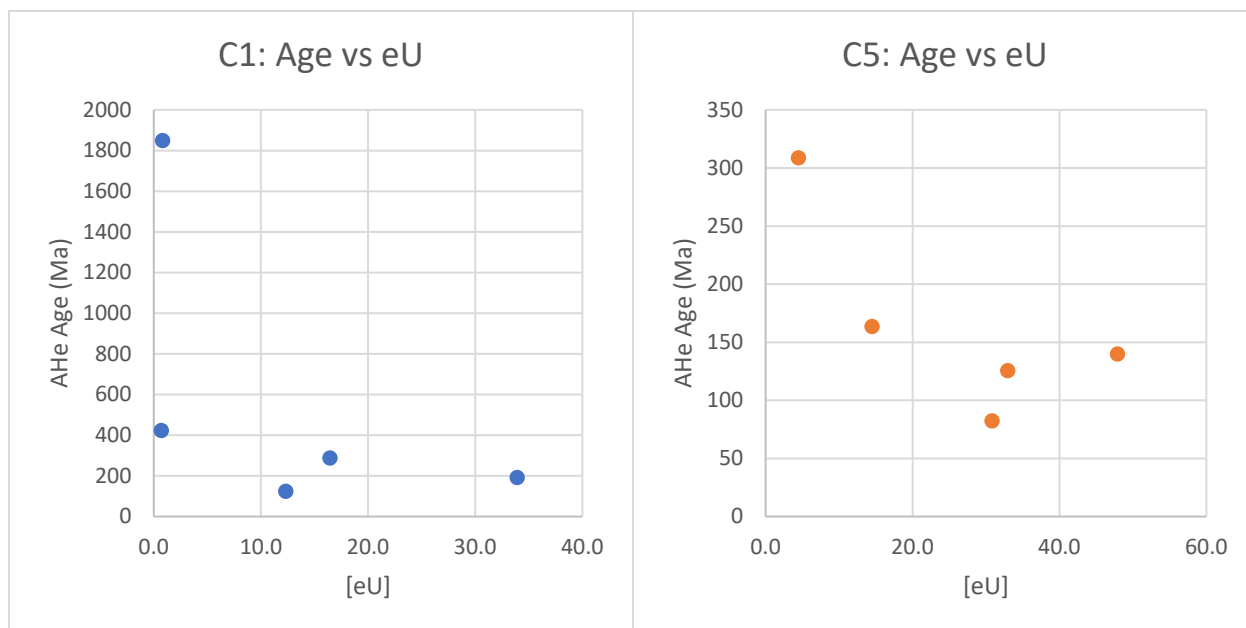
AHe single-grain ages vs. grain size (approximated by "r": radius of a sphere with an equivalent surface area to volume ratio as the apatite grain) also display no trend.
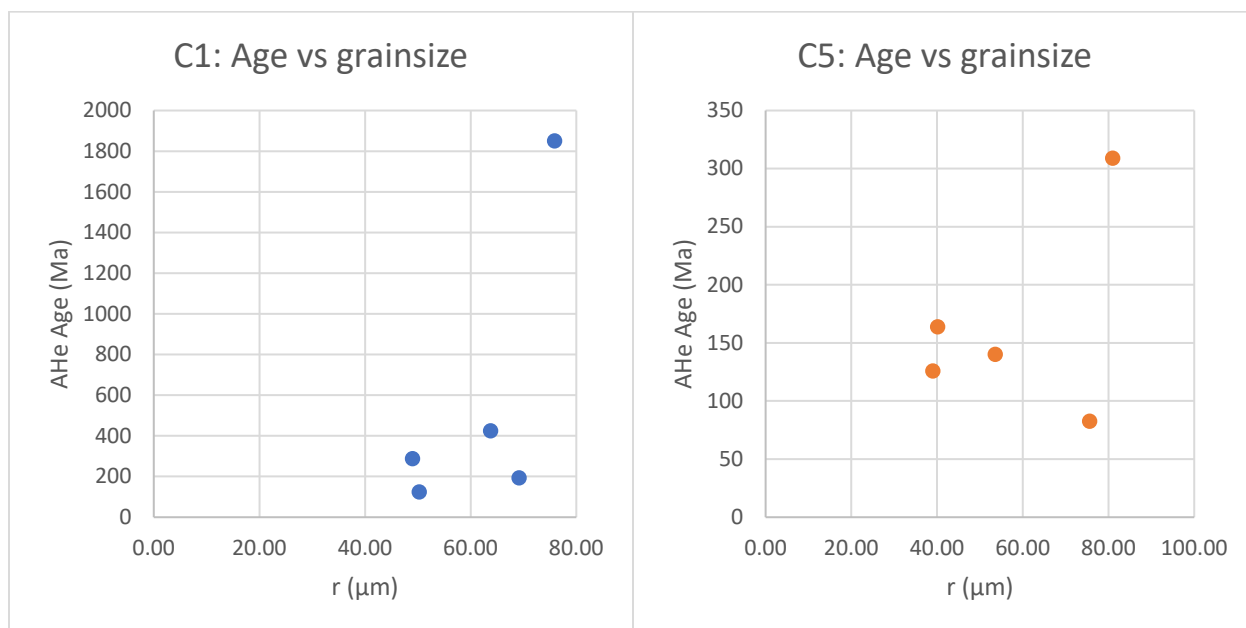
Supplementary File B. Inverse Thermal Models

In this supplementary file, the screenshots of HeFTy (Ketcham, 2005) inverse thermal models are included. The following information is presented for each sample: the time-temperature history path envelopes (good paths in purple and acceptable paths in green), the best-fit (black path) and weighted mean path (thick blue path), and the constraint boxes which includes stratigraphic age and paleo-temperature (olive box; Woodrow et al., 1973); AFT track length distribution, calculated track length distribution based on best-fit path; model goodness-of-fit (GOF) statistics and the age of the oldest fission track that has not been completely annealed ("Old"; Ketcham, 2005); AHe diffusion profile and GOF statistics when present; and vitrinite reflectance (%R_o) output, which includes modeled and measured values (">" sign means the %R_o calculation does not include a depositional event). See Chapter 1 supplementary information for further discussion on development of inverse thermal models and constraints.

In this file, thermal models constrained with and without additional apatite (U-Th)/He (AHe) dates are included. AHe data contained single-grain age variation with outliers significantly older than AFT ages (Table 2). The addition of AHe data in inverse thermal modeling generally yielded more tightly constrained time-temperature path envelopes through the PRZ (~30-90 °C) but sample C1 was unable to model any good or acceptable paths using both AHe and AFT data. Given that AHe single-grain ages contained significant variation and AFT data contains the kinetic parameter (i.e. fission track length), as discussed in the paper, when the model was unable to produce paths with AHe and AFT data, AFT data was used exclusively.

C1 – with AHe data
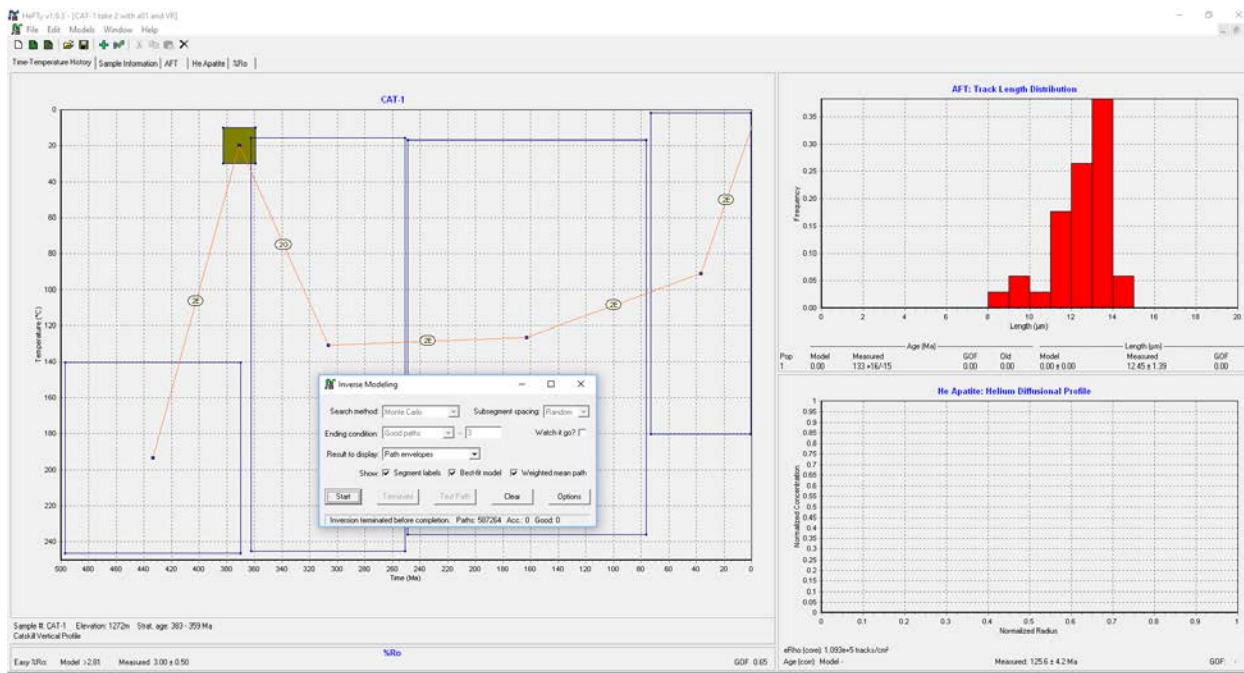
C1 – without AHe data
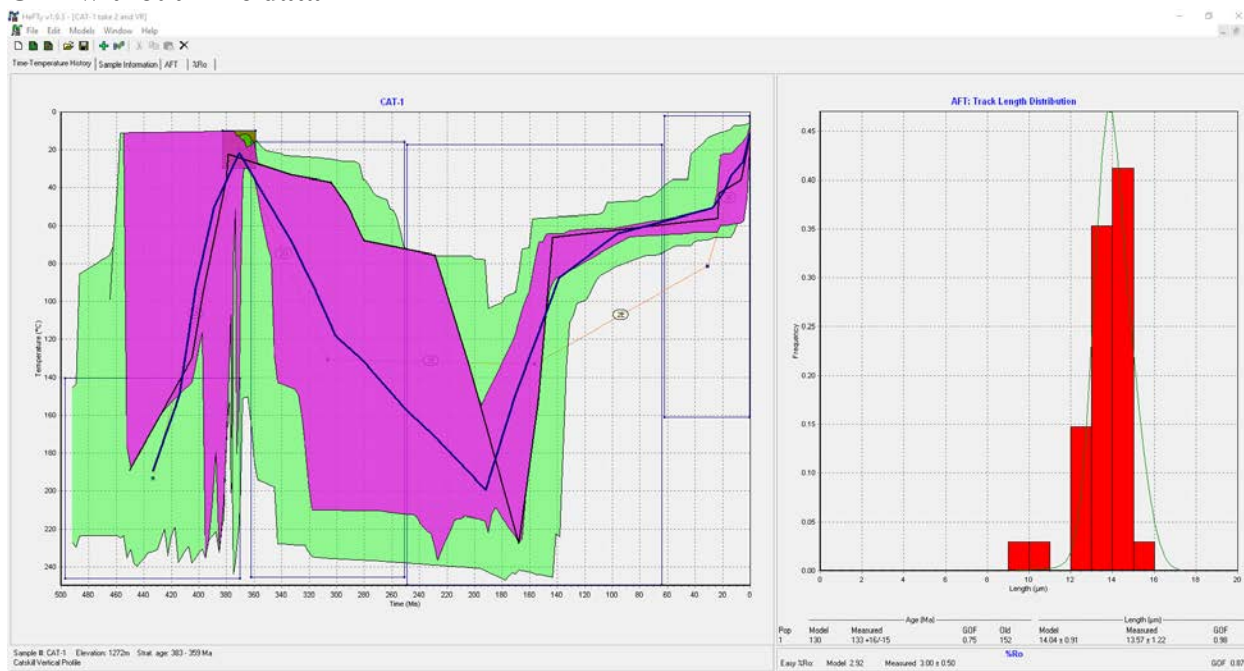
C2
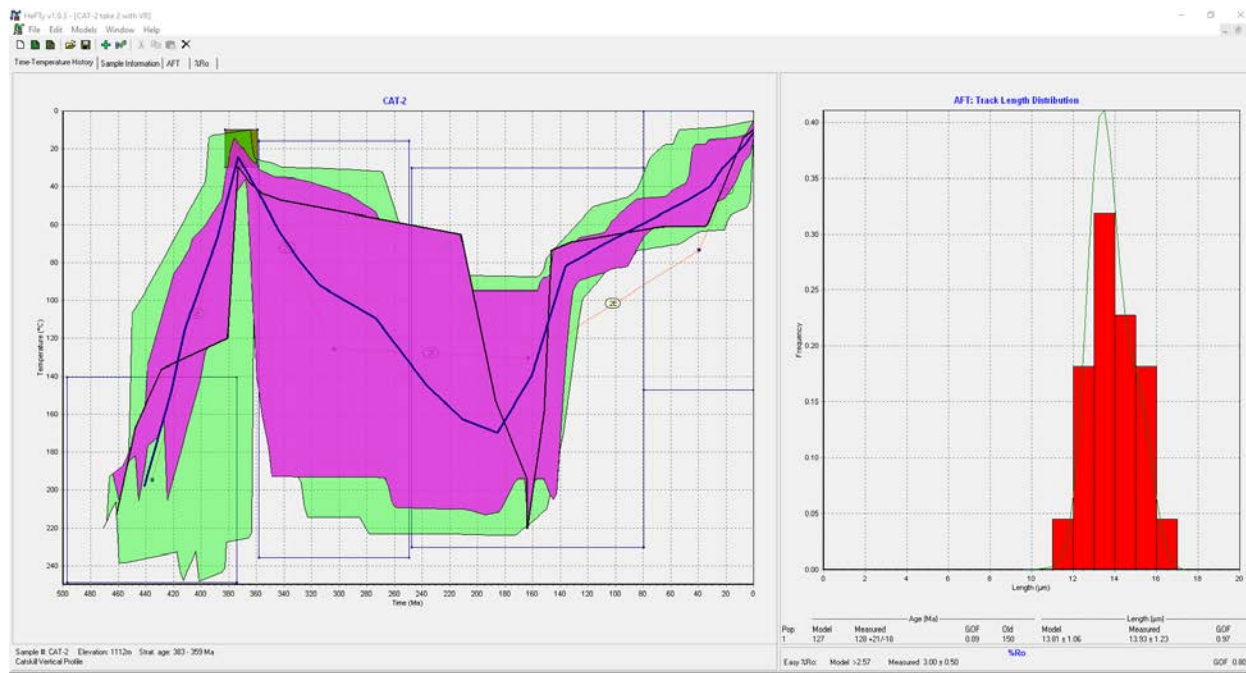
C3 – with AHe data

C3 – without AHe data
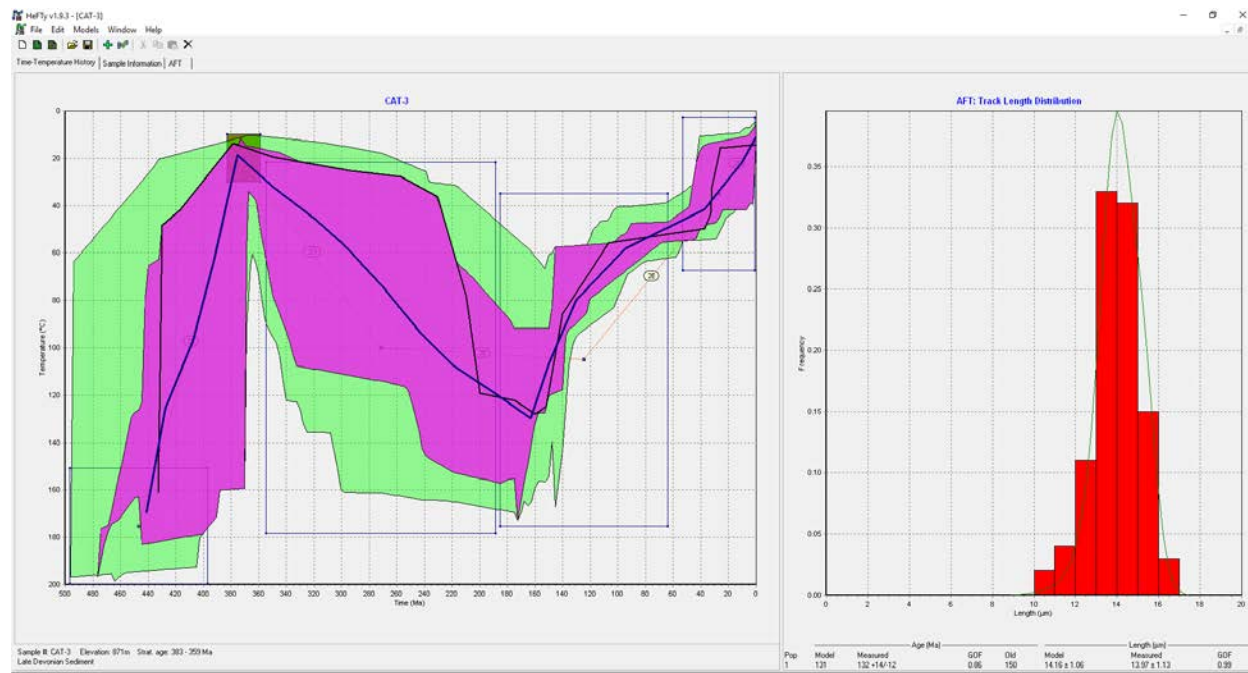
C5
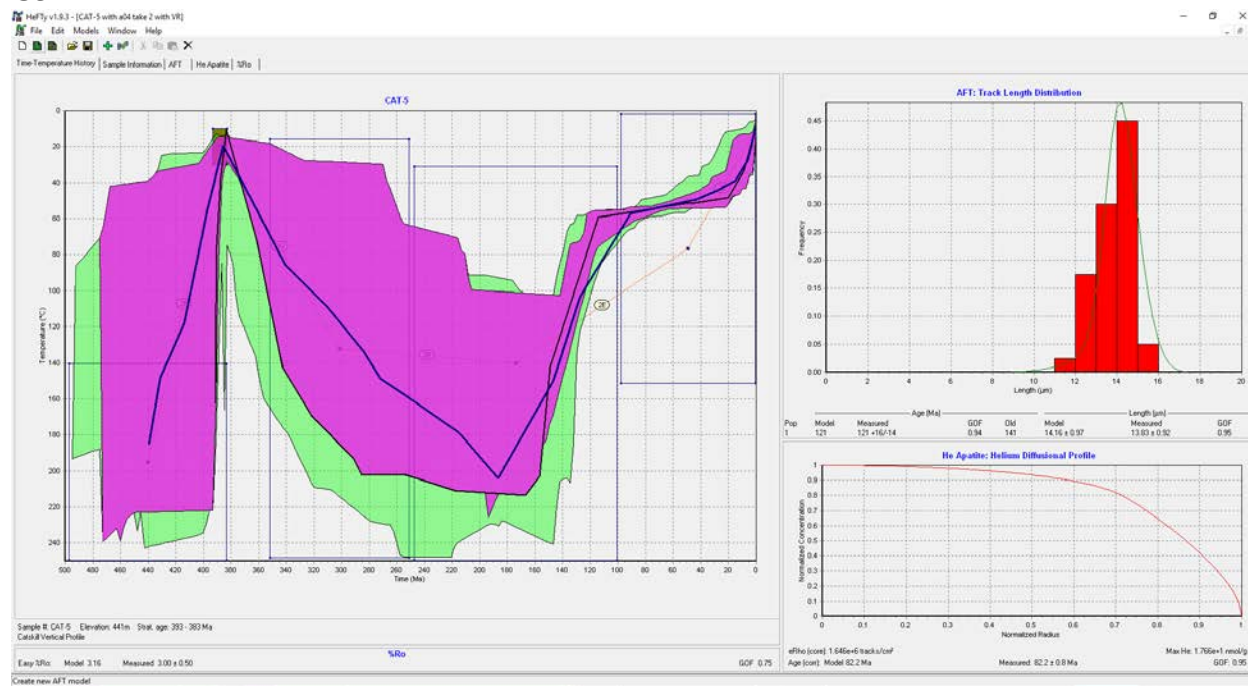
C6
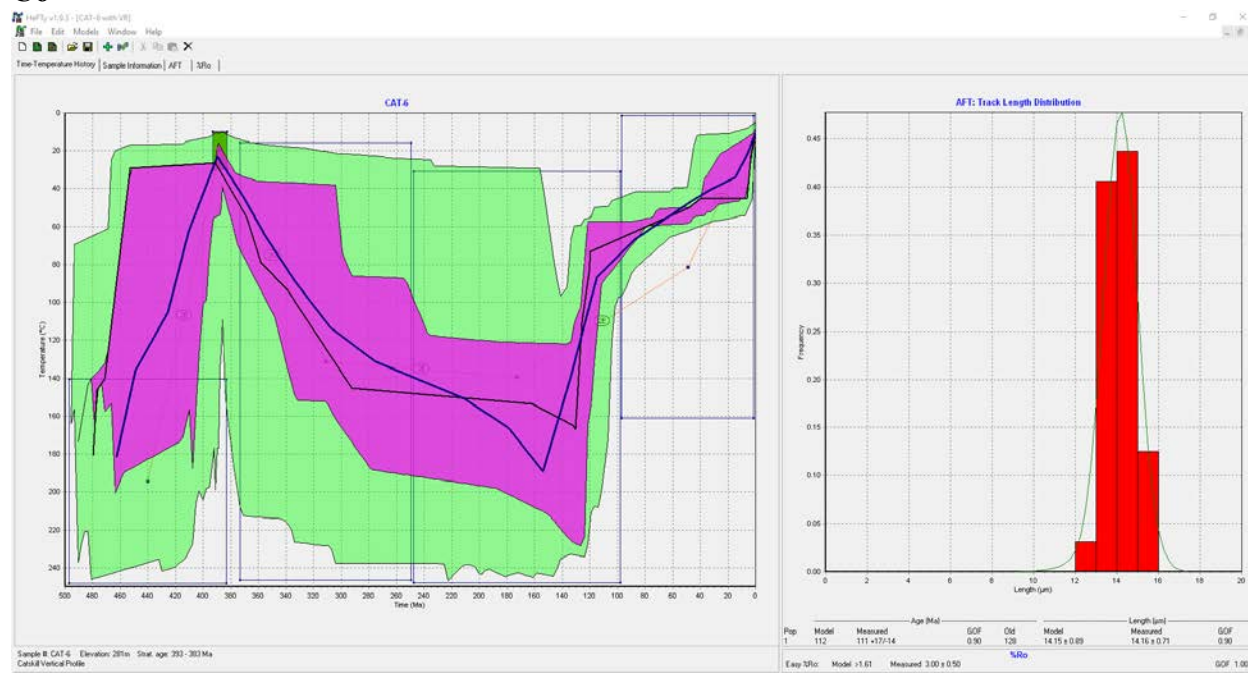
Appendix C: Supplementary material for Chapter Three

Appalachian Low-Temperature Thermochronology Database (AppLTDB) Information Guide:

Database was created without spaces to allow for seamless loading into ArcGIS.
Can be ordered in alphabetical order (row # and Ref_Order) or from north to south (N-S_Order), which was determined by arranging studies by latitude.
Location Data:
Sample ID and location data (latitude/longitude in decimal degrees) is from published tables (Table), GPS measured values (Measured), manually georeferenced pdfs in ArcGIS (Manual_Georef) or published georeferenced figures (GeoTiff).
Elevation (meters) is from published tables (Table), text of the paper (Text), GPS measured values (Measured) or estimated on Google Earth Pro (GoogleEarthPro). Negative values indicate depth of sample below surface.
AFT Age Data:
Apatite fission-track ages (AFT_age; Ma), 1-sigma error (AFT_1sig), chi-squared % values (chi2; when reported), mean track length (MTL; µm), and standard deviation (Std_Dev; µm)
AHe Age Data:
Apatite (U-Th)/He ages (AHe_age; Ma), 2-sigma analytical error (AHe_2sig) and single-grain age variation (Var; when reported)
Physiographic Provinces:
Physiographic province (Province) polygons were determined and drawn into ArcGIS from Soeder et al. (2014). Polygon layer was joined with sample point data to determine province of each sample location.
Rift Basins (Rift_Basins) polygons were drawn into ArcGIS from Withjack et al. (2012). Polygon layer was joined with sample point data to determine if sample lay within a rift basin. Output dash if not within rift basin.
Lithology
United State lithologic maps from the USGS The State Geologic Map Compilation (SGMC) Geodatabase of the Conterminous United States (Horton, 2017). Polygon layer was joined with sample point data to determine lithology of each sample location.
Information includes: original map unit label from state geologic maps (ORIG_LABEL); SGMC map unit label (SGMC_LABEL); unique value for every unite in the SGMC (UNIT_LINK), also the easiest way to look up details on the USGS Mineral Resources Online Spatial Database; USGS state agency code (SOURCE); unit formational/depositional age (UNIT_AGE); lithology ranked by the SGMC compiler as a major component of the geologic unit (ROCKTYPE1); lithology ranked by the SGMC compiler as the second major component of the geologic unit (ROCKTYPE2).
HydroSHEDS Database
USGS database of geo-references catchment boundaries (Lehner et al., 2008). Database name is an abbreviation of: **Hydro**logical data and maps based on **SH**uttle **E**levation **D**erivatives at multiple **S**cales (http://www.hydrosheds.org)**.**
Drainage polygon layer was joined with sample point data to determine which catchment each sample location was within.
Which part of the Atlantic (i.e. North, Middle, or South) or Gulf of Mexico catchments drain to (Drain_To) was determined using Pazzaglia and Brandon (1996).

Appalachian Low-Temperature Thermochronology Database (AppLTDB)

Ordering			Location Data							AFT Data					AHe Data			Physiographic_Provinces		Lithology (USGS)							HydroSHEDS Database	
Row	Ref_Order	N-S_Order	Study	Sample_ID	Latitude	Longitude	Loc_Data	Elevation	Elev_Data	AFT_age	AFT_1sig	chi2	MTL	Std_Dev	AHe_age	AHe_2sig	Var	Province	Rift_Basin	ORIG_LABEL	SGMC_LABEL	UNIT_LINK	SOURCE	UNIT_AGE	ROCKTYPE1	ROCKTYPE2	Drainage	Drain_To
3	Ref01	NS09	Amidonetal.,2016	V14	43.997	-71.201	GeoTIFF	514	Table	-	-	-	-	-	88	3	4	Taconic_Acadian_Terrane	-	J4hx	J4hx;0	NHJ4hx;0	NH001	Jurassic	quartz syenite		Saco	North_Atlantic
4	Ref01	NS09	Amidonetal.,2016	V13	43.997	-71.201	GeoTIFF	204	Table	82	8	-	-	-	131	5	5	Taconic_Acadian_Terrane	-	J4hx	J4hx;0	NHJ4hx;0	NH001	Jurassic	quartz syenite		Saco	North_Atlantic
5	Ref01	NS09	Amidonetal.,2016	V15	43.997	-71.201	GeoTIFF	-122	Table	68	6	-	-	-	65	4	6	Taconic_Acadian_Terrane	-	J4hx	J4hx;0	NHJ4hx;0	NH001	Jurassic	quartz syenite		Saco	North_Atlantic
6	Ref01	NS09	Amidonetal.,2016	V16	43.997	-71.201	GeoTIFF	-404	Table	-	-	-	-	-	60	10	16	Taconic_Acadian_Terrane	-	J4hx	J4hx;0	NHJ4hx;0	NH001	Jurassic	quartz syenite		Saco	North_Atlantic
7	Ref01	NS09	Amidonetal.,2016	V17	43.997	-71.201	GeoTIFF	-695	Table	62	6	-	-	-	40	6	15	Taconic_Acadian_Terrane	-	J4hx	J4hx;0	NHJ4hx;0	NH001	Jurassic	quartz syenite		Saco	North_Atlantic
8	Ref02	NS19	Blackmeretal.,1994	BE-10	41.17164	-77.02536	Manual_Georef	320	Table	146	8	89	12.4	1.8	-	-	-	Valley_and_Ridge	-	St	St;19	PASt;19	PA002	Silurian	quartzite	sandstone	Susquehanna	Mid_Atlantic
9	Ref02	NS19	Blackmeretal.,1994	BE-11	41.1333	-77.14227	Manual_Georef	500	Table	163	11	66	11.8	2.4	-	-	-	Valley_and_Ridge	-	Or	Or;15	PAOr;15	PA002	Ordovician	shale	siltstone	Susquehanna	Mid_Atlantic
10	Ref02	NS19	Blackmeretal.,1994	BE-7	41.0616	-77.27868	Manual_Georef	380	Table	155	9	13	11.5	2.6	-	-	-	Valley_and_Ridge	-	Oj	Oj;15	PAOj;15	PA002	Ordovician	sandstone	shale	Susquehanna	Mid_Atlantic
11	Ref02	NS19	Blackmeretal.,1994	CK-1	41.28803	-77.66841	Manual_Georef	400	Table	148	9	5	11.4	2.7	-	-	-	Appalachian	-	MDhm	MDhm;13	PAMDhm;13	PA002	Mississippian and Devonian	sandstone	siltstone	Susquehanna	Mid_Atlantic
12	Ref02	NS19	Blackmeretal.,1994	CK-10	41.49612	-77.17936	Manual_Georef	442	Table	155	10	5	11.9	2.2	-	-	-	Appalachian	-	Dck	Dck;12	PADck;12	PA002	Devonian	sandstone	siltstone	Susquehanna	Mid_Atlantic
13	Ref02	NS19	Blackmeretal.,1994	CK-11	41.49181	-76.58156	Manual_Georef	375	Table	134	7	5	11.3	2.6	-	-	-	Appalachian	-	Mb	Mb;10	PAMb;10	PA002	Mississippian	sandstone	conglomerate	Susquehanna	Mid_Atlantic
14	Ref02	NS19	Blackmeretal.,1994	CK-12	41.47325	-75.70214	Manual_Georef	341	Table	134	7	5	12.3	2.2	-	-	-	Valley_and_Ridge	-	Dck	Dck;12	PADck;12	PA002	Devonian	sandstone	siltstone	Susquehanna	Mid_Atlantic
15	Ref02	NS19	Blackmeretal.,1994	CK-3	40.18229	-78.04512	Manual_Georef	320	Table	125	8	5	11.7	2.3	-	-	-	Valley_and_Ridge	-	Dck	Dck;12	PADck;12	PA002	Devonian	sandstone	siltstone	Susquehanna	Mid_Atlantic
16	Ref02	NS19	Blackmeretal.,1994	CK-7	39.80811	-79.46094	Manual_Georef	402	Table	151	21	5	11.6	2.4	-	-	-	Appalachian	-	Pp	PAp;6	PAPAp;6	PA002	Pennsylvanian	sandstone	conglomerate	Mississippian	Gulf_of_Mexico
17	Ref02	NS19	Blackmeretal.,1994	CK-8	41.29969	-78.17528	Manual_Georef	256	Table	154	8	5	10.7	2.9	-	-	-	Appalachian	-	Pp	PAp;6	PAPAp;6	PA002	Pennsylvanian	sandstone	conglomerate	Susquehanna	Mid_Atlantic
18	Ref02	NS19	Blackmeretal.,1994	CK-9	41.193	-77.36691	Manual_Georef	177	Table	167	11	7	11.7	2.2	-	-	-	Valley_and_Ridge	-	Dlh	Dlh;15	PADlh;15	PA002	Devonian	mudstone	siltstone	Susquehanna	Mid_Atlantic
19	Ref02	NS19	Blackmeretal.,1994	D-3	40.58535	-78.39483	Manual_Georef	439	Table	137	13	5	11.8	2.7	-	-	-	Appalachian	-	Dlh	Dlh;15	PADlh;15	PA002	Devonian	mudstone	siltstone	Susquehanna	Mid_Atlantic
20	Ref02	NS19	Blackmeretal.,1994	D-4	40.47676	-77.15693	Manual_Georef	168	Table	164	19	5	12.3	1.9	-	-	-	Valley_and_Ridge	-	Dciv	Dciv;17	PADciv;17	PA002	Devonian	siltstone	mudstone	Susquehanna	Mid_Atlantic
21	Ref02	NS19	Blackmeretal.,1994	D-5	41.10177	-76.34846	Manual_Georef	469	Table	123	9	5	11.4	2.1	-	-	-	Valley_and_Ridge	-	Dcsc	Dcsc;17	PADcsc;17	PA002	Devonian	mudstone	siltstone	Susquehanna	Mid_Atlantic
22	Ref02	NS19	Blackmeretal.,1994	D-7	41.36782	-75.56402	Manual_Georef	463	Table	111	7	5	11.9	2.3	-	-	-	Appalachian	-	Dcd	Dcd;17	PADcd;17	PA002	Devonian	sandstone	siltstone	Susquehanna	Mid_Atlantic
23	Ref02	NS19	Blackmeretal.,1994	J-1	40.94349	-77.58054	Manual_Georef	274	Table	142	11	25	12.0	2.6	-	-	-	Valley_and_Ridge	-	St	St;19	PASt;19	PA002	Silurian	quartzite	sandstone	Susquehanna	Mid_Atlantic
24	Ref02	NS19	Blackmeretal.,1994	PA-13	40.93552	-78.5689	Manual_Georef	402	Table	131	15	5	11.9	2.2	-	-	-	Appalachian	-	Pcg	PAcg;6	PAPAcg;6	PA002	Pennsylvanian	shale	sandstone	Susquehanna	Mid_Atlantic
25	Ref02	NS19	Blackmeretal.,1994	PA-15	39.9887	-79.18929	Manual_Georef	469	Table	153	16	5	11.9	2.2	-	-	-	Appalachian	-	Pcg	PAcg;6	PAPAcg;6	PA002	Pennsylvanian	shale	sandstone	Mississippian	Gulf_of_Mexico
26	Ref02	NS19	Blackmeretal.,1994	PA-17	39.84323	-80.42626	Manual_Georef	-107	Table	144	11	5	11.0	2.5	-	-	-	Appalachian	-	Pg	Pg;0	PAPg;0	PA002	Permian	sandstone	shale	Mississippian	Gulf_of_Mexico
27	Ref02	NS19	Blackmeretal.,1994	PA-2	40.59571	-78.49401	Manual_Georef	457	Table	139	16	5	11.9	2.4	-	-	-	Appalachian	-	Pa	PAa;6	PAPAa;6	PA002	Pennsylvanian	sandstone	shale	Susquehanna	Mid_Atlantic
28	Ref02	NS19	Blackmeretal.,1994	PA-3	40.2655	-78.8385	Manual_Georef	555	Table	133	10	45	11.9	2.4	-	-	-	Appalachian	-	Pcc	PAcc;6	PAPAcc;6	PA002	Pennsylvanian	shale	siltstone	Mississippian	Gulf_of_Mexico
29	Ref02	NS19	Blackmeretal.,1994	PA-9	40.86381	-79.5731	Manual_Georef	354	Table	184	10	5	12.5	2.0	-	-	-	Appalachian	-	Pa	PAa;6	PAPAa;6	PA002	Pennsylvanian	sandstone	shale	Mississippian	Gulf_of_Mexico
30	Ref02	NS19	Blackmeretal.,1994	PG-1	40.67591	-79.05684	Manual_Georef	396	Table	141	10	5	12.2	2.6	-	-	-	Appalachian	-	Pcg	PAcg;6	PAPAcg;6	PA002	Pennsylvanian	shale	sandstone	Mississippian	Gulf_of_Mexico
31	Ref02	NS19	Blackmeretal.,1994	PL-1	41.20324	-76.06149	Manual_Georef	165	Table	144	9	31	12.7	1.7	-	-	-	Valley_and_Ridge	-	Mp	Mp;11	PAMp;11	PA002	Mississippian	sandstone	siltstone	Susquehanna	Mid_Atlantic
32	Ref02	NS19	Blackmeretal.,1994	PL-2	41.4443	-75.64281	Manual_Georef	305	Table	140	8	45	12.3	1.9	-	-	-	Appalachian	-	Pl	PAl;7	PAPAl;7	PA002	Pennsylvanian	sandstone	siltstone	Susquehanna	Mid_Atlantic
33	Ref02	NS19	Blackmeretal.,1994	PL-6	40.7263	-76.44836	Manual_Georef	290	Table	141	10	55	13.1	1.5	-	-	-	Valley_and_Ridge	-	Dcd	Dcd;17	PADcd;17	PA002	Devonian	sandstone	siltstone	Susquehanna	Mid_Atlantic
34	Ref02	NS19	Blackmeretal.,1994	PM-1	40.14781	-80.172	Manual_Georef	347	Table	172	9	45	12.0	2.0	-	-	-	Appalachian	-	Pg	Pg;0	PAPg;0	PA002	Permian	sandstone	shale	Mississippian	Gulf_of_Mexico
35	Ref02	NS19	Blackmeretal.,1994	PM-2	39.88219	-80.41208	Manual_Georef	347	Table	167	9	5	11.5	2.5	-	-	-	Appalachian	-	Pg	Pg;0	PAPg;0	PA002	Permian	sandstone	shale	Mississippian	Gulf_of_Mexico
36	Ref02	NS19	Blackmeretal.,1994	PMN-1	39.84161	-79.92677	Manual_Georef	235	Table	142	12	5	11.8	2.2	-	-	-	Appalachian	-	Pm	PAm;6	PAPAm;6	PA002	Pennsylvanian	limestone	shale	Mississippian	Gulf_of_Mexico
37	Ref03	NS26	Boettcher&Milliken,1994	KY49_A	37.34292	-82.38047	Manual_Georef	220	Table	98	7	13	12.4	2.1	-	-	-	Appalachian	-	PAbl	PAbl;0	KYPAbl;0	KY001	Pennsylvanian	shale	siltstone	Mississippian	Gulf_of_Mexico
38	Ref03	NS26	Boettcher&Milliken,1994	VA26_B	37.32707	-82.18038	Manual_Georef	280	Table	104	8	44	12.6	1.6	-	-	-	Appalachian	-	@w	PAw;0	VAPAw;0	VA003	Pennsylvanian	sandstone	siltstone	Mississippian	Gulf_of_Mexico
39	Ref03	NS26	Boettcher&Milliken,1994	KY112_C	37.37566	-82.52885	Manual_Georef	240	Table	125	10	43	12.1	1.8	-	-	-	Appalachian	-	PAbl	PAbl;0	KYPAbl;0	KY001	Pennsylvanian	shale	siltstone	Mississippian	Gulf_of_Mexico
40	Ref03	NS26	Boettcher&Milliken,1994	VA24_D	37.21949	-82.20206	Manual_Georef	450	Table	92	7	24	12.3	1.8	-	-	-	Appalachian	-	@n	PAn;0	VAPAn;0	VA003	Pennsylvanian	shale	siltstone	Mississippian	Gulf_of_Mexico
41	Ref03	NS26	Boettcher&Milliken,1994	KY115_E	37.22283	-82.56396	Manual_Georef	420	Table	120	10	18	12.5	1.6	-	-	-	Appalachian	-	PAbl	PAbl;0	KYPAbl;0	KY001	Pennsylvanian	shale	siltstone	Mississippian	Gulf_of_Mexico
42	Ref03	NS26	Boettcher&Milliken,1994	VA4_F	37.26837	-82.2967	Manual_Georef	550	Table	123	8	9	12.1	1.5	-	-	-	Appalachian	-	@n	PAn;0	VAPAn;0	VA003	Pennsylvanian	shale	siltstone	Mississippian	Gulf_of_Mexico
43	Ref03	NS26	Boettcher&Milliken,1994	VA6_G	37.13783	-82.40346	Manual_Georef	550	Table	98	8	59	12.2	1.5	-	-	-	Appalachian	-	@wg	PAwg;0	VAPAwg;0	VA003	Pennsylvanian	sandstone	siltstone	Mississippian	Gulf_of_Mexico
44	Ref03	NS26	Boettcher&Milliken,1994	VA19_H	37.15527	-82.58703	Manual_Georef	700	Table	137	8	8	12.9	1.3	-	-	-	Appalachian	-	@n	PAn;0	VAPAn;0	VA003	Pennsylvanian	shale	siltstone	Mississippian	Gulf_of_Mexico
45	Ref03	NS26	Boettcher&Milliken,1994	KY46A_I	37.6149	-82.27152	Manual_Georef	220	Table	127	8	15	12.5	1.7	-	-	-	Appalachian	-	PAbl	PAbl;0	KYPAbl;0	KY001	Pennsylvanian	shale	siltstone	Mississippian	Gulf_of_Mexico
46	Ref03	NS26	Boettcher&Milliken,1994	KY109_J	37.43917	-82.49349	Manual_Georef	220	Table	131	8	16	12.9	1.7	-	-	-	Appalachian	-	PAbl	PAbl;0	KYPAbl;0	KY001	Pennsylvanian	shale	siltstone	Mississippian	Gulf_of_Mexico
47	Ref04	NS03	Doherty&Lyons, 1980	1_VT-AV-1-73	44.89355	-71.55512	Manual_Georef	729	GoogleEarthPro	114	8	-	-	-	-	-	-	Taconic_Acadian_Terrane	-	ws	ws;0	VTws;0	VT001	Permian-Triassic	syenite	quartz syenite	Connecticut	Mid_Atlantic
48	Ref04	NS03	Doherty&Lyons, 1980	2_NH-AV-2-73	44.73824	-71.55696	Manual_Georef	798	GoogleEarthPro	96	10	-	-	-	-	-	-	Taconic_Acadian_Terrane	-	Jc1b	Jc1b;0	NHJc1b;0	NH001	Middle - Late? Jurassic	granite		Connecticut	Mid_Atlantic
49	Ref04	NS03	Doherty&Lyons, 1980	4_NH-WN-6-73	43.55587	-71.36665	Manual_Georef	253	GoogleEarthPro	90	10	-	-	-	-	-	-	Taconic_Acadian_Terrane	-	J7x	J7x;0	NHJ7x;0	NH001	Jurassic	syenite		Merrimac	Mid_Atlantic
50	Ref04	NS03	Doherty&Lyons, 1980	5_NH-WN-7-73	43.498	-71.1826	Manual_Georef	278	GoogleEarthPro	81	8	-	-	-	-	-	-	Taconic_Acadian_Terrane	-	Kc1b	Kc1b;0	NHKc1b;0	NH001	Early Cretaceous	granite		Merrimac	Mid_Atlantic
51	Ref04	NS03	Doherty&Lyons, 1980	6_NH-PK-8-73	43.10379	-71.2015	Manual_Georef	141	GoogleEarthPro	122	12	-	-	-	-	-	-	Taconic_Acadian_Terrane	-	K9AB	K9AB;0	NHK9AB;0	NH001	Cretaceous	diorite	gabbro	Piscataqua	North_Atlantic
52	Ref04	NS03	Doherty&Lyons, 1980	7_NH-PL-9-73	43.90956	-71.52684	Manual_Georef	701	GoogleEarthPro	102	16	-	-	-	-	-	-	Taconic_Acadian_Terrane	-	Jc1b	Jc1b;0	NHJc1b;0	NH001	Middle - Late? Jurassic	granite		Merrimac	Mid_Atlantic
53	Ref04	NS03	Doherty&Lyons, 1980	8_VT-AS-10-73	43.43108	-72.44545	Manual_Georef	708	GoogleEarthPro	101	6	-	-	-	-	-	-	Taconic_Acadian_Terrane	-	ws	ws;0	VTws;0	VT001	Permian-Triassic	syenite	quartz syenite	Connecticut	Mid_Atlantic
54	Ref04	NS03	Doherty&Lyons, 1980	9_NH-NC-11-73	43.99293	-71.08628	Manual_Georef	136	GoogleEarthPro	94	8	-	-	-	-	-	-	Taconic_Acadian_Terrane	-	PM1m	PAM1m;0	NHPAM1m;0	NH001	Mississippian - Pennsylvanian	granite		Saco	North_Atlantic
55	Ref04	NS03	Doherty&Lyons, 1980	10_NH-FN-12-73	44.15513	-71.69194	Manual_Georef	945	GoogleEarthPro	82	12	-	-	-	-	-	-	Taconic_Acadian_Terrane	-	Jc1b	Jc1b;0	NHJc1b;0	NH001	Middle - Late? Jurassic	granite		Merrimac	Mid_Atlantic
a	Ref05	NS24	Kunketal.,2005	4-MatherGorge	39.0278	-77.2785	Table	72	GoogleEarthPro	131	16	1	14.0	1.2	-	-	-	Piedmont	-	u	u;0	VAu;0	VA003	Proterozoic	ultramafitite (komatiite)		Potomac	Mid_Atlantic
57	Ref05	NS24	Kunketal.,2005	5-MatherGorge	39.0118	-77.252	Table	68	GoogleEarthPro	138	14	9	13.2	1.6	-	-	-	Piedmont	-	[Zms	CAZms;0	VACAZms;0	VA003	Proterozoic Z-Cambrian	schist	gneiss	Potomac	Mid_Atlantic
58	Ref05	NS24	Kunketal.,2005	12-MatherGorge	38.9587	-77.2054	Table	52	GoogleEarthPro	155	13	89	13.9	1.3	-	-	-	Piedmont	-	[Zms	CAZms;0	VACAZms;0	VA003	Proterozoic Z-Cambrian	schist	gneiss	Potomac	Mid_Atlantic
59	Ref05	NS24	Kunketal.,2005	18-Sykesville	38.9668	-77.1526	Table	15	GoogleEarthPro	155	14	39	13.2	1.4	-	-	-	Piedmont	-	Water	water;0	MDwater;0	MD001	Holocene	water		Potomac	Mid_Atlantic
60	Ref05	NS24	Kunketal.,2005	19-Sykesville	38.9718	-77.1383	Table	80	GoogleEarthPro	179	15	43	14.3	1.4	-	-	-	Piedmont	-	Pzk	PZk;6	MDPZk;6	MD001	Ordovician	biotite gneiss		Potomac	Mid_Atlantic
61	Ref05	NS24	Kunketal.,2005	20-Sykesville	38.9288	-77.1174	Table	7	GoogleEarthPro	157	18	61	13.6	1.3	-	-	-	Piedmont	-	water	water;0	VAwater;0	VA003	Holocene	water		Potomac	Mid_Atlantic
62	Ref05	NS24	Kunketal.,2005	24-Laurel	38.9268	-77.0439	Table	32	GoogleEarthPro	198	21	16	13.5	1.3	-	-	-	Piedmont	-	Ql	Ql;5	MDQl;5	MD001	Quaternary	gravel	sand	Potomac	Mid_Atlantic
63	Ref07	NS21	McKeonetal.,2014	APL-BUTL-00	41	-74.3333	Table	126	Table	-	-	-	-	-	126	4	39	Valley_and_Ridge	-	Ylo	Ylo;11	NJYlo;11	NJ001	Middle Proterozoic	gneiss	granofels	Passaic_Raritan	Mid_Atlantic
64	Ref07	NS21	McKeonetal.,2014	APL-CHFD-00	39.8708	-75.5958	Table	48	Table	-	-	-	-	-	164	5	79	Piedmont	-	fgh	pCAfgh;14	PApCAfgh;14	PA002	Precambrian	felsic gneiss	mafic gneiss	Delaware	Mid_Atlantic
65	Ref07	NS21	McKeonetal.,2014	APL-JJ-99	40.8583	-74.9833	Table	122	Table	-	-	-	-	-	94	2	28	Valley_and_Ridge	-	Cl	CAl;6	NJCAl;6	NJ001	Middle and Lower Cambrian	dolostone (dolomite)	shale	Delaware	Mid_Atlantic
66	Ref07	NS21	McKeonetal.,2014	APL-LBCL-00	40.4583	-75.55	Table	153	Table	-	-	-	-	-	72	1	5	Valley_and_Ridge	-	Clv	CAlv;23	PACAlv;23	PA002	Cambrian	dolostone (dolomite)	shale	Delaware	Mid_Atlantic
67	Ref07	NS21	McKeonetal.,2014	APL-MORR-00	40.2	-74.7708	Table	6	Table	-	-	-	-	-	118	4	14	Piedmont	Newark_Basin	Qt	Qt;0	PAQt;0	PA002	Quaternary	sand	clay or mud	Delaware	Mid_Atlantic
68	Ref07	NS21	McKeonetal.,2014	APL-SCDM-00	40.0708	-75.3083	Table	15	Table	-	-	-	-	-	183	7	14	Piedmont	Newark_Basin	OCc	OCAc;0	PAOCAc;0	PA002	Ordovician and Cambrian	limestone	phyllite	Delaware	Mid_Atlantic
69	Ref07	NS21	McKeonetal.,2014	APL-SMT-99	40.6	-75.3833	Table	229	Table	-	-	-	-	-	155	7	5	Valley_and_Ridge	-	gn	pCAgn;14	PApCAgn;14	PA002	Precambrian	felsic gneiss	mafic gneiss	Delaware	Mid_Atlantic
70	Ref07	NS21	McKeonetal.,2014	APL-VSP-00	40.6917	-74.9	Table	183	Table	-	-	-	-	-	117	4	43	Valley_and_Ridge	-	Yp	Yp;11	NJYp;11	NJ001	Middle Proterozoic	paragneiss	amphibolite	Passaic_Raritan	Mid_Atlantic
71	Ref07	NS21	McKeonetal.,2014	NC-MM-4a	35.7351	-82.1026	Table	443	Table	-	-	-	-	-	83	1	39	Blue_Ridge	-	Ybgg	Ybgg;2	NCYbgg;2	NC002	Middle Proterozoic	granitic gneiss	amphibolite	Santee	South_Atlantic
72	Ref07	NS21	McKeonetal.,2014	NC-MM-6	35.7512	-82.1527	Table	688	Table	-	-	-	-	-	70	1	45	Blue_Ridge	-	Zabg	Zabg;2	NCZabg;2	NC002	Late Proterozoic	gneiss	conglomerate	Santee	South_Atlantic
73	Ref07	NS21	McKeonetal.,2014	NC-MM-7	35.7623	-82.1578	Table	794	Table	-	-	-	-	-	89	3	43	Blue_Ridge	-	Zabg	Zabg;2	NCZabg;2	NC002	Late Proterozoic	gneiss	conglomerate	Santee	South_Atlantic
74	Ref07	NS21	McKeonetal.,2014	NC-MM-9	35.7653	-82.1675	Table	1044	Table	-	-	-	-	-	80	2	28	Blue_Ridge	-	Zabg	Zabg;2	NCZabg;2	NC002	Late Proterozoic	gneiss	conglomerate	Santee	South_Atlantic
75	Ref07	NS21	McKeonetal.,2014	NC-MM-16	35.7644	-82.2647	Table	2034	Table	-	-	-	-	-	171	7	62	Blue_Ridge	-	Zatw	Zatw;2	NCZatw;2	NC002	Late Proterozoic	metasedimentary rock	mica schist	Mississippian	Gulf_of_Mexico
76	Ref07	NS21	McKeonetal.,2014	NC-SY-2AB	35.4605	-83.1441	Table	1780	Table	-	-	-	-	-	143	5	88	Blue_Ridge	-	Zgs	Zgs;2	NCZgs;2	NC002	Late Proterozoic	metasedimentary rock	slate	Mississippian	Gulf_of_Mexico
77	Ref07	NS21	McKeonetal.,2014	NC-SY-3	35.461	-83.1274	Table	1686	Table	-	-	-	-	-	128	4	90	Blue_Ridge	-	Zgs	Zgs;2	NCZgs;2	NC002	Late Proterozoic	metasedimentary rock	slate	Mississippian	Gulf_of_Mexico
78	Ref07	NS21	McKeonetal.,2014	NC-SY-5	35.4493	-83.1044	Table	1419	Table	-	-	-	-	-	77	2	45	Blue_Ridge	-	Zgs	Zgs;2	NCZgs;2	NC002	Late Proterozoic	metasedimentary rock	slate	Mississippian	Gulf_of_Mexico
79	Ref07	NS21	McKeonetal.,2014	NC-SY-7	35.4437	-83.0833	Table	1092	Table	-	-	-	-	-	81	1	57	Blue_Ridge	-	ZYbn	ZYbn;2	NCZYbn;2	NC002	Middle/Late Proterozoic	biotite gneiss	amphibolite	Mississippian	Gulf_of_Mexico
80	Ref07	NS21	McKeonetal.,2014	NC-SY-8	35.4632	-83.0982	Table	932	Table	-	-	-	-	-	87	2	5	Blue_Ridge	-	Zgs	Zgs;2	NCZgs;2	NC002	Late Proterozoic	metasedimentary rock	slate	Mississippian	Gulf_of_Mexico
81	Ref07	NS21	McKeonetal.,2014	NC-SY-9	35.4075	-83.1236	Table	808	Table	-	-	-	-	-	76	1	32	Blue_Ridge	-	ZYbn	ZYbn;2	NCZYbn;2	NC002	Middle/Late Proterozoic	biotite gneiss	amphibolite	Mississippian	Gulf_of_Mexico
82	Ref07	NS21	McKeonetal.,2014	NC-SY-10	35.3937	-83.178	Table	695	Table	-	-	-	-	-	90	2	16	Blue_Ridge	-	ZYbn	ZYbn;2	NCZYbn;2	NC002	Middle/Late Proterozoic	biotite gneiss	amphibolite	Mississippian	Gulf_of_Mexico
83	Ref07	NS21	McKeonetal.,2014	NC-SY-11	35.3224	-83.1719	Table	634	Table	-	-	-	-	-	100	2	29	Blue_Ridge	-	ZYbn	ZYbn;2	NCZYbn;2	NC002	Middle/Late Proterozoic	biotite gneiss	amphibolite	Mississippian	Gulf_of_Mexico
84	Ref07	NS21	McKeonetal.,2014	NC-SY-12	35.4271	-83.4584	Table	520	Table	-	-	-	-	-	169	8	80	Blue_Ridge	-	Ybgg	Ybgg;2	NCYbgg;2	NC002	Middle Proterozoic	granitic gneiss	amphibolite	Mississippian	Gulf_of_Mexico
85	Ref07	NS21	McKeonetal.,2014	NC-SY-13	35.3722	-83.565	Table	530	Table	-	-	-	-	-	112	2	38	Blue_Ridge	-	Zhha	Zhha;2	NCZhha;2	NC002	Late Proterozoic	metasedimentary rock	mica schist	Mississippian	Gulf_of_Mexico
86	Ref07	NS21	McKeonetal.,2014	NC-SY-14	35.4469	-83.8148	Table	402	Table	-	-	-	-	-	163	5	71	Blue_Ridge	-	Zchs	Zchs;2	NCZchs;2	NC002	Late Proterozoic	slate	phyllite	Mississippian	Gulf_of_Mexico
87	Ref07	NS21	McKeonetal.,2014	H4	35.4678	-83.1416	Table	1659	Table	-	-	-	-	-	92	2	51	Blue_Ridge	-	Zgs	Zgs;2	NCZgs;2	NC002	Late Proterozoic	metasedimentary rock	slate	Mississippian	Gulf_of_Mexico
88	Ref07	NS21	McKeonetal.,2014	H8	35.4672	-83.1512	Table	1400	Table	-	-	-	-	-	164	4	75	Blue_Ridge	-	Zgs	Zgs;2	NCZgs;2	NC002	Late Proterozoic	metasedimentary rock	slate	Mississippian	Gulf_of_Mexico
89	Ref07	NS21	McKeonetal.,2014	H9	35.4758	-83.1592	Table	1227	Table	-	-	-	-	-	142	3	104	Blue_Ridge	-	Zgs	Zgs;2	NCZgs;2	NC002	Late Proterozoic	metasedimentary rock	slate	Mississippian	Gulf_of_Mexico
90	Ref07	NS21	McKeonetal.,2014	H11	35.4747	-83.1824	Table	933	Table	-	-	-	-	-	145	4	73	Blue_Ridge	-	Zgs	Zgs;2	NCZgs;2	NC002	Late Proterozoic	metasedimentary rock	slate	Mississippian	Gulf_of_Mexico
91	Ref07	NS21	McKeonetal.,2014	H12	35.4693	-83.2152	Table	757	Table	-	-	-	-	-	156	4	67	Blue_Ridge	-	Ybgg	Ybgg;2	NCYbgg;2	NC002	Middle Proterozoic	granitic gneiss	amphibolite	Mississippian	Gulf_of_Mexico
92	Ref07	NS21	McKeonetal.,2014	CH01	35.1059	-82.624	Table	961	Table	-	-	-	-	-	118	3	73	Blue_Ridge	-	CZgs	CAZgs;5	SCCAZgs;5	SC001	Cambrian or Neoproterozoic	mica schist	amphibolite	Santee	South_Atlantic
93	Ref08	NS06	Miller&Lakatos,1983	AN-27	44.133	-73.952	GeoTIFF	1380	Table	147	10	-	-	-	-	-	-	Adirondacks	-	a	Ya;1	NYYa;1	NY001	Middle Proterozoic	metavolcanic rock	paragneiss	St.Lawrence	North_Atlantic
94	Ref08	NS06	Miller&Lakatos,1983	AN-3	44.133	-73.952	GeoTIFF	908	Table	137	12	-	-	-	-	-	-	Adirondacks	-	a	Ya;1	NYYa;1	NY001	Middle Proterozoic	metavolcanic rock	paragneiss	St.Lawrence	North_Atlantic
95	Ref08	NS06	Miller&Lakatos,1983	F-4A	44.328	-74.258	GeoTIFF	486	Table	125	4	-	-	-	-	-	-	Adirondacks	-	a	Ya;1	NYYa;1	NY001	Middle Proterozoic	metavolcanic rock	paragneiss	St.Lawrence	North_Atlantic
96	Ref08	NS06	Miller&Lakatos,1983	W-2A	44.232	-73.475	GeoTIFF	134	Table	107	10	-	-	-	-	-	-	Adirondacks	-	a	Ya;1	NYYa;1	NY001	Middle Proterozoic	metavolcanic rock	paragneiss	St.Lawrence	North_Atlantic
97	Ref08	NS06	Miller&Lakatos,1983	W-2B	44.232	-73.475	GeoTIFF	-184	Table	86	12	-	-	-	-	-	-	Adirondacks	-	a	Ya;1	NYYa;1	NY001	Middle Proterozoic	metavolcanic rock	paragneiss	St.Lawrence	North_Atlantic
98	Ref09	NS13	Miller&Duddy,1989	MD1	42.20952	-74.01339	Manual_Georef	297	GoogleEarthPro	108	9	-	-	-	-	-	-	Valley_and_Ridge	-	Dhmo	Dhmo;2	NYDhmo;2	NY001	Middle Devonian	shale	sandstone	Hudson	Mid_Atlantic
99	Ref09	NS13	Miller&Duddy,1989	MD2	42.18573	-73.99851	Manual_Georef	153	GoogleEarthPro	155	7	15	13.6	1.1	-	-	-	Valley_and_Ridge	-	Dhpl	Dhpl;2	NYDhpl;2	NY001	Middle Devonian	shale	sandstone	Hudson	Mid_Atlantic
100	Ref09	NS13	Miller&Duddy,1989	MD3	42.19167	-74.02826	Manual_Georef	445	GoogleEarthPro	164	11	-	-	-	-	-	-	Valley_and_Ridge	-	Dhmo	Dhmo;2	NYDhmo;2	NY001	Middle Devonian	shale	sandstone	Hudson	Mid_Atlantic
101	Ref09	NS13	Miller&Duddy,1989	MD4	42.42069	-74.46548	Manual_Georef	352	GoogleEarthPro	145	14	75	14.1	1.1	-	-	-	Appalachian	-	Dhmo	Dhmo;2	NYDhmo;2	NY001	Middle Devonian	shale	sandstone	Hudson	Mid_Atlantic
102	Ref09	NS13	Miller&Duddy,1989	MD5	42.40582	-74.48035	Manual_Georef	430	GoogleEarthPro	100	8	-	-	-	-	-	-	Appalachian	-	Dgu	Dgu;2	NYDgu;2	NY001	Middle Devonian	shale	siltstone	Hudson	Mid_Atlantic
103	Ref09	NS13	Miller&Duddy,1989	MD6	42.50922	-74.98402	Manual_Georef	348	GoogleEarthPro	132	15	-	-	-	-	-	-	Appalachian	-	Dhmo	Dhmo;2	NYDhmo;2	NY001	Middle Devonian	shale	sandstone	Susquehanna	Mid_Atlantic
104	Ref09	NS13	Miller&Duddy,1989	MD7	42.44524	-76.02221	Manual_Georef	391	GoogleEarthPro	146	12	-	-	-	-	-	-	Appalachian	-	Ds	Ds;2	NYDs;2	NY001	Upper Devonian	shale	siltstone	Susquehanna	Mid_Atlantic
105	Ref09	NS13	Miller&Duddy,1989	MD8	42.93089	-76.58929	Manual_Georef	191	GoogleEarthPro	142	20	2	14.6	1.2	-	-	-	Appalachian	-	Don	Don;2	NYDon;2	NY001	Middle Devonian	limestone	chert	St.Lawrence	North_Atlantic
106	Ref09	NS13	Miller&Duddy,1989	MD9	42.9673	-78.78086	Manual_Georef	200	GoogleEarthPro	248	13	1	13.5	2.4	-	-	-	Appalachian	-	Sab	Sab;4	NYSab;4	NY001	Upper Silurian	dolostone (dolomite)	shale	St.Lawrence	North_Atlantic
107	Ref09	NS13	Miller&Duddy,1989	MD10	42.81166	-74.69903	Manual_Georef	446	GoogleEarthPro	246	17	61	14.2	1.2	-	-	-	Appalachian	-	Dhg	Dhg;2	NYDhg;2	NY001	Lower Devonian	limestone	dolostone (dolomite)	Hudson	Mid_Atlantic
108	Ref09	NS13	Miller&Duddy,1989	MD11	42.9716	-76.04838	Manual_Georef	306	GoogleEarthPro	228	17	65	14.8	1.1	-	-	-	Appalachian	-	Do	Do;2	NYDo;2	NY001	Lower Devonian	sandstone	limestone	St.Lawrence	North_Atlantic
109	Ref09	NS13	Miller&Duddy,1989	MD12	42.91635	-76.76377	Manual_Georef	135	GoogleEarthPro	149	9	24	14.4	1.5	-	-	-	Appalachian	-	Sab	Sab;4	NYSab;4	NY001	Upper Silurian	dolostone (dolomite)	shale	St.Lawrence	North_Atlantic
110	Ref09	NS13	Miller&Duddy,1989	MD13	42.94834	-77.31631	Manual_Georef	209	GoogleEarthPro	200	7	85	14.1	1.4	-	-	-	Appalachian	-	Don	Don;2	NYDon;2	NY001	Middle Devonian	limestone	chert	St.Lawrence	North_Atlantic
111	Ref09	NS13	Miller&Duddy,1989	MD14	42.18275	-74.09369	Manual_Georef	804	GoogleEarthPro	126	10	10	14.5	1.0	-	-	-	Appalachian	-	Dhmo	Dhmo;2	NYDhmo;2	NY001	Middle Devonian	shale	sandstone	Hudson	Mid_Atlantic
112	Ref09	NS13	Miller&Duddy,1989	MD15	42.15301	-74.10559	Manual_Georef	649	GoogleEarthPro	153	14	-	-	-	-	-	-	Appalachian	-	Dhmo	Dhmo;2	NYDhmo;2	NY001	Middle Devonian	shale	sandstone	Hudson	Mid_Atlantic
113	Ref09	NS13	Miller&Duddy,1989	MD16	42.15734	-75.16723	Manual_Georef	376	GoogleEarthPro	188	10	9	13.7	1.6	-	-	-	Appalachian	-	Dsw	Dsw;2	NYDsw;2	NY001	Upper Devonian	shale	sandstone	Delaware	Mid_Atlantic
114	Ref09	NS13	Miller&Duddy,1989	MD17	42.35219	-75.09453	Manual_Georef	442	GoogleEarthPro	160	10	-	-	-	-	-	-	Appalachian	-	Dhmo	Dhmo;2	NYDhmo;2	NY001	Middle Devonian	shale	sandstone	Susquehanna	Mid_Atlantic
115	Ref09	NS13	Miller&Duddy,1989	MD18	41.47977	-74.7252	Manual_Georef	388	GoogleEarthPro	159	19	3	14.0	1.2	-	-	-	Appalachian	-	Dsw	Dsw;2	NYDsw;2	NY001	Upper Devonian	shale	sandstone	Delaware	Mid_Atlantic
116	Ref09	NS13	Miller&Duddy,1989	MD19	41.43033	-74.71938	Manual_Georef	288	GoogleEarthPro	136	11	-	-	-	-	-	-	Appalachian	-	Dhmo	Dhmo;2	NYDhmo;2	NY001	Middle Devonian	shale	sandstone	Delaware	Mid_Atlantic
117	Ref09	NS13	Miller&Duddy,1989	MD20	41.45359	-74.87351	Manual_Georef	275	GoogleEarthPro	135	17	1	14.1	1.1	-	-	-	Appalachian	-	Dww	Dww;2	NYDww;2	NY001	Upper Devonian	shale	sandstone	Delaware	Mid_Atlantic
118	Ref09	NS13	Miller&Duddy,1989	MD21	41.50012	-74.94622	Manual_Georef	311	GoogleEarthPro	181	13	-	-	-	-	-	-	Appalachian	-	Dww	Dww;2	NYDww;2	NY001	Upper Devonian	shale	sandstone	Delaware	Mid_Atlantic
119	Ref09	NS13	Miller&Duddy,1989	MD22	41.56992	-75.01019	Manual_Georef	237	GoogleEarthPro	130	8	84	14.1	1.1	-	-	-	Appalachian	-	Dwh	Dwh;2	NYDwh;2	NY001	Upper Devonian	sandstone	shale	Delaware	Mid_Atlantic
120	Ref09	NS13	Miller&Duddy,1989	MD23	41.77057	-75.03928	Manual_Georef	366	GoogleEarthPro	128	10	-	-	-	-	-	-	Appalachian	-	Dwh	Dwh;2	NYDwh;2	NY001	Upper Devonian	sandstone	shale	Delaware	Mid_Atlantic
121	Ref09	NS13	Miller&Duddy,1989	MD24	41.86654	-74.99856	Manual_Georef	558	GoogleEarthPro	168	11	39	14.4	1.0	-	-	-	Appalachian	-	Dwh	Dwh;2	NYDwh;2	NY001	Upper Devonian	sandstone	shale	Delaware	Mid_Atlantic
122	Ref09	NS13	Miller&Duddy,1989	MD25	41.87235	-75.10616	Manual_Georef	545	GoogleEarthPro	116	12	-	-	-	-	-	-	Appalachian	-	Dwh	Dwh;2	NYDwh;2	NY001	Upper Devonian	sandstone	shale	Delaware	Mid_Atlantic

Appalachian Low-Temperature Thermochronology Database (Appl.TDB)

Ordering			Study	Sample_ID	Location Data		Elevation	Ref_Data	Use_Data	AFT Data						Age Data				Physiographic_Province			ORIG_LABEL	SGWC_LABEL	UNIT_LINK	SOURCE	Lithology (USGS) UNIT_AGE	ROCKTYPE1	ROCKTYPE2	HydroSHEDS Database	
Row_Ref_Order	N-S_Order				Latitude	Longitude				AFT_Age	AFT_1sig	chi2	MTL	Std_Dev		Ahe_Age	Ahe_1sig	Var		Province	HP_Basin									Drainage	Drain_Tb

Appalachian Low-Temperature Thermochronology Database (Appl.TDB)

Ordering		Study	Sample_ID	Location Data			Elevation	Rev_Data	AFT Data					Ahe Data			Physiographic_Province		ORIG_LABEL	SGMC_LABEL	UNIT_LINK	SOURCE	Lithology (USGS)	ROCKTYPE1	ROCKTYPE2	HydroSHEDS Database	
Row Ref. Order	N-S_Order			Latitude	Longitude	Loc_Data			AFT_age	AFT_1sig	ch2	MTL	MTL_1sig_Dev	Ahe_age	Ahe_1sig	Var	Province	H.F. Basin					UNIT_AGE			Drainage	Drain_To

Appalachian Low-Temperature Thermochronology Database (Appl.TDB)

Row Ref. Order	N-S_Order	Study	Sample_ID	Latitude	Longitude	Loc_Data	Elevation	Rev_Data	AFT_Age	AFT_1sig	chi2	MTL	Std_Dev	Ahe_age	Ahe_1sig	1g	Var	Province	H.P_Basin	ORIG_LABEL	SGMC_LABEL	UNIT_LINK	SOURCE	UNIT_AGE	ROCKTYPE1	ROCKTYPE2	Drainage	Down_Tb
363	N502	Roden-Tice&Tice,2005	48ADK	43.7	-74.383	Table	1049	GoogleEarthPro	146	15		13.0	1.3					Adirondacks		asch	asch	NYY001	NY001	Middle Proterozoic	gneiss	anorthosite	Hudson	Mid_Atlantic
364	N502	Roden-Tice&Tice,2005	49ADK	44.368	-75.263	Table	227	GoogleEarthPro	146	15								Adirondacks		Yuch;1	Yuch;1	NYYbq;1	NY001	Middle Proterozoic	paragneiss	gneiss	Hudson	Mid_Atlantic
365	N502	Roden-Tice&Tice,2005	50ADK	44.069	-75.365	Table	285	GoogleEarthPro	142	15		12.7	1.5					Adirondacks		Ybqp;1	Ybqp;1	NYYbq;1	NY001	Middle Proterozoic	paragneiss	amphibolite	St_Lawrence	North_Atlantic
366	N502	Roden-Tice&Tice,2005	51ADK	44.069	-75.362	Table	299	GoogleEarthPro	161	22								Adirondacks		Ybqp;1	Ybqp;1	NYYbq;1	NY001	Middle Proterozoic	paragneiss	gneiss	St_Lawrence	North_Atlantic
367	N502	Roden-Tice&Tice,2005	52ADK	44.069	-75.362	Table	279	GoogleEarthPro	107	13		13.3						Adirondacks		Ybqp;1	Ybqp;1	NYYbq;1	NY001	Middle Proterozoic	paragneiss	metasedimentary rock	North_Atlantic	North_Atlantic
368	N502	Roden-Tice&Tice,2005	53ADK	43.875	-73.75	Table	100	GoogleEarthPro	108	18								Valley_and_Ridge		Oc	Occ;1	NYOc;1	NY001	Middle Ordovician	black shale		Mid_Atlantic	Mid_Atlantic
369	N502	Roden-Tice&Tice,2005	54ADK	43.13	-73.643	Table	118	GoogleEarthPro	108	18								Valley_and_Ridge		Omi	Omi;1	NYOmi;1	NY001	Ordovician	shale	slate	Hudson	Mid_Atlantic
370	N502	Roden-Tice&Tice,2005	55E-NY	43.062	-73.694	Table	105	GoogleEarthPro	115	13								Valley_and_Ridge		Oag	Oag;1	NYOag;1	NY001	Middle Ordovician	graywacke	shale	Hudson	Mid_Atlantic
371	N502	Roden-Tice&Tice,2005	56E-NY	42.959	-73.508	Table	381	GoogleEarthPro	134	13								Valley_and_Ridge		Cn	On;2	NYOn;2	NY001	Cambrian	graywacke	graywacke	Hudson	Mid_Atlantic
372	N502	Roden-Tice&Tice,2005	57E-NY	42.689	-73.398	Table	203	GoogleEarthPro	142	19								Taconic_Acadian_Terrane		Cn	On;2	NYOn;2	NY001	Cambrian	shale	quartzite	Hudson	Mid_Atlantic
373	N502	Roden-Tice&Tice,2005	58E-NY	42.494	-73.53	Table	301	GoogleEarthPro	121	12								Taconic_Acadian_Terrane		Cr	Cn;2	NYCn;2	NY001	Cambrian	graywacke	shale	Hudson	Mid_Atlantic
374	N502	Roden-Tice&Tice,2005	59E-NY	42.75	-73.517	Table	116	GoogleEarthPro	117	17								Taconic_Acadian_Terrane		Cr	Cn;2	NYCn;2	NY001	Cambrian	shale	shale	Hudson	Mid_Atlantic
375	N502	Roden-Tice&Tice,2005	60E-NY	42.787	-73.398	Table	331	GoogleEarthPro	121	15								Taconic_Acadian_Terrane		Cr	Cn;2	NYCn;2	NY001	Cambrian	phyllite	quartzite	Mid_Atlantic	Mid_Atlantic
376	N502	Roden-Tice&Tice,2005	61E-NY	42.319	-73.517	Table	462	GoogleEarthPro	178	26								Taconic_Acadian_Terrane		Ca	Oa;2	NYCa;2	NY001	Cambrian	phyllite	shale	St_Lawrence	North_Atlantic
377	N502	Roden-Tice&Tice,2005	62FRONT	44.504	-75.623	Table	101	GoogleEarthPro	178	26								Adirondacks		Obk	Obk;1	NYObk;1	NY001	Lower Ordovician	dolostone (dolomite)	limestone	St_Lawrence	North_Atlantic
378	N502	Roden-Tice&Tice,2005	63FRONT	44.504	-75.837	Table	161	GoogleEarthPro	103	19								Adirondacks		Obk	Obk;1	NYObk;1	NY001	Lower Ordovician	dolostone (dolomite)	limestone	St_Lawrence	North_Atlantic
379	N502	Roden-Tice&Tice,2005	64VT	43.603	-73	Table	263	GoogleEarthPro	103	19								Taconic_Acadian_Terrane		CА	OА;0	VTCА;0	VT001	Cambrian	quartzite	sandstone	North_Atlantic	North_Atlantic
380	N502	Roden-Tice&Tice,2005	65VT	43.52	-72.993	Table	258	GoogleEarthPro	117	18		13.3	1.6					Taconic_Acadian_Terrane		Cc	OcА;0	VTOcА;0	VT001	Cambrian	quartzite	sandstone	North_Atlantic	North_Atlantic
381	N502	Roden-Tice&Tice,2005	66VT	43.515	-73.11	Table	81	GoogleEarthPro	97	14		13.3	1.5					Taconic_Acadian_Terrane		Cc	OcА;0	VTOcА;0	VT001	Cambrian	biotite gneiss	gneiss	Mid_Atlantic	Mid_Atlantic
382	N502	Roden-Tice&Tice,2005	67VT	43.521	-73.313	Table	446	GoogleEarthPro	103	12								Taconic_Acadian_Terrane		CdA	OcdA;0	VTOcdA;0	VT001	Cambrian	dolostone (dolomite)	dolostone (dolomite)	Mid_Atlantic	Mid_Atlantic
383	N502	Roden-Tice&Tice,2005	68VT	42.878	-73.117	Table	510	GoogleEarthPro	116	13		13.3						Taconic_Acadian_Terrane		pC	pCA;0	VTpCA;0	VT001	Precambrian	biotite gneiss	amphibolite	Connecticut	Mid_Atlantic
384	N502	Roden-Tice&Tice,2005	69VT	43.229	-72.888	Table	98	GoogleEarthPro	127	13								Taconic_Acadian_Terrane		pC	pCA;0	VTpCA;0	VT001	Precambrian	biotite gneiss	conglomerate	St_Lawrence	North_Atlantic
385	N502	Roden-Tice&Tice,2005	70VT	44.469	-73.029	Table	92	GoogleEarthPro	116	13								Taconic_Acadian_Terrane		Cp	OAp;0	VTOAp;0	VT001	Cambrian	schist	conglomerate	St_Lawrence	North_Atlantic
386	N502	Roden-Tice&Tice,2005	71VT	44.443	-73.02	Table	101	GoogleEarthPro	127	13								Taconic_Acadian_Terrane		Cp	OAp;0	VTOAp;0	VT001	Cambrian	schist	conglomerate	St_Lawrence	North_Atlantic
387	N502	Roden-Tice&Tice,2005	72VT	44.377	-72.888	Table	101	GoogleEarthPro	106	15								Taconic_Acadian_Terrane		Cu	OAu;0	VTOAu;0	VT001	Cambrian	mica schist	phyllite	St_Lawrence	North_Atlantic
388	N502	Roden-Tice&Tice,2005	73VT	44.149	-72.888	Table	414	GoogleEarthPro	109	25								Taconic_Acadian_Terrane		nhu	VTnhu;0	VTnhu;0	VT001	Precambrian	granitic gneiss		Mid_Atlantic	Mid_Atlantic
389	N502	Roden-Tice&Tice,2005	74VT	43.974	-72.482	Table	353	GoogleEarthPro	123	15			1.5					Taconic_Acadian_Terrane		pCA0	pCAn;0	VTpCAn;0	VT001	Precambrian	quartzite	mica schist	Mid_Atlantic	Mid_Atlantic
390	N502	Roden-Tice&Tice,2005	75VT	43.892	-72.398	Table	319	GoogleEarthPro	113	12								Taconic_Acadian_Terrane		Dw;0	VTDw;0	VTDw;0	VT001	Devonian	quartzite	schist	Connecticut	Mid_Atlantic
391	N502	Roden-Tice&Tice,2005	76VT	43.825	-72.398	Table	319	GoogleEarthPro	106	15								Taconic_Acadian_Terrane		Dw;0	VTDw;0	VTDw;0	VT001	Devonian	phyllite	phyllite	Connecticut	Mid_Atlantic
392	N502	Roden-Tice&Tice,2005	77VT	43.825	-72.332	Table	353	GoogleEarthPro	116	12		12.9						Taconic_Acadian_Terrane		Dg	VTDg;0	VTDg;0	VT001	Devonian	limestone	mica schist	Connecticut	Mid_Atlantic
393	N502	Roden-Tice&Tice,2005	78VT	43.696	-72.401	Table	460	GoogleEarthPro	124	24								Taconic_Acadian_Terrane		Dg	VTDg;0	VTDg;0	VT001	Devonian	phyllite	phyllite	Connecticut	Mid_Atlantic
394	N502	Roden-Tice&Tice,2005	79VT	43.327	-72.463	Table	123	GoogleEarthPro	119	23								Taconic_Acadian_Terrane		Dg	VTDg;0	VTDg;0	VT001	Devonian	phyllite	amphibolite	Connecticut	Mid_Atlantic
395	N502	Roden-Tice&Tice,2005	80VT	43.327	-72.83	Table	221	GoogleEarthPro	106	17								Taconic_Acadian_Terrane		pC	pCA;0	VTpCA;0	VT001	Precambrian	biotite gneiss	amphibolite	Connecticut	Mid_Atlantic
396	N502	Roden-Tice&Tice,2005	81VT	43.323	-72.823	Table	410	GoogleEarthPro	123	14		13.4						Taconic_Acadian_Terrane		pCA0	pCA;0	VTpCA;0	VT001	Precambrian	marble	granulite	Connecticut	Mid_Atlantic
397	N502	Roden-Tice&Tice,2005	82VT	42.887	-72.073	Table	737	GoogleEarthPro	143	13								Taconic_Acadian_Terrane		pCm	pCAm;0	VTpCAm;0	VT001	Precambrian	mica schist	quartzite	St_Lawrence	North_Atlantic
398	N502	Roden-Tice&Tice,2005	83VT	42.46	-72.652	Table	172	GoogleEarthPro	123	20								Taconic_Acadian_Terrane		Omc	VTOmc;1	VTOmc;1	VT001	Ordovician	biotite gneiss	amphibolite	St_Lawrence	North_Atlantic
399	N502	Roden-Tice&Tice,2005	84VT	43.114	-72.888	Table	370	GoogleEarthPro	119	19								Taconic_Acadian_Terrane		pC	pCA;0	VTpCA;0	VT001	Precambrian			St_Lawrence	Mid_Atlantic
400	N502	Roden-Tice&Tice,2005	85VT	44.588	-71.549	Table	275	GoogleEarthPro	106	21								Taconic_Acadian_Terrane		hu0	VThu;0	VThu;0	VT001	Ordovician			Mid_Atlantic	Mid_Atlantic
401	N502	Roden-Tice&Tice,2005	86VT	44.922	-72.149	Table	367	GoogleEarthPro	104	15			1.6					Taconic_Acadian_Terrane		nhu;0	VTnhu;0	VTnhu;0	VT001	Devonian	granitic gneiss		North_Atlantic	Mid_Atlantic
402	N501	Roden-Tice et al.,2009	87NH	42.834	-72.358	Table	148	GoogleEarthPro	128	19		13.1						Taconic_Acadian_Terrane		Oo1-3A	Oo1-3A;0	NHOo1-3A;0	NH001	Late Ordovician	granite	granite	Mid_Atlantic	Mid_Atlantic
403	N501	Roden-Tice et al.,2009	88NH	42.792	-72.455	Table	123	GoogleEarthPro	96	22								Taconic_Acadian_Terrane		Dk2A	Dk2A;0	NHDk2A;0	NH001	Early Devonian	granite	granite	Connecticut	Mid_Atlantic
404	N501	Roden-Tice et al.,2009	89NH	42.923	-72.541	Table	228	GoogleEarthPro	92	22								Taconic_Acadian_Terrane		Oo1-3A	Oo1-3A;0	NHOo1-3A;0	NH001	Late Ordovician	granite	granodiorite	Connecticut	Mid_Atlantic
405	N501	Roden-Tice et al.,2009	90NH	43.179	-72.447	Table	104	GoogleEarthPro	106	17								Taconic_Acadian_Terrane		Dbz0	Dbz0;0	NHDbz0;0	NH001	Early Devonian	granodiorite	tonalite	Connecticut	Mid_Atlantic
406	N501	Roden-Tice et al.,2009	91NH	43.902	-71.993	Table	327	GoogleEarthPro	79	9		13.1						Taconic_Acadian_Terrane		Oo2-3A0	Oo2-3A;0	NHOo2-3A;0	NH001	Late Ordovician	trondhjemite		Mid_Atlantic	Mid_Atlantic
407	N501	Roden-Tice et al.,2009	92NH	43.842	-71.365	Table	217	GoogleEarthPro	83	11		13.0						Taconic_Acadian_Terrane		D3B0	D3B0;0	NHD3B0;0	NH001	Early-Late Devonian	granodiorite		Merrimac	Mid_Atlantic
408	N501	Roden-Tice et al.,2009	93NH	43.842	-71.509	Table	99	GoogleEarthPro	114	17		13.4	1.6					Taconic_Acadian_Terrane		Dlu	Dlu;0	NHDlu;0	NH001	Late Devonian	metasedimentary rock	tonalite	Mid_Atlantic	North_Atlantic
409	N501	Roden-Tice et al.,2009	94NH	43.456	-71.156	Table	296	GoogleEarthPro	128	14								Taconic_Acadian_Terrane		Oca	Oca;0	NHOca;0	NH001	Middle Ordovician	mica schist		Merrimac	Mid_Atlantic
410	N501	Roden-Tice et al.,2009	95MA	42.428	-72.158	Table	93	GoogleEarthPro	115	18								Taconic_Acadian_Terrane		Ops	Ops;0	NHOps;0	NH001	Ordovician	granitic gneiss	amphibolite	Connecticut	Mid_Atlantic
411	N501	Roden-Tice et al.,2009	96MA	42.708	-73.086	Table	270	GoogleEarthPro	70	9								Taconic_Acadian_Terrane		Srf	Srf;0	NHSrf;0	NH001	Late Devonian	mica schist	amphibolite	Housatonic	Mid_Atlantic
412	N501	Roden-Tice et al.,2009	97MA	42.186	-73.158	Table	502	GoogleEarthPro	126	19		12.7	1.7					Taconic_Acadian_Terrane		Yb	Yb;0	MAYb;0	MA001	Proterozoic Y	granitic gneiss	conglomerate	Hudson	Mid_Atlantic
413	N501	Roden-Tice et al.,2009	98MA	42.185	-73.158	Table	471	GoogleEarthPro	170	22			1.5					Taconic_Acadian_Terrane		Yhb;0	Yhb;0	MAYhb;0	MA001	Proterozoic Y	mafic gneiss	gneiss	Connecticut	Mid_Atlantic
414	N501	Roden-Tice et al.,2009	99MA	42.569	-73.251	Table	559	GoogleEarthPro	125	31		12.4						Taconic_Acadian_Terrane		Yo	Yo;0	MAYo;0	MA001	Proterozoic Y	gneiss	phyllite	Connecticut	Mid_Atlantic
415	N501	Roden-Tice et al.,2009	100MA	42.516	-72.807	Table	528	GoogleEarthPro	150	15		12.7	1.7					Taconic_Acadian_Terrane		Dbg;0	Obg;0	MADbg;0	MA001	Proterozoic Y	mica schist	schist	Connecticut	Mid_Atlantic
416	N501	Roden-Tice et al.,2009	101MA	42.43	-72.789	Table	405	GoogleEarthPro	136	17		12.8						Taconic_Acadian_Terrane		Dw;0	Dw;0	MADw;0	MA001	Lower Devonian	quartzite	granulite	Connecticut	Mid_Atlantic
417	N501	Roden-Tice et al.,2009	102MA	42.179	-72.798	Table	306	GoogleEarthPro	130	17								Taconic_Acadian_Terrane		Dg	Dg;0	MADg;0	MA001	Lower Devonian	schist	quartzite	Merrimac	Mid_Atlantic
418	N501	Roden-Tice et al.,2009	103MA	42.142	-72.888	Table	94	GoogleEarthPro	104	13								Taconic_Acadian_Terrane		Ocas	Oca;0	MADw;0	MA001	Lower Devonian	pelitic schist	granulite	Merrimac	Mid_Atlantic
419	N501	Roden-Tice et al.,2009	104MA	42.438	-72.529	Table	128	GoogleEarthPro	126	10								Taconic_Acadian_Terrane		Dbz0	Dbz0;0	NHDbz0;0	NH001	Early Devonian	mica schist	gneiss	Connecticut	Mid_Atlantic
420	N501	Roden-Tice et al.,2009	105MA	42.186	-73.073	Table	294	GoogleEarthPro	125	17		12.8						Taconic_Acadian_Terrane		Dcl;0	Dcl;0	NHDcl;0	NH001	Late Devonian	granitic gneiss	amphibolite	Connecticut	Mid_Atlantic
421	N501	Roden-Tice et al.,2009	106MA	42.185	-73.289	Table	470	GoogleEarthPro	135	16								Taconic_Acadian_Terrane		Dclm;0	DclAm;0	NHDclAm;0	NH001	Late Devonian	granitic gneiss	gneiss	Connecticut	Mid_Atlantic
422	N501	Roden-Tice et al.,2009	107MA	42.186	-73.427	Table	374	GoogleEarthPro	136	14								Taconic_Acadian_Terrane		Dclm;0	Dclm;0	NHDclm;0	NH001	Late Devonian	mafic gneiss	amphibolite	Connecticut	Mid_Atlantic
423	N501	Roden-Tice et al.,2009	108MA	42.313	-73.122	Table	463	GoogleEarthPro	145	22								Taconic_Acadian_Terrane		Dbz0	Dbz0;0	NHDbz0;0	NH001	Early Devonian	mica schist	conglomerate	Connecticut	Mid_Atlantic
424	N501	Roden-Tice et al.,2009	109MA	42.313	-73.077	Table	510	GoogleEarthPro	139	17								Taconic_Acadian_Terrane		Dw;0	Dw;0	MADw;0	MA001	Lower Devonian	schist	granitic gneiss	Connecticut	Mid_Atlantic
425	N501	Roden-Tice et al.,2009	110CT	42.001	-72.888	Table	358	GoogleEarthPro	124	16		12.8	1.4					Taconic_Acadian_Terrane		Ocm0	Ocm0	CTOcm0	CT001	Middle Ordovician	schist	schist	Housatonic	Mid_Atlantic
426	N501	Roden-Tice et al.,2009	111CT	42	-73.251	Table	472	GoogleEarthPro	137	17								Taconic_Acadian_Terrane		Og	Og;0	CTOg;0	CT001	Middle Ordovician	gneiss	schist	Housatonic	Mid_Atlantic
427	N501	Roden-Tice et al.,2009	112CT	41.842	-73.229	Table	402	GoogleEarthPro	142	17								Taconic_Acadian_Terrane	Hartford_Basin	Og;0	Og;0	CTOg;0	CT001	Middle Ordovician	gneiss	schist	Housatonic	Mid_Atlantic
428	N501	Roden-Tice et al.,2009	s90-76	42.834	-72.358	Table	148	GoogleEarthPro	128	19								Taconic_Acadian_Terrane		Oo1-3A0	Oo1-3A;0	NHOo1-3A;0	NH001	Late Ordovician	granite	granite	Mid_Atlantic	Mid_Atlantic
429	N501	Roden-Tice et al.,2009	s90-77	42.792	-72.455	Table	123	GoogleEarthPro	96	22								Taconic_Acadian_Terrane		Dk2A	Dk2A;0	NHDk2A;0	NH001	Early Devonian	granite	granite	Connecticut	Mid_Atlantic
430	N501	Roden-Tice et al.,2009	s90-78	42.923	-72.541	Table	234	GoogleEarthPro	118	14			1.4					Taconic_Acadian_Terrane		Oo1-3A0	Oo1-3A;0	NHOo1-3A;0	NH001	Late Ordovician	granite	granodiorite	Connecticut	Mid_Atlantic
431	N501	Roden-Tice et al.,2009	s90-81	43.179	-72.447	Table	107	GoogleEarthPro	106	17								Taconic_Acadian_Terrane		Dbz0	Dbz0;0	NHDbz0;0	NH001	Early Devonian	pelitic schist	metasedimentary rock	Connecticut	Mid_Atlantic
432	N501	Roden-Tice et al.,2009	s91-63	43.456	-72.043	Table	109	GoogleEarthPro	98	12		13.0						Taconic_Acadian_Terrane		Srl0	Srl0	NHSrl0;0	NH001	Lower Silurian (Llandoverian)	tonalite	granodiorite	Merrimac	Mid_Atlantic
433	N501	Roden-Tice et al.,2009	s91-65	43.229	-71.726	Table	198	GoogleEarthPro	104	11		12.9						Taconic_Acadian_Terrane		Dclm;0	DclAm;0	NHDclAm;0	NH001	Late Devonian	tonalite	tonalite	Merrimac	Mid_Atlantic
434	N501	Roden-Tice et al.,2009	s92-9	43.228	-71.57	Table	178	GoogleEarthPro	90	11			1.7					Taconic_Acadian_Terrane		Dclm;0	Dclm;0	NHDclm;0	NH001	Late Devonian	granite	granite	Merrimac	Mid_Atlantic
435	N501	Roden-Tice et al.,2009	s92-10	43.425	-71.726	Table	301	GoogleEarthPro	94	10		12.5	1.7					Taconic_Acadian_Terrane		Dclm;0	Dclm;0	NHDclm;0	NH001	Late Devonian	granodiorite	granodiorite	Saco	Mid_Atlantic
436	N501	Roden-Tice et al.,2009	s92-11	43.186	-71.994	Table	231	GoogleEarthPro	81	10								Taconic_Acadian_Terrane		D10	D10;0	MED10;0	ME001	Devonian	slate	schist	Piscataqua	Mid_Atlantic
437	N501	Roden-Tice et al.,2009	s92-12	43.456	-72.252	Table	339	GoogleEarthPro	99	11		13.0						Taconic_Acadian_Terrane		D5md0	MED5md0	MED5md0	ME001	Devonian - Mississippian	granite	granite	Saco	Connecticut
438	N501	Roden-Tice et al.,2009	s92-14	43.456	-71.874	Table	385	GoogleEarthPro	90	13			2.5					Taconic_Acadian_Terrane		D3;0	D3;0	MED3;0	ME001	Devonian - Silurian?	metasedimentary rock		St_Lawrence	Connecticut
439	N501	Roden-Tice et al.,2009	s92-15	44.224	-70.669	Table	408	GoogleEarthPro	90	10		12.8						Taconic_Acadian_Terrane		nhu	VTnhu;0	VTnhu;0	VT001	Silurian?	metavolcanic rock	slate	Androscoggin	Androscoggin
440	N501	Roden-Tice et al.,2009	s93-116	44.338	-70.708	Table	408	GoogleEarthPro	116	13								Taconic_Acadian_Terrane		nhu	VTnhu;0	VTnhu;0	VT001	Middle - Upper Ordovician	meta-basalt		Androscoggin	Androscoggin
441	N501	Roden-Tice et al.,2009	s94-18	44.663	-70.804	Table	316	GoogleEarthPro	94	10								Taconic_Acadian_Terrane		nhu	VTnhu;0	VTnhu;0	VT001	Upper to Middle Silurian (Ludlovian and Wenlockian)	meta-basalt		Androscoggin	Androscoggin
442	N501	Roden-Tice et al.,2009	s94-19	44.4	-70.611	Table	235	GoogleEarthPro	98	12								Taconic_Acadian_Terrane		Sfr	Sfr;0	NHSfr;0	NH001	Upper to Middle Silurian (Ludlovian and Wenlockian)	meta-basalt		Saco	Mid_Atlantic
443	N501	Roden-Tice et al.,2009	s94-22	44.807	-70.672	Table	285	GoogleEarthPro	128	12								Taconic_Acadian_Terrane		Sdfb	Sdfb;0	NHSdfb;0	NH001	Early Devonian	phyllite	mica schist	Connecticut	Mid_Atlantic
444	N501	Roden-Tice et al.,2009	s94-30	43.456	-70.911	Table	352	GoogleEarthPro	113	11								Taconic_Acadian_Terrane		MD1m	MD1m;0	NHMD1m;0	NH001	Early Devonian	phyllite	phyllite	St_Lawrence	Connecticut
445	N501	Roden-Tice et al.,2009	s92-6	43.474	-70.787	Table	99	GoogleEarthPro	94	9								Taconic_Acadian_Terrane		SdfV	SdfV;0	NHSdfV;0	NH001	Late Ordovician	granodiorite		Androscoggin	Mid_Atlantic
446	N501	Roden-Tice et al.,2009	s92-8	43.456	-70.787	Table	211	GoogleEarthPro	101	14								Taconic_Acadian_Terrane		Oh2-9A	Oh2-9A;0	NHOh2-9A;0	NH001	Late Ordovician	granodiorite		Saco	Mid_Atlantic
447	N501	Roden-Tice et al.,2009	s93-1	44.687	-71.874	Table	288	GoogleEarthPro	125	23								Taconic_Acadian_Terrane		nhu	VTnhu;0	VTnhu;0	VT001	Late Ordovician	granodiorite	granodiorite	Connecticut	Connecticut
448	N501	Roden-Tice et al.,2009	s93-3	44.828	-71.964	Table	215	GoogleEarthPro	128	13								Taconic_Acadian_Terrane		nhu	VTnhu;0	VTnhu;0	VT001	Early-Late Devonian	granodiorite	granodiorite	Connecticut	Connecticut
449	N501	Roden-Tice et al.,2009	s93-6	44.931	-72.252	Table	380	GoogleEarthPro	90	13		10.6	1.3					Taconic_Acadian_Terrane		nhu	VTnhu;0	VTnhu;0	VT001	Late Ordovician	trondhjemite	calc-silicate rock	Connecticut	Connecticut
450	N501	Roden-Tice et al.,2009	s93-8	44.941	-71.874	Table	205	GoogleEarthPro	140	14		12.8	1.8					Taconic_Acadian_Terrane		nhu	VTnhu;0	VTnhu;0	VT001	Late Ordovician	tonalite	calc-silicate rock	Connecticut	Connecticut
451	N501	Roden-Tice et al.,2009	s93-52	44.244	-72.142	Table	135	GoogleEarthPro	116	12								Taconic_Acadian_Terrane		hu0	VThu;0	VThu;0	VT001	Late Ordovician	granodiorite	metasedimentary rock	Connecticut	Connecticut
452	N501	Roden-Tice et al.,2009	s93-53	43.999	-72.447	Table	352	GoogleEarthPro	98	13		12.7						Taconic_Acadian_Terrane		Dg;0	VTDg;0	VTDg;0	VT001	Ordovician	phyllite		Connecticut	Connecticut
453	N501	Roden-Tice et al.,2009	s93-54	43.825	-72.447	Table	122	GoogleEarthPro	104	12								Taconic_Acadian_Terrane		Dg;0	VTDg;0	VTDg;0	VT001	Devonian	phyllite	tonalite	Connecticut	Connecticut
454	N501	Roden-Tice et al.,2009	s93-55	43.662	-72.254	Table	218	GoogleEarthPro	94	14		12.5	1.7					Taconic_Acadian_Terrane		Dbz0	Dbz0;0	NHDbz0;0	NH001	Early Devonian	granodiorite		Connecticut	Connecticut
455	N501	Roden-Tice et al.,2009	s93-106	43.683	-72.269	Table	198	GoogleEarthPro	100	14								Taconic_Acadian_Terrane		Oo1b	Oo1b;0	NHOo1b;0	NH001	Late Ordovician	granite	tonalite	Connecticut	Connecticut
456	N501	Roden-Tice et al.,2009	s93-111	43.177	-72.269	Table	126	GoogleEarthPro	104	13		13.0						Taconic_Acadian_Terrane		Oo1b	Oo1b;0	NHOo1b;0	NH001	Late Ordovician	granite	granodiorite	Connecticut	Connecticut
457	N501	Roden-Tice et al.,2009	s93-112	43.159	-72.269	Table	198	GoogleEarthPro	95	10		12.8	1.3					Taconic_Acadian_Terrane		Oo1b	Oo1b;0	NHOo1b;0	NH001	Late Ordovician	tonalite		Connecticut	Connecticut
458	N501	Roden-Tice et al.,2009	s93-114	43.186	-72.294	Table	285	GoogleEarthPro	121	13								Taconic_Acadian_Terrane		Op	Op;0	NHOp;0	NH001	Middle - Upper Ordovician	slate	tonalite	Connecticut	Connecticut
459	N501	Roden-Tice et al.,2009	s93-121	43.902	-71.993	Table	327	GoogleEarthPro	79	9		13.1						Taconic_Acadian_Terrane		Oo2-3A0	Oo2-3A;0	NHOo2-3A;0	NH001	Late Ordovician	trondhjemite		Mid_Atlantic	Mid_Atlantic
460	N501	Roden-Tice et al.,2009	s93-1	43.842	-71.365	Table	217	GoogleEarthPro	83	11		13.0						Taconic_Acadian_Terrane		D3B0	D3B0;0	NHD3B0;0	NH001	Early-Late Devonian	granodiorite		Merrimac	Mid_Atlantic
461	N501	Roden-Tice et al.,2009	s93-6	44.828	-72.252	Table	503	GoogleEarthPro	70	10		13.4						Taconic_Acadian_Terrane		Dbz0	Dbz2b;0	NHDbz2b;0	NH001	Early-Late Devonian	granodiorite	tonalite	Merrimac	Mid_Atlantic
462	N501	Roden-Tice et al.,2009	s93-57	44.445	-71.191	Table	288	GoogleEarthPro	85	14		1.6						Taconic_Acadian_Terrane		Oai	Oai;0	NHOai;0	NH001	Middle Ordovician	metavolcanic rock	metasedimentary rock	Androscoggin	North_Atlantic

155

Appalachian Low-Temperature Thermochronology Database (Appl.TDB)

Row Ref. Order	N-S_Order	Study	Sample_ID	Latitude	Longitude	Elevation	Dev_Data	Loc_Data	AFT_Age	AFT_1sig	ch2	MTL	Std_Dev	Ahe_Age	Ahe_1sig	Var	Physiographic_Province	Rift_Basin	ORIG_LABEL	STRUC_LABEL	UNIT_LABEL	UNIT_LINK	SOURCE	UNIT_AGE	ROCKTYPE1	ROCKTYPE2	Drainage	Trib_To
483	Ref17	Roden-T.cetal.,2009	s03-58		-71.367			GoogleEarthPro	85								Taconic_Acadian_Terrane		Db2b	Db2b;0	Db2b;0	NHDb2b;0	NH;001	Middle Ordovician	metasedimentary rock	metasedimentary rock	Androscoggin	North_Atlantic

(Table continues — the remaining columns/rows comprise the Appalachian Low-Temperature Thermochronology Database, Rows 483–602, with sample identifiers, geographic coordinates, apatite fission-track (AFT) and apatite (U-Th)/He (Ahe) age data, physiographic province, USGS lithology, rock types, and HydroSHEDS drainage attributes.)

Appalachian Low-Temperature Thermochronology Database (Appl.TDB)

Row Ref_Order	N-S_Order	Study	Sample_ID	Latitude	Longitude	Loc_Data	Elevation	Rev_Data	AFT_Age	AFT_1sig	ch2	MTL	Std_Dev	Ahe_age	Ahe_1sig	Var	Province	RiftBasin	ORIG_LABEL	SGMC_LABEL	UNIT_LINK	SOURCE	UNIT_AGE	ROCKTYPE1	ROCKTYPE2	Drainage	Drain_To
603	Ref24	NS08	Taylor&Fitzgerald,2010	ADK04-10	43.42722	-73.74167	Manual_Georef	619	Table	96	3	6	13.3	1.2				Adirondacks	-	phgs	Yphgs;1	NYYphgs;1	NYD01	Middle Proterozoic	granulite	felsic gneiss	St.Lawrence	North_Atlantic
604	Ref24	NS08	Taylor&Fitzgerald,2010	ADK04-8	43.42778	-73.74028	Manual_Georef	543	Table	93	1	0	13.6	1.3				Adirondacks	-	phgs	Yphgs;1	NYYphgs;1	NYD01	Middle Proterozoic	granulite	felsic gneiss	St.Lawrence	North_Atlantic
605	Ref24	NS08	Taylor&Fitzgerald,2010	ADK04-9	43.4275	-73.7375	Manual_Georef	434	Table	100	4	10	13.2	1.4				Adirondacks	-	phgs	Yphgs;1	NYYphgs;1	NYD01	Middle Proterozoic	granulite	felsic gneiss	St.Lawrence	North_Atlantic
606	Ref24	NS08	Taylor&Fitzgerald,2010	ADK03-17	43.42722	-73.72194	Manual_Georef	314	Table	101	4	19	12.8	1.4				Adirondacks	-	phgs	Yphgs;1	NYYphgs;1	NYD01	Middle Proterozoic	granulite	felsic gneiss	St.Lawrence	North_Atlantic
607	Ref24	NS08	Taylor&Fitzgerald,2010	ADK03-10	43.42639	-73.72778	Manual_Georef	229	Table	101	4	30	12.9	1.3				Adirondacks	-	phgs	Yphgs;1	NYYphgs;1	NYD01	Middle Proterozoic	granulite	felsic gneiss	St.Lawrence	North_Atlantic
608	Ref24	NS08	Taylor&Fitzgerald,2010	ADK03-11	43.41111	-73.71389	Manual_Georef	128	Table	98	3	39	12.9	1.3				Adirondacks	-	hbg	Yhbg;1	NYYhbg;1	NYD01	Middle Proterozoic	paragneiss	metasedimentary rock	St.Lawrence	North_Atlantic
609	Ref25	NS25	Tsengel et al.,1999	9-Campbell	37.993	-77.35	GeoTIFF	-150	Table	203	17							Coastal	Taylorsville_Basin	Tc	Tc;0	VATc;0	VAD03	Tertiary	sand	silt	Rappahannock	Mid_Atlantic
610	Ref25	NS25	Tsengel et al.,1999	9-Campbell	37.993	-77.35	GeoTIFF	-450	Table	157	12							Coastal	Taylorsville_Basin	Tc	Tc;0	VATc;0	VAD03	Tertiary	sand	silt	Rappahannock	Mid_Atlantic
611	Ref25	NS25	Tsengel et al.,1999	9-Campbell	37.993	-77.35	GeoTIFF	-615	Table	147	8							Coastal	Taylorsville_Basin	Tc	Tc;0	VATc;0	VAD03	Tertiary	sand	silt	Rappahannock	Mid_Atlantic
612	Ref25	NS25	Tsengel et al.,1999	9-Campbell	37.993	-77.35	GeoTIFF	-1040	Table	143	12							Coastal	Taylorsville_Basin	Tc	Tc;0	VATc;0	VAD03	Tertiary	sand	silt	Rappahannock	Mid_Atlantic
613	Ref25	NS25	Tsengel et al.,1999	9-Campbell	37.993	-77.35	GeoTIFF	-1550	Table	155	10							Coastal	Taylorsville_Basin	Tc	Tc;0	VATc;0	VAD03	Tertiary	sand	silt	Rappahannock	Mid_Atlantic
614	Ref25	NS25	Tsengel et al.,1999	9-Campbell	37.993	-77.35	GeoTIFF	-1675	Table	136	15							Coastal	Taylorsville_Basin	Tc	Tc;0	VATc;0	VAD03	Tertiary	sand	silt	Rappahannock	Mid_Atlantic
615	Ref25	NS25	Tsengel et al.,1999	6-Butler	38.153	-77.156	GeoTIFF	-350	Table	144	9							Coastal	Taylorsville_Basin	Qph	Qph;0	VAQph;0	VAD03	Quaternary	gravel	sand	Rappahannock	Mid_Atlantic
616	Ref25	NS25	Tsengel et al.,1999	6-Butler	38.153	-77.156	GeoTIFF	-1675	Table	135	10							Coastal	Taylorsville_Basin	Qph	Qph;0	VAQph;0	VAD03	Quaternary	gravel	sand	Rappahannock	Mid_Atlantic
617	Ref25	NS25	Tsengel et al.,1999	7-Payne	38.099	-77.072	GeoTIFF	-900	Table	171	8							Coastal	Taylorsville_Basin	water	water;0	VAwater;0	VAD03	Holocene	water		Rappahannock	Mid_Atlantic
618	Ref25	NS25	Tsengel et al.,1999	7-Payne	38.099	-77.072	GeoTIFF	-1675	Table	154	8							Coastal	Taylorsville_Basin	water	water;0	VAwater;0	VAD03	Holocene	water		Rappahannock	Mid_Atlantic
619	Ref25	NS25	Tsengel et al.,1999	4-Bowie-Fogg	38.198	-76.971	GeoTIFF	-1650	Table	153	13							Coastal	Taylorsville_Basin	Qbs	Qbs;0	VAQbs;0	VAD03	Quaternary	sand	silt	Potomac	Mid_Atlantic
620	Ref25	NS25	Tsengel et al.,1999	8-Ellis	38.021	-76.979	GeoTIFF	-515	Table	178	12							Coastal	Taylorsville_Basin	Tc	Tc;0	VATc;0	VAD03	Tertiary	sand	silt	Rappahannock	Mid_Atlantic
621	Ref25	NS25	Tsengel et al.,1999	8-Ellis	38.021	-76.979	GeoTIFF	-1650	Table	152	13							Coastal	Taylorsville_Basin	Tc	Tc;0	VATc;0	VAD03	Tertiary	sand	silt	Rappahannock	Mid_Atlantic
622	Ref25	NS25	Tsengel et al.,1999	5-Roberts	38.15	-76.973	GeoTIFF	-1045	Table	175	15							Coastal	Taylorsville_Basin	psg	psg;0	VApsg;0	VAD03	Tertiary	gravel	sand	Potomac	Mid_Atlantic
623	Ref26	NS10	West&Roden-Tice,2003	ME-1	43.884	-70.088	GoogleEarthPro	56	Table	92	14	87						Taconic_Acadian_Terrane	-	O2cr	O2cr;0	MEO2cr;0	ME001	Ordovician - Precambrian Z	mudstone	sandstone	Casco_Bay	North_Atlantic
624	Ref26	NS10	West&Roden-Tice,2003	ME-2	43.889	-70	GoogleEarthPro	40	Table	89	13	81						Taconic_Acadian_Terrane	-	O2c	O2c;0	MEO2c;0	ME001	Ordovician - Precambrian Z	mafic/metavolcanic rock	felsic metavolcanic rock	Casco_Bay	North_Atlantic
625	Ref26	NS10	West&Roden-Tice,2003	ME-3	43.914	-70.035	GoogleEarthPro	57	Table	113	13	93	12.9	1.6				Taconic_Acadian_Terrane	-	SOv	SOv;0	MESOv;0	ME001	Silurian - Ordovician	sandstone	quartzite	Casco_Bay	North_Atlantic
626	Ref26	NS10	West&Roden-Tice,2003	ME-5	43.781	-69.912	GoogleEarthPro	1	Table	159	19	68	12.6	1.2				Taconic_Acadian_Terrane	-	O2cr	O2cr;0	MEO2cr;0	ME001	Ordovician - Precambrian Z	mudstone	sandstone	Casco_Bay	North_Atlantic
627	Ref26	NS10	West&Roden-Tice,2003	ME-6	43.904	-69.848	GoogleEarthPro	53	Table	159	19	68	12.6	1.4				Taconic_Acadian_Terrane	-	D1	D1;0	MED1;0	ME001	Devonian	slate	schist	Kennebec	North_Atlantic
628	Ref26	NS10	West&Roden-Tice,2003	ME-7	43.878	-69.825	GoogleEarthPro	21	Table	140	16	0	12.6	1.5				Taconic_Acadian_Terrane	-	O2ce	O2ce;0	MEO2ce;0	ME001	Ordovician - Precambrian Z	mafic/metavolcanic rock	felsic metavolcanic rock	Androscoggin	North_Atlantic
629	Ref26	NS10	West&Roden-Tice,2003	ME-8	43.919	-69.875	GoogleEarthPro	25	Table	140	19	79	12.8	1.5				Taconic_Acadian_Terrane	-	O2c	O2c;0	MEO2c;0	ME001	Carboniferous	granite		Casco_Bay	North_Atlantic
630	Ref27	NS05	Wrensel,2008	m3-38	43.849	-70.447	GoogleEarthPro	109	Table	117	17	89						Taconic_Acadian_Terrane	-	C3b(m)	C3b(m);0	MEC3b(m);0	ME001	Carboniferous	granite		Kennebec	North_Atlantic
631	Ref27	NS05	Wrensel,2008	m3-63	44.211	-70.812	GoogleEarthPro	76	Table	111	12	58	12.7	1.9	121			Taconic_Acadian_Terrane	-	D1	D1;0	MED1;0	ME001	Devonian	granite		Kennebec	North_Atlantic
632	Ref27	NS05	Wrensel,2008	m3-64	44.255	-70.097	GoogleEarthPro	42	Table	120	12	78	12.8	1.7				Taconic_Acadian_Terrane	-	D1	D1;0	MED1;0	ME001	Devonian	slate	schist	Eastern_Coastal	North_Atlantic
633	Ref27	NS05	Wrensel,2008	m3-65	44.334	-69.097	GoogleEarthPro	72	Table	140	20	8						Taconic_Acadian_Terrane	-	OCAp	OCAp;0	MEOCAp;0	ME001	Ordovician - Cambrian	granite		Eastern_Coastal	North_Atlantic
634	Ref27	NS05	Wrensel,2008	m3-66	44.261	-69.317	GoogleEarthPro	104	Table	109	13	49	12.7	1.5	102		6	Taconic_Acadian_Terrane	-	D1	D1;0	MED1;0	ME001	Devonian	mafic/metavolcanic rock	felsic metavolcanic rock	Central_Coastal	North_Atlantic
635	Ref27	NS05	Wrensel,2008	m3-67	44.321	-69.383	GoogleEarthPro	97	Table	139	12	69	13.1	1.3				Taconic_Acadian_Terrane	-	O2cev	O2cev;0	MEO2cev;0	ME001	Ordovician - Precambrian Z	mafic/metavolcanic rock	felsic metavolcanic rock	Central_Coastal	North_Atlantic
636	Ref27	NS05	Wrensel,2008	m3-69	44.38	-69.413	GoogleEarthPro	105	Table	119	20	2	13.0	1.6				Taconic_Acadian_Terrane	-	O2c	O2c;0	MEO2c;0	ME001	Ordovician - Precambrian Z	quartz monzonite		Kennebec	North_Atlantic
637	Ref27	NS05	Wrensel,2008	m3-72	44.347	-69.786	GoogleEarthPro	94	Table	118	17	87						Taconic_Acadian_Terrane	-	D4d(m)	D4d(m);0	MED4d(m);0	ME001	Devonian	syenite		Kennebec	North_Atlantic
638	Ref27	NS05	Wrensel,2008	m3-73	44.324	-70.059	GoogleEarthPro	191	Table	125	20	29	12.4	1.8	103		6	Taconic_Acadian_Terrane	-	C7	C7;0	MEC7;0	ME001	Carboniferous	syenite		Kennebec	North_Atlantic
639	Ref27	NS05	Wrensel,2008	m3-74	44.082	-69.702	GoogleEarthPro	72	Table	129	16	73	12.5	1.9	103			Taconic_Acadian_Terrane	-	C1	C1;0	MEC1;0	ME001	Devonian	syenite		Central_Coastal	North_Atlantic
640	Ref27	NS05	Wrensel,2008	m3-75	44.224	-69.463	GoogleEarthPro	154	Table	131	14	21						Taconic_Acadian_Terrane	-	D7	D7;0	MED7;0	ME001	Devonian	granite		Central_Coastal	North_Atlantic
641	Ref27	NS05	Wrensel,2008	m3-76	44.275	-69.647	GoogleEarthPro	92	Table	133	13	66						Taconic_Acadian_Terrane	-	D1	D1;0	MED1;0	ME001	Devonian	granite		Kennebec	North_Atlantic
642	Ref27	NS05	Wrensel,2008	m3-77	43.422	-70.406	GoogleEarthPro	16	Table	120	12	27						Taconic_Acadian_Terrane	-	C1	C1;0	MEC1;0	ME001	Carboniferous	gabbro	diorite	Piscataqua	North_Atlantic
643	Ref27	NS05	Wrensel,2008	m3-78	43.542	-70.521	GoogleEarthPro	36	Table	147	15	36	12.7	1.5	119			Taconic_Acadian_Terrane	-	C9	C9;0	MEC9;0	ME001	Carboniferous	granite		Saco	North_Atlantic
644	Ref27	NS05	Wrensel,2008	m3-80	43.476	-70.317	GoogleEarthPro	101	Table	126	17	98	13.2	1.7				Taconic_Acadian_Terrane	-	C1(m)	C1(m);0	MEC1(m);0	ME001	Devonian	granite		Piscataqua	North_Atlantic
645	Ref27	NS05	Wrensel,2008	m3-81	43.344	-70.683	GoogleEarthPro	65	Table	115	13	0	12.0	2.3	126		8	Taconic_Acadian_Terrane	-	D1(m)	D1(m);0	MED1(m);0	ME001	Devonian	granite	felsic metavolcanic rock	Piscataqua	North_Atlantic
646	Ref27	NS05	Wrensel,2008	m3-118	43.419	-70.735	GoogleEarthPro	90	Table	108	17	31	13.0	1.0	110		7	Taconic_Acadian_Terrane	-	C1(m)	C1(m);0	MEC1(m);0	ME001	Devonian	mafic/metavolcanic rock	felsic metavolcanic rock	Piscataqua	North_Atlantic
647	Ref27	NS05	Wrensel,2008	m3-119	43.273	-70.651	GoogleEarthPro	59	Table	105	15	100	13.3	1.3				Taconic_Acadian_Terrane	-	D1	D1;0	MED1;0	ME001	Devonian	granodiorite		Piscataqua	North_Atlantic
648	Ref27	NS05	Wrensel,2008	m3-120	43.264	-70.68	GoogleEarthPro	63	Table	118	18	78	13.5	1.3				Taconic_Acadian_Terrane	-	D2	D2;0	MED2;0	ME001	Devonian	mafic/metavolcanic rock	felsic metavolcanic rock	Piscataqua	North_Atlantic
649	Ref27	NS05	Wrensel,2008	m4-33	44.092	-69.957	GoogleEarthPro	82	Table	118	21	48						Taconic_Acadian_Terrane	-	O2c	O2c;0	MEO2c;0	ME001	Ordovician - Precambrian Z	mafic/metavolcanic rock	felsic metavolcanic rock	Androscoggin	North_Atlantic
650	Ref27	NS05	Wrensel,2008	m4-35	44.191	-69.716	GoogleEarthPro	38	Table	122	16	23	13.0	1.4	111			Taconic_Acadian_Terrane	-	O2c	O2c;0	MEO2c;0	ME001	Ordovician - Precambrian Z	mafic/metavolcanic rock	felsic metavolcanic rock	Kennebec	North_Atlantic
651	Ref27	NS05	Wrensel,2008	m4-36	44.244	-69.576	GoogleEarthPro	45	Table	110	16	85	13.0	1.5				Taconic_Acadian_Terrane	-	O2c	O2c;0	MEO2c;0	ME001	Ordovician - Precambrian Z	granite		Central_Coastal	North_Atlantic
652	Ref27	NS05	Wrensel,2008	m4-37	44.175	-70.084	GoogleEarthPro	81	Table	95	12	6	12.6		121		7	Taconic_Acadian_Terrane	-	O2c	O2c;0	MEO2c;0	ME001	Devonian	mafic/metavolcanic rock	felsic metavolcanic rock	Androscoggin	North_Atlantic
653	Ref27	NS05	Wrensel,2008	m4-38	44.089	-69.835	GoogleEarthPro	108	Table	119	15	77			118		7	Taconic_Acadian_Terrane	-	O2c	O2c;0	MEO2c;0	ME001	Devonian	mafic/metavolcanic rock	felsic metavolcanic rock	Androscoggin	North_Atlantic
654	Ref27	NS05	Wrensel,2008	m4-39	44.096	-69.872	GoogleEarthPro	56	Table	124	19	91	13.0	1.8				Taconic_Acadian_Terrane	-	O2c	O2c;0	MEO2c;0	ME001	Ordovician - Precambrian Z	slate	schist	Androscoggin	North_Atlantic
655	Ref27	NS05	Wrensel,2008	m4-40	44.089	-69.816	GoogleEarthPro	21	Table	121	21	51						Taconic_Acadian_Terrane	-	O2c	O2c;0	MEO2c;0	ME001	Ordovician - Precambrian Z	slate	schist	Kennebec	North_Atlantic
656	Ref27	NS05	Wrensel,2008	m4-41	43.996	-69.804	GoogleEarthPro	41	Table	159	28	72						Taconic_Acadian_Terrane	-	O2ce	O2ce;0	MEO2ce;0	ME001	Ordovician - Precambrian Z	slate	schist	Kennebec	North_Atlantic
657	Ref27	NS05	Wrensel,2008	m4-42	44.098	-69.655	GoogleEarthPro	77	Table	134	16	79						Taconic_Acadian_Terrane	-	O2ce	O2ce;0	MEO2ce;0	ME001	Ordovician - Precambrian Z	slate	schist	Central_Coastal	North_Atlantic
658	Ref27	NS05	Wrensel,2008	m4-43	44.111	-69.624	GoogleEarthPro	56	Table	117	14	71						Taconic_Acadian_Terrane	-	O2ce	O2ce;0	MEO2ce;0	ME001	Ordovician - Precambrian Z	sandstone	limestone	Central_Coastal	North_Atlantic
659	Ref27	NS05	Wrensel,2008	m4-44	44.061	-69.538	GoogleEarthPro	17	Table	126	15	90	12.5	1.9	101		6	Taconic_Acadian_Terrane	-	DOb	DOb;0	MEDOb;0	ME001	Devonian - Ordovician	granite		Central_Coastal	North_Atlantic
660	Ref27	NS05	Wrensel,2008	m4-45	44.099	-69.417	GoogleEarthPro	96	Table	100	13	6						Taconic_Acadian_Terrane	-	D1(m)	D1(m);0	MED1(m);0	ME001	Devonian	quartz monzonite		Central_Coastal	North_Atlantic
661	Ref27	NS05	Wrensel,2008	m4-47	44.314	-69.705	GoogleEarthPro	71	Table	112	16	23						Taconic_Acadian_Terrane	-	D4d(m)	D4d(m);0	MED4d(m);0	ME001	Devonian	granodiorite		Kennebec	North_Atlantic
662	Ref27	NS05	Wrensel,2008	m4-49	44.332	-69.397	GoogleEarthPro	255	Table	103	14	83						Taconic_Acadian_Terrane	-	D1	D1;0	MED1;0	ME001	Devonian	granodiorite		Kennebec	North_Atlantic
663	Ref27	NS05	Wrensel,2008	m4-51	43.632	-71.993	GoogleEarthPro	303	Table	100	14	72	12.7	2.0				Taconic_Acadian_Terrane	-	Db2b	Db2b;0	NHDb2b;0	NH001	Early Devonian	granodiorite	tonalite	Connecticut	Mid_Atlantic

Supplementary Table 2. Summary of information on samples with mean apatite fission-track lengths >14 µm

Study	Lat., Long. (°) Elev. (m)	AFT Age (Ma) (± 1σ)	χ² prob. (%)	Mean Track Length (µm)	Std. Dev. (µm)	Physiographic Province	Catchment Drainage Outlet
Kunk et al., 2005	39.028, -77.279 72	131 ± 16	1	14.0	1.2	Piedmont	Mid. Atlantic
Kunk et al., 2005	38.972, -77.138 80	179 ± 15	43	14.3	1.4	Piedmont	Mid. Atlantic
Miller & Duddy, 1989	42.421, -74.465 352	145 ± 14	75	14.1	1.1	Appalachian Basin	Mid. Atlantic
Miller & Duddy, 1989	42.931, -76.589 191	142 ± 20	2	14.6	1.2	Appalachian Basin	North Atlantic
Miller & Duddy, 1989	42.812, -74.699 446	246 ± 17	61	14.2	1.2	Appalachian Basin	Mid. Atlantic
Miller & Duddy, 1989	42.972, -76.048 306	228 ± 17	65	14.8	1.1	Appalachian Basin	North Atlantic
Miller & Duddy, 1989	42.916, -76.764 135	149 ± 9	24	14.4	1.5	Appalachian Basin	North Atlantic
Miller & Duddy, 1989	42.948, -77.316 209	200 ± 7	85	14.1	1.4	Appalachian Basin	North Atlantic
Miller & Duddy, 1989	42.183, -74.094 804	126 ± 10	10	14.5	1.0	Appalachian Basin	Mid. Atlantic
Miller & Duddy, 1989	41.48, -74.725 388	159 ± 19	3	14.0	1.2	Appalachian Basin	Mid. Atlantic
Miller & Duddy, 1989	41.454, -74.874 275	135 ± 17	1	14.1	1.1	Appalachian Basin	Mid. Atlantic
Miller & Duddy, 1989	41.57, -75.01 237	130 ± 8	84	14.1	1.1	Appalachian Basin	Mid. Atlantic
Miller & Duddy, 1989	41.867, -74.999 558	168 ± 11	39	14.4	1.0	Appalachian Basin	Mid. Atlantic
Miller & Duddy, 1989	41.98, -75.225 406	140 ± 11	18	14.4	1.2	Appalachian Basin	Mid. Atlantic
Miller & Duddy, 1989	42.32, -77.401 410	142 ± 12	91	14.0	1.3	Appalachian Basin	Mid. Atlantic
Miller & Duddy, 1989	41.749, -74.507 339	114 ± 9	17	14.1	1.0	Appalachian Basin	Mid. Atlantic
Miller & Duddy, 1989	42.099, -74.567 612	118 ± 9	16	14.1	1.3	Appalachian Basin	Mid. Atlantic
Miller & Duddy, 1989	41.998, -74.406 1105	116 ± 23	81	14.6	1.3	Appalachian Basin	Mid. Atlantic
Miller & Duddy, 1989	41.915, -74.275 486	138 ± 14	-	14.5	0.7	Ridge and Valley	Mid. Atlantic

Study	Lat., Long. (°) Elev. (m)	AFT Age (Ma) (± 1σ)	χ² prob. (%)	Mean Track Length (µm)	Std. Dev. (µm)	Physiographic Province	Catchment Drainage Outlet
Roden & Miller, 1989	40.932, -75.186 404	144 ± 8	5	14.0	1.2	Ridge and Valley	Mid. Atlantic
Roden & Miller, 1989	40.511, -77.581 135	245 ± 13	5	14.1	1.7	Ridge and Valley	Mid. Atlantic
Roden & Miller, 1991	41.066, -74.027 72	161 ± 12	85	14.1	1.6	Hartford Rift Basin	Mid. Atlantic
Roden & Miller, 1991	40.959, -74.185 76	196 ± 23	98	14.8	1.0	Hartford Rift Basin	Mid. Atlantic
Roden & Miller, 1991	41.389, -72.613 102	154 ± 11	58	14.0	1.4	Hartford Rift Basin	Mid. Atlantic
Roden-Tice & Wintsch, 2002	42.46, -72.26 159	143 ± 21	-	14.1	1.2	Taconic and Acadian Terrane	Mid. Atlantic
Roden-Tice et al., 2000	44.05, -73.46 83	123 ± 14	-	14.0	1.4	Adirondacks	North Atlantic
Steckler et al., 1993	40.888, -74.167 51	136 ± 7	27	14.3	1.0	Newark Rift Basin	Mid. Atlantic
Steckler et al., 1993	41.111, -74.063 157	157 ± 10	1	14.2	1.1	Newark Rift Basin	Mid. Atlantic
Steckler et al., 1993	41.016, -74.272 93	138 ± 9	35	14.1	1.1	Newark Rift Basin	Mid. Atlantic
Steckler et al., 1993	41.238, -74.005 53	171 ± 9	36	14.1	1.1	Newark Rift Basin	Mid. Atlantic

This table summarizes the pertinent information from the AppLTDB (Supplementary material) collected on samples with mean apatite fission-track lengths >14 µm. AFT age likely represents the timing of rapid cooling for that sample (i.e. Gleadow et al., 1986; Green et al., 1989). Physiographic province and catchment drainage outlet are included for reference with figure 5 and the discussion. Lat. = latitude; Long. = longitude; Elev. = elevation; AFT = apatite fission-track; Std. Dev. = standard deviation.

References

Amidon, W. H., Roden-Tice, M. K., Anderson, A. J., McKeon, R. E., and Shuster, D. L. (2016). Late cretaceous unroofing of the White Mountains, New Hampshire, USA: An episode of passive margin rejuvenation? *Geology*, *44*(6), 415–418.

Armstrong, P.A. (2005) Thermochronometers in sedimentary basins. *Rev. Mineral. Geochem.*, **58**, 499-525.

Ault, A.K., Flowers, R.M., and Bowring, S.A. (2013). Phanerozoic surface history of the Slave craton. *Tectonics*, *32*(5), 1066–1083.

Babault, J., Loget, N., Van Den Driessche, J., Castelltort, S., Bonnet, S. & Davy, P. (2006) Did the Ebro basin connect to the Mediterranean before the Messinian salinity crisis?. *Geomorphology*, **81**(1-2), 155-165.

Bailey, D.G. & Lupulescu, M.V. (2015) Spatial, temporal, mineralogical, and compositional variations in Mesozoic kimberlitic magmatism in New York State. *Lithos,* **212**, 298-310.

Barbarand, J., Carter, A., Wood, I. & Hurford, T. (2003) Compositional and structural control of fission-track annealing in apatite. *Chem. Geol.*, *198*, 107–137.

Beamud, E., Muñoz, J. A., Fitzgerald, P. G., Baldwin, S. L., Garcés, M., Cabrera, L., & Metcalf, J. R. (2010) Magnetostratigraphy and detrital apatite fission track thermochronology in syntectonic conglomerates: Constraints on the exhumation of the South-Central Pyrenees. *Basin Research*, *23*(3), 309–331.

Beaumont, C., Quinlan, G.M. & Hamilton, J. (1987) The Alleghanian orogeny and its relationship to the evolution of the eastern interior, North America. In: *Sedimentary Basins and Basin-forming Mechanisms* (Ed. by C. Beaumont & A.J. Tankard), *Mem. Can. Soc. Petrol. Geol.*, **12**, 425-445.

Bishop, P. (2007). Long-term landscape evolution: linking tectonics and surface processes. *Earth Surface Processes and Landforms*, *32*(3), 329-365.

Blackmer, G.C., Omar, G. I. & Gold, D.P. (1994) Post-Alleghanian Unroofing History of the Appalachian Basin, Pennsylvania, from Fission Track Analysis and Thermal Models. *Tectonics*, **13**, 1259–1276.

Blakey, R.C. (2013). North American Key Time-slices Series. Colorado Plateau Geosystems Inc., Deep Time Maps™.

Boettcher, S.S. & Milliken, K.L. (1994). Mesozoic-Cenozoic Unroofing of the Southern Appalachian Basin: Apatite Fission Track Evidence from Middle Pennsylvanian Sandstones. *J. Geol.*, *102*, 655–668.

Braun, D.D. (1989) The depth of post middle Miocene erosion and the age of the present landscape, in The Rivers and Valleys of Pennsylvania, Then and Now, edited by W. D. Sevon, pp. 16-20, Fieldtrip Guidebook ,Harrisburg Arear Geological Society, Harrisburg, Pa.

Braun, J. (2002). Quantifying the effect of recent relief changes on age-elevation relationships. *Earth and Planetary Science Letters*, *200*(3–4), 331–343.

Bray, R.J., Green, P.F. & Duddy, I.R. (1992) Thermal History Reconstruction Using Apatite Fission Track Analysis and Vitrinite Reflectance: A Case Study from the UK East Midlands and Southern North Sea. *Geol. Soc. London Spec. Publ.,* **67**, 3–25.

Brown, R.W., Beucher, R., Roper, S., Persano, C., Stuart, F. & Fitzgerald, P.G. (2013) Natural age dispersion arising from the analysis of broken crystals. Part I: Theoretical basis and

implications for the apatite (U–Th)/He thermochronometer. *Geochim. Cosmochim. Acta*, *122*, 478-497.

Burtner, R.L., Nigrini, A. & Donelick, R.A. (1994) Thermochronology of Lower Cretaceous Source Rocks in the Idaho-Wyoming Thrust Belt. *AAPG Bull.,* **78**, 1613–1636.

Carlson, W.D., Donelick, R.A. & Ketcham R.A. (1999) Variability of apatite fission-track annealing kinetics: I. Experimental results. *Am. Mineral.,* **84**, 1213–1223.

Chyi, L.L., Barnett, R.G., Burford, A.E., Quick, T.J. & Gray, R.J. (1987) Coalification patterns of the Pittsburgh coal: their origin and bearing on hydrocarbon maturation. *Int. J. Coal Geol.*, **7**, 69-83.

Coney, P.J., Muñoz, J., McClay, K.R. & Evenchick, C.A. (1996) Syntectonic burial and post-tectonic exhumation of the southern Pyrenees foreland fold-thrust belt. *J. Geol. Soc. Lond.*, **153**(1), 9-16.

Corrigan, J., Cervany, P.F., Donelick, R.A. & Bergman, S.C. (1998) Postorogenic denudation along the late Paleozoic Ouachita trend, south central United States of America: Magnitude and timing constraints from apatite fission track data. *Tectonics*, **17**, 587-603.

Crowley, K.D., Cameron, M. & Schaefer, R.L. (1991) Experimental studies of annealing of etched fission tracks in fluorapatite. *Geochim. Cosmochim. Acta,* **55**, 1449–1465.

Daniels, E.J., Altaner, S.P., Marshak, E. & Eggleston, J.R. (1990) Hydrothermal alteration in anthracite from eastern Pennsylvania: implications for mechanisms of anthracite formation. *Geology*, **18**, 247-250.

Davis, W.M. (1889) The river and valleys of Pennsylvania: National Geographic Magazine, v. 1, p. 183–253.

de Boer, J.Z., McHone, J.G., Puffer, J.H., Ragland, P.C. and Whittington, D., 1988. Mesozoic and Cenozoic magmatism. In: R.E. Sheridan and J.A. Grow (Editors), The Geology of North America, Volume I-2. The Atlantic Continental Margin, U.S. Geol. Soc. Am., Boulder, Colo., pp. 217-241.

de Bruijne, C.H. & Andriessen, P.A.M. (2002) Far field effects of Alpine plate tectonism in the Iberian microplate recorded by fault-related denudation in the Spanish Central System. *Tectonophysics*, **349**(1-4), 161-184.

Dicken, C.L., Nicholson, S.W., Horton, J.D., Kinney, S.A., Gunther, G., Foose, M.P. & Mueller, J. A.L. (2005) Preliminary integrated geologic map databases for the United States: Delaware, Maryland, New York, Pennsylvania, and Virginia. *U.S. Geol. Surv.*, Open Report **2005-1325**.

Doherty, J. T., & Lyons, J. B. (1980). Mesozoic erosion rates in northern New England. Geological Society of America Bulletin, 91(Part 1), 16–20.

Donelick, R.A., Ketcham R.A. & Carlson, W.D. (1999) Variability of apatite fission-track annealing kinetics: II. Crystallographic orientation effects. *Am. Mineral.*, **84**, 1224–1234.

Donelick, R.A., O'Sullivan, P.B. & Ketcham R.A. (2005) Apatite fission-track analysis. *Rev. Mineral. Geochem.*, **58**, 49–94.

Dorobek, S. (1989) Migration of orogenic fluids through the Siluro-Devonian Helderberg Group during the late Paleozoic deformation; Constraints on fluid sources and implications for thermal histories of sedimentary basins. *Tectonophysics*, **159**, 25–45.

East, J.A., Swezey, C.S., Repetski, J.E. & Hayba, D.O. (2012) Thermal maturity map of Devonian shale in the Illinois, Michigan, and Appalachian basins of North America. *U.S. Geol. Surv.*, Sci. Invest. Map **3214**.

Eaton, D.W. & Frederiksen, A. (2007) Seismic Evidence for Convection-Driven Motion of the North American Plate. *Nature,* **446**, 428–431.

Ehlers, T.A. & Farley, K.A. (2003) Apatite (U-Th)/He thermochronometry: methods and applications to problems in tectonic and surface processes. *Earth Planet. Sci. Lett.*, **206**, 1–14.

Epstein, A.G., Epstein, J.B. & Harris, L.D. (1977) Conodont Color Alteration - an Index to Organic Metamorphism. *U.S. Geol. Surv.,* Professional Paper **995**, 1-27.

Ettensohn, F.R. (1985). The Catskill Delta complex and the Acadian Orogeny: A model. *Geological Society of America Special Papers*, *201*, 39–49.

Ettensohn, F.R. (2008) The Appalachian foreland basin in eastern United States. In: *Sedimentary basins of the World* (Ed. by K.J. Hsü), Section: *The Sedimentary Basins of the United States and Canada* (Ed. by A.D. Miall), **5**, 105-179.

Faill, R. T. (1973). Tectonic development of the Triassic Newark-Gettysburg basin in Pennsylvania. *Geological Society of America Bulletin*, *84*(3), 725-740.

Faill, R.T. (1985) The Acadian Orogeny and the Catskill Delta. *Geol. Soc. Am., Spec. Pap.*, **201**, 15–38.

Faill, R.T. (1997a). A geologic history of the north-central Appalachians. Part 1. Orogenesis from the Mesoproterozoic through the Taconic orogeny. *American Journal of Science*.

Faill, R.T. (1997b). A geologic history of the north-central Appalachians, part 2: The Appalachian basin from the Silurian through the Carboniferous. *American Journal of Science*, *297*, 729–761.

Faill, R.T. (1998). A geologic history of the north-central Appalachians, part 3. The Alleghany orogeny. *American Journal of Science*, *298*, 131–179.

Fairhead, J.D., and Binks, R.M. (1991) Differential opening of the Central and South Atlantic Oceans and the opening of the West African rift system: Tectonophysics, v. 187, p. 191–203.

Farley, K.A. (2002) (U-Th)/He Dating: Techniques, Calibrations, and Applications. *Rev. Mineral. Geochem.*, **47,** 819–844.

Farley, K.A., Wolf, R.W., Silver, L.T. (1996) The effects of long alpha-stopping distances on (U-Th)/He ages. *Geochim. Cosmochim. Acta*, **60**, 4223-4229.

Fitzgerald, P.G., Baldwin, S.L., Webb, L.E. & O'Sullivan, P.B. (2006) Interpretation of (U-Th)/He single grain ages from slowly cooled crustal terranes: A case study from the Transantarctic Mountains of southern Victoria Land. *Chem. Geol.*, **225**, 91–120.

Fitzgerald and Malusà (2018) Concept of the exhumed partial annealing (retention) zone and age-elevation profiles in thermochronology. In: *Fission-track thermochronology and its application to geology* (Ed. by M.G. Malusà and P.G. Fitzgerald), Springer, Berlin (Chapter 9).

Flowers, R.M., Ketcham, R.A., Shuster, D.L. & Farley, K.A. (2009) Apatite (U-Th)/He thermochronometry using a radiation damage accumulation and annealing model. *Geochim. Cosmochim. Acta*, **73**, 2347–2365.

Flowers, R.M. & Kelley, S.A. (2011) Interpreting data dispersion and "inverted" dates in apatite (U-Th)/He and fission-track datasets: An example from the US midcontinent. *Geochim. Cosmochim. Acta*, **75**, 5169-5186.

Foscolos, A.E., Powell, T. G. & Gunther, P.R. (1976) The use of clay minerals and inorganic and organic geochemical indicators for evaluating the degree of diagenesis and oil generating potential of shales. *Geochim. Cosmochim. Acta*, **40**, 953-966.

Friedman, G.M. (1987) Vertical Movements of the Crust: Case Histories from the Northern Appalachian Basin. *Geology*, **15**, 130–1133.

Friedman, G.M. & Sanders, J.E. (1982) Time-temperature-burial significance of Devonian anthracite implies former great (approx 6.5km) depth of burial of Catskill Mountains, New York. *Geology*, **10**, 93–96.

Galbraith, R.F. (1990) The radial plot: graphical assessment of spread in ages. *International Journal of Radiation Applications and Instrumentation. Part D. Nuclear Tracks and Radiation Measurements*, **17**(3), 207-214.

Galbraith, R.F. & Laslett, G.M. (1993) Statistical models for mixed fission track ages. *Nucl. Tracks Radiat. Meas.*, **21**, 459–470.

Gallagher, K. (2012) Transdimensional inverse thermal history modeling for quantitative thermochronology. J. Geophys. Res. Solid Earth 117 (B2).

Gallagher, K., Brown, R. & Johnson, C. (1998) Fission Track Analysis and Its Applications to Geological Problems. *Annu. Rev. Earth Planet Sci.*, **26**, 519–72.

Gallen, S.F., Wegmann, K.W. & Bohnenstieh, D.R. (2013) Miocene rejuvenation of topographic relief in the southern Appalachians. *GSA Today*, **23**, 4–10.

Gerlach, J.B. & Cercone, K.R. (1993). Former Carboniferous overburden in the northern Appalachian Basin: a reconstruction based on vitrinite reflectance. *Org. Geochem.*, **20**, 223–232.

Gleadow, A.J.W. & Duddy, I.R. (1981) A Natural Long-Term Track Annealing Experiment for Apatite. *Nuclear Tracks*, **5**, 169–174.

Gleadow, A.J.W., Duddy, I.R. & Lovering, J.F. (1983) Fission Track Analysis: A New Tool for the Evaluation of Thermal Histories and Hydrocarbon Potential. *APPEA J.,* **23**, 93-102.

Gleadow, A.J.W. & Duddy, I.R. (1984) Fission track dating and thermal history analysis of apatites from wells in the north-west Canning Basin. In: *Canning Basin, W.A.- petroleum geology and mineral potential* (Ed. by P.G. Purcell), *Geol. Soc. Australia, Petrol. Explor. Soc. Australia*, 277-287.

Gleadow, A.J.W., Duddy, I.R., Green, P.F. & Hegarty, K.A. (1986) Fission track lengths in the apatite annealing zone and the interpretation of mixed ages. *Earth Planet. Sci. Lett.*, **78**, 245-254.

Gleadow, A.J.W. & Fitzgerald, P.G. (1987) Uplift History of the Transantarctic Mountains: New Evidence from Fission Track Dating of Basement Apatites in the Dry Valleys Area, Southern Victoria Land. *Earth Planet. Sci. Lett.*, **82**, 1–14.

Gleadow, A. J., & Brown, R. W. (2000). Fission-track thermochronology and the long-term denudational response to tectonics. *Geomorphology and global tectonics*, 57-75.

Green, P.F., Duddy, I.R., Gleadow, A.J.W., Tingate, P.R. & Laslett, G.M. (1986) Thermal annealing of fission tracks in apatite: 1. A qualitative description. *Chem. Geol.: Isotope Geoscience section*, **59**, 237-253.

Green, P.F., Duddy, I.R., Gleadow, A. J.W. & Lovering, J. F. (1989) Apatite fission-track analysis as a paleotemperature indicator for hydrocarbon exploration. In: *Thermal history of sedimentary basins* (Ed. by N.D. Naeser & T.H. McCulloh), 181-195.

Green, P.F., Duddy, I.R. & Bray, R.J. (1995) Applications of Thermal History Reconstruction in Inverted Basins. *Geol. Soc. London Spec. Publ.*, **88**, 149–165.

Green, P.F. & Duddy, I.R. (2012) Thermal history reconstruction in sedimentary basins using apatite fission-track analysis and related techniques. *Analyzing the thermal history of sedimentary basins: Methods and case studies: SEPM Special Publication*, **103**, 65-104.

Green, P.F. & Duddy, I.R. (2018) Apatite (U-Th-Sm)/He thermochronology on the wrong side of the tracks. *Chem. Geol.*, **488**, 21-33.

Green, P.F., Japsen, P., Chalmers, J.A., Bonow, J.M., & Duddy, I.R. (2018) Post-breakup burial and exhumation of passive continental margins: Seven propositions to inform geodynamic models. *Gondwana Research*, *53*, 58-81.

Gurney, G.G. & Friedman, G.M. (1986) Burial history of Cherry Valley carbonate sequence, from Cherry Valley, New York. *Am. Assoc. Pet. Geol., Bull.*, 70.CONF-8610158.

Hack, J.T. (1960) Interpretation of erosional topography in humid temperate regions: American Journal of Science, v. 258-A, p. 80–97.

Hack, J.T. (1982) Physiographic divisions and differential uplift in the Piedmont and Blue Ridge: U.S. Geological Survey Professional Paper 1265-P, p. 1–49.

Hack, J. T. (1989). Geomorphology of the Appalachian highlands. *The Appalachian-Ouachita Orogen in the United States, The Geology of North America*, *2*, 459-470.

Hames, W., McHone, J. G., Renne, P., & Ruppel, C. (2003). The Central Atlantic magmatic province: Insights from fragments of Pangea. *Washington DC American Geophysical Union Geophysical Monograph Series*, *136*.

Harrison, M.J., Marshak, S. & Onasch, C.M. (2004) Stratigraphic control of hot fluids on anthracitization, Lackawanna synclinorium, Pennsylvania. *Tectonophysics*, **378**, 85-103.

Harrison, T.M. & Zeitler, P.K. (2005) Fundamentals of noble gas thermochronometry. *Rev. Mineral. Geochem.*, **58**, 123-149.

Hatcher, R. D. (2002). Alleghanian (Appalachian) orogeny, a product of zipper tectonics: Rotational transpressive continent-continent collision and closing of ancient oceans along irregular margins. *Geological Society of America Special Paper*, *364*, 199–208.

Hatcher Jr., R.D. (2010) The Appalachian orogen: A brief summary. In: *From Rodinia to Pangea: The Lithotectonic Record of the Appalachian Region* (Ed. by R.P. Tollo, M.J. Bartholomew, J.P. Hibbard & P.M. Karabinos), *GSA Memoir*, **206**, 1-19.

Hatcher Jr, R. D., Thomas, W. A., & Viele, G. W. (Eds.). (1989). *The Appalachian-Ouachita Orogen in the United States*. Geological Society of America.

Heaman, L.M. & Kjarsgaard, B.A. (2000) Timing of eastern North American kimberlite magmatism; continental extension of the Great Meteor Hotspot track? *Earth Planet. Sci. Lett.,* **178**, 253–268.

Hijmans, R.J., Cameron, S.E., Parra, J.L., Jones, P.G. & Jarvis, A. (2005) Very high resolution interpolated climate surfaces for global land areas. *Int. J. Climatol.*, **25**, 1965–1978.

Horton, J.D. (2017) The State Geologic Map Compilation (SGMC) geodatabase of the conterminous United States (ver. 1.1, August 2017): U.S. Geological Survey data release.

House, M.A., Farley, K.A. & Kohn, B.P. (1999) An empirical test of helium diffusion in apatite: borehole data from the Otway basin, Australia. *Earth Planet. Sci. Lett.*, **170**, 463-474.

Hower, J.C. & Gayer, R.A. (2002) Mechanisms of coal metamorphism: case studies from Paleozoic coalfields. *Int. J. Coal Geol.*, **50**, 215-245.

Hulver, M.L. (1997) Post-orogenic evolution of the Appalachian mountain system and its foreland. PhD Thesis, University of Chicago, Chicago, IL.

Hurford, A.J. & Green, P.F. (1983) The Zeta Age Calibration of Fission-Track Dating. *Chem. Geol.*, **41**, 285–317.

Hurford, A.J. (2018) An Historical Perspective on Fission-Track Thermochronology. In: *Fission-track thermochronology and its application to geology* (Ed. by M.G. Malusà and P.G. Fitzgerald), Springer, Berlin (Chapter 1).

Isachsen, Y.W. (1975) Possible evidence for contemporary doming of the Adirondack Mountains, New York, and suggested implications for regional tectonics and seismicity. Tectonophysics, 29: 161-181.

Isachsen, Y.W. (1981) Contemporary doming of the Adirondack Mountains: further evidence from releveling. Tectonophysics 71:95–96.

Isachsen, Y.W., Landing, E., Lauber, J.M., Rickard, L.V. & Rogers, W.B. (1991) The geology of New York: a simplified account. N.Y. State Mus. Education Leaflet 28, New York State Museum/Geological Survey.

Isachsen, Y. W., & Kelly, W. M. (1992). The Adirondacks: Still rising after all these years. *Natural History, May Issue*.

Issler, D. R. (1996) An inverse model for extracting thermal histories from apatite fission track data: instructions and software for the Windows 95 environment. Geol. Surv. Can. Open File Rep. 2325.

Jarvis A., Reuter, H.I., Nelson, A. & Guevara, E. (2008) Hole-filled seamless SRTM data V4, *International Centre for Tropical Agriculture (CIAT)*, available from http://srtm.csi.cgiar.org.

Jiang, S. (2012). Clay minerals from the perspective of oil and gas exploration. In: *Clay Minerals in Nature - Their Characterization, Modification and Application* (Ed. by M. Valaškova & G.S. Martynkova), InTech.

Johnsson, M.J. (1985) Late Paleozoic-Middle Mesozoic uplift rate, cooling rate and geothermal gradient for south-central New York state. *Nucl. Tracks Radiat. Meas.*, **10**(3), 295–301.

Johnsson, M.J. (1986) Distribution of maximum burial temperatures across northern Appalachian Basin and implications for Carboniferous sedimentation patterns. *Geology*, **14**, 384–387.

Judson, S. (1975) Evolution of Appalachian Topography. In: *Theories of Landform Development, Proceedings of the 6th Geomorphology Symposium* (Ed. by W.N. Melhore and R.C. Flemal), 29-44. Publications in Geomorphology, State University of New York at Binghamton.

Ketcham, R.A. (2005) Forward and Inverse Modeling of Low-Temperature Thermochronometry Data. *Rev. Mineral. Geochem.*, **58**, 275–314.

Ketcham, R.A. (2012) Basin Thermal History Analysis Using (U-Th)/ He Thermochronometry. *SPEM Spec. Pub.*, **103**, 105–123.

Ketcham, R.A., Donelick R.A. & Carlson W.D. (1999) Variability of apatite fission-track annealing kinetics: III. Extrapolation to geological time scales. *Am. Mineral.*, **84**, 1235-1255.

Ketcham, R.A., Carter, A., Donelick, R.A., Barbarand, J. & Hurford, A.J. (2007) Improved measurement of fission-track annealing in apatite using *c*-axis projection. *Am. Mineral.*, **92**, 799-810.

Ketcham, R.A., Gautheron, C. & Tassan-Got, L. (2011) Accounting for long alpha-particle stopping distances in (U-Th-Sm)/He geochronology: Refinement of the baseline case. *Geochim. Cosmochim. Acta*, **75**, 7779–7791.

Ketcham, R.A., van der Beek, P., Barbarand, J., Bernet, M. & Gautheron, C. (2018) Reproducibility of Thermal History Reconstruction from Apatite Fission-Track and (U-Th)/He Data. *Geochemistry, Geophysics, Geosystems*.

Klitgord, K.D., Hutchinson, D.R. & Schouten, H. (1988) U.S. Atlantic continental margin: structural and tectonic framework. In: *The Geology of North America, the Atlantic*

Continental Margin, U.S. (Ed. by R.E. Sheridan & J.A. Grow), 19-57, Decade of North American Geology Series, **2**, Geological Society of America, Boulder, CO.

Kohn, B., Chung, L. & Gleadow, A.J.W. (2018) Fission-track analysis: field collection, sample preparation and data acquisition. In: *Fission-track thermochronology and its application to geology* (Ed. by M.G. Malusà and P.G. Fitzgerald), Springer, Berlin (Chapter 2).

Kunk, M. J., Wintsch, R. P., Naeser, C. W., Naeser, N. D., Southworth, C. S., Drake, A. A., & Becker, J. L. (2005). Contrasting tectonothermal domains and faulting in the Potomac terrane, Virginia-Maryland - Discrimination by40Ar/39Ar and fission-track thermochronology. Bulletin of the Geological Society of America, 117(9–10), 1347–1366.

Lakatos, S. & Miller, D.S. (1983). Fission-track analysis of apatite and zircon defines a burial depth of 4 to 7 km for lowermost Upper Devonian, Catskill Mountains, New York. *Geology*, **11**, 103–104.

Lash, G.G. & Blood, D.R. (2007) Origin of Early Overpressure in the Upper Devonian Catskill Delta Complex, Western New York State. *Basin Res.*, **19**, 51–66.

Lash, G. G., and Engelder, T. (2009). Tracking the burial and tectonic history of Devonian shale of the Appalachian basin by analysis of joint intersection style. *Bulletin of the Geological Society of America*, *121*(1–2), 265–277.

Laslett, G.M., Green, P.F., Duddy, I.R. & Gleadow, A.J.W. (1987) Thermal annealing of fission tracks in apatite 2. A quantitative analysis. *Chem. Geol.: Isotope Geoscience Section*, **65**, 1-13.

Lehner, B., Verdin, K., Jarvis, A. (2008): New global hydrography derived from spaceborne elevation data (HydroSHEDS). Eos, Transactions, AGU, 89(10): 93-94.

Levine, J.R. (1986) Deep burial of coal-bearing strata, Anthracite region, Pennsylvania: sedimentation or tectonics. *Geology*, **14**, 577-580.

Lindberg, F.A. (1985) Northern Appalachian Region: COSUNA Project. *American Association of Petroleum Geologists*, Tulsa, OK.

Malusà, M.G. & Fitzgerald, P.G. (2018) From cooling to exhumation: setting the reference frame for the interpretation of thermochronologic data. In: *Fission-track thermochronology and its application to geology* (Ed. by M.G. Malusà and P.G. Fitzgerald), Springer, Berlin (Chapter 8).

Marzoli, A., Renne, P.R., Piccirillo, E.M., Ernesto, M., Bellieni, G. & deMin, A. (1999) Extensive 200-million-year-old continental flood basalts of the Central Atlantic Magmatic Province. *Science*, 284, 616–618.

McHone, J. G. (1988). Tectonic and paleostress patterns of Mesozoic intrusions in eastern North America. In *Developments in Geotectonics* (Vol. 22, pp. 607-620). Elsevier.

McHone, J.G. (1992) Mafic dike suites within Mesozoic igneous provinces of New England and Atlantic Canada, *in* Puffer, J.H. and Ragland, P.C., eds., Eastern North American Mesozoic Magmatism: Geological Society of America Special Paper 268.

McKeon, R.E., Zeitler, P.K., Pazzaglia, F.J., Idleman, B.D. & Enkelmann, E. (2014) Decay of an old orogen: Inferences about appalachian landscape evolution from low-temperature thermochronology. *Geol. Soc. Am. Bull.*, **126**, 31–46.

Meesters, A.G.C.A. & Dunai, T.J. (2002) Solving the production–diffusion equation for finite diffusion domains of various shapes: Part II. Application to cases with a-ejection and nonhomogeneous distribution of the source. Chemical Geology 186, 347–363.

Miller, D. S., & Lakatos, S. (1983). Uplift rate of Adirondack anorthosite measured by fission-track analysis of apatite. Geology, 11(5), 284–286.

Miller, D.S. & Duddy, I.R. (1989) Early Cretaceous Uplift and Erosion of the Northern Appalachian Basin, New York , Based on Apatite Fission Track Analysis. *Earth Planet. Sci. Lett.*, **93**, 35–49.

Miller, S.R., Sak, P.B., Kirby, E. & Bierman, P.R. (2013) Neogene rejuvenation of central Appalachian topography: Evidence for differential rock uplift from stream profiles and erosion rates. *Earth Planet. Sci. Lett.*, **369**, 1–12.

Moodie, A.J., Pazzaglia, F.J., & Berti, C. (2018). Exogenic forcing and autogenic processes on continental divide location and mobility. *Basin Research*, *30*(2), 344-369.

Moucha, R., Forte, A.M., Mitrovica, J.X., Rowley, D.B., Quere, S., Simmons, N.A. & Grand, S.P. (2008) Dynamic topography and long-term sea-level variations: There is no such thing as a stable continental platform. *Earth Planet. Sci. Lett.*, **271**, 101–108.

Naeser, C.W. (1981) The Fading of Fission Tracks in the Geologic Environment- Data from Deep Drill Holes. *Nuclear Tracks*, **5**, 248–250.

Naeser, N.D., Naeser, C.W. & McCulloh, T.H. (1989). The application of fission-track dating to the depositional and thermal history of rocks in sedimentary basins. In: *Thermal history of sedimentary basins* (Ed. by N.D. Naeser & T.H. McCulloh), 157-180, Springer, New York, NY.

Naeser, C. W., Naeser, N. D., Newell, W. L., Southworth, S., Edwards, L. E., & Weems, R. E. (2016). Erosional and depositional history of the Atlantic passive margin as recorded in detrital zircon fission-track ages and lithic detritus in Atlantic Coastal Plain sediments. *American Journal of Science*, *316*(2), 110-168.

Nielsen, S.B., Clausen, O.R. & Mcgregor, E. (2017) basin%Ro: A vitrinite reflectance model derived from basin and laboratory data. *Basin Research*, **29**, 515–536.

Nomade, S., Knight, K. B., Beutel, E., Renne, P. R., Verati, C., Féraud, G., Marzoli, A., Youbi, N. & Bertrand, H. (2007). Chronology of the Central Atlantic Magmatic Province: implications for the Central Atlantic rifting processes and the Triassic–Jurassic biotic crisis. *Palaeogeography, Palaeoclimatology, Palaeoecology*, *244*(1-4), 326-344.

Oliver, J. (1986) Fluids expelled tectonically from orogenic belts: their role in hydrocarbon migration and other geologic phenomena. *Geology*, **14**, 99–102.

Olsen, P.E., Kent, D.V., Et-Touhami, M. & Puffer, J. (2003) Cyclo-, magneto-, and bio-stratigraphic constraints on the duration of the CAMP event and its relationship to the Triassic–Jurassic boundary. In: Hames, W. E., McHone, J. G., Renne, P. R. & Ruppel, C. (eds) The Central Atlantic Magmatic Province, Insights from Fragments of Pangea. American Geophysical Union, Geophysical Monograph, 136, 7–32.

Pazzaglia, F.J. & Gardner, T.W. (1994) Late Cenozoic flexural deformation of the middle U.S. Atlantic passive margin. *J. Geophys. Res.*, **99**, 12143–112157.

Pazzaglia, F.J. & Brandon, M.T. (1996) Macrogeomorphic evolution of the post-Triassic Appalachian Mountains determined by deconvolution of the offshore basin sedimentary record. *Basin Research*, **8**, 1–24.

Poag, C.W. (Ed.) (1985) Geologic Evolution of the United States Atlantic Margin, pp. 217–263. Van Nostrand Reinhold, New York.

Poag, C.W. (1992) U.S. middle Atlantic continental rise: Provenance, dispersal, and deposition of Jurassic to Quaternary sediments. In: Geologic Evolution of Atlantic continental rises (Ed. by C. W. Poag and P. C. Graciansky), Van Nostrand Reinhold, New York.

Poag, C.W., and Sevon, W.D. (1989) A record of Appalachian denudation in post-rift Mesozoic and Cenozoic sedimentary deposits of the U.S. Middle Atlantic continental margin: Geomorphology, v. 2, no. 1–3, p. 119–157.

Poag, C.W. and Ward, L. W. (1993) Allostratigraphy of the U.S. middle Atlantic continental margin – characteristics, distribution, and depositional history of principal unconformity-bounded upper Cretaceous and Cenozoic sedimentary units. Prof. Pap. U.S. Geol. Surv., 1542.

Rast, N. (1989) The evolution of the Appalachian chain, in Bally, A. W. and Palmer, A. R. eds., The geology of North America—an overview, Geological Society of America, The geology of North America, Boulder, CO, v. A, pp. 323–348.

Rast, N., & Skehan, J. W. (1993). Mid-Paleozoic orogenesis in the North Atlantic: the Acadian orogeny. In *The Acadian Orogeny: Recent Studies in New England, Maritime Canada and the Autochthonous Foreland* (Vol. 245, pp. 1-25).

Reed, J.S., Spotila, J.A., Eriksson, K.A. & Bodnar, R.J. (2005) Burial and exhumation history of Pennsylvanian strata, central Appalachian Basin: An integrated study. *Basin Research*, **17**, 259-268.

Reiners, P.W. & Farley, K.A. (2001) Influence of Crystal Size on Apatite (U-Th)/He Thermochronology: An Example from the Bighorn Mountains, Wyoming. *Earth Planet. Sci. Lett.*, **188**, 413–420.

Reiners, P.W., Zhou, Z., Ehlers, T.A., Changhai, X., Brandon, M.T., Donelick, R.A. and Nicolescu, S. (2003) Post-progenic evolution of the Dabie Shan, eastern China, from (U-Th)/He and fission track thermochronology. Am J Sci 303:489-518.

Repetski, J.E., Ryder, R.T., Weary, D.J., Harris, A.G. & Trippi, M.H. (2008) Thermal Maturity Patterns (CAI and% Ro) in Upper Ordovician and Devonian Rocks of the Appalachian Basin. A Major Revision of U.S. Geol. Surv. Map I–917–E, Using New Subsurface Collections. *U.S. Geol. Surv.*, Sci. Invest. Map **3006**, 26.

Riccio, S.J., Fitzgerald, P.G., Benowitz, J.A. and Roeske, S.M. (2014). The role of thrust faulting in the formation of the eastern Alaska Range: Thermochronological constraints from the Susitna Glacier Thrust Fault region of the intracontinental strike-slip Denali Fault system. *Tectonics*, *1*(3), 144–173.

Roden, M.K. (1991) Apatite Fission-Track Thermochronology of the Southern Appalachian Basin: Maryland, West Virginia, and Virginia. *J. Geol.*, **99**, 41–53.

Roden, M.K. & Miller, D.S. (1989) Apatite fission-track thermochronology of the Pennsylvania Appalachian Basin. *Geomorphology*, **2**, 39–51.

Roden, M.K. & Miller, D.S. (1991) Tectono-thermal history of Hartford, Deerfield, Newark and Taylorsville Basins, eastern United States, using fission-track-analysis. *Schweiz. Mineral. Petrogr. Mitt.*, **71**, 187–203.

Roden-Tice, M.K., Tice, S.J. & Schofield, I.S. (2000) Evidence for Differential Unroofing in the Adirondack Mountains, New York State, Determined by Apatite Fission-Track Thermochronology. *J. Geol.*, **108**, 155–169.

Roden-Tice, M.K. & Wintsch, R.P. (2002) Early Cretaceous Normal Faulting in Southern New England: Evidence from Apatite and Zircon Fission-Track Ages. *J. Geol.*, **110**, 159–178.

Roden-Tice, M.K. & Tice, S.J. (2005) Regional-Scale Mid-Jurassic to Late Cretaceous Unroofing from the Adirondack Mountains through Central New England Based on Apatite Fission-Track and (U-Th)/He Thermochronology. *J. Geol.*, **113**, 535–552.

Roden-Tice, M.K., West Jr., D.P., Potter, J.K., Raymond, S.M. & Winch, J.L. (2009) Presence of a Long-Term Lithospheric Thermal Anomaly: Evidence from Apatite Fission-Track Analysis in Northern New England. *J. Geol.*, **117**, 627–641.

Roden-Tice, M. K., Eusden, J. D., & Wintsch, R. P. (2012). Apatite fission-track evidence for the Cretaceous development of kilometer-scale relief and steady-state Tertiary topography in New England. Geomorphology, 141–142, 114–120.

Ruppert, L.F., Hower, J.C., Ryder, R.T., Levine, J.R., Trippi, M.H. & Grady, W.C. (2010) Geologic controls on thermal maturity patterns in Pennsylvanian coal-bearing rocks in the Appalachian basin. *Int. J. Coal Geol.*, **81**, 169–181.

Ryder, R.T., Hackley, P.C., Trippi, M.H. & Alimi, H. (2013) Evaluation of thermal maturity in the low maturity Devonian shales of the northern Appalachian Basin. *American Association of Petroleum Geologists Search and Discovery Article*, 10477.

Schettino, A., & Turco, E. (2009). Breakup of Pangaea and plate kinematics of the central Atlantic and Atlas regions. *Geophysical Journal International*, *178*(2), 1078-1097.

Shorten and Fitzgerald (in review) Post-orogenic thermal history and exhumation of the Northern Appalachian Basin: Low-temperature thermochronologic constraints, Basin Research.

Shorten and Fitzgerald (in press Chapter 2) Episodic exhumation of the Appalachian Orogen in the Catskill Mountains.

Sobel, E.R. & Seward, D. (2010) Influence of Etching Conditions on Apatite Fission-Track Etch Pit Diameter. *Chem. Geol.*, **271**, 59–69.

Soeder, D. J., Enomoto, C. B., & Chermak, J. A. (2014). The Devonian Marcellus Shale and Millboro Shale. Field Guides, 35, 129-160.

Spotila, J.A., Bank, G.C., Reiners, P.W., Naeser, C.W., Naeser, N.D. & Henika, B.S. (2004) Origin of the Blue Ridge escarpment along the passive margin of Eastern North America. *Basin Research*, **16**, 41–63.

Steckler, M. S., Omar, G. I., Karner, G. D., & Kohn, B. P. (1993). Pattern of hydrothermal circulation within the Newark basin from fission-track analysis. Geology, 21(8), 735-738.

Sweeney, J.J. & Burnham, A.K. (1990) Evaluation of a Simple Model of Vitrinite Reflectance Based on Chemical Kinetics. *AAPG Bull.*, **74**, 1559-1570.

Taylor, J.P. & Fitzgerald, P.G. (2010) Low-temperature thermal history and landscape development of the eastern Adirondack Mountains, New York: Constraints from apatite fission-track thermochronology and apatite (U-Th)/He dating. *Bull. Geol. Soc. Am.*, **123**, 412–426.

Thiede, R.C., Bookhagen, B., Arrowsmith, J.R., Sobel, E.R. & Strecker, M.R. (2004) Climatic control on rapid exhumation along the Southern Himalayan Front. *Earth Planet. Sci. Lett.*, **222**, 791–806.

Tissot B.P., Welte, D.H. (1978) *Petroleum formation and occurrence: a new approach to oil and gas exploration*. Springer-Verlag, Berlin.

Tobin, R.C. & Claxton, B.L. (2000) Multidisciplinary thermal maturity studies using vitrinite reflectance and fluid inclusion microthermometry: a new calibration of old techniques. *Bull. Am. Assoc. Petrol. Geol.*, **84**, 1647-1665.

Tseng, H. Y., Burruss, R. C., Onstott, T. C., & Omar, G. (1999). Paleofluid-flow circulation within a Triassic rift basin: Evidence from oil inclusions and thermal histories. *Bulletin of the Geological Society of America*, *111*(2), 275–290.

Vermeesch, P. (2008) RadialPlotter: A Java application for fission track, luminescence and other radial plots. *Radiation Measurements*, **44**, 409–410.

Ver Straeten, C.A. (2009) The classic Devonian of the Catskill front: A foreland basin record of Acadian orogenesis. In: *New York State Geological Association, 81st Annual Meeting Guidebook* (Ed. by F. Vollmer), 7-1–7-54.

Ver Straeten, C.A. (2010) Lessons from the foreland basin: Northern Appalachian basin perspectives on the Acadian orogeny. In: *From Rodinia to Pangea: The Lithotectonic Record of the Appalachian Region (Ed. by R.P. Tollo). Geol. Soc. Am. Mem.*, **206**, 251-282.

Ver Straeten, C. A. (2013) Beneath it all: bedrock geology of the Catskill Mountains and implications of its weathering. *Annals of the New York Academy of Sciences*, (March), 1-39.

Vitorello, I. & Pollack, H.N. (1980) On the Variation of Continetal Heat Flow with Age and the Thermal Evolution of Continents. *J. Geophys. Res.*, **85**, 983–995.

Weary, D.J., Ryder, R.T. & Nyahay, R. (2000) Thermal maturity patterns (CAI and %R$_o$) in the Ordovician and Devonian rocks of the Appalachian basin in New York State. *U.S. Geol. Surv.*, Open Report **2000-496**.

Weisberg, W.R., Metcalf, J.R. & Flowers, R.M. (2018) Distinguishing slow cooling versus multiphase cooling and heating in zircon and apatite (U-Th)/He datasets: The case of the McClure Mountain syenite standard. *Chemical Geology*, (in press).

West, D.P., Jr., Lux, D.R., and Hussey, A.M., II (1993) Contrasting thermal histories across the Flying Point fault, southwestern Maine: Evidence for Mesozoic displacement: Geological Society of America Bulletin, v. 105, p. 1478–1490.

West Jr, D. P., & Roden-Tice, M. K. (2003). Late Cretaceous reactivation of the Norumbega fault zone, Maine: Evidence from apatite fission-track ages. *Geology*, *31*(7), 649-652.

West Jr., D. P., Roden-Tice, M. K., Potter, J. K., and Barnard, N. Q. (2008). Assessing the role of orogen-parallel faulting in post-orogenic exhumation: low-temperature thermochronology across the Norumbega Fault System, Maine. *Canadian Journal of Earth Sciences*, *45*(3), 287–301.

Wildman, M., Brown, R., Beucher, R., Persano, C., Stuart, F., Gallagher, K., Schwanethal, J. and Carter, A. (2016) The chronology and tectonic style of landscape evolution along the elevated Atlantic continental margin of South Africa resolved by joint apatite fission track and (U-Th-Sm)/He thermochronology. *Tectonics*, **35**(3), 511-545.

Wildman, M., Cogné, N. and Beucher, R. (2018) Fission-track Thermochronology Applied to the Evolution of Passive Continetal Margins. In: *Fission-track thermochronology and its application to geology* (Ed. by M.G. Malusà and P.G. Fitzgerald), Springer, Berlin (Chapter 20).

Wilkins, S., Mount, V., Mahon, K., Perry, A. & Koenig, J. (2014) Characterization and development of subsurface fractures observed in the Marcellus Formation, Appalachian Plateau, north-central Pennsylvania. *AAPG Bulletin*, **98**, 2301-2345.

Withjack, M.O., Schlische, R.W. & Olsen, P.E. (1998) Diachronous rifting, drifting, and inversion on the passive margin of central eastern North America: an analog for other passive margins. *AAPG Bull.*, **82**, 817–835.

Withjack, M.O. & Schlische, R.W. (2005) A review of tectonic events on the passive margin of eastern North America. In: *Petroleum Systems of Divergent Continental Margin Basins (Ed. by P.J. Post, N.C. Rosen, D.L. Olson, S.L. Palmes, K.T. Lyons & G.B. Newton)*. 25th Bob S. Perkins Research Conference, Gulf Coast Section of SEPM, Houston, TX, 203-235.

Withjack, M. O., Schlische, R. W., & Olsen, P. E. (2012). Development of the passive margin of eastern North America: Mesozoic rifting, igneous activity, and breakup. In *Regional Geology and Tectonics: Phanerozoic Rift Systems and Sedimentary Basins* (pp. 300-335).

Wojcik, K.M., Goldstein, R.H. & Walton, A.W. (1994) History of diagenetic fluids in a distant foreland area, Middle and Upper Pennsylvanian Cherokee basin, Kansas, USA: fluid inclusion evidence. *Geochim. Cosmochim. Acta*, **58**, 1175-1191.

Wolf, R.A., Farley, K.A. & Silver, L.T. (1996) Helium diffusion and low-temperature thermochronometry of apatite. *Geochim. Cosmochim. Acta*, **60**, 4231-4240.

Wolf, R.A., Farley, K.A., Kass, D.M. (1998) Modeling of the temperature sensitivity of the apatite (U-Th)/He thermochronometer. *Chem. Geol.*, **148**, 105-114.

Woodrow, D.L., Fletcher, F.W. & Ahrnsbrak, W.F. (1973) Paleogeography and paleoclimate at the deposition sites of the Devonian Catskill and old red facies. *Bull. Geol. Soc. Am.*, **84**, 3051–3064.

Zeitler, P.K., Herczig, A.L., McDougall, I. & Honda, M. (1987) U-Th-He dating of apatite: A potential thermochronometer. *Geochim. Cosmochim. Acta*, **51**, 2865–2868.

Zhang, E. & Davis, A. (1993) Coalification patterns of the Pennsylvanian coal measures in the Appalachian foreland basin, western and south-central Pennsylvania. *Bull. Geol. Soc. Am.*, **105**, 162-174.

Vita

Chilisa M. Shorten   Department of Earth Sciences
cmshorte@syr.edu   Syracuse University

EDUCATION

Ph.D. in Earth Sciences   2013 – 2018
Department of Earth Sciences, Syracuse University
B.S. Cum Laude in Geology   2007 – 2010
Department of Geology and Environmental Science, University of Pittsburgh

PROFESSIONAL AND TEACHING EXPERIENCE

Syracuse University Department of Earth Sciences, **Teaching Assistant**   2013 – 2018
Chevron Energy Technology Company, **Earth Science Internship**   Summer 2017
Syracuse University Department of Earth Sciences, **Teaching Instructor**   Summer 2016
Environmental Resources Management, **Associate Geologist**   2011 – 2013
Groundwater and Environmental Services, **Staff Geologist**   2010 – 2011

PUBLICATIONS

Shorten, C.S. & Fitzgerald, P.G. (in review). Post-orogenic thermal history and exhumation of the Northern Appalachian Basin: Low-temperature thermochronologic constraints. *Basin Research*.

PRESENTATIONS

Shorten, C.S. & Fitzgerald, P.G. (2018). Post-Orogenic Exhumation of the Northern Appalachian Basin and the Timing of Hydrocarbon Generation: Low-Temperature Thermochronological Constraints from New York and Pennsylvania. *AAPG Annual Convention and Exhibition,* abstract no.2832784. Poster, AAPG ACE, Salt Lake City, UT.

Shorten, C.S. & Fitzgerald, P.G. (2018). Post-Orogenic Exhumation of the Northern Appalachian Basin and the Timing of Hydrocarbon Generation: Low-Temperature Thermochronological Constraints from the Northern Appalachian Basin and the Catskills. *GSA Abstracts with Programs*, v.50, no.2, paper no.14-3. Oral Presentation, NE GSA Meeting, Burlington, VT.

Shorten, C.S. & Fitzgerald, P.G. (2017). Post-orogenic thermal history and exhumation of the Northern Appalachian Basin constrained through low-temperature thermochronology. *GSA Abstracts with Programs*, v.49, no.2, paper no.14-11. Poster, NE/NC GSA Meeting, Pittsburgh, PA.

Shorten, C.S. & Fitzgerald, P.G. (2015). Post-orogenic thermal history and exhumation of the Northern Appalachian Basin constrained through low-temperature thermochronology. *GSA Abstracts with Programs*, v.47, no.7, p.799, paper no.316-7. Poster, GSA Annual Meeting, Baltimore, MD.

ACADEMIC AWARDS AND CERTIFICATIONS

SU Outstanding Teaching Assistant Award   2017
Certificate in University Teaching, SU Graduate School and Dept. of Earth Science   2017
Certificate of Professional Development, SU Women in Science and Engineering   2016
K. Douglas Nelson Award for graduate research in geophysics and tectonics   2015

PROFESSIONAL MEMBERSHIPS

AAPG (since 2013); **AAPG Division of Professional Affairs** (provisional member, since 2018); **GSA** (since 2013); **GSA Structure and Tectonics Division** (since 2014); **AGU** (since 2013)